AN EXPERIMENTAL INVESTIGATION ON THE BIOMECHANICS OF BONE FRAGILITY IN TYPE 2 DIABETES

Marissa Britton B.E.

OLLSCOIL NA GAILLIMHE
UNIVERSITY OF GALWAY

A thesis submitted to the University of Galway as fulfilment of the requirements for the Degree of Doctor of Philosophy

2023

Discipline of Biomedical Engineering,
College of Science and Engineering,
University of Galway

Supervisor of Research:
Dr. Ted Vaughan

ABSTRACT

Type 2 diabetic patients experience up to a 3-fold increase in bone fracture risk. Paradoxically, type 2 diabetes is associated with a normal or increased bone mineral density (BMD) when compared to non-diabetic patients. The current leading hypothesis is that the hyperglycaemic state leads to non-enzymatic glycation in collagen causing the formation of crosslinks, known as Advanced Glycation End Products (AGEs), stiffening the overall collagen network leading to more brittle behaviour. While the relationship between AGE accumulation and bone biomechanics has been widely suggested, a causal relationship has not yet been established, suggesting that other tissue-level mechanisms may be responsible for fragility. The objective of this thesis is to investigate the biomechanics of type 2 diabetic bone fragility through a multiscale experimental strategy that considers structural, mechanical and compositional features of in vitro and ex vivo human tissue samples.

Initially, an in vitro glycation model was used to simulate diabetic conditions in twenty anatomically adjacent pairs of cortical bone from a single bovine femur. Mechanical characterisation was carried out using 3-point bend, fracture toughness, and nanoindentation testing, while bone composition was analysed by quantifying the accumulation of fluorescent AGEs. A study was also carried out on human trabecular and cortical bone tissue, obtained from femoral heads of patients undergoing total hip replacement, to evaluate the effect of type 2 diabetes on bone biomechanics. Mechanical testing was carried out on isolated trabecular cores using monotonic and cyclic compression loading and nanoindentation experiments, with bone microdamage analysed using micro-computed tomography (micro-CT) imaging. Bone composition was evaluated using Raman spectroscopy, high-performance liquid chromatography, fluorometric spectroscopy. Finally, the effect of type 2 diabetes on the trabecular microarchitecture in the femoral head was also evaluated through a macro- and micro-regional analysis of micro-CT based images.

It was found that AGEs were not detrimental to the mechanical properties of bone tissue, with AGE accumulation actually found to enhance several pre- and post-yield properties of the in vitro glycated bovine tissue. It was also found that human type 2 diabetic bone had altered mechanical, compositional, and morphological properties compared to non-type 2 diabetic bone. High-resolution (10μm) micro-CT imaging showed that cores taken from the central trabecular region of femoral head had higher bone mineral density, bone volume, trabecular thickness and reduced trabecular separation. These samples of human type 2 diabetic bone also had enhanced macro-mechanical compressive and fatigue properties, with many significant differences remaining even when normalised against the bone volume. Using nanoindentation, tissue-level mechanical properties of cortical and trabecular bone was unchanged in type 2 diabetic samples compared to controls. Through compositional analysis, higher levels of furosine were found in type 2 diabetic trabecular bone and an increase in both furosine and carboxymethyl-lysine (an AGE) was found in cortical bone. Raman spectroscopy showed that type 2 bone had a higher mineral-to-matrix ratio, carbonate substitution and reduced crystallinity compared to the controls. Finally, regional differences within micro regions of the femoral head of type 2 diabetic samples compared to non-type 2 diabetic samples were found, along with regional differences within each macro region within each group were found. In conclusion, this thesis shows that type 2 diabetes leads to distinct changes in both organic and mineral phases of the bone tissue matrix, but these changes did not coincide with any reduction in the mechanical properties of the tissue under either monotonic or cyclic loading. While this enhances the current understanding of type 2 diabetic bone, this thesis provides no evidence that AGE accumulation is responsible for diabetic bone fragility and further investigations are required to elucidate the mechanisms responsible for bone fragility in type 2 diabetes.

LIST OF PUBLICATIONS

Journal Articles

The following publications have arisen from the work presented in this thesis:

Britton, M., Parle, E., Vaughan, T.J. "An investigation on the effects of in vitro induced advanced glycation end-products on cortical bone fracture mechanics at fall-related loading rates" (2023) Journal of the Mechanical Behaviour of Biomedical Materials

The following manuscripts are currently in preparation:

Britton M., Monahan, G.E., Schiavi-Tritz, J., Beljebbar, A., Van Gulick, L., Owieka, A., Jaisson, S., Kerdjoudj, H., Vaughan, T.J. "Investigating the Mechanical Properties and Microdamage Accumulation of Human Type 2 Diabetic Bone" *In preparation*

Britton M., Monahan, G.E., Vaughan, T.J. "An Investigation of Regional Heterogeneity within the ex vivo Femoral Head of Type 2 Diabetic Patients" *In preparation*

The following publications have been generated separate to this thesis:

Monahan, G. E., Schiavi-Tritz, J., **Britton, M.**, Vaughan, T.J. "Longitudinal Alterations in Bone morphology, Mechanical Integrity and Composition in Type-2 Diabetes in a Zucker Diabetic Fatty(ZDF) Rat" (2023) Bone

Dubus, M., Scomazzon, L., Ledouble, C., Braux, J., Beljebbar, A., Van Gulick, L., Baldit, A., Gorin, C., Alem, H., Bouland, N., **Britton, M**., Schiavi, J., Vaughan, T.J., Mauprivez, C., Kerdjoudj, H. "Hybrid Mineral/Organic Material Induces Bone Bridging and Bone Volume Augmentation in Rat Calvarial Critical Size Defects" (2022) Cells

Peer-Reviewed International Conferences

Podium presentation at the annual meeting of Orthopaedic Research Society, Dallas, Texas, USA. February 2023.

Podium presentation at the annual meeting of ICORS World Orthopaedic Congress, Edinburgh, Scotland. September 2022.

Podium presentation at the annual meeting of Word Congress of Biomechanics, Taipei, Taiwan. July 2022.

Podium presentation at the annual meeting of European Solid Mechanics Conference, Galway, Ireland. July 2022.

Podium presentation at the annual meeting of the European Society of Biomechanics, Porto, Portugal. June 2022.

Poster presentation at the annual meeting of Orthopaedic Research Society, Tampa, Florida, USA. February 2022.

Podium presentation at the annual meeting of the European Society of Biomechanics, Milan, Italy. July 2021.

Peer-Reviewed National Conferences

Podium presentations at 25th, 26th, 27th and 28th Annual conference of the Section of Bioengineering of the Royal Academy of Medicine in Ireland (BINI), January 2019, 2020, May 2022 and January 2023.

ACKNOWLEDGEMENTS

I would like to take this opportunity to express my sincere gratitude to everyone who has supported me throughout my studies. First and foremost, I would like to express my sincere thanks and gratitude to my supervisor Dr. Ted Vaughan, for his support, encouragement, and direction throughout my studies. I am truly grateful for your expertise and insights.

I would also like to extend my thanks to Dr. Jessica Schiavi-Tritz for her invaluable advice, support, and encouragement throughout this process. Jess, I appreciate all our research discussions and the wonderful company you provided in Reims and Dallas!

A special thank you goes out to all the current and former members of the Vaughan research group. Many thanks to my friends Masooma, Ruth, Swati, Vatsal, Vinnie, Anneke, Ryan, Dave, Tecla, Martina, Mahtab, Sam, Darshan, Thomas, and all the members of Pints for PhDs and An Detective for the lunchtime chats, laughter, conference trips, and ice cream breaks. Special thanks to my colleague and good friend, Genna, for always making time for diabetic research discussions and being excellent company during conferences and trips. Thanks also to Flavia for the daily chats, big and small, and coffee breaks, especially during the past year. I would also like to thank Ciara for the countless miles ran, hours of chats, sea swims, and craic. My sincere appreciation goes to the technical staff, especially Dave Connolly, for their assistance and expertise in the lab. Thanks also to Pat Kelly for machining all the necessary rigs and end-caps!

To all my housemates in Dún and the members of Spider Arms, thank you for the laughter, adventures, nights out, and fun.

To my family, Mam, Dad, Kate, Cathal, and Liam – thank you for your unconditional love, support, and encouragement throughout the years. Last but not least, Aidan, thank you for everything, especially, your constant love, support, encouragement and understanding.

DECLARATION OF ORIGINALITY

I declare that the work presented in this thesis is my own.

Marissa Britton

TABLE OF CONTENTS

CHAPTER 1

Introduction

Skeletal health is an important issue for older adults as the fracture risk increases exponentially with age (Schwartz 2003). According to recent statistics, approximately 4 million bone fragility fractures occur annually in the EU, leading to an approximate cost of €37 billion to healthcare systems (Kanis et al. 2021). Type 2 diabetes (T2D) has recently emerged as an independent risk factor for bone fragility fractures, with T2D patients having up to a three-fold increased fracture risk at the hip and other non-vertebral sites compared to non-diabetic patients (Bonds et al. 2006; Janghorbani et al. 2007; Vestergaard 2007; Schwartz et al. 2011; Napoli et al. 2014). Additionally, vertebral fracture risk has been found to be increased in people with T2D (Koromani et al. 2021), this is important as vertebral fractures, unlike non-vertebral fractures, can often occur without a fall (Tsuda 2017). However, there is a lack of understanding of the mechanisms that underlie this T2D bone fragility as, paradoxically, T2D patients have a normal or increased bone mineral density (BMD) compared to non-diabetic patients (Heilmeier et al. 2015; Melton et al. 2008a). This is in contrast to changes that take place in osteoporosis, which has been widely characterised as a disease of bone loss or reduced BMD (World Health Organization 1994; Pahr and Zysset 2016). This creates clinical challenges as current diagnostic techniques cannot accurately predict fracture probability in T2D patients, as these

tend to be based on measurements bone density through dual-energy x-ray absorptiometry (DXA) scanning (Kanis et al. 2000), for example. This also implies that T2D has a deleterious effect on bone quality, whereby the intrinsic material properties of the bone matrix are altered and contribute to impaired biomechanical behaviour. However, there remains a lack of detailed quantitative information about how bone tissue properties are affected in individuals with T2D. This, coupled with bone's complex hierarchical structural organisation and associated fracture mechanics, means there is a severe lack of understanding of (i) the sub-tissue physiochemical alterations that take place in type 2 diabetic bone disease and (ii) how these changes compromise overall structural integrity of the tissue. To understand the precise mechanisms leading to the increase in fracture risk for T2D patients, a comprehensive understanding is required on the multiscale mechanical, morphological and compositional characteristics of human T2D bone. The work of this thesis adopts mechanical testing, compositional and morphological analysis techniques to investigate the effect of T2D on bone biomechanics.

1.2 T2D Background

Diabetes is a chronic metabolic disease (Laakso 1999; American Diabetes Association 2010; Shanbhogue et al. 2016) that affects the body's ability to produce and respond to insulin. Diabetes is characterised by hyperglycaemia, which can be associated with permanent damage and failure of various organs and tissues. T2D is much more common than type 1 diabetes, accounting for ~90-95% of those with diabetes (American Diabetes Association 2010). T2D is caused by a combination of reduction in insulin-stimulated glucose uptake and a deficient compensatory insulin secretory response. T2D patients have an increased risk of developing a number of serious life-threatening health problems, leaving them with higher medical care costs, reduced quality of life and increased mortality (Baena-Díez et al. 2016). Most T2D patients are overweight or obese (Bain et al. 2016), which in itself provides some level of insulin resistance. With an increase in age, obesity and inactivity, the risk of developing T2D

increases (American Diabetes Association 2010). The global incidence of diabetes has been growing over recent decades. By 2045, it is estimated that 9.9% of the population will have diabetes. The worldwide annual cost of diabetes is 850 billion USD, or 780 billion euros (Cho et al. 2018). In Ireland, the estimated annual cost of diabetes is 2 billion euros, which equates to 12-14% of the total annual healthcare budget according to a report by Diabetes Ireland (2018).

T2D can lead to a range of health complications that include diabetic retinopathy, neuropathy and cardiomyopathy. While these chronic health conditions are widely associated with T2D, T2D has also been associated with up to a 3-fold increase in bone fracture risk (Janghorbani et al. 2007). The emergence of bone fragility as an additional disease complication is concerning, particularly seeing as these patients generally experience no reduction in bone mineral density (BMD). While these higher levels of BMD are strongly associated with the increased BMI that is generally prevalent in T2D patients (Felson et al. 1993; Thomas et al. 2001), it has been shown that increased BMD and increased fragility remains even after the data is adjusted for BMI, suggesting that other factors such as hyperinsulinemia may contribute to increased BMD (Reid et al. 1993; Strotmeyer et al. 2004; De Liefde et al. 2005; Oei et al. 2013). Despite most T2D patients having a relatively higher BMD, it is suggested that T2D is associated with a low bone turnover state with reduced bone formation (Achemlal et al., 2005; Bloomfield et al., 2008; Moseley, 2012a). While the onset of T2D leads to increased bone fragility, these patients also experience an impaired fracture healing response due to the disease state, with increased incidence of complications compared to healthy individuals (Folk et al. 1999; Retzepi and Donos 2010; Jiao et al. 2015), including delayed healing time, non-union or re-dislocation. This highlights the distinct need to better understand bone fragility in T2D and protect against fractures in this patient population. With the rapidly increasing prevalence of T2D across the global population (International Diabetes Federation 2021), there is an urgent need to

understand the precise mechanisms, composition and morphological properties of T2D bone that may influence the increased fragility in T2D bone at the population level.

1.3 Advanced Glycation End-products

T2D disrupts metabolic and cellular functions throughout the body. The hyperglycaemic state is accompanied by other pathophysiological changes that include increased bone marrow adiposity, the release of inflammatory factors and higher oxidative stress. These systemic changes disrupt normal bone metabolism, whereby the normal maintenance of the bone tissue matrix is disrupted. These results in a range of sub-tissue alterations to both the organic and mineral phases of the bone matrix, which impairs local tissue biomechanics and ultimately weakens the overall structure. However, the precise sub-tissue alterations that take place and mechanisms that impair whole-bone fracture mechanics in T2D remains poorly understood.

The leading hypothesis for the cause of the increased bone fragility in T2D is that the hyperglycaemic state leads to an acceleration of non-enzymatic glycation in collagen, causing the formation of crosslinks and adducts throughout the protein network, known as advanced glycation end-products (AGEs). AGEs are generated from the sequential non-enzymatic chemical glycoxidation of protein amino groups accumulating in various collagenous tissues, including bone, as a function of time and glucose concentration (Singh et al. 2001). Previous studies have linked AGE accumulations with alterations in the mechanical properties of collagenous tissues and have proposed that these unwanted crosslinks may stiffen the overall collagen network leading to more brittle behaviour and bone fragility (Bank et al. 1998; Vashishth et al. 2001). Increased accumulation of AGEs in bone has been linked with aging (Zimmermann et al. 2011), chronic kidney disease (Damrath et al. 2021) and T2D (Karim and Bouxsein 2016). Wang et al. (2002) reported that elderly bone has decreased mechanical properties and increased concentration of the AGE, pentosidine. They found that pentosidine was negatively correlated with ultimate bending stress, total work-to-fracture and the critical

stress intensity factor. While it has been widely hypothesised that AGE accumulation is correlated with increased fragility in T2D (Schwartz and Sellmeyer 2007; Vashishth 2007; Saito and Marumo 2010; Saito and Marumo 2015; Sihota et al. 2021), the correlation between increased AGEs and decreased mechanical properties has not been conclusively demonstrated in T2D. **In particular, the difficulty in obtaining direct measurements from bone tissue in vivo means that quantitative data describing precisely how bone tissue properties are affected by AGE accumulation in human patients with T2D is limited.**

1.4 Biomechanics of T2D Bone Tissue

There are distinct challenges in understanding the mechanisms responsible for the increased bone fragility in T2D. While population-level studies have identified increased fracture risk for T2D patients (Janghorbani et al. 2007; Vestergaard 2007), there is a distinct lack of data describing the tissue-level biomechanics of T2D bone. In fact, much of the current understanding of the mechanics of bone fragility in T2D has been generated using in vitro models, whereby animal or human tissue was immersed in a ribose solution to promote non-enzymatic glycation of the protein network. These studies have shown contradictory results, with some studies finding an increase in the yield stress and strain of glycated samples (Vashishth et al. 2001), while other studies have found impaired post-yield properties of glycated samples (Tang et al. 2007; Willett et al. 2013; Jia et al. 2021), and others finding no observable differences in the mechanical properties of glycated samples (Viguet-Carrin et al. 2008). While these studies have provided some insight into the role of AGEs on bone biomechanics, the results have been highly contradictory, with the wide variation in results possibly arising from the difficulties in reducing inter-specimen variability in specimens. Furthermore, in vitro glycation studies have tended to focus on elastic tissue mechanics, with studies that examine the fracture mechanics of in vitro glycated samples only appearing recently (Merlo et al. 2020; Jia et al. 2021). **Determining the precise role of AGE**

accumulation on bone tissue fracture mechanics has proven difficult and experimental approaches that reduce specimen variability are required.

While in vitro models have provided certain insight into the mechanics of glycated bone tissue, these still do not fully represent the T2D disease state, and biomechanical data from human tissue has become increasingly important. In this context, detailed biomechanical studies on human tissue have really only emerged in the past five years, with the majority of these characterising the uniaxial compression behaviour of trabecular cores that have been extracted from femoral heads of patients with T2D. Interestingly, the majority of these studies have found that the mechanical properties of trabecular bone tissue in T2D are similar (Karim et al. 2018; Parle et al. 2020) or even enhanced (Hunt et al. 2019) compared to non-T2D controls. However, cyclic reference point indentation has found higher creep indentation distance in cortical bone (Karim et al. 2018), which does provide evidence of impaired tissue-level properties in T2D. More interestingly, despite the assumption that AGEs accumulate in the bone tissue of people with T2D, the evidence for this is actually quite scarce and even conflicting. Several studies on human tissue have found no differences in the amount of fluorescent AGEs in T2D (Hunt et al. 2019; Karim et al. 2018) with only a limited number of studies showing an increase in either fluorescent (Sihota et al. 2021) or non- fluorescent AGEs (Karim et al. 2018). Thus, the relevance of AGE accumulation and its contribution towards skeletal fragility in T2D remains unknown (Karim et al. 2018) and this recent research suggests that other mechanisms may also contribute to bone fragility in T2D. These could include other alterations to the mineral or organic phases of the bone matrix taking place, with several studies observing altered mineral distributions (Parle et al. 2020), changes to collagen matrix and a more heterogeneous distribution of microdamage (Sacher et al. 2022) in T2D bone. While such mechanisms may contribute to bone fragility in T2D, there remains a lack of experimental investigations on human T2D tissue that provides quantitative data on the role of the bone matrix on the tissue

biomechanics, and whole bone fragility. Furthermore**,** existing experimental biomechanical investigations have been largely carried using monotonic loading conditions, which may not fully capture the possible mechanisms of fragility in T2D, which could include the accumulation of microdamage under cyclic loading (Tang and Vashishth, 2010). **To further elucidate the relationship between T2D and increased fracture risk in human bone, more comprehensive studies are required that systematically investigate the mechanical, morphological, and compositional properties of T2D tissue.**

1.5 Bone Mineral Density

Population-level studies have provided direct evidence that T2D bone is subject to changes in bone density and morphology, with several studies identifying higher BMD values in the femoral neck (Melton et al. 2008b; Heilmeier et al. 2015), lumbar spine (Strotmeyer et al. 2004; Melton et al. 2008b), distal radius (Melton et al. 2008b; Petit et al. 2010) and the distal tibia (Petit et al. 2010) of T2D patients. While these studies show that T2D undergoes distinct structural changes, the imaging modalities used are generally low resolution through DXA scanning, quantitative computed tomography (QCT) or peripheral QCT (pQCT), which means that the precise nature of changes to the local microarchitecture remain poorly understood. While many studies have reported similar or improved trabecular bone microarchitecture in T2D patients compared to non-diabetic controls, studies using high resolution pQCT (HR-pQCT) have reported that cortical bone could also be negatively impacted in T2D. This is evidenced by findings of increased cortical porosity or lower cortical density (Burghardt et al. 2010; Patsch et al. 2013; Yu et al. 2014). The majority of HR-pQCT investigation of diabetic bone to date has been carried out on T2D bone with some recent research being carried out on type 1 diabetic bone (Sewing et al. 2022). Studies that have conducted detailed micro-CT on human bone are currently limited and have generally evaluated isolated trabecular cores from the primary loading axis or the central region of the femoral head (Karim et al. 2018; Parle et

al. 2020; Piccoli et al. 2020; Sihota et al. 2021; Yadav et al. 2022) or femoral neck (Hunt et al. 2019; Cirovic et al. 2022). However, it is known that in other disease states, such as osteoporosis, trabecular bone can undergo distinct regional changes from the primary loading axis (Homminga 2003) that weakens the structure significantly for non-typical loading. **It is apparent that T2D affects the morphological properties of bone. It is essential that the precise effect of T2D on the morphological properties of bone are better understood and that detailed microstructural information that goes beyond BMD is needed. Additionally, the regional changes within the T2D femoral head, including areas outside of the primary loading axis, in bone density and microarchitecture.**

1.6 Objectives

The global objective of this thesis is to investigate the biomechanics of type 2 diabetic bone fragility through a multiscale experimental strategy that considers structural, mechanical and compositional features of in vitro and ex vivo human tissue samples. This work will help elucidate the underlying mechanisms that are responsible for bone fragility in T2D that could contribute to the development of more effective clinical fracture risk assessment strategies. The specific objectives to:

1. Establish an in vitro glycation model of T2D to investigate the relationship between AGE accumulation and the fracture mechanics of ex vivo bovine cortical bone tissue.
2. Investigate the roles of bone composition and micro-damage accumulation on the mechanical properties of human T2D femoral head trabecular bone tissue under both monotonic and cyclic loading.
3. Evaluate the regional morphological properties of ex vivo T2D femoral heads through micro-CT and image analysis and investigate inter- and intra-regional heterogeneity in the trabecular microarchitecture with the onset of disease.

1.7 Thesis Structure

The outline of this thesis is as follows:

Chapter 2 outlines existing literature relevant to T2D and bone. This chapter describes the structure and function of bone and details the effect of T2D on it. It also provides a review of various experimental techniques that have been employed to evaluate the mechanical behaviour, composition and morphology of bone.

Chapter 3 presents an experimental investigation into in vitro AGE accumulation in bovine cortical bone and the influence it has on mechanical and compositional properties. The mechanical properties of rectangular specimens of bone are assessed using three-point bend, fracture toughness and nanoindentation tests. The composition of the bone is analysed using fluorometric spectrometry.

Chapter 4 demonstrates an experimental investigation into the mechanics, microdamage accumulation, composition, and morphology of trabecular cores of T2D bone. The biomechanics is evaluated through monotonic and cyclic compression, while composition is analysed using high-performance liquid chromatography, Raman and fluorometric spectroscopy. The morphological properties and microdamage accumulation are assessed using micro computed tomography. Additionally, nanoindentation of both cortical and trabecular T2D bone is carried out to determine tissue level properties.

In Chapter 5, a regional morphological assessment of trabecular region of the T2D femoral head is presented. Femoral heads are scanned using micro computed tomography. The trabecular region is segmented into thirty-seven regions of interest. These regions of interest are then compared to non-T2D regions of interest. Regional changes within the T2D femoral heads are also assessed. The bone mineral density distribution is also investigated.

In Chapter 6, the main findings of this thesis are outlined and suggestions for future research are presented.

1.8 References

Achemlal, Lahsen, Saida Tellal, Fouad Rkiouak, Abderrazak Nouijai, Ahmed Bezza, El Mostapha Derouiche, Driss Ghafir, and Abdellah El Maghraoui. 2005. 'Bone metabolism in male patients with type 2 diabetes', *Clinical Rheumatology*, 24: 493-96.

American Diabetes Association. 2010. 'Diagnosis and classification of diabetes mellitus', *Diabetes Care*, 33.

Baena-Díez, Jose Miguel, Judit Peñafiel, Isaac Subirana, Rafel Ramos, Roberto Elosua, Alejandro Marín-Ibañez, María Jesús Guembe, Fernando Rigo, María José Tormo-Díaz, Conchi Moreno-Iribas, Joan Josep Cabré, Antonio Segura, Manel García-Lareo, Agustín Gómez De La Cámara, José Lapetra, Miquel Quesada, Jaume Marrugat, Maria José Medrano, Jesús Berjón, Guiem Frontera, Diana Gavrila, Aurelio Barricarte, Josep Basora, Jose María García, Natalia C. Pavone, David Lora-Pablos, Eduardo Mayoral, Josep Franch, Manel Mata, Conxa Castell, Albert Frances, and María Grau. 2016. 'Risk of cause-specific death in individuals with diabetes: A competing risks analysis', *Diabetes Care*, 39: 1987-95.

Bain, SC, M Feher, D Russell-Jones, and K Khunti. 2016. 'Management of type 2 diabetes: t he current situation and key opportunities to improve care in the UK', *Diabetes, Obesity and Metabolism*, 18: 1157-66.

Bank, Ruud A., Michael T. Bayliss, Floris P. J. G. Lafeber, Alice Maroudas, and Johan M. Tekoppele. 1998. "Ageing and zonal variation in post-translational modification of collagen in normal human articular cartilage The age-related increase in non-enzymatic glycation affects biomechanical properties of cartilage." In *Biochem. J*, 345-51.

Bloomfield, Susan A., Harry A. Hogan, Michael D. Delp, Rhonda D. Prisby, Joshua M. Swift, Susan A. Bloomfield, Harry A. Hogan, and Michael D. Delp. 2008. 'Altered bone mass, geometry and mechanical properties during the development and progression of type 2 diabetes in the Zucker diabetic fatty rat', *Journal of Endocrinology*.

Bonds, Denise E., Joseph C. Larson, Ann V. Schwartz, Elsa S. Strotmeyer, John Robbins, Beatriz L. Rodriguez, Karen C. Johnson, and Karen L. Margolis. 2006. 'Risk of Fracture in Women with Type 2 Diabetes: the Women's Health Initiative Observational Study', *The Journal of Clinical Endocrinology & Metabolism*, 91: 3404-10.

Burghardt, Andrew J., Ahi S. Issever, Ann V. Schwartz, Kevin A. Davis, Umesh Masharani, Sharmila Majumdar, and Thomas M. Link. 2010. 'High-Resolution Peripheral Quantitative Computed Tomographic Imaging of Cortical and Trabecular Bone Microarchitecture in Patients with Type 2 Diabetes Mellitus', *The Journal of Clinical Endocrinology & Metabolism*, 95: 5045-55.

Cho, N. H., J. E. Shaw, S. Karuranga, Y. Huang, J. D. da Rocha Fernandes, A. W. Ohlrogge, and B. Malanda. 2018. 'IDF Diabetes Atlas: Global estimates of diabetes prevalence for 2017 and projections for 2045', *Diabetes Research and Clinical Practice*, 138: 271-81.

Cirovic, Aleksandar, Jelena Jadzic, Danica Djukic, Danijela Djonic, Vladimir Zivkovic, Slobodan Nikolic, Marija Djuric, and Petar Milovanovic. 2022. 'Increased Cortical Porosity, Reduced Cortical Thickness, and Reduced Trabecular and Cortical Microhardness of the Superolateral Femoral Neck Confer the Increased Hip Fracture Risk in Individuals with Type 2 Diabetes', *Calcified Tissue International*, 111: 457-65.

Damrath, John G, Amy Creecy, Joseph M Wallace, and Sharon M Moe. 2021. 'The impact of advanced glycation end products on bone properties in chronic kidney disease', *Current Opinion in Nephrology and Hypertension*, 30: 411-17.

De Liefde, II, Marjolein van der Klift, CEDH De Laet, PLA Van Daele, Albert Hofman, and HAP Pols. 2005. 'Bone mineral density and fracture risk in type-2 diabetes mellitus: the Rotterdam Study', *Osteoporosis International*, 16: 1713-20.

Diabetes Ireland. 2018. "Diabetes Ireland. Diabetes Ireland highlights escalating cost of treating diabetes complications to TDs on World Diabetes Day." In.: Diabetes Ireland.

Felson, David T., Yuqing Zhang, Marian T. Hannan, and Jennifer J. Anderson. 1993. 'Effects of weight and body mass index on bone mineral density in men and women: The framingham study', *JOURNAL OF BONE AND MINERAL RESEARCH*, 8: 567-73.

Folk, J. W., A. J. Starr, and J. S. Early. 1999. 'Early wound complications of operative treatment of calcaneus fractures: analysis of 190 fractures', *J Orthop Trauma*, 13: 369-72.

Heilmeier, U., D. R. Carpenter, J. M. Patsch, R. Harnish, G. B. Joseph, A. J. Burghardt, T. Baum, A. V. Schwartz, T. F. Lang, and T. M. Link. 2015. 'Volumetric femoral BMD, bone geometry, and serum sclerostin levels differ between type 2 diabetic postmenopausal women with and without fragility fractures', *Osteoporosis International*, 26: 1283-93.

Homminga, J.J. 2003. 'Towards a rational definition of osteoporosis', Technische Universiteit Eindhoven.

Hunt, Heather B, Ashley M Torres, Pablo M Palomino, Eric Marty, Rehan Saiyed, Matthew Cohn, Jonathan Jo, Stephen Warner, Grazyna E Sroga, and Karen B King. 2019. 'Altered tissue composition, microarchitecture, and mechanical performance in cancellous bone from men with type 2 diabetes mellitus', *JOURNAL OF BONE AND MINERAL RESEARCH*, 34: 1191-206.

International-Diabetes-Federation. 2021. "IDF Diabetes Atlas 2021 10th Edition." In. https://diabetesatlas.org: International Diabetes Federation.

Janghorbani, M., R. M. Van Dam, W. C. Willett, and F. B. Hu. 2007. 'Systematic Review of Type 1 and Type 2 Diabetes Mellitus and Risk of Fracture', *American Journal of Epidemiology*, 166: 495-505.

Jia, Shaowei, He Gong, Haipeng Cen, Peipei Shi, Rui Zhang, Zhaowei Li, and Xuewei Bi. 2021. 'Influence of non-enzymatic glycation on the mechanical properties of cortical bone', *Journal of the Mechanical Behavior of Biomedical Materials*, 119: 104553-53.

Jiao, H., E. Xiao, and D. T. Graves. 2015. 'Diabetes and Its Effect on Bone and Fracture Healing', *Curr Osteoporos Rep*, 13: 327-35.

Kanis, J. A., C. C. Glüer, and International Osteoporosis Foundation for the Committee of Scientific Advisors. 2000. 'An Update on the Diagnosis and Assessment of Osteoporosis with Densitometry', *Osteoporosis International*, 11: 192-202.

Kanis, John A., Nicholas Norton, Nicholas C. Harvey, Trolle Jacobson, Helena Johansson, Mattias Lorentzon, Eugene V. McCloskey, Carl Willers, and Fredrik Borgström. 2021. 'SCOPE 2021: a new scorecard for osteoporosis in Europe', *Archives of Osteoporosis*, 16: 82.

Karim, Lamya, and Mary L. Bouxsein. 2016. 'Effect of type 2 diabetes-related non-enzymatic glycation on bone biomechanical properties', *Bone*, 82: 21-27.

Karim, Lamya, Julia Moulton, Miranda Van Vliet, Kelsey Velie, Ann Robbins, Fatemeh Malekipour, Ayesha Abdeen, Douglas Ayres, and Mary L. Bouxsein. 2018. 'Bone microarchitecture, biomechanical properties, and advanced glycation end-products in the proximal femur of adults with type 2 diabetes', *Bone*, 114: 32-39.

Koromani, Fjorda, Samuel Ghatan, Mandy van Hoek, M. Carola Zillikens, Edwin H. G. Oei, Fernando Rivadeneira, and Ling Oei. 2021. 'Type 2 Diabetes Mellitus and Vertebral Fracture Risk', *Current Osteoporosis Reports*, 19: 50-57.

Laakso, Markku. 1999. 'Hyperglycemia and cardiovascular disease in type 2 diabetes', *Diabetes*, 48: 937-42.

Melton, L. J., Cynthia L. Leibson, Sara J. Achenbach, Terry M. Therneau, and Sundeep Khosla. 2008a. 'Fracture Risk in Type 2 Diabetes: Update of a Population-Based Study', *JOURNAL OF BONE AND MINERAL RESEARCH*, 23: 1334-42.

Melton, L. J., B. Lawrence Riggs, Cynthia L. Leibson, Sara J. Achenbach, Jon J. Camp, Mary L. Bouxsein, Elizabeth J. Atkinson, Richard A. Robb, and Sundeep Khosla. 2008b. 'A Bone Structural Basis for Fracture Risk in Diabetes', *The Journal of Clinical Endocrinology & Metabolism*, 93: 4804-09.

Merlo, Kelly, Jacob Aaronson, Rachana Vaidya, Taraneh Rezaee, Vijaya Chalivendra, and Lamya Karim. 2020. 'In Vitro-Induced High Sugar Environments Deteriorate Human Cortical Bone Elastic Modulus and Fracture Toughness', *Journal of Orthopaedic Research®*, 38: 972-83.

Moseley, Kendall F. 2012. "Type 2 diabetes and bone fractures." In, 128-35. NIH Public Access.

Napoli, Nicola, Elsa S. Strotmeyer, Kristine E. Ensrud, Deborah E. Sellmeyer, Douglas C. Bauer, Andrew R. Hoffman, Thuy Tien L. Dam, Elizabeth Barrett-Connor, Lisa Palermo, Eric S. Orwoll, Steven R. Cummings, Dennis M. Black, and Ann V. Schwartz. 2014. 'Fracture risk in diabetic elderly men: The MrOS study', *Diabetologia*, 57: 2057-65.

Oei, Ling, M. Carola Zillikens, Abbas Dehghan, Gabriëlle H. S. Buitendijk, Martha C. Castaño-Betancourt, Karol Estrada, Lisette Stolk, Edwin H. G. Oei, Joyce B. J. Van Meurs, Joseph A. M. J. L. Janssen, Albert Hofman, Johannes P. T. M. Van Leeuwen, Jacqueline C. M. Witteman, Huibert A. P. Pols, André G. Uitterlinden, Caroline C. W. Klaver, Oscar H. Franco, and Fernando Rivadeneira. 2013. 'High bone mineral density and fracture risk in type 2 diabetes as skeletal complications of inadequate glucose control: The Rotterdam study', *Diabetes Care*, 36: 1619-28.

Pahr, Dieter H., and Philippe K. Zysset. 2016. 'Finite Element-Based Mechanical Assessment of Bone Quality on the Basis of In Vivo Images', *Current Osteoporosis Reports*, 14: 374-85.

Parle, Eoin, Sherdya Tio, Annie Behre, John J. Carey, Colin G. Murphy, Timothy F. O'Brien, William A. Curtin, Stephen R. Kearns, John P. McCabe, Cynthia M. Coleman, Ted J. Vaughan, and Laoise M. McNamara. 2020. 'Bone Mineral Is More Heterogeneously Distributed in the Femoral Heads of Osteoporotic and Diabetic Patients: A Pilot Study', *JBMR Plus*, 4: e10253-e53.

Patsch, Janina M., Andrew J. Burghardt, Samuel P. Yap, Thomas Baum, Ann V. Schwartz, Gabby B. Joseph, and Thomas M. Link. 2013. 'Increased cortical porosity in type 2 diabetic postmenopausal women with fragility fractures', *JOURNAL OF BONE AND MINERAL RESEARCH*, 28: 313-24.

Petit, Moira A., Misti L. Paudel, Brent C. Taylor, Julie M. Hughes, Elsa S. Strotmeyer, Ann V. Schwartz, Jane A. Cauley, Joseph M. Zmuda, Andrew R. Hoffman, and Kristine E. Ensrud. 2010. 'Bone mass and strength in older men with type 2 diabetes: The Osteoporotic Fractures in Men Study', *JOURNAL OF BONE AND MINERAL RESEARCH*, 25: 285-91.

Piccoli, Alessandra, Francesca Cannata, Rocky Strollo, Claudio Pedone, Giulia Leanza, Fabrizio Russo, Valentina Greto, Camilla Isgrò, Carlo Cosimo Quattrocchi, Carlo Massaroni, Sergio Silvestri, Gianluca Vadalà, Tiziana Bisogno, Vincenzo Denaro, Paolo Pozzilli, Simon Y. Tang, Matt J. Silva, Caterina Conte, Rocco Papalia, Mauro Maccarrone, and Nicola Napoli. 2020. 'Sclerostin Regulation, Microarchitecture, and Advanced Glycation End-Products in the Bone of Elderly Women With Type 2 Diabetes', *JOURNAL OF BONE AND MINERAL RESEARCH*, 35: 2415-22.

Reid, I. R., M. C. Evans, G. J. S. Cooper, R. W. Ames, and J. Stapleton. 1993. 'Circulating insulin levels are related to bone density in normal postmenopausal women', *American Journal of Physiology - Endocrinology and Metabolism*, 265: 655-59.

Retzepi, M., and N. Donos. 2010. 'The effect of diabetes mellitus on osseous healing', *Clin Oral Implants Res*, 21: 673-81.

Sacher, S. E., H. B. Hunt, S. Lekkala, K. A. Lopez, J. Potts, A. K. Heilbronner, E. M. Stein, C. J. Hernandez, and E. Donnelly. 2022. 'Distributions of Microdamage Are Altered Between Trabecular Rods and Plates in Cancellous Bone From Men With Type 2 Diabetes Mellitus', *J Bone Miner Res*, 37: 740-52.

Saito, Marumo, and KMSKM Marumo. 2010. 'Collagen cross-links as a determinant of bone quality: a possible explanation for bone fragility in aging, osteoporosis, and diabetes mellitus', *Osteoporosis International*, 21: 195-214.

Saito, Mitsuru, and Keishi Marumo. 2015. 'Effects of Collagen Crosslinking on Bone Material Properties in Health and Disease', *Calcified Tissue International*, 97: 242-61.

Schwartz, A. V. 2003. 'Diabetes Mellitus: Does it Affect Bone?', *Calcified Tissue International*, 73: 515-19.

Schwartz, Ann V., and Deborah E. Sellmeyer. 2007. 'Diabetes, fracture, and bone fragility', *Current Osteoporosis Reports*, 5: 105-11.

Schwartz, Ann V., Eric Vittinghoff, Douglas C. Bauer, Teresa A. Hillier, Elsa S. Strotmeyer, Kristine E. Ensrud, Meghan G. Donaldson, Jane A. Cauley, Tamara B. Harris, Annemarie Koster, Catherine R. Womack, Lisa Palermo, and Dennis M. Black. 2011. 'Association of BMD and FRAX score with risk of fracture in older adults with type 2 diabetes', *JAMA - Journal of the American Medical Association*, 305: 2184-92.

Sewing, Lilian, Laura Potasso, Sandra Baumann, Denis Schenk, Furkan Gazozcu, Kurt Lippuner, Marius Kraenzlin, Philippe Zysset, and Christian Meier. 2022. 'Bone Microarchitecture and Strength in Long-Standing Type 1 Diabetes', *JOURNAL OF BONE AND MINERAL RESEARCH*, 37: 837-47.

Shanbhogue, Vikram V., Deborah M. Mitchell, Clifford J. Rosen, and Mary L. Bouxsein. 2016. 'Type 2 diabetes and the skeleton: new insights into sweet bones', *The Lancet Diabetes & Endocrinology*, 4: 159-73.

Sihota, Praveer, Ram Naresh Yadav, Ruban Dhaliwal, Jagadeesh Chandra Bose, Vandana Dhiman, Deepak Neradi, Shailesh Karn, Sidhartha Sharma, Sameer Aggarwal, Vijay G. Goni, Vishwajeet Mehandia, Deepak Vashishth, Sanjay Kumar Bhadada, and Navin Kumar. 2021. 'Investigation of mechanical, material and compositional determinants of human trabecular bone quality in type 2 diabetes', *The Journal of Clinical Endocrinology & Metabolism*, XX: 1-19.

Singh, R., A. Barden, T. Mori, and L. Beilin. 2001. 'Advanced glycation end-products: A review', *Diabetologia*, 44: 129-46.

Strotmeyer, Elsa S., Jane A. Cauley, Ann V. Schwartz, Michael C. Nevitt, Helaine E. Resnick, Joseph M. Zmuda, Douglas C. Bauer, Frances A. Tylavsky, Nathalie De Rekeneire, Tamara B. Harris, and Anne B. Newman. 2004. 'Diabetes is associated independently of body composition with BMD and bone volume in older white and black men and women: The health, aging, and body composition study', *JOURNAL OF BONE AND MINERAL RESEARCH*, 19: 1084-91.

Tang, S. Y. Y., U. Zeenath, and D. Vashishth. 2007. 'Effects of non-enzymatic glycation on cancellous bone fragility', *Bone*, 40: 1144-51.

Thomas, T., B. Burguera, L. J. Melton, E. J. Atkinson, W. M. O'Fallon, B. L. Riggs, and S. Khosla. 2001. 'Role of serum leptin, insulin, and estrogen levels as potential mediators of the relationship between fat mass and bone mineral density in men versus women', *Bone*, 29: 114-20.

Tsuda, T. 2017. 'Epidemiology of fragility fractures and fall prevention in the elderly: a systematic review of the literature', *Curr Orthop Pract*, 28: 580-85.

Vashishth, D., G. J. Gibson, J. I. Khoury, M. B. Schaffler, J. Kimura, and D. P. Fyhrie. 2001. 'Influence of nonenzymatic glycation on biomechanical properties of cortical bone', *Bone*, 28: 195-201.

Vashishth, Deepak. 2007. 'The role of the collagen matrix in skeletal fragility', *Current Osteoporosis Reports*, 5: 62-66.

Vestergaard, P. 2007. 'Discrepancies in bone mineral density and fracture risk in patients with type 1 and type 2 diabetes—a meta-analysis', *Osteoporosis International*, 18: 427-44.

Viguet-Carrin, S., D. Farlay, Y. Bala, F. Munoz, M. L. Bouxsein, and P. D. Delmas. 2008. 'An in vitro model to test the contribution of advanced glycation end products to bone biomechanical properties', *Bone*, 42: 139-49.

Wang, X., X. Shen, X. Li, and C. Mauli Agrawal. 2002. 'Age-related changes in the collagen network and toughness of bone', *Bone*, 31: 1-7.

Willett, Thomas L., Sibi Sutty, Anne Gaspar, Nick Avery, and Marc Grynpas. 2013. 'In vitro non-enzymatic ribation reduces post-yield strain accommodation in cortical bone', *Bone*, 52: 611-22.

World Health Organization. 1994. *Assessment of fracture risk and its application to screening for postmenopausal osteoporosis: report of a WHO study group [meeting held in Rome from 22 to 25 June 1992]* (World Health Organization).

Yadav, Ram Naresh, Praveer Sihota, Deepak Neradi, Jagadeesh Chandra Bose, Vandana Dhiman, Shailesh Karn, Sidhartha Sharma, Sameer Aggarwal, Vijay G. Goni, Sanjay Kumar Bhadada, and Navin Kumar. 2022. 'Effects of type 2 diabetes on the viscoelastic behavior of human trabecular bone', *Medical Engineering & Physics*, 104: 103810.

Yu, E. W., M. S. Putman, N. Derrico, G. Abrishamanian-Garcia, J. S. Finkelstein, and M. L. Bouxsein. 2014. 'Defects in cortical microarchitecture among African-American women with type 2 diabetes', *Osteoporosis International*, 26: 673-79.

Zimmermann, Elizabeth A., Eric Schaible, Hrishikesh Bale, Holly D. Barth, Simon Y. Tang, Peter Reichert, Bjoern Busse, Tamara Alliston, Joel W. Ager, and Robert O. Ritchie. 2011. 'Age-related changes in the plasticity and toughness of human cortical bone at multiple length scales', *Proceedings of the National Academy of Sciences of the United States of America*, 108: 14416-21.

CHAPTER 2

Literature Review

This chapter provides an overview of the literature relevant to the subject areas of this thesis. In Section 2.1, a background to bone function and structure is provided, while details of the biomechanical properties of cortical and trabecular are presented in Section 2.2. An overview of bone diseases is presented in Section 2.3, while Section 2.4 reviews type 2 diabetes and its relationship to fragility fractures in bone.

2.2 Bone Structure and Function

2.2.1 Background

The adult human skeleton is composed of 206 bones and provides the framework to support the body, protect internal organs and enable movement and locomotion through contraction of the attached muscles. Bone tissue can be described as a naturally occurring composite material whose constituent phases (organic and inorganic) are hierarchically organised to provide exceptional mechanical properties with high stiffness and excellent resistance to fracture. In addition, bone is a mechanosensitive tissue that constantly adapts to accommodate the demands of the loading environment. This mechanical loading encountered due to daily activities regulates tissue homeostasis, which optimises tissue composition and structure and the associated load-bearing capacity (Cowin, 2001; Currey, 2006). For example, even before birth,

the mechanical forces generated by foetal kicks and movements are thought to contribute to regulating the shape of bones (Verbruggen et al. 2018). The morphology of the different bones of the skeleton are "built" to resist the specific local deformations and loads that they are subjected to. Long bones are comprised of an outer shell, or cortex, of compact bone tissue, while the medullary cavity contains the bone marrow and resident hematopoietic and mesenchymal stem cells as shown in Figure 2.1. This structure is sufficiently stiff to accommodate loading due to body weight, while also being lightweight to allow the body movement (Currey 2012; Seeman and Delmas 2006).

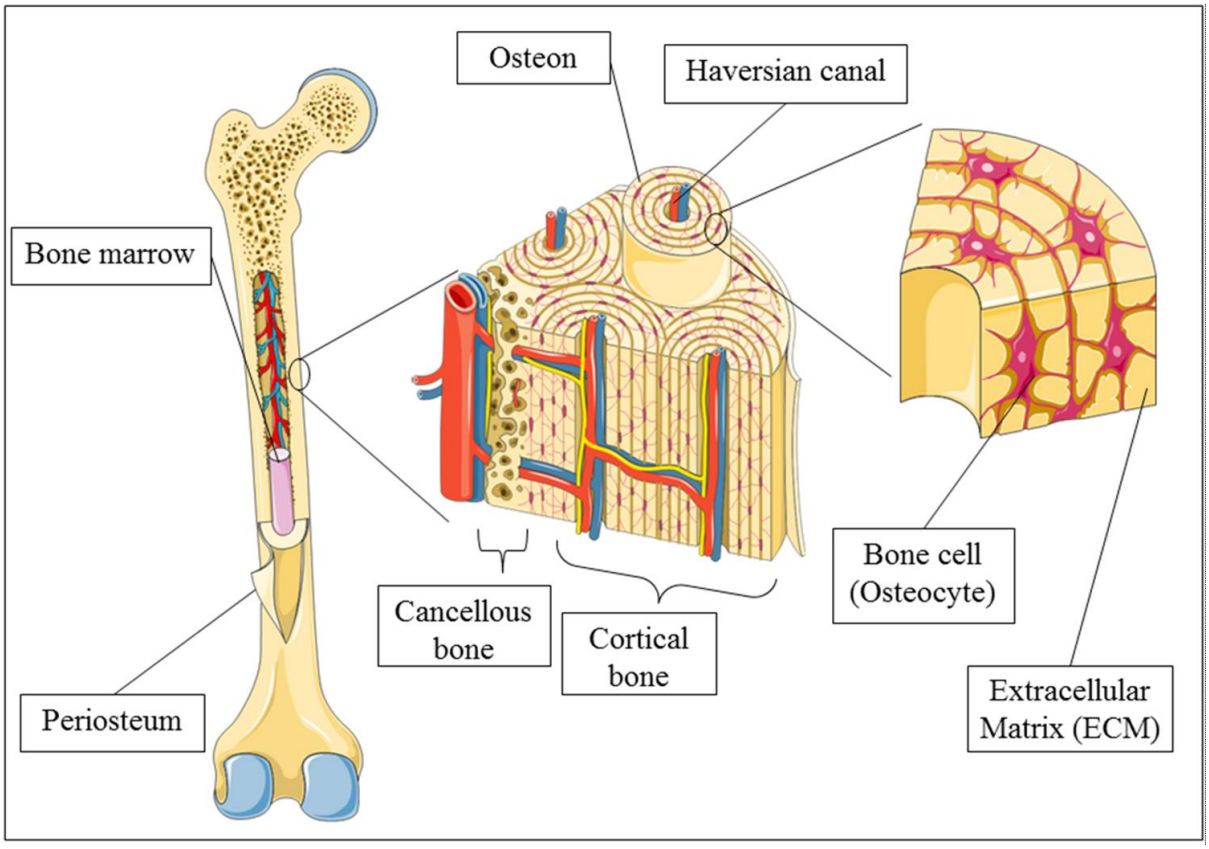

Figure 2.1 Schematic overview of bone, depicting gross overview, and cellular distribution. In particular, osteoprogenitors may be found abundantly in the periosteum and bone marrow, where they perform critical roles in bone repair. Additionally, bone is observed to be highly vascularized, in both the intramedullary canal and periosteal region (Chao Le Meng et al. 2013).

2.2.2 Bone Structure

Bone has a hierarchical structure that has an intricate organisation of material constituents over many length scales (Rho et al. 1998), as shown schematically in Figure 2.2. At the sub-nanostructural level, the tissue is comprised of collagen molecules, minerals, water and non-collagenous proteins that dictate the overall performance of the bone. These components are organised into arrays that form mineralised collagen fibrils at the nanoscale, which may be considered universal building blocks of the tissue., Mineralised collagen fibril arrays are assembled together to form the fibres at the nano-structural level and are embedded in the extrafibrillar matrix, which is composed of extrafibrillar minerals and non-collagenous proteins (NCPs) (McNally et al. 2012; Sroga and Vashishth 2012). The mineralised collagen fibrils are then organised by layering to form lamellae at the sub-microstructural level. At the microstructural-level, layers of lamellar bone form concentric cylinders in the form of osteons, which have central channels to accommodate the bone vasculature (Weiner and Wagner, 1998). Another type of bone tissue present in both cortical and trabecular bone is woven bone. Woven bone, unlike lamellar bone, can be formed de novo and typically functions as a provisional structure that precedes the development of lamellar bone during bone formation and growth (Martin and Burr 1989). Woven bone is a less organized structure in comparison to lamellar bone and it can be identified by its unorganised arrangement of collagen fibres (Turner 1992). At the macro-structural level, bone may be categorised as cortical bone or trabecular bone. While cortical and trabecular bone differ in their development, architecture and function, they are fundamentally comprised of similar sub-microstructural constituents and together form the whole bone (Cowin, 2001).

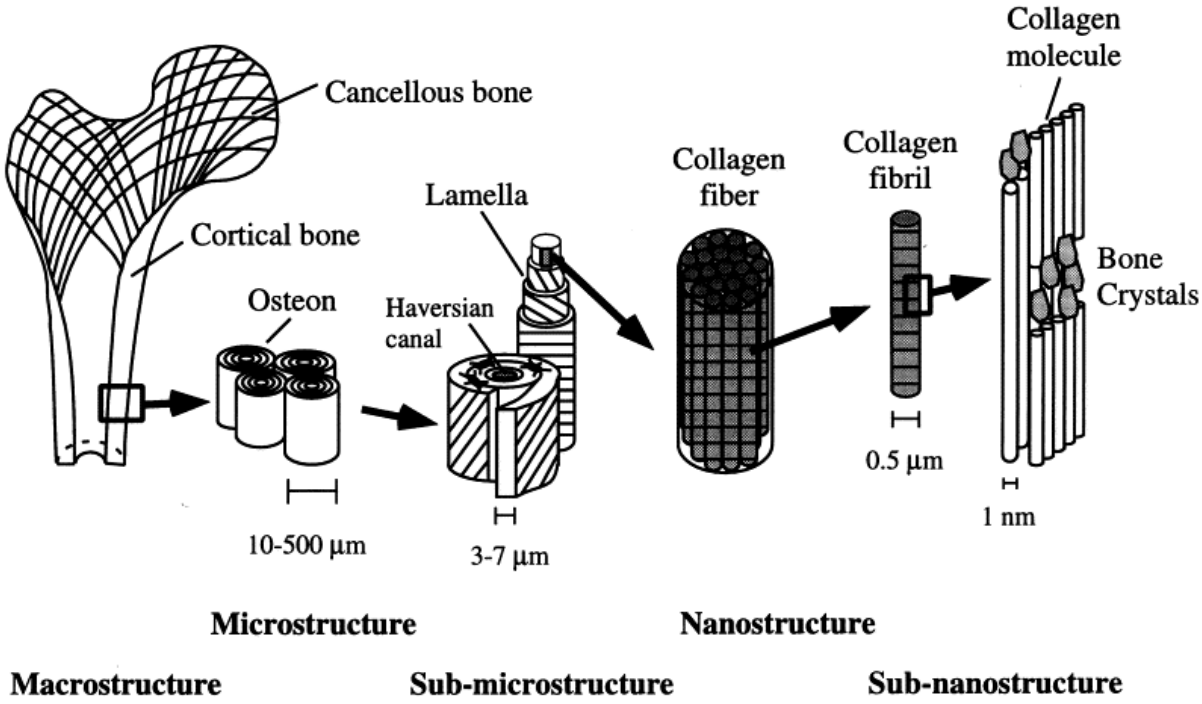

Figure 2.2 Hierarchical structural organization of bone. Macrostructure with cortical and cancellous bone; microstructure with osteons with Haversian systems, sub-microstructure with lamellae; nanostructure with collagen fibre assemblies of collagen fibrils; and sub-nanostructure with bone mineral crystals and collagen molecules (Rho et al. 1998).

2.2.2.1 Cortical Bone

Cortical bone, also known as compact bone, is a dense, solid material with microscopic channels and low porosity of ~2% (Patsch et al. 2013; Wölfel et al. 2022). It is mainly found in the shaft of long bones and forms the outer surface of all bones. Cortical bone is primarily responsible for the protective and supportive function of the skeleton. At the microstructural level, the cortical bone is composed of primarily lamellae (Figure 2.3) and woven bone can also be present. The lamellae exist in three main configurations in function of the location and/or the size of the animal:

1) concentric lamellar surfaces surround the Harversian channel that contain blood vessels and nerves, that form the osteon;

2) circumferential lamellae that are composed of layers of lamellae that extend around part or all the circumference of the shaft; and

3) interstitial lamellae fill the gaps between the haversian system, they are composed angular fragments of old concentric or circumferential lamellae (Cowin, 2001).

Additionally in the bones of animals that grow rapidly, such as ovine and bovine bone, another type of bone tissue is also present in the cortical bone, known as plexiform bone. This bone is very similar in structure to laminar bone but has a denser vascularisation system. Longitudinal, radial and circumferential primary osteons form a three-dimensional symmetrical network (Hillier and Bell 2007).

2.2.2.2 Trabecular Bone

Trabecular bone, also known as cancellous bone, is highly porous and has a spongy foam-like structure that provides space for the bone marrow. Trabecular bone is made up of interconnected microstructural components called trabeculae (Figure 2.3) that vary from rod-like to plate-like shapes. Their density, orientation and shape vary depending on the anatomical location, with their geometric features driven by the magnitude and direction of the external loading that is applied (Huiskes et al. 1987; Carter et al. 1996; Morgan and Keaveny 2001). There are several characteristics of bone microarchitecture that can be measured, which are discussed in detail in Section 2.2.3. The microstructure of trabecular bone is distinct to cortical bone as it does not have osteons but is instead comprised of lamellar bone. In addition, there is no direct vascularisation and therefore the bone cells in this part of bone depend on fluid exchange from the neighbouring marrow spaces for nutrients and oxygen. However, the metabolic activity of cells in trabecular bone is higher than in cortical bone leading to a higher bone remodelling rate. Trabecular bone has a 26% per year turnover rate compared to 3% for cortical bone (Webster and Jee 1983; Oftadeh et al. 2015)

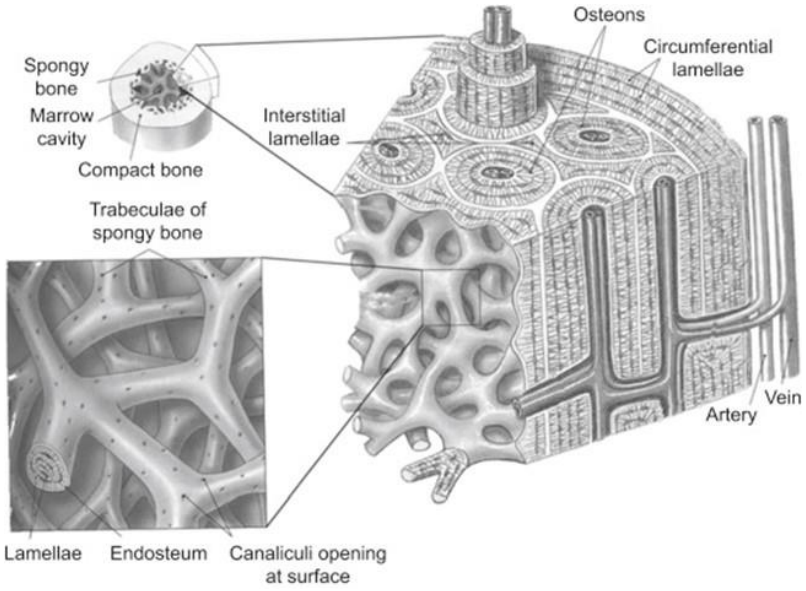

Figure 2.3 Schematic of cortical and trabecular bone in more detail (Lacroix 2019).

2.2.3 Bone Morphology

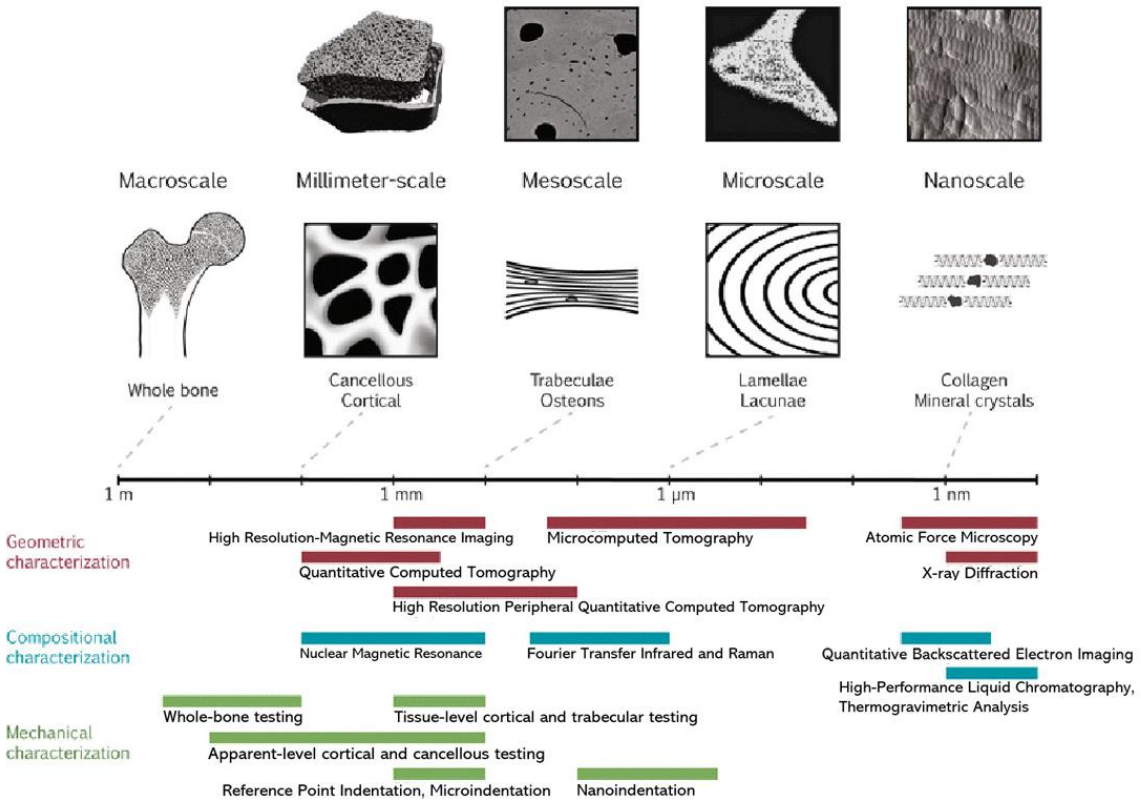

Figure 2.4 Bone quality measurement techniques depicted on a logarithmic scale of the hierarchical structure of bone. Representative images of bone using the imaging techniques of high-resolution peripheral quantitative computed tomography (HR-pQCT), quantitative backscattered electron imaging (qBEI), Fourier transform infrared (FTIR) imaging of crystallinity, and atomic force microscopy (AFM) are shown. The field of view of the representative images corresponds with the scale bar. Along the bottom, each characterization technique is categorized as geometric, compositional, or mechanical and is depicted by a bar showing the approximate range of resolutions currently achievable (Hunt and Donnelly 2016).

A range of non-invasive imaging techniques are used to assess bone morphology (Figure 2.4), with detailed quantitative assessment of the bone microarchitecture providing insight into both morphological and topographical features of the 3D porous structure. Previously, bone morphological parameters were determined using 2D sections of bone biopsies (Parfitt et al. 1983; Bouxsein et al. 2010). For in vivo assessment of 3D bone geometry at the macroscale, techniques include using quantitative computed tomography (QCT) (Hayes et al. 1991) and high resolution peripheral QCT (HR-pQCT) (Dall'Ara et al. 2012). While QCT is capable of

obtaining coarse geometric measurements of volumetric BMD (vBMD), it is incapable of measuring specific features of the trabecular architecture due a relatively low in-plane resolution of ~0.5 mm. On the other hand, HR-pQCT can be used to image trabecular morphology at peripheral sites, such as the distal radius, with an isotropic resolution of ~60-80 µm (Klose-Jensen et al. 2020). At this resolution, features of microarchitecture and morphology of trabecular bone, such as bone volume fraction (BV/TV), trabecular thickness (Tb.Th), trabecular separation (Tb.Sp) and trabecular number (Tb.N) can be determined.

For more detailed evaluation on ex vivo samples, micro-computed tomography (micro-CT) based techniques enable detailed evaluation of bone structure at the sub-millimetre resolution, with recent advancements even allowing a sub-micrometre level of resolution (Donnelly 2011; Bouxsein et al. 2010). The general set-up of a micro-CT is shown in Figure 2.5, whereby X-ray radiation is used to capture 2D cross sectional images of samples, which are then reconstructed into a 3D visualisation, enabling the analysis of the structure and density. Radiographic principles form the foundation of CT, in which electrons are guided from a cathode to strike a heavy metal anode. This releases X-ray radiation that is directed through the sample to a scintillator, which transforms it into visible light and detected by a photodetector (Landis and Keane 2010). By comparing the x-ray attenuation in the bone with that of the hydroxyapatite (HA) standard, micro-CT scans can be used to estimate the regional density of bone tissue.

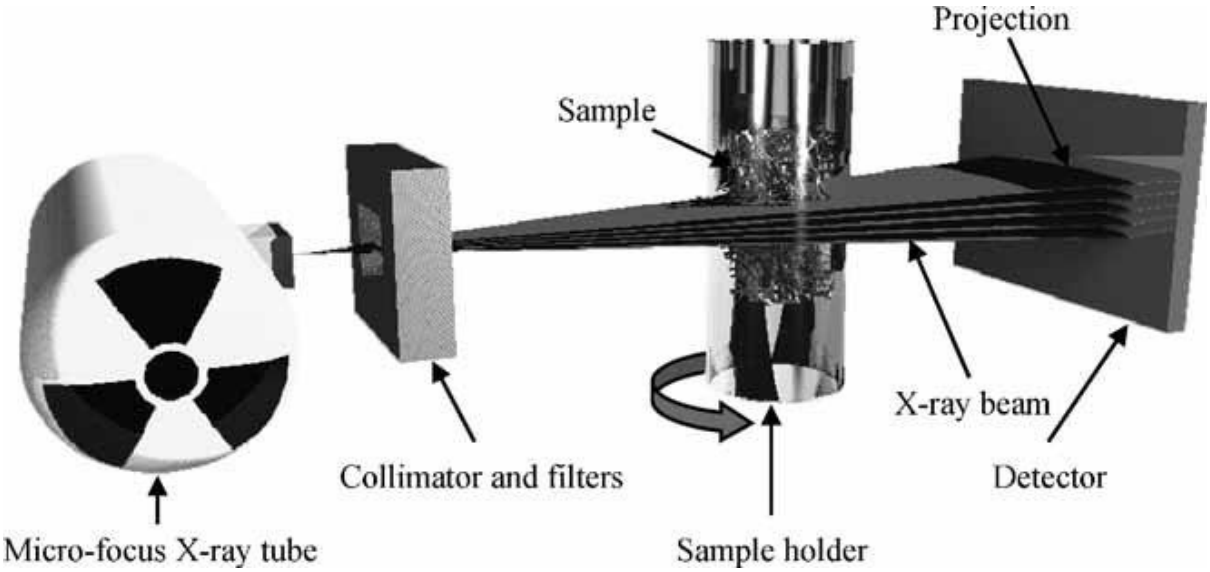

Figure 2.5 Schematic of Micro-CT (Bouxsein et al. 2010)

To gain a complete description of trabecular morphology using micro-CT analysis, 3D algorithms were developed due to the mixture of rod-like and plate-like trabeculae inside the underlying trabecular structure (Hildebrand et al. 1999; Laib et al. 1997). Table 2.1 provides a summary of the morphological features of bone that can be quantified with high-resolution micro-CT scans, with several of these parameters closely correlated to the mechanical function of the tissue (Zysset 2003; Maquer et al. 2015; Musy et al. 2017), meaning that they have gained widespread use in understanding bone biomechanics. The measurement of bone volume (BV) and the total volume of interest (TV) are determined by assigning a threshold that allows the separation of the bone from the background medium or surrounding tissue based on density. Bone volume fraction (BV/TV) can then be determined from the ratio of these two indices. The area of bone surface (BS) can be measured using a marching-cubes algorithm (Lorensen and Cline 1987) to triangulate the object surface. Sphere-fitting method 3D calculations (Hildebrand and Rüegsegger 1997a) are used to measure mean trabecular thickness (Tb.Th), mean trabecular separation (Tb.Sp), and mean trabecular number (Tb.N). This sphere-fitting method is calculated from the average diameter of the largest sphere that can be fitted in an entirely enclosed within the object for Tb.Th or background for Tb.Sp, as shown in Figure 2.6.

The mean trabecular number is calculated using the distance-transformation method as the inverse of the mean distance between the structure's mid-axes (Danielsson 1980; Bouxsein et al. 2010).

Table 2.1 Definition and description of 3D morphological features for trabecular and cortical bone microarchitecture adapted from Bouxsein et al. *2010.*

Abbreviation	Variable	Description	Standard unit
TV	Total volume	Volume of the entire region of interest	mm^3
BV	Bone volume	Volume of the region segmented as bone	mm^3
BS	Bone surface	Surface of the region segmented as bone	mm^2
BV/TV	Bone volume fraction	Ratio of the segmented bone volume to the total volume of the region of interest	%
BS/TV	Bone surface density	Ratio of the segmented bone surface to the total volume of the region of interest	mm^2/mm^3
BS/BV	Specific bone surface	Ratio of the segmented bone surface to the segmented bone volume	mm^2/mm^3
Conn.D	Connectivity density	A measure of the degree of connectivity of trabeculae normalized by TV	$1/mm^3$
SMI	Structure model index	An indicator of the structure of trabeculae; SMI will be 0 for parallel plates and 3 for cylindrical rods (Hildebrand 1997).	Dimensionless
Tb.N	Trabecular number	Measure of the average number of trabeculae per unit length	1/mm
Tb.Th	Trabecular thickness	Mean thickness of trabeculae, assessed using direct 3D methods	Mm
Tb.Sp	Trabecular separation	Mean distance between trabeculae, assessed using direct 3D methods	Mm
DA	Degree of anisotropy	1 = isotropic, >1 = anisotropic by definition; DA = length of longest divided by shortest mean intercept length vector	Dimensionless
MIL	Mean intercept length	Measurements of structural anisotropy	Dimensionless
Tt.Ar	Total cross-sectional area	Total cross-sectional area inside the periosteal envelope	mm^2
Ct.Ar	Cortical area	Cortical bone area = cortical volume (Ct.V) ÷ (number of slices × slice thickness)	mm^2
Ct.Th	Cortical thickness	Average cortical thickness	mm
Ct.Ar/Tt.Ar	Cortical bone fraction	Cortical area fraction	%
Ct.Po	Cortical porosity	In a given cortical region, the volume of pores (Po.V, mm3) ÷ total volume of cortical bone compartment (Ct.V, mm3)	%

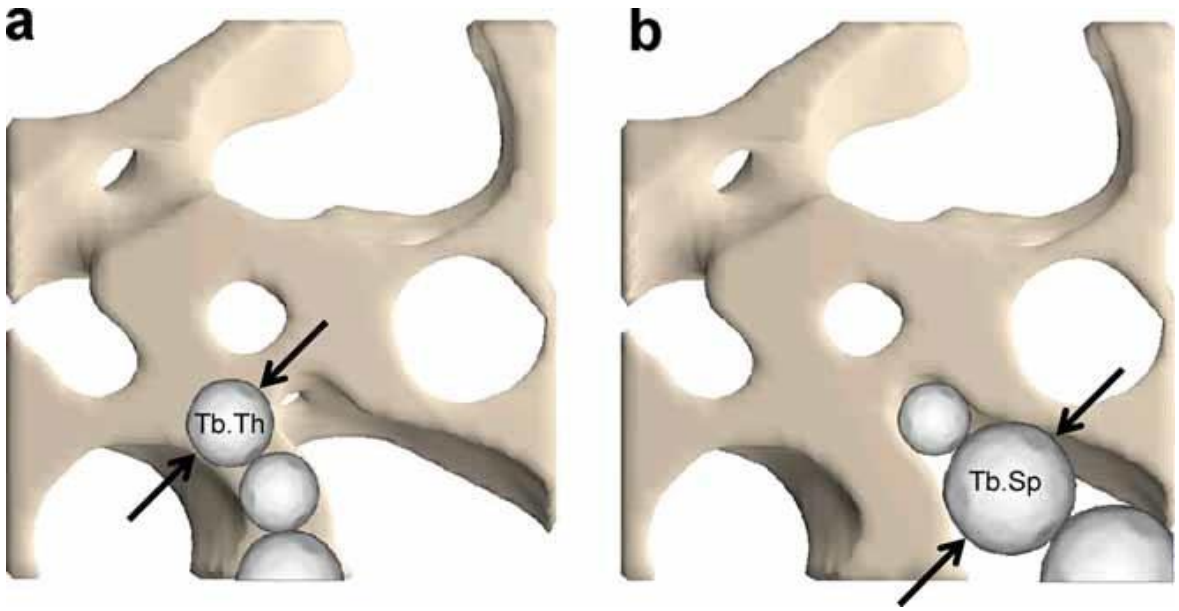

Figure 2.6 Schematic representation of trabecular thickness and trabecular separation 3D sphere fitting method calculation (Bouxsein et al.*2010).*

The mean intercept length (MIL) method (Whitehouse 1974) provides a measure of the degree of anisotropy (DA) of the trabecular structure. Connectivity density (Conn.D) is a measure of the degree of connectivity of trabeculae normalized by TV. The Euler number is used to derive the quantity of connections that must be severed in order to divide an object into two parts, with this number divided by the total volume to get the Conn.D (Odgaard and Gundersen 1993). The structural model index (SMI), is a measure of how plate like or rod like characteristic of the trabecular structure, with 0 being plate like and 4 being a sphere (Hildebrand and Rüegsegger 1997b). The SMI calculation involves first fitting a mesh of triangles to the bone surface and computing its total area by summing the areas of all triangles (S). The mesh is then expanded a small distance (r) in the direction of the vertex normals of the triangles, and the surface area is measured again. The change in surface area (S') is divided by r to obtain an approximate surface area derivative, which is then multiplied by the bone volume (V) to obtain the final SMI value.

$$SMI = \frac{6 \times \frac{S'}{r} \times V}{S^2} \quad (1.1)$$

If the SMI values are positive the surface is convex and if the values are negative the surface is concave (Scanco). Cortical bone may also be defined by several characteristic parameters that can be determined by micro-CT. These include total cross-sectional area (Tt.Ar), cortical bone area (Ct.Ar), cortical thickness (Ct.Th), cortical bone fraction (Ct.Ar/Tt.Ar), and cortical porosity (Ct.Po).

2.2.4 Bone Matrix

2.2.4.1 Bone Composition

Bone is a composite material comprising of an organic protein network of collagenous and non-collagenous proteins, combined with inorganic hydroxyapatite mineral crystals. Type I collagen, a triple helical protein, is the most abundant collagen protein in the body and represents 90% of the organic phase of the bone tissue (Cowin, 2001). It is composed of tropocollagen fibrils that consist of two identical amino-acid α_1 chains and one α_2 chain, which coil around each other to form a three-strand alpha-helix rope-like structure (Miller, 1984). These fibrils assemble to form fibres that are primarily responsible for providing strength and flexibility to the tissue structure, while also supplying bone cells with a scaffold for attachment (Saito and Marumo 2015).

About 10% of the organic phase consists of non-collagenous proteins, which include osteocalcin, osteonectin, osteopontin, bone sialoprotein and many other proteins (Cowin, 2001). Non-collagenous proteins play important roles in the formation, maintenance, and repair of bone tissue. They have a variety of functions including regulation of bone mineral deposition and binding collagen fibres together. The most abundant non-collagenous protein found in bone is osteocalcin (OC), which possesses a high affinity for binding to hydroxyapatite (HA) (Ritter et al. 1992). OC, along with osteopontin (OPN), plays a crucial role in facilitating the bonding

process at the interfaces between HA minerals in the extrafibrillar space (Hauschka and Carr 1982). While their contribution towards tissue stiffness is minor (Morgan et al. 2015), it has become apparent that their role in intrinsic toughening, one of the primary contributors towards healthy tissue's excellent fracture resistance, is considerable (Fantner et al. 2005; Tavakol and Vaughan 2020, 2022).

The inorganic phase of the bone matrix contributes to 65% of the overall weight composition of bone tissue and is composed of mineral including an analogue of impure hydroxyapatite, $Ca_{10}(PO_4)_6(OH)_2$, containing other elements such as carbonate, citrate, magnesium, fluoride, and strontium (Cowin, 2001). The mineral phase tends to reside within the overlap and gap regions of collagen fibrils, and can take the form of needle-like, plate-like or rod-like crystals. The mineral crystals are first deposited in discrete sites in the collagenous matrix. As the bone matures, the impurities in the mineral crystals reduce and they grow in size due to the addition of ions and the aggregation of other crystals at the mineralisation sites.

2.2.4.2 Bone cells, modelling and remodelling

Bone cells are responsible for bone formation and the long-term maintenance of the tissue. Bone modelling consists of the formation of the bone during embryogenesis, growth during childhood and deposition of new bone during adaptation, while bone remodelling is the process by which the matrix is renewed continually. There are four main cell types that are found in bone: osteoblasts, osteocytes, osteoclasts and bone lining cells.

Osteoblasts are the bone forming cells that originate from mesenchymal stem cells (MSC) and are responsible for the production of the bone matrix, which initially is an unmineralised tissue (the osteoid). Once the matrix has been synthesised there are three possible pathways for osteoblasts. In the first instance some osteoblasts flatten and become quiescent bone lining cells. Another possible outcome is death by apoptosis. However, most osteoblasts become encased in the bone matrix leading them to further differentiate into osteocytes (Ottewell 2016). Once the organic matrix is formed, osteoblasts and osteocytes produce enzymes, matrix proteins and cytokines that will organise the maturation of the tissue with the calcification and reorganisation of the matrix (Wang et al. 2013; Weiner and Wagner 1998). Osteocytes are encased in a lacunae and their star-like shape (see Figure 2.7) leads to the formation a network of thin canaliculi permeating the entire bone matrix, known as the osteocyte lacuna-canalicular system (Hadjidakis and Androulakis 2006). This canalicular system allows for cell-cell communication. Osteocytes are mechanosensitive cells that are capable of detecting mechanical strain, hydrostatic pressures and fluid flow through the presence of a range of mechanosensors on the cell surface (Reitsma et al. 2007). In response to these mechanical forces, osteocytes release a range of signalling molecules that initiate the remodelling process (see Figure 2.8). An increase in mechanical stimulation leads to an increase in bone formation, while a decrease in mechanical stimulation leads to an increase in bone resorption and decrease in bone formation this is known as the mechanostat hypothesis (Frost 1987; Frost 2003). Daily

loading of bone induces the formation of microcracks within the matrix. Kennedy et al. (2014) found that in the areas around microcracks the expression of osteoclastogenic proteins RANKL and VEGF were increased. The microcracks are repaired, during the remodelling process, and the structure is modified in response to stress and other biomechanical forces (Hadjidakis and Androulakis, 2006).

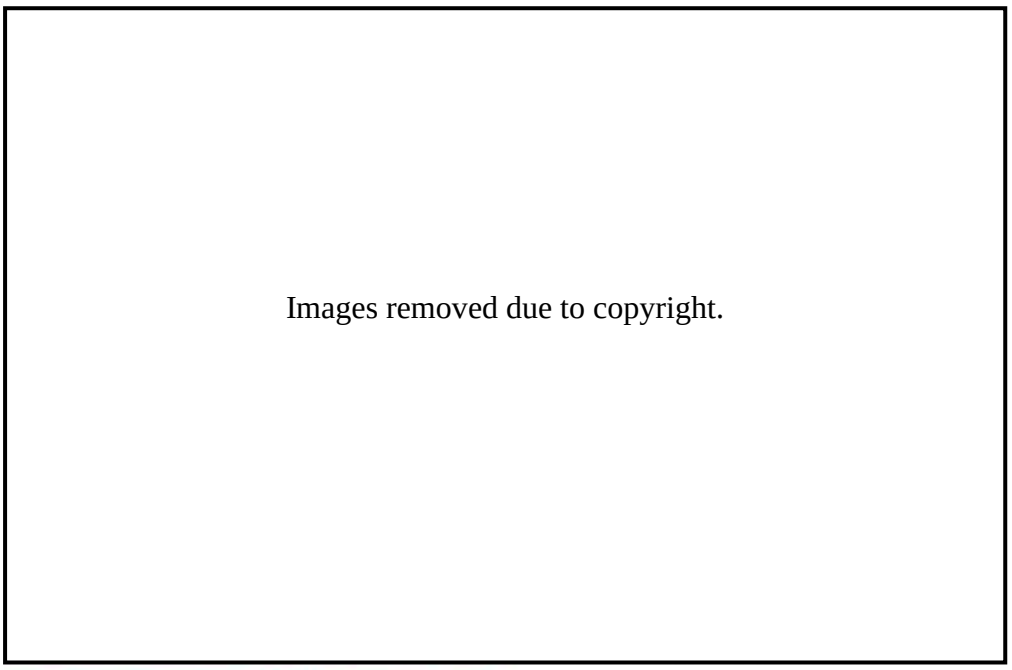

Figure 2.7 Images of osteocytes
(a) Three-dimensional reconstruction image of the avian osteocyte network by IMARIS software. Note the ordered array of the osteocytes in chick bone. (b) Field emission scanning electron microscope images of chick osteocyte. (Robling and Bonewald 2020) Previously adapted from (Tanaka-Kamioka et al. 1998).

Osteoclasts are giant multinucleated cells derived from hematopoietic stem cells that are stimulated by RANKL (Rucci 2008) and are responsible for resorption of the bone at the beginning of the remodelling process. When the osteoclasts become activated, they secrete enzymes, digest the organic collagen and proteins, and an acidic solution, that dissolves the inorganic mineral phase (Brandi, 2009). This results in a concave surface that has been eaten away by the osteoclasts and starts the progenitor cells recruitment of the osteoblasts to lay down new bone until the resorbed bone is replaced (Hadjidakis and Androulakis, 2006). Osteoblasts

and osteoclasts form the bone multicellular unit that reconstructs bone in distinct locations on the cortical and trabecular bone. The external size and contours of bone and its internal architecture are modified by deposition or removal of bone from the surface of the bone, causing cortical and trabecular thickening during growth and thinning during ageing (Seeman and Delmas, 2006).

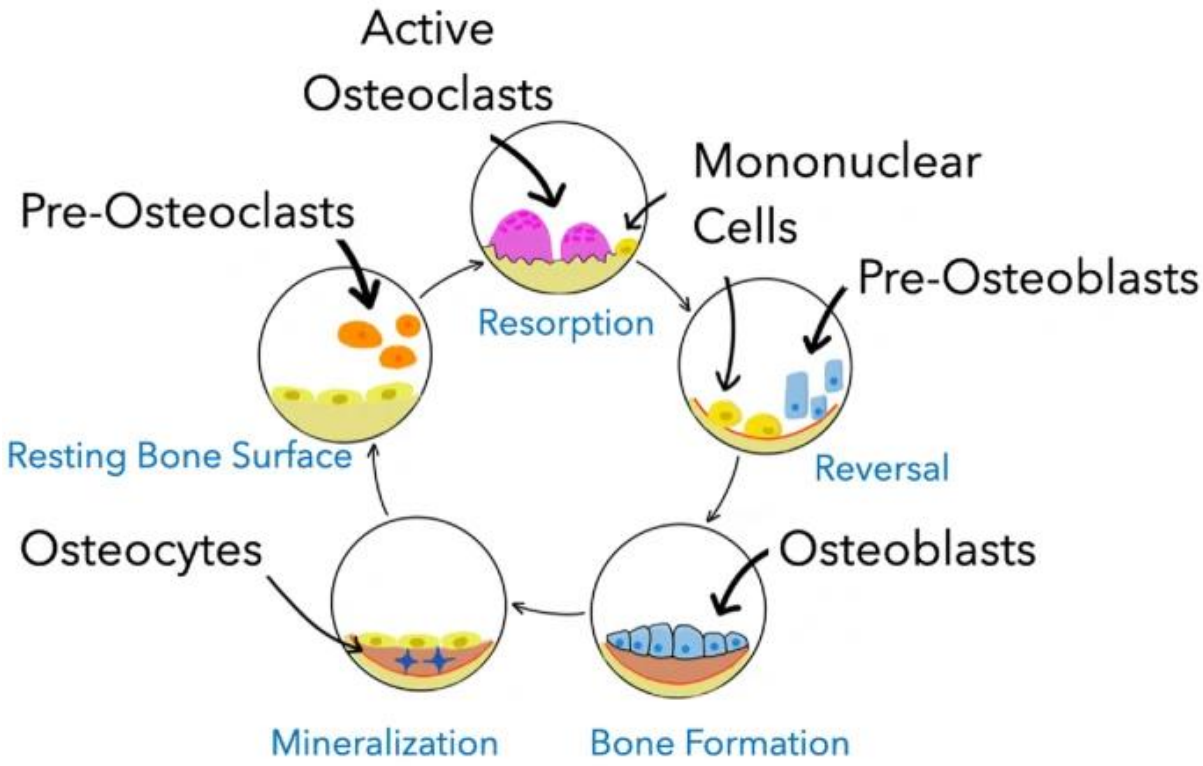

Figure 2.8 Schematic of bone remodelling process (Liang et al. 2021).

2.2.4.3 Enzymatic Crosslinks

The organic bone matrix is a network of proteins that is primarily bound through the formation of enzymatic crosslinks between neighbouring proteins. Enzymatic crosslinks form in bone through a process involving the activation of the enzyme lysil oxidase (LOX) that binds collagen fibrils through the formation of lysine-lysine covalent bond between telopeptide (terminus) ends. These crosslinks results in a staggered arrangement of fibrils that stabilise the collagen molecules and prevents the sliding of micro-fibrils past-one another (Tabacco and

Rubin, 2020), which provides a critical contribution to the overall strength of bone tissue (Saito and Marumo 2015). Five different types of enzymatic crosslinks have been reported in bone collagen. Immature divalent crosslinks of dihydroxylysinonorleucine (DHLNL), hydroxylysinonorleucine (HLNL), and lysinonorleucine (LNL) are found between collagen fibrils, which over time develop into mature trivalent crosslinks of pyridinoline (PYD) and deoxypyridinoline (DPD) (Arakawa et al. 2020).

2.2.4.4 Non-Enzymatic Crosslinks

Non-enzymatic glycation (NEG) mediated crosslinks and products form from the existence of reducing sugars in the extracellular space that react non-enzymatically with amino groups in proteins, lipids and nucleic acids. The molecules go through a series of chemical reactions forming Schiff bases and Amadori products and produce Advanced Glycation End-products (AGEs) (Suzuki et al. 2022; Willett et al. 2022; Gautieri et al. 2017; Grandhee and Monnier 1991). This process is known as the Maillard reaction, which is made up of three distinct phases (Figure 2.9). The early stage involves a reducing sugar (i.e. such as glucose, ribose, fructose) reacting with a free amino group, which results in the formation of an unstable compound, known as the Schiff base. Thereafter, it undergoes rearrangement to a more stable form, known as the Amadori product. During the intermediate stage, the Amadori product degrades to form a variety of reactive dicarbonyl compounds such as glyocal, methylglyoxal, deoxyglucosones through chemical reactions such as dehydration and oxidation. Finally, irreversible molecules, known as AGEs, are created during the later stages of glycation, leading to their accumulation within the matrix (Singh et al. 2014). Primarily, proteins with long half-lives that contain exposed lysine residues are affected by the accumulation of AGEs as their formation is endogenous and relatively slow (Sensi et al. 1995; Yamagishi 2011; Dyer et al. 1993; Ansari and Dash 2013). Collagen generally has a long half-live, with type I collagen in bone having a half-life of 1-2 years (Snedeker and Gautieri 2014). Proteins with AGE accumulation undergo

considerable alterations brought on by cross-linkage formation and changes in local ionic charge. Enzymatic functions are modified due to the altered microenvironment caused by AGE accumulation, leading to changes in enzyme activity. Additionally, AGEs bind to receptors, such as the receptor for AGEs (RAGE) and, through intracellular signal transduction, cause inflammation (Suzuki et al. 2022). Increased accumulation of AGEs in bone are known to occur in aging (Zimmermann et al. 2011), chronic kidney disease (Damrath et al. 2021) and type 2 diabetes (Karim and Bouxsein 2016).

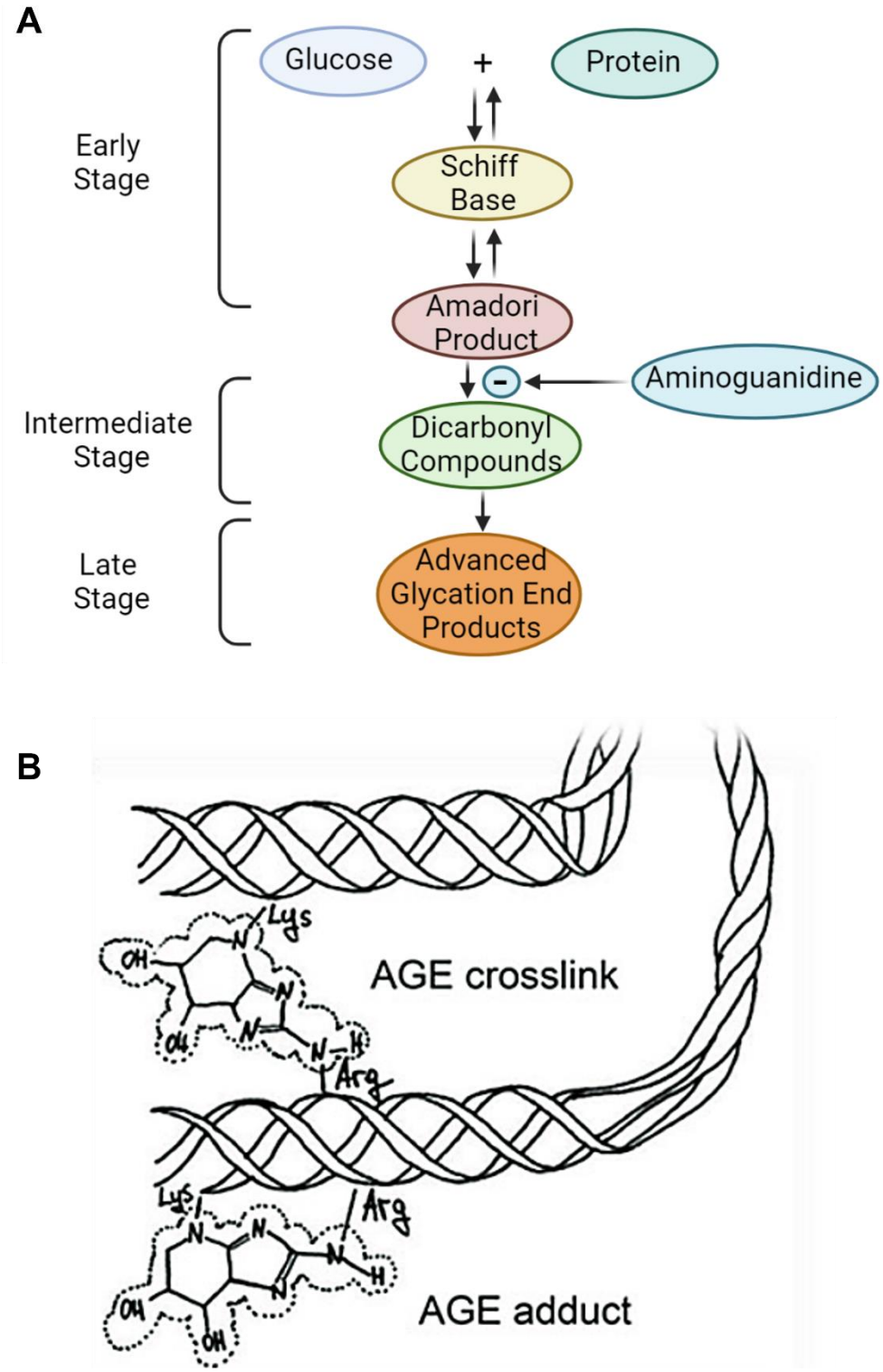

Figure 2.9 (A) Formation of advanced glycation end products (AGEs) AGEs are formed in three stages: early, intermediate, and late stage. In an early stage, sugars react with a free amino group to form Schiff base which undergoes a rearrangement to a more stable product known as Amadori product. In an intermediate stage, Amadori product degrades to a variety of reactive dicarbonyl compounds. In the late stage of the glycation process AGEs (irreversible compounds) are formed. Image adapted (Singh, Bali et al. *2014). (B) Adducts and crosslinking AGEs on collagen molecule. (Gautieri* et al.*2017)*

To date, as many as 40 different AGEs have been identified in vivo (Arakawa et al. 2020). AGEs are classified into groups based on their ability to fluoresce and whether they are crosslinks or adducts (Suzuki et al. 2022). Crosslinked AGEs form covalent bonds between neighbouring proteins or lipids, while adducting AGEs modify the sidechain of a protein or a lipid (Figure 2.9). Adducts affect the structure of the amino acid itself, which can change the microenvironment of the modified protein sites and therefore influence how the protein functions. This is in contrast to crosslink-based AGEs that simply bind or connect proteins and lipids together (Nagai et al. 2014). Pyrraline, Imidazolones, Carboxyethyl-lysine (CEL) and Carboymethyl-lysine (CML) are non-fluorescent and non-crosslinked AGEs. In particular, CML is an AGE that has been identified in bone tissue that changes the ionic charge of the collagen molecule from positive to negative through the addition of a carboxyl group to the latent amine of a lysine (Willett et al. 2022). Glyoxal lysine dimer (GOLD), methylglyoxal lysine dimer (MOLD), and Glucosepane are non-fluorescent and crosslinked AGEs. Argpyrimidine is a fluorescent and non-crosslinked AGE. The chemical structures of these AGEs are shown schematically in Figure 2.10. Pentosidine is a fluorescent, crosslinked AGE and is one of the only fluorescent AGEs that can be precisely quantified in bone as it fluoresces naturally and has the ability to endure hydrolysis (Burr and Allen 2019; Willett et al. 2022). However, despite being relatively easy to measure, it has been noted recently that pentosidine is much less abundant in bone than other AGEs (Arakawa et al. 2020).

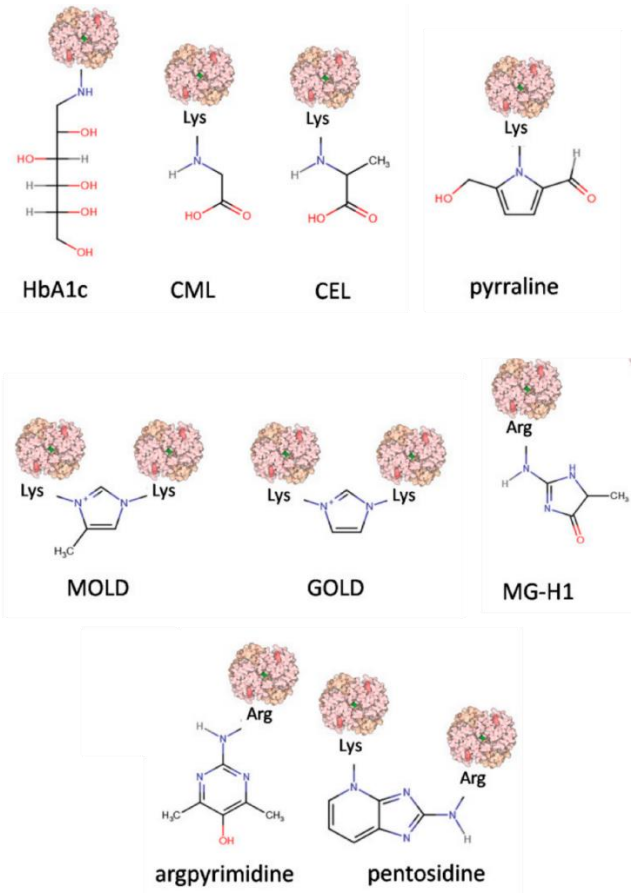

Figure 2.10 Chemical structure representations of AGEs.

Modified protein surface models (light pink) are based on the structure of human haemoglobin adapted from (Twarda-Clapa et al. 2022).

2.2.4.5 Characterisation of the Bone Matrix

Raman Spectroscopy

Raman spectroscopy is a non-destructive technique that provides detailed information about chemical structure and composition of materials by analysing the vibrational modes of molecules. The tissue quality of bone can be assessed using this technique. It is based on the Raman effect, which occurs when light interacts with matter and some of the photons in the light are scattered in a way that results in a shift in their energy. This shift is related to the vibrational energy of the molecule. In Raman spectroscopy, a laser beam is focused on a sample, and the scattered light is collected and analysed. The resulting spectrum (Figure 2.11) can provide information about the chemical composition and molecular structure of the sample. Raman spectroscopy has become a valuable technique in the evaluation of bone quality and composition. This is because the method can be used to analyse fresh, fixed and embedded bone specimens. It can also be used, with limitations, for non-invasive in vivo measurements. This technique provides details about the bone's mineral and collagen components and also sheds light on the impact of different matrix proteins on bone material characteristics. Furthermore, the Raman spectrum of bone carries information not only about the bone mineral's crystalline structure, which influences bone hardness, but also about the alignment of mineral crystals in relation to the collagen fibril axis (Mandair and Morris 2015). There are several common Raman spectroscopy parameters (Table 2.2) used to quantify bone quality, such as the mineral-to-matrix ratio, carbonate-to-phosphate ratio, crystallinity, and the matrix maturity (Unal et al. 2018).

Table 2.2 Raman measurements related to bone quality assessment.

Parameter	Calculation	Description
Mineral-to-matrix ratio	Ratio of the area of the PO_4^{-3} peak to area of amide I, amide III, or CH_2.	Linked to phosphate or carbonate mineralisation of bone (Mandair and Morris 2015).
Carbonate-to-phosphate ratio	Ratio of the area of CO_3^{-2} to area of PO_4^{-3}	Level that carbonate ions substitute phosphate in the mineral phase of the bone (Morris and Mandair 2011).
Crystallinity	Inverse full width half max of PO_4^{-3} peak	Structure of mineral crystals (Morris and Mandair 2011; Mandair and Morris 2015).
Matrix maturity	Ratio of amide I peak to the right shoulder 1660/1690 cm^{-1}	Degree of maturity of collagen(Pezzotti et al. 2017) .

Image removed due to copyright.

Figure 2.11 Baselined-corrected Raman spectrum of mouse cortical bone. Major bone mineral and matrix collagen band positions and associated spectral regions are marked (Mandair and Morris 2015).

High performance Liquid Chromatography

High performance Liquid Chromatography (HPLC) is a powerful analytical technique used to separate, identify, and quantify individual components of complex mixtures based on their physical and chemical properties. In HPLC, a liquid sample is injected into a column filled with a stationary phase material, typically a solid material with a liquid or a gel. The column is connected to a pump, which pushes a solvent through the column at high pressure, carrying the sample with it. The individual components of the sample interact differently with the stationary phase and the solvent, leading to different retention times and ultimately separation of the components. HPLC can be used to measure AGEs such as pentosidine (Hunt et al. 2018), carboxy methyl lysine (CML) (Hein et al. 2003) and furosine (Sell 1997), an early glycation marker.

2.3 Bone Biomechanics

2.3.1 General Experimental Testing of Bone

The mechanical analysis of bone tested under uniaxial compression or tension involves calculating the effective stress (σ) and strain (ε). Stress is fundamentally defined as force (F) divided by the area (A) over which the force is acting.

$$\sigma = \frac{F}{A} \tag{1.2}$$

The resulting deformation that occurs when a force is applied to any material is known as strain, which may be defined as the change in length (ΔL) divided by the initial length (L_0).

$$\varepsilon = \frac{\Delta L}{L_o} \tag{1.3}$$

Another standard method of testing bone is three-point bend (3PB) tests, which requires a different calculation of stress and strain due to the test geometry and configuration, shown in Figure 2.12, whereby a point load is applied to a beam-shaped specimen that is simply

supported across a span of two supports. Under this loading regime, the flexural stress (σ_f) is calculated by:

$$\sigma_f = \frac{3FL}{2bd^2} \tag{1.4}$$

where F is the load applied, L is the support span, b is the width and d is the depth. Flexural strain (ε_f) is calculated by:

$$\varepsilon_f = \frac{6Dd}{L^2} \tag{1.5}$$

where D is the maximum deflection.

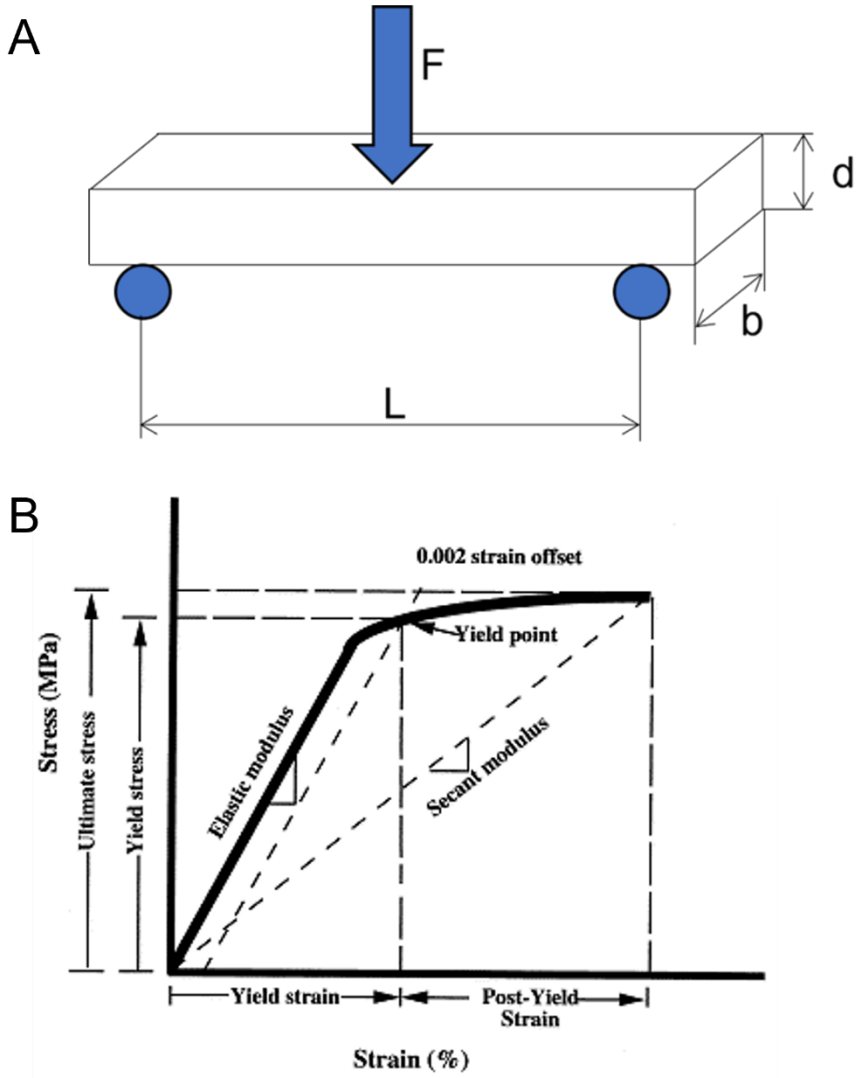

Figure 2.12 A) Schematic of 3-point bend test. B) Schematic of a typical stress-strain curve for cortical bone with the elastic and post-yield properties (Vashishth et al. 2001).

From the apparent stress-strain curve (Figure 2.12), several key quantities can be determined. The modulus of a material defined as the slope of the stress-strain curve in over strain. The apparent modulus (E) of a material is generally defined as the slope of the stress-strain curve over the initial linear region, with several different approaches used to evaluate this parameter. Different approaches to measure elastic modulus include a linear curve fit to the data from the steepest part of the stress strain curve (O'Mahony et al. 2000) and the slope of the initial 0.1% strain range of the stress-strain curve (Keaveny et al. 1999). The secant modulus (E_S) is defined as the slope between the origin and any point of interest on a stress-strain curve. The yield point denotes the point at which the behaviour of linear elasticity deviates noticeably. The yield point is defined as the point at which the stress-strain curve and a line with an elastic modulus-equivalent slope and a 0.2% strain-intercept. This point allows the determination of yield stress (σ_y) and yield strain (ε_y). Beyond this limit, the material also builds up irreversible strains called plastic strains. In many materials, the yield point is also regarded as the beginning of failure, with material properties being divided into pre-yield, or elastic properties and post-yield or plastic properties. The peak stress on the stress-strain curved is defined as the ultimate strength (σ_{ult}), which is the point at which the material has failed entirely and cannot carry any further load. After this point, the material undergoes structural collapse. The energy absorbed by the material or strain energy can be obtained by measuring the area under the stress-strain curve (also termed the toughness and work). This value is normalised to the volume of the test sample and is described in terms of Joules per cubic meter.

2.3.2 Experimental Testing of Cortical Bone

The mechanical properties of cortical bone have been characterised through a range of techniques, including uniaxial tension, uniaxial compression and three-point bend (3PB) testing, as summarised in Table 2.3. The shape of the cortical specimens can vary depending on the test, which cylindrical (Dong et al. 2012), dumbbell (Mirzaali et al. 2016), dog bone

(Katzenberger et al. 2020), beam (Cuppone et al. 2004) and pin (Stefan et al. 2010) shaped specimens. Notched specimens of cortical bone have also been used to characterise fracture toughness, which is an important characteristic of a material that describes the resistance of a material to crack propagation and the work required to fracture the material. This method will be discussed in detail in section 2.3.4.

2.3.2.1 Cortical Bone Experimentally Derived Mechanical Properties

Cortical bone is an anisotropic material that exhibits higher mechanical properties in the longitudinal direction compared to the transverse direction. Table 2.3 presents the mechanical properties of cortical bone. Cortical bone is considerably stiffer compared to trabecular bone, which is due to the densely packed arrangement of cortical bone. Cortical bone experiences a ~1.5-2% decrease in stiffness and strength per decade of life (Burstein et al. 1976), which is due to a gradual loss in mineral and increased porosity (Reilly et al. 1974; Hayes 1991). Porosity plays an important role in the mechanical integrity of cortical bone and can explain ~70% of variability in the measured modulus and ~55% of variability of the yield stress of cortical bone (Dong and Guo 2004).

Table 2.3 Mechanical properties of longitudinal cortical bone under uniaxial tensile (UT), uniaxial compression (UC) and three-point bend tests (3PB).

Anatomic Location	Modulus (GPa)	Yield Stress (MPa)	Yield Strain (%)	Test	Reference
Femur *Human*	19.9±1.8	107.9±12.3	0.73±0.05	UT	(Bayraktar et al. 2004)
Femur *Human*	18.6 ± 1.9			3PB	(Cuppone et al. 2004)
Femur *Human*	18.97 ± 1.84	147.89 ± 16.36	0.98 ± 0.09	UC	(Dong et al. 2012)
Femur *Bovine*	22.6 ± 1.2			UC	(Novitskaya et al. 2011)
Femur *Bovine*	9.9 ± 2.7	281 ± 42.4		UT	(Ferreira et al. 2006)
Tibia *Bovine*	17.85 ± 1.0			3PB	(Stefan et al. 2010)

2.3.3 Experimental Testing of Trabecular Bone

Mechanical testing of trabecular bone is generally performed on cubic or cylindrical cores under hydration. Figure 2.13 presents examples of mechanical tests for trabecular bone. Uniaxial compression tests are commonly used to determine the mechanical properties of trabecular bone. Uniaxial compression is applied by compressing a trabecular core or cube between two rigid platens. However, care must be taken to reduce end-artefacts (Linde and Hvid 1989) (Odgaard and Linde 1991). To reduce the unwanted effects of end-artefacts the extracted trabecular samples are often embedded in endcaps (Keaveny et al. 1997; Morgan and Keaveny 2001; Karim et al. 2018; Sihota et al. 2021). Other methods, to test trabecular bone include ultrasonic testing of trabecular samples and tension, compression or bending tests of single trabeculae. Nanoindentation can be used to assess tissue-level characteristics and is discussed in detail in section 2.2.4.5.

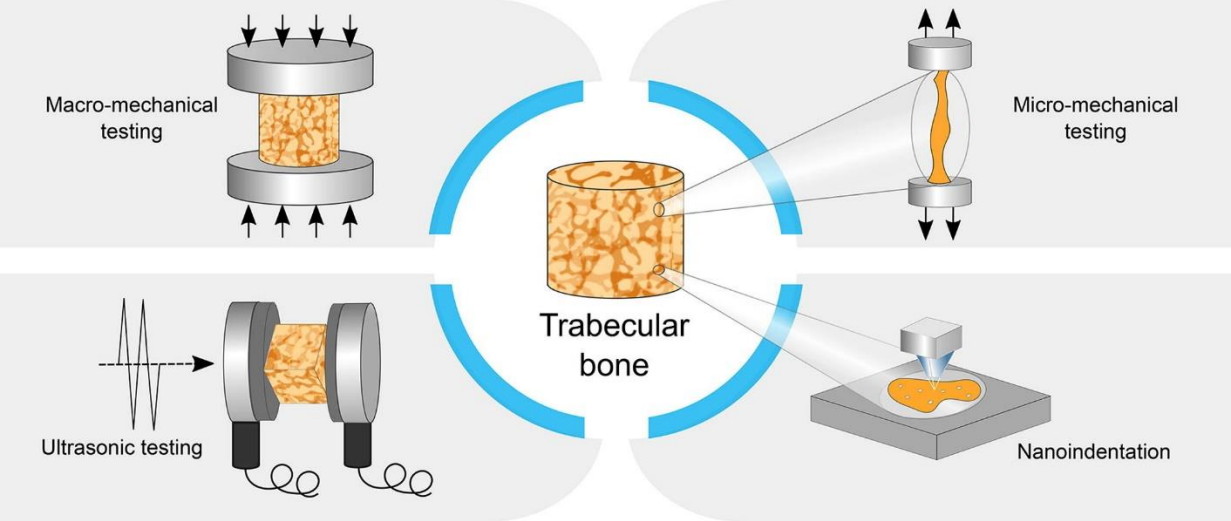

Figure 2.13 Schematic of experimental mechanical tests of trabecular bone. Including macro-mechanical testing on trabecular core, micro-mechanic testing on single trabeculae, ultrasonic testing on trabecular core and nanoindentation at the tissue level (Wu et al. 2018).

The compressive stress-strain behaviour of trabecular bone is similar to that of a cellular solid, which can be seen in Figure 2.14. There are three distinct regions in the curve: linear elastic, a plateau of stress, and finally densification. During the linear elastic phase, the trabeculae bend elastically. This is followed by a near-constant stress plateau caused by buckling of trabeculae. Finally, when the trabeculae close enough to touch, densification occurs, and the stress increases rapidly (Gibson 1985; Gibson 2005).

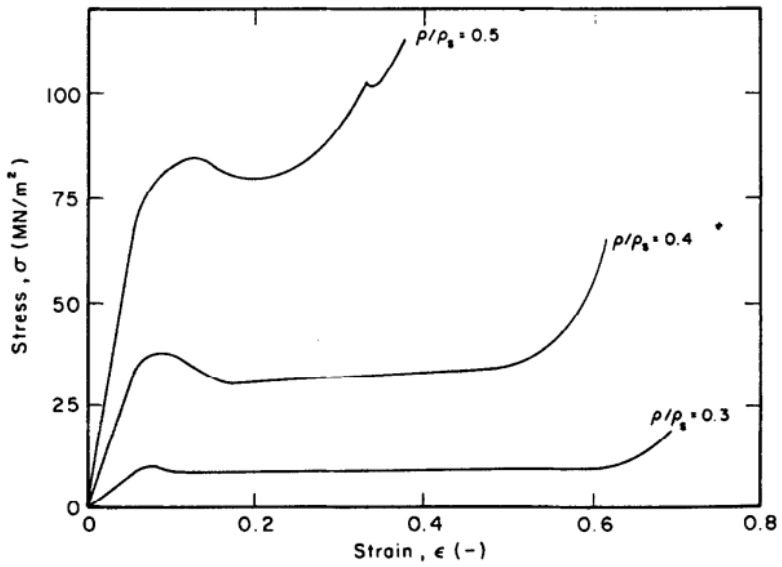

Figure 2.14 Stress-strain curves for cancellous bone. As relative density increases, Young's modulus and compressive strength increase. The strain at which the trabecular walls touch, and densification occurs decreases (Gibson 1985) previously modified from (Hayes and Carter 1976).

2.3.3.1 Trabecular Bone Experimentally Derived Mechanical properties.

The mechanical properties of the trabecular bone are influenced by many factors including the BMD (Kopperdahl and Keaveny 1998), the microarchitecture (Teo et al. 2007), the loading direction (Zysset and Curnier 1995; Öhman et al. 2007; Shi et al. 2009), and age (McCalden and McGeough 1997), and anatomical location. (Morgan and Keaveny 2001; Morgan et al. 2003; Nazarian et al. 2007). Table 2.4 summarises the mechanical properties of trabecular bone. Generally, the mechanical properties of trabecular bone are assessed in quasi-static conditions under monotonic compression loading by using cylindrical or cubic cores, despite the fact that fractures are a result of traumatic loading that take place at high strain-rates. The elastic behaviour of trabecular bone in compression and tension has been shown to be the same (Ashman et al. 1989; Røhl et al. 1991), while the yield strain of trabecular bone is approximately 1% and is higher in compression than tension (Morgan and Keaveny 2001).

Table 2.4 Mechanical properties of human trabecular bone samples tested in monotonic compression.

Anatomic Location	Apparent Modulus (MPa)	Yield Stress (MPa)	Yield Strain (%)	Density (g/cm^3)	Reference
Femoral Neck	3,230±936	17.45±6.15	0.85±0.10	0.58±0.11	(Morgan and Keaveny 2001)
Femoral Neck	3,132 ± 1466	18.72 ± 8.88			(Wang et al. 2015)
Femoral Head	635 ± 265	6.7 ± 2.7	1.11±0.21		(Homminga et al. 2002)
Femoral head	566 ± 174	2.29 ± 1.54			(Karim et al. 2018)
Greater Trochanter	622±302	3.21±1.83	0.70±0.05	0.22±0.05	(Morgan and Keaveny 2001)
Vertebra	344±148	2.02±0.92	0.77±0.06	0.18±0.05	(Morgan and Keaveny 2001)
Proximal Tibia	1,091±634	5.83±3.42	0.73±0.06	0.23±0.06	(Morgan and Keaveny 2001)
Proximal Tibia	485±333				(Røhl et al. 1991)
Mean of several locations	597.9	8.975	1.521		(Rincón-Kohli and Zysset 2009)

While the reported apparent moduli and yield stress of human trabecular bone vary greatly depending on anatomical location (344 MPa – 3,230 MPa) (Table 2.4), the primary factor that contributes to the mechanical properties of trabecular bone is the apparent density. The apparent density, also known as the BMD, is the product of bone tissue density and bone volume fraction (Goulet et al. 1994; Keller 1994). Biomechanical testing has shown that the relationship between the apparent elastic modulus and the density of trabecular bone can be described by both power law (Figure 2.15) (Morgan and Keaveny 2001; Hernandez et al. 2001; Zysset 2003) and linear functions (Ciarelli et al. 2000; Oftadeh et al. 2015). Bone volume fraction can explain 80-95% of the variation in elastic properties of trabecular bone (Kabel et al. 1999; Zysset 2003). The microarchitectural features of trabecular bone also contribute to mechanical properties, with more plate-like or more rod-like structures possible across different anatomic locations. For example, trabecular bone from the proximal femur tends to be high density and has a microarchitecture that is more plate-like in structure. Conversely,

trabecular bone from vertebral bodies tend to be lower density and morphologically more rod-like in structure (Hildebrand et al. 1999). Furthermore, it has been found that trabecular bone tissue from the proximal femur has a higher effective modulus than vertebral samples with similar BV/TV (Morgan et al. 2003).

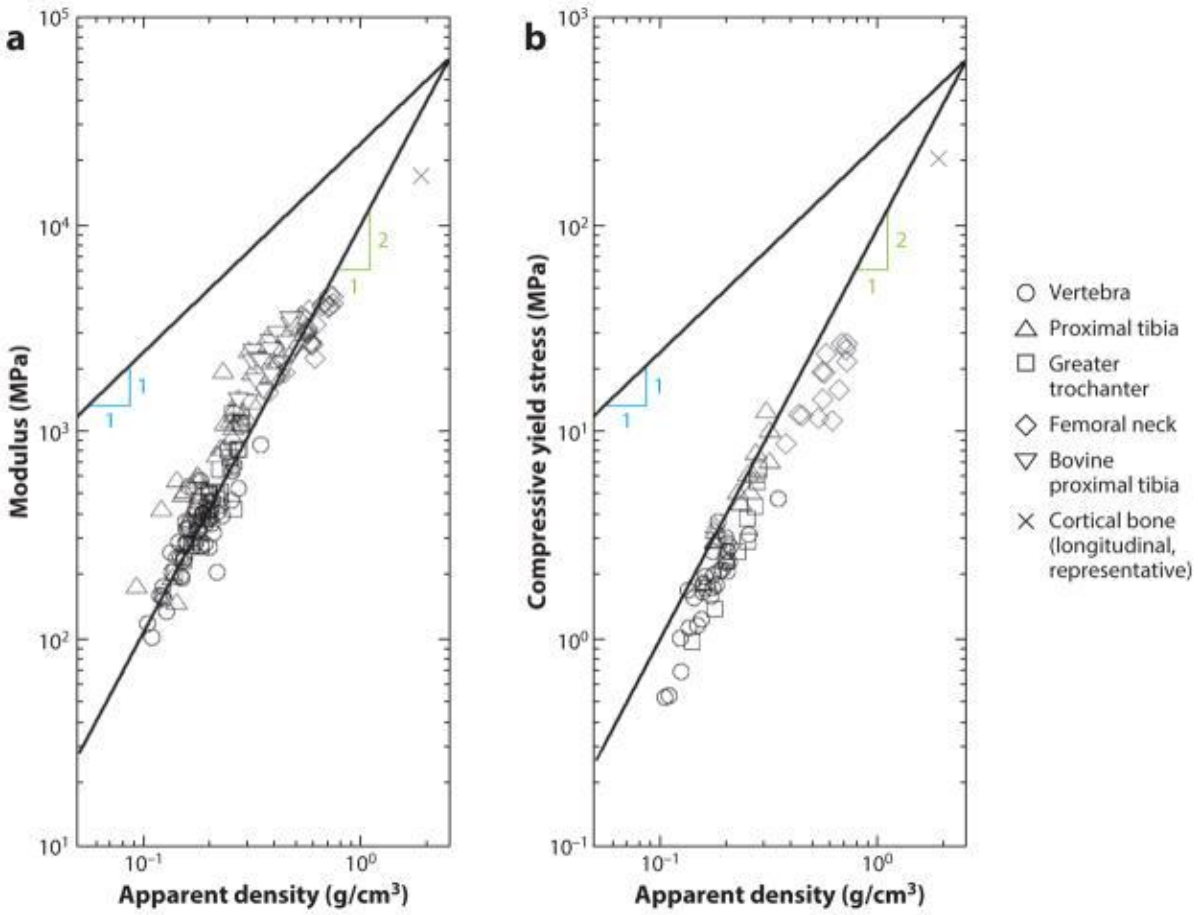

Figure 2.15 Log–log plots of bone strength as functions of apparent density. (a) Young's modulus and (b) compressive yield strength as functions of apparent density. Lines indicating power-law exponents of one and two are drawn on the plots. From (Morgan et al. 2018) previously Modified from (Morgan and Keaveny 2001) (Morgan et al. 2003).

2.3.4 Bone Fracture Behaviour

Bone's ability to resist fracture depends on several factors including the amount of bone present, the spatial distribution of the bone mass, the cortical and trabecular microarchitecture and the intrinsic properties of each of the bone components (Brandi 2009). Microdamage

consists of an accumulation of diffuse damage and linear microcracks. Diffuse damage is the earliest form of damage to occur and can form with modest cyclic loads or constant loads over a long period of time. It consists of clusters of cracks at the sub-lamellar level of 1μm or less. Furthermore, diffuse damage generally occurs in regions of the bone that experience tensile stress and it is not a precursor of linear microcracks. Linear microcracks form under the repetitive activities of daily life, such as walking and running, in the interstitial bone, they are in the order of 50-100 μm. Unlike diffuse damage, linear microcracks are more likely to form in regions of bone that undergo shear or compressive loading (Seref-Ferlengez et al. 2015). Microdamage facilitates the dissipation of energy across multiple levels of bone hierarchy and helps resist fracture. The quality of the organic matrix, collagen, and non-collagenous proteins is a key contributor of bone's ability to form microdamage. The composition of bone, and its capacity to disperse deformation energy without allowing initial cracks to propagate at the lamellar level in the case of trabecular bone, and at the lamellar and osteon level in the case of cortical bone, are important factors of bone toughness (Hahn 1984; Peterlik et al. 2006; Vashishth 2007).

Launey et al. (2010), who have carried out much of the work on bone toughness, give a detailed review of the mechanisms of bone toughness. The toughness of bone arises from the interplay between extrinsic and intrinsic toughening mechanisms, with the former dominating at length scales greater than 1 μm and the latter active primarily at length scales less than 1 μm (Figure 2.16). Each level of hierarchy exhibits distinct toughening mechanisms when the tissue is externally loaded. At the molecular level of tropocollagen molecules and mineralised collagen fibrils, intrinsic mechanisms such as molecular uncoiling and intermolecular sliding occur. These intrinsic toughening mechanisms enhance the resistance to fracture by forming larger, local yield regions around crack-like defects, protecting the integrity of the entire structure by allowing for localised failure.

At the level of fibril arrays, fibrillar sliding and microcracking are observed. The collagen fibres are made up of twisted mineralised collagen fibrils that are held together by a thin layer of extrafibrillar matrix. During deformation, fracture is resisted by the breaking of sacrificial bonds in the extrafibrillar matrix. Microcracking in bone is the prevalent mechanism of microscale deformation, providing an intrinsic contribution to the toughness of bone and an essential phenomenon for the development of the most potent extrinsic toughening mechanisms, such as crack bridging and crack deflection, that occur at larger length scales. Microcracking may also play a crucial role in signalling the remodelling of bone tissue.

In cortical bone, microcracks tend to form along the cement lines or hyper-mineralised interfaces between the bone matrix and secondary osteon structures, and along the boundaries of primary osteons. These microcracks typically have a spacing of tens to hundreds of micrometres and are oriented along the long axis of the bone, which contributes to the anisotropy of bone toughness. Such microcracks are formed due fracture of hydroxyapatite crystals surrounding collagen fibres or delamination at the crystal/fibre interfaces. Microcracking plays a crucial role in crack bridging and crack deflection, which are the most effective toughening mechanisms in bone.

At larger length scales, the energy dissipation capacity of bone increases through crack bridging by collagen fibrils at the interface of fibril arrays. At the largest length scales, in the range of 10–100 μm, extrinsic toughening mechanisms predominate, and extensive crack deflection and crack bridging by uncracked ligaments occur as a result of microcracking. Microcracking is a key mechanism for extrinsic toughening in bone, as it leads to crack deflection/twist and crack bridging. The competition between the direction of maximum mechanical driving force and the path of weakest microstructural resistance determines the path of least resistance for microcracking. In the longitudinal orientation of bone, these paths are aligned, resulting in high toughness. However, in the transverse orientation, the maximum driving force is parallel to the

crack tip while the weakest paths are perpendicular to it. This makes bone tougher to break in the transverse direction due to significant deflection of cracks. Fracture toughness is more than five times higher in the transverse direction than in the longitudinal direction. The difference in toughness between these two orientations can be attributed to the different toughening mechanisms, primarily crack deflection/twist in the transverse direction and crack bridging in the longitudinal direction (Launey et al. 2010).

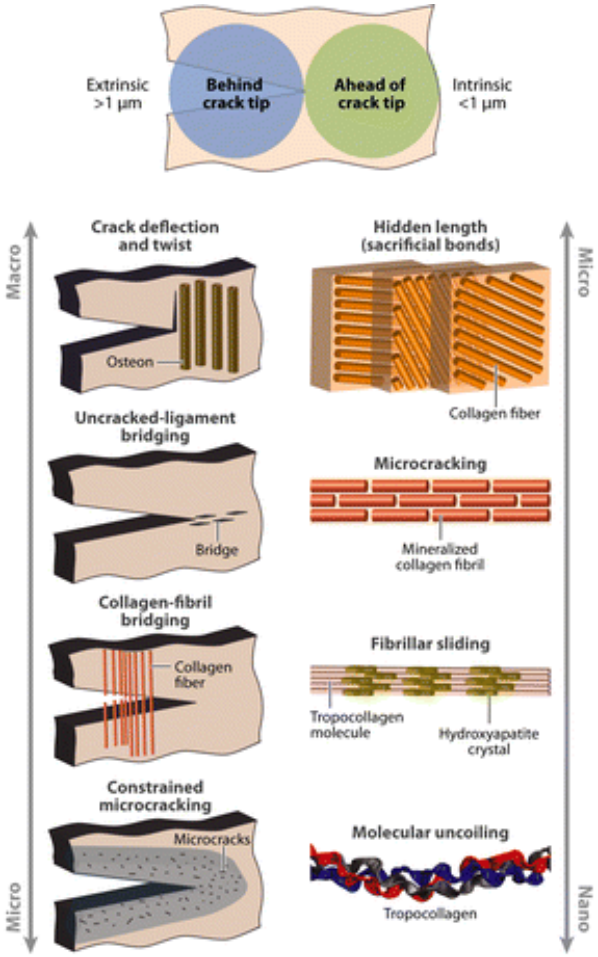

Launey ME, et al. 2010.
Annu. Rev. Mater. Res. 40:25–53

Figure 2.16 Measurement of bone toughness

The toughness of bone results from a mutual competition between extrinsic (crack-tip shielding) toughening mechanisms, which predominate at length scales at more than 1 μm, and intrinsic (plastic deformation) toughening mechanisms, which are active at length scales at primarily less than 1 μm. Distinct toughening mechanisms occur at each level of hierarchy. Molecular uncoiling and intermolecular sliding of molecules are observed at the smallest level of tropocollagen molecules and mineralized collagen fibrils. Microcracking and fibrillar sliding are observed at the level of fibril arrays. At larger levels, the breaking of sacrificial bonds contributes to increasing the energy dissipation capacity of bone at the interface of fibril arrays, together with crack bridging by collagen fibrils. At the largest length scales in the 10–100-μm range, the primary sources of toughening are extrinsic and result from extensive crack deflection and crack bridging by uncracked ligaments, both mechanisms that are motivated by the occurrence of microcracking. (Launey et al. 2010)

2.3.4.1 Linear-elastic fracture mechanics

Standard test methods using linear-elastic fracture mechanics have been developed to measure the plane-strain fracture toughness in mode I for metallic materials (ASTM E399-90) have been developed by ASTM, these methods have also been applied to bone (Table 2.5). The most common specimen set-ups used to determine the fracture toughness, $K_{I,}$ are the single-edge notched three-point bend specimen (SENB) and the compact-tension specimens (Figure 2.17), which are respectively calculated as follows:

$$K_I = \frac{PS}{BW^{\frac{3}{2}}} f\left(\frac{a}{W}\right) \tag{1.6}$$

And

$$K_I = \frac{P}{BW^{\frac{1}{2}}} f'\left(\frac{a}{W}\right) \tag{1.7}$$

Where P is the applied load, S is the loading span (the distance between specimen supports), B is the specimen thickness, W is the specimen depth, a is the crack depth, and $f\left(\frac{a}{W}\right)$ and $f'\left(\frac{a}{W}\right)$ are geometric functions of a/W for SENB and compact-tension specimens, respectively, as provided in ASTM 1820. The toughness, $K_{c,}$ of a material is defined by the critical load at crack initiation or instability, provided small-scale yielding conditions are present. In situations where there are also plane-strain conditions, the corresponding plane strain fracture toughness is referred to as K_{IC} and can be regarded as a material characteristic specific to those conditions. When toughness is measured using these methods, the results are singular and only pertain to crack initiation being equivalent with instability. Furthermore, there is no incorporation of any involvement of plastic or inelastic deformation.

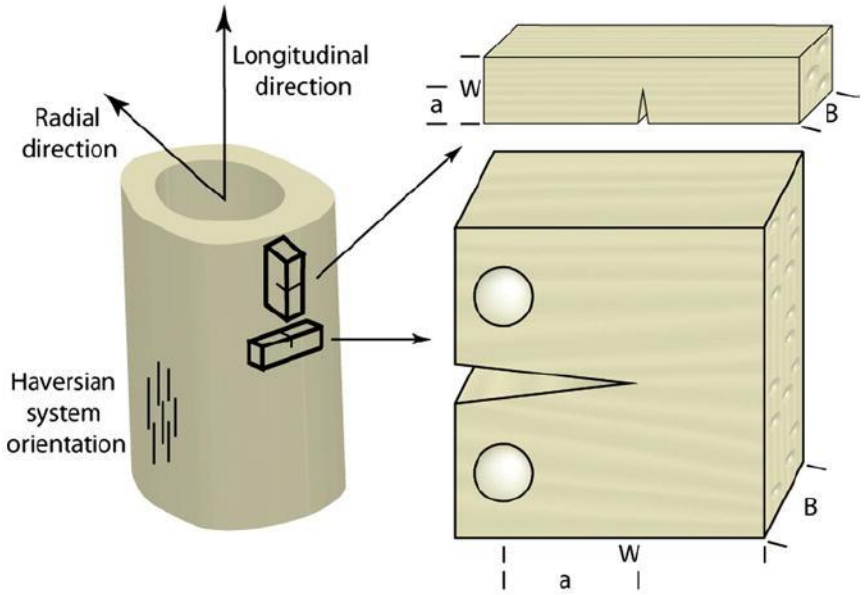

Figure 2.17 Schematic diagrams of samples removed from mammalian long bone. Samples can be fabricated to test bone in the transverse or the longitudinal directions. Shown here are the SE(B) and C(T) geometries for testing the transverse and longitudinal directions respectively. (Ritchie et al. 2008)

2.3.4.2 Non-Linear-elastic fracture mechanics

When extensive plastic deformation occurs, non-linear-elastic fracture mechanics aim to offer improved methods of assessing fracture toughness. Just as *K* serves as the characterising parameter for the linear-elastic singularity, the J-integral, *J*, performs a similar function for the nonlinear-elastic singularity by uniquely characterising the crack-tip stress and strain fields. Assuming that the applicability of *J* extends to length scales comparable to fracture events, it can be employed as a parameter to associate with the commencement and progression of cracks in materials that experience some degree of inelastic deformation. At the point of fracture initiation, $J = J_c$, which can serve as an indicator of the fracture toughness related to crack initiation (Ritchie et al. 2008).

J can be defined as the rate of change in potential energy per unit increase in crack areas for a non-linear elastic solid. Standard test methods for measuring non-linear elastic fracture mechanics have also been developed by ASTM, to measure fracture toughness and crack extension R-curves (ASTM 1820). Again, standard specimen configurations include SENB

and compact tension specimens. In the case of three-point bending SENB and compact tension set-ups, *J* is given by:

$$J = \frac{{K_I}^2}{E'} + \frac{\eta}{B(W-a)} A_{pl} \tag{1.8}$$

where η is a geometric factor and A_{pl} is the area under the plastic portion of the curve. Like linear-elastic fracture mechanics, the fracture toughness can be characterised in terms of J_c and the R-curve providing a measure of crack-growth toughness. In contrast to the *K*-based measurements, the *J*-based measurements include the important contribution of inelasticity in the quantitative assessment of fracture toughness. This aspect is particularly significant for bone, primarily due to the presence of diffuse damage and the formation of microcracks that function as inelastic mechanisms (Ritchie et al. 2008).

Table 2.5 Fracture toughness properties of cortical bone. K_c is critical stress intensity factor, J_{Ic} is crack-initiation fracture toughness, T is transverse, and L is longitudinal.

Anatomic Location	Fracture toughness	Type of Fracture toughness	Reference
Tibia (T) *Human* *Bovine*	 4.05-4.35 MPam$^{1/2}$ 4.68-6.73 MPam$^{1/2}$	K_c	(Norman et al. 1995)
Femur (T) Femur (L) Tibia (T) *Bovine*	3.48±0.33 MPam$^{1/2}$ 2.30±0.27 MPam$^{1/2}$ 4.53±0.98 MPam$^{1/2}$	K_c	(Lucksanasombool et al. 2001)
Femur (T) *Bovine*	5.5 MPam$^{1/2}$	K_c	(Yan et al. 2008)
Femur (L) *Human* Tibia (L) *Bovine*	3.1±1.8 mJ/mm^2 3.5±1.6 mJ/mm^2	J_{Ic}	(Woodside and Willett 2016)

2.3.5 Tissue-level Mechanical Properties

Due to the complex hierarchical structure, it is challenging to determine true tissue-level properties of either cortical or trabecular bone. Traditionally, indentation has been used to determine the hardness of materials and in recent years it has been used to determine the properties of biological materials such as bone as shown in Table 2.6. The standard method for estimating the modulus and hardness of a material through indentation with a Berkovich tip was developed by Oliver and Pharr (Oliver and Pharr 2004; Oliver and Pharr 1992). Nanoindentation uses an indenter tip that is applied to the material using an increasing load and the area of the indent is then estimated. Diamond is a common material for nanoindentation tips, which come in a variety of shapes, including spherical, conical, and most frequently three-sided pyramidal or Berkovich shapes as they are the easiest to manufacture (Zysset 2009). Nanoindentation can be load (mN) controlled or displacement (nm) controlled. During the test, the loading, unloading curve and tip displacement are measured. An indentation sequence consists of using a constant rate to load to maximum load and using the same rate to unload. To minimise the effect of viscoelastic behaviour and thermal drift on the property measurements a hold period can be implemented at the peak load, creating a trapezoidal like curve. The material's elastic modulus can be estimated based on this curve.

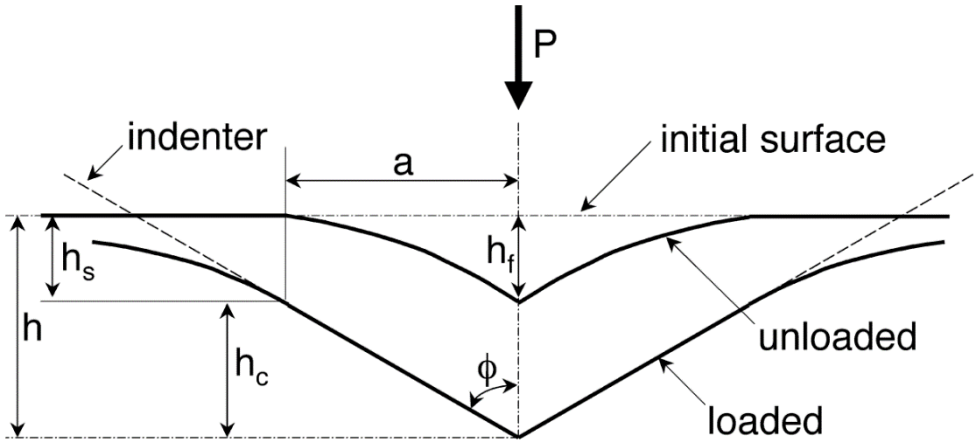

Figure 2.18 Schematic illustration of the unloading process showing parameters characterizing the contact geometry (Oliver and Pharr 2004).

The Oliver and Pharr method involves fitting the power-law relation to the upper portion of the load-displacement curve's unloading segment,

$$P = \alpha\left(h - h_f\right)^m \tag{1.9}$$

where P is the indentation load, α and m are power law fitting constants, h is the indentation displacement and h_f is the irreversible depth of indentation once the indenter is fully unloaded. From the above power-law relation, the initial unloading stiffness is determined,

$$S = \frac{dP}{dh} \tag{1.10}$$

$$S = m\alpha\left(h_{max} - h_f\right)^{m-1} \tag{1.11}$$

The contact depth can be determined by calculating the distance between,

$$h_c = h_{max} - h_s \tag{1.12}$$

$$h_c = h_{max} - \epsilon\frac{P_{max}}{S} \tag{1.13}$$

where h_s is the sink-in depth, ϵ is a constant based on the geometry of the tip.

Hardness, *H*, is determined using the equation:

$$H = \frac{P_{max}}{A} \tag{1.14}$$

Where *A* is the contact area of the indentation. To determine *A* the nanoindentation instrument must be calibrated by determining the shape function constant $(C_1, \ldots, C_8)$ that best fit the relationship between the projected contact area of the indentation made by the indenter, A, and the contact depth, h_c.

$$\begin{aligned} A = {} & C_0h_c^2 + C_1h_c + C_2h_c^{1/2} + C_3h_c^{1/4} + C_4h_c^{1/8} \\ & + C_5h_c^{1/16} + C_6h_c^{1/32} + C_7h_c^{1/64} + C_8h_c^{1/128} \end{aligned} \tag{1.15}$$

The elastic modulus is measured through its relationship to the contact area and recorded unloading stiffness by:

$$S = \beta \frac{2}{\sqrt{\pi}} E^* \sqrt{A} \tag{1.16}$$

where E^* is the effective modulus defined by:

$$E^* = \frac{dP}{dh} \frac{\sqrt{\pi}}{2\sqrt{A}} \tag{1.17}$$

$$\frac{1}{E^*} = \frac{1 - {v_s}^2}{E_s} + \frac{1 - {v_i}^2}{E_i} \tag{1.18}$$

With the elastic displacements that occur in both specimens, the Young's modulus E_s and Poisson's ratio v_s and the indenter, E_i and v_i, being taken into account.

Table 2.6 Mechanical properties of cortical and trabecular bone determined from nanoindentation. T is transverse and L is longitudinal.

Anatomic Location	Type	Modulus (GPa)	Hardness (GPa)	Reference
Vertebra *Human (dry)*	Cortical Osteon Cortical Interstitial Trabecular	22.5 ±1.3 25.8 ±0.7 13.4 ±2.0	0.614 ±0.042 0.736 ±0.034 0.468 ±0.079	(Rho et al. 1997)
Femoral Neck *Human (wet)*	Cortical Osteon Cortical Interstitial Trabecular	15.8 ±5.3 17.5 ±5.3 11.4 ±5.6	0.234 - 0.760	(Zysset et al. 1999)
Femur *Human (dry)*	Cortical Trabecular	20.02 ±0.27 18.14 ±1.7		(Turner et al. 1999)
Vertebral *Bovine (dry)*	Cortical Osteon (L) Cortical Interstitial (L) Cortical (T) Trabecular (L) Trabecular (T)	24.7 ± 2.5 30.1 ± 2.4 19.8 ± 1.6 20 ± 2 14.7 ± 1.9	0.811 ±0.155 0.892 ±0.1 13 0.647 ±0.060 0.528 ±0.095 0.410 ±0.063	(Wang et al. 2006)
Vertebral *Human (wet)* *Human (dry)*	Trabecular Trabecular	12.3 15.4		(Wolfram et al. 2010)

2.4 Bone Diseases and Fractures

According to recent statistics, approximately 3.5 million bone fragility fractures occur annually in the EU, leading to an approximate cost of €37 billion to healthcare systems (Hernlund et al. 2013). These fractures have considerable impact on patients, leading to substantial pain, disability and even premature death (Adachi et al. 2001). Bone fragility fractures are highly correlated with aging and/or the onset various bone-related diseases. During the aging process, there is a general reduction in bone mineral density that starts in the third decade of life, and continues thereafter through each year of life. Cortical bone loss arises after menopause or sex-steroid-deficiency in aging men and is associated with increasing cortical porosity. Changes linked with increasing age in human trabecular bone include decreased Tb.N, Tb.Th and Conn.D. In particular, trabecular thinning appears to be the main contributing factor to bone loss in men, while women tend to lose more bone through decreases in Tb.N (Boskey and Imbert 2017). It has been found that the compressive strength of trabecular bone decreases by 8.5% with every decade (McCalden and McGeough 1997). The fatigue life of older trabecular bone is also reduced, with the number of cycles to a specified test endpoint is significantly lower in older compared to younger samples of trabecular bone (Green et al. 2011). These changes coincide with reduced density making the elderly population more susceptible to fractures. While age-related bone loss affects the general population of both men and women, it is more prominent in women post-menopause, where they are highly susceptible to the onset of osteoporosis.

2.4.1 Osteoporosis

Osteoporosis is by far the most studied bone disease and is primarily characterised as a disease of bone loss. Osteoporosis means ‘porous’ bone and it is a skeletal metabolic disease that is characterised by reduced bone density through microarchitectural deterioration of bone tissue. Osteoporosis leads to increased higher fracture risk, with fragility fractures causing severe pain

and disability (Clynes et al. 2020). It is caused by an inhibited remodelling process that leads to excessive resorption and unmatched levels of formation leading to a net loss of bone mass (Lerner 2006; Riggs et al. 2002). Osteoporosis can develop due to multiple cause, including estrogen deficiency (post-menopausal), natural aging, and thyroid pathologies. Osteoporosis is characterised by reduced bone mineral density (BMD) resulting from changes in the microarchitecture and composition of bone. In the early stages of osteoporosis bone loss occurs, however, there is no change in tissue mineralisation and collagen maturity (O'Sullivan 2020). Microarchitecturally, the trabeculae undergo thinning, leading to a decrease in bone density. There is also an increase in porosity of the cortical bone, accompanied by thinning of the cortical bone itself. Loss of trabecular connectivity is another notable change, and the microarchitecture becomes more anisotropic as a compensatory response to bone mass loss. However, as osteoporosis progresses the bone loss is reduced and compensatory action of secondary new bone formation, and mineralisation of exiting tissue occur along with trabecular thickening (Allison and McNamara 2019; O'Sullivan et al. 2020; O'Sullivan 2020). Compositionally, the osteoporotic bone has been shown to exhibit higher levels of mineralisation of trabeculae (Busse et al. 2009; McNamara 2010). Alterations also occur in the collagen of the bone, with collagen synthesis being increased (Mansell and Bailey 2003) with some evidence for decreased enzymatic crosslinks and increased AGE crosslinks in osteoporotic bone as is also seen in type 2 diabetic bone (Saito and Marumo 2010).

According to statistics from the International Osteoporosis Foundation, globally, one in three women and one in five men over the age of 50 will experience an osteoporotic fracture during their lifetime. The global aging population paired with changes in lifestyle habits has contributed to a significant increase in the incidence of osteoporosis and related fractures, a trend that is expected to continue into the future. As a result of its widespread occurrence, osteoporosis is recognised as a critical public health issue (Genant et al. 1999).

In the management of patients with osteoporosis, effective fracture risk assessment strategies are crucial to clinicians, not only in diagnosing bone pathologies, but also in guiding treatment strategies and informing when pharmacological intervention may be required (Unnanuntana et al. 2010). The current gold standard for fracture risk prediction technique is a dual x-ray absorption (DXA) scan. This scan measures the BMD of a patient and from this a fracture risk can be calculated in terms of a T-score, which provides a diagnostic classification of the severity of the disease. The T-score is the number of standard deviations above or below the average BMD of a young adult reference population. A T-score of -1.0 or above is normal BMD, between -1.0 and -2.5 is low bone mass or osteopenia, while -2.5 and below is osteoporotic (Gourlay et al. 2012).

However, despite this, the clinical screening and assessment of BMD through DXA scanning is only effective in capturing 50-70% of the variation in whole bone strength (Lochmüller et al. 1998; Melton 1995; Unnanuntana et al. 2010). The World Health Organization Fracture Risk Algorithm (FRAX) score is also used, which can provide improved estimates of fracture probability compared to BMD alone (Kanis et al. 2009). The FRAX algorithm makes an empirically-based adjustment of the fracture probability based on other known independent risk factors (e.g. age, sex or family history (Kanis et al. 2009)).

2.4.2 Diabetes and Bone

Clinical assessment of fracture risk becomes even more challenging in other bone-related diseases where there is no reduction in BMD. In particular, it has been reported that T2D patients have an increased fracture risk of up to three fold at hip and other non-vertebral sites when compared to non-diabetic patients, despite an increased BMD (Bonds et al. 2006; Janghorbani et al. 2007; Vestergaard 2007; Schwartz et al. 2011; Napoli et al. 2014). This presents distinct clinical challenges in terms of both assessment and treatment of type 2 diabetic bone disease, as traditional screening methods using DXA scanning are based on BMD

measurement are unable to provide quantitative measures of fracture probability. Even the FRAX algorithm underestimates fracture probability in T2D, due to relatively the high BMD of these patients (Giangregorio et al. 2012).

2.4.2.1 Type 2 Diabetes Epidemiology

Diabetes is a chronic metabolic disease with significant comorbidities. It affects the body's ability to produce and respond to insulin and is characterised by hyperglycaemia. The chronic hyperglycaemia of diabetes is associated with permanent damage and failure of various organs. T2D is much more common than type 1 diabetes, accounting for ~90-95% of those with diabetes. T2D is caused by a combination of reduction in insulin-stimulated glucose uptake and a deficient compensatory insulin secretory response. In some cases, a level of hyperglycaemia sufficiently high to cause pathological and functional changes in different tissues can exist for an extended period of time before the T2D is detected and diagnosed. Most T2D patients are obese, which in itself provides some level of insulin resistance. With an increase in age, higher levels of obesity and reduced activity, the risk of developing T2D also increases.

T2D patients have an increased risk of developing a number of serious life-threatening health problems, leaving them with higher medical care costs, reduced quality of life and increased mortality. High glucose levels cause vascular damage throughout the body affecting the heart, eyes, kidneys, nerves, and result in many complications. The global incidence of diabetes has been growing over recent decades. By 2045, it is estimated that 9.9% of the population will have diabetes. The global cost of diabetes annually is 850 billion USD (Cho et al. 2018), with an estimated annual cost of 2 billion euros in Ireland (Diabetes Ireland 2018). With the increasing T2D patient population, there is an increasingly urgent need to understand the effect that diabetes has on the body and in this case, of particular interest is the effect diabetes has on

the bone. T2D is particularly prevalent in developed regions such as Western Europe and shows a distribution pattern that matches socio-economic development (Khan et al. 2020).

T2D is normally diagnosed by a glycated haemoglobin (HbA_{1c}) test result of 48 mmol/mol (6.5%) or above. T2D diabetes can also be diagnosed by measuring the blood glucose measures during a 75 g oral glucose tolerance test, with diabetes being defined as a fasting glucose of ≥7.0 mmol/litre and/or 2-hour post-challenge glucose of ≥11.1 mmol/litre by the World Health Organisation (WHO) (Forouhi and Wareham, 2019).

2.4.2.2 Bone Fragility in Type 2 Diabetes (T2D)

A summary of fracture risk in T2D patients is shown in Table 2.7. Strotmeyer et al. (2005) presented one of the first studies to investigate fracture risk in T2D by examining whether impaired fasting glucose was associated with higher fracture rates in older adults. It was found that T2D patients had a 64% higher incidence in bone fractures at all sites, compared to non-diabetic participants Following this, Bonds et al. (2006) investigated fracture risk in women with clinically diagnosed T2D in the Women's Health Initiative Observational Cohort, which is a prospective study of postmenopausal women (n=93,676). This cohort were compared to women without diagnosed diabetes and it was found that women with T2D were at an increased risk for fracture compared to non-diabetic controls, with an adjusted relative risk (RR) of between 1.20 and 1.33 depending on fracture site. Janghorbani et al. (2007) conducted a systematic review of published data on the association between diabetes mellitus and fracture. This review found that T2D was associated with an increased risk of hip fracture in both men (RR = 2.8) and women (RR = 2.1). Vestergaard et al. (2007) conducted a meta-analysis on the effect of diabetes on bone mineral density (BMD) and fracture risk and found that there was a higher risk of hip fractures among patients with T2D, with a RR of 1.38 compared to non-diabetic controls. A meta-regression analysis also indicated that BMI was a significant determinant of BMD in both the spine and hip, while glycated haemoglobin (HbA1C) was not

found to be associated with BMD. Following on from this, Schwartz et al. (2007) investigated the potential links between femoral neck BMD T-score, FRAX score, and the risk of hip and non-spine fractures in older individuals with T2D. In these older individuals, it was found that both femoral neck BMD T-score and FRAX score were positively correlated with hip and non-spine fracture risk. However, the study also revealed that for a given T-score and age, or for a given FRAX score, older adults with T2D had a higher risk of fractures than those without T2D. More recently, Oei et al. (2013) examined the impact of glucose control on skeletal complications in a cohort of 4,135 individuals from the Rotterdam study. Among the 420 participants with T2D at baseline, they were categorized into three comparison groups based on their level of glucose control: adequately controlled diabetes (ACD) with 203 individuals, inadequately controlled diabetes (ICD) with 217 individuals, and no diabetes with 3,715 individuals. The results showed that participants with ICD had a 47-62% higher risk of fractures compared to those without diabetes, while those with ACD had a similar risk of fractures as individuals without diabetes. This was followed up by Napoli et al. (2014) explored the link between diabetes and non-vertebral fractures in elderly men by analysing data from the Osteoporotic Fractures in Men study. The results indicated that the risk of non-vertebral fractures was greater among men with diabetes compared to normo-glycemic men, with a RR of 1.3. Additionally, this risk was even higher in men who were using insulin, with a relative risk of 2.46. However, after making adjustments for multiple variables, the risk of non-vertebral fractures remained significantly elevated only among men with diabetes who were using insulin, with an adjusted RR of 1.74. Wang et al. (2016) performed a meta-analysis of eight studies to evaluate the associated between diabetes and vertebral fracture risk. The results of this analysis revealed the pooled RR of vertebral fracture for diabetic individuals was 2.03.

Overall, it is clear these studies provide evidence of an increase in fracture risk for T2D patients. In those with T2D, the increase in fracture risk is met with an impaired fracture healing

(Schwartz 2003), with diabetic patients having healing times prolonged by up to 87% (Loder 1988). Due to this slower fracture healing, fractures can have a profound effect on the quality of life of T2D patients and can lead to substantial disability and morbidity. T2D patients have an increased mortality risk of when compared to non-diabetic patients (Ahn et al. 2020).

Table 2.7 Summary of fracture risk in T2D patients, where RR is relative risk, ICD is inadequately controlled T2D, ACD is adequately controlled T2D.

Fracture Location	Summary RR (% increase in fracture)	Reference
All	1.64 (64%)	(Strotmeyer et al. 2005)
All	1.2	(Bonds et al. 2006)
Hip (female)	2.1	(Janghorbani et al. 2007)
Hip (male)	2.8	
Hip	1.38	(Vestergaard 2007)
Hip (female)	1.88	(Schwartz et al. 2011)
Non-Spine (female)	1.52	
Hip (male)	5.71	
Non-Spine (male)	2.17	
All (ICD)	1.47-1.62 (47-62%)	(Oei et al. 2013)
All (ACD)	No difference	
Non-Vertebral	1.3	(Napoli et al. 2014)
Non-Vertebral (using Insulin)	2.46	
Vertebral	2.03	(Wang et al. 2016)

2.5 Mechanisms of Bone Fragility in T2D

2.5.1 Diabetes and Bone Metabolism/Cellular Mechanisms

Insulin, produced in the pancreas, is an anabolic hormone that regulates the levels of glucose in the blood. Responding to insulin resistance, the pancreatic islets enhance their cell mass and insulin secretory activity. If the functional development of pancreatic islet β-cells do not counteract the degree of insulin resistance, insulin deficiency and T2D develop. T2D causes the development of long-term macro-vascular and micro-vascular complications. Insulin resistance is generally present throughout the development from prediabetes to overt T2D. The onset of T2D and its evolution are largely affected by the progressive failure of β-cells to produce sufficient levels of insulin (Donath and Shoelson, 2011). It is thought that the

hyperglycaemic state due to T2D leads to increased levels of sugar in the blood and causes an increase in non-enzymatic crosslinks and adducts known as AGEs. The onset of type 2 diabetes and the hyperglycaemic state also leads to other distinct changes in systemic biochemical factors. In particular, the hyperglycaemic state in T2D leads to complex pathophysiological changes that include increased bone marrow adiposity, the release of inflammatory factors (e.g. IL1, IL-6 (Graves and Kayal 2008)) and higher oxidative stress. This is known to disrupt bone homeostasis (Paschou et al. 2017), whereby osteoblasts, osteoclasts and osteocytes are impacted by the hyperglycaemic state of T2D. It has been shown that T2D is associated with decreased bone remodelling. Lower levels of bone formation markers, osteocalcin (Kunutsor et al. 2015), procollagen type 1 N-terminal propeptide (P1NP) and C-terminal telopeptide, CTX (Purnamasari et al. 2017), and bone resorption markers RANKL and TRAP5b (Sassi et al. 2018) are found in T2D, implying that bone turnover in T2D is lower (Purnamasari et al. 2017; Sassi et al. 2018; Tanaka et al. 2018; Levinger et al. 2016).

AGEs affect cellular activity in bone in T2D. However, to date, there is not a clear understanding of this. Through interaction with the AGE-specific receptor (RAGE), the build-up of AGEs in the bone's extracellular matrix (ECM) controls osteoblast proliferation and differentiation. RAGE binding activates NF-KB in osteoblasts increasing cytokine production. In addition to upregulating the formation of reactive oxygen species, the AGE-RAGE binding interaction also increases inflammation in the bone microenvironment, which in turn causes bone loss. A build-up of AGEs in the body can hinder osteoblast differentiation and proliferation, decrease osteocalcin secretion, and disrupt cell adhesion and matrix interactions, all of which have an impact on bone formation (Burr and Allen 2019). Several in vitro studies have suggested that the presence of AGEs lead to a deleterious effect on osteoblast activity (Mercer et al. 2007; Sanguineti et al. 2008) by reducing osteoblastic attachment to the collagen matrix (McCarthy et al. 2004), preventing osteoblast proliferation and differentiation (Kume

et al. 2005; Katayama et al. 1996), inhibiting mineralisation of osteoblastic cells and decreasing osteocalcin RNA expression (Ogawa et al. 2007). Incubation of human osteoblast with Pentosidine resulted in a significant decrease in alkaline phosphatase (ALP), and receptor for AGE (RAGE) mRNA levels (Sanguineti et al. 2008). In vitro studies have also found that AGEs alter osteoclast behaviour, although the precise mechanism by which they do this is unclear as the findings have been contradictory.

Additionally, AGEs might control osteoclast activity and osteoclastogenisis, with their presence slowing osteoclastic resorption. This may be due in part to a decline in collagen's solubility caused by the presence of AGEs (Valcourt et al. 2007). These combined effects could be responsible for the normal or even increased bone mass seen in T2D patients (Burr and Allen 2019). A decrease in osteoclastogenisis has been reported (Gangoiti et al. 2013). It has also been shown that AGEs increase osteoclast activity in a rodent model (Miyata et al. 1997). Likewise, a recent study found that the local concentration of AGES was positively correlated with the bone resorption activities of osteoclasts (Dong et al. 2011). Conversely, a previous in vitro study found that bone treated with pentosidine had significantly inhibited resorption (Valcourt et al. 2007).

2.5.2 Altered Bone Matrix

2.5.2.1 Matrix

This altered bone remodelling process and hyperglycaemic state negatively impacts the underlying composition of the bone matrix. As described in Section 2.2.4.4, AGEs have been found to accumulate in T2D bone tissue, leading to an altered collagen matrix. Hunt et al. (2019) evaluated the bone matrix of T2D patients and found an increase in the AGE pentosidine and the sugar:matrix ratio in T2D bone and that the enzymatic crosslink Pyd trended towards being lower in the T2D group compared to the non-T2D group. Following on from this, Wölflel et al. (2020) found no differences in enzymatic crosslinking or matrix maturity of T2D bone

compared to controls. However, an increase in carboxymethyl lysine (CML) was found in the T2D samples. Sihota et al. (2021) found a higher fluorescent AGE accumulation and non-enzymatic crosslink ratio, a lower enzymatic crosslink ratio and an altered secondary structure of Amide I and Amide II proteins in T2D bone after fracture compared to non-T2D controls. Recently, Wölfel et al. (2022) revealed a higher carbonate-to-amide I ratio in T2D with high porosity (T2DwHP) compared to control and T2D as the carbonate-to-phosphate ratio was similar across all groups it has been postulated that T2DwHP have a lower amide I content. Wölfel et al. (2022) also found no difference in the level of fluorescent AGE accumulation in T2D compared to non-T2D samples. Lekkala et al. (2023) found an elevation in fluorescent advanced glycation end products (AGEs) and pentosidine in both trabecular and cortical iliac bone among postmenopausal women. Additionally, they observed an increase in the non-enzymatic crosslink ratio in the cortical bone of T2D samples when compared to non-T2D samples. However, no significant differences were observed in terms of the mineral-to-matrix ratio, carbonate to phosphate ratio, or crystallinity.

2.5.2.2 Mineral

T2D also impacts mineralisation of the tissue, with recent work demonstrating that hyperglycaemia disrupts the mineralisation phase of osteoblasts (Ghodsi et al. 2016). This has been proposed to alter mineralisation quality, with recent work using ZDF rats showing that mineral constituents at the sub-tissue level are altered, suggesting secondary mineralisation does not proceeding correctly (Monahan et al. 2023). Parle et al. (2020) have shown that mineral is more heterogeneously distributed in human type 2 diabetic tissue by analysing bone mineral density distribution through mineral density histograms from micro-CT. Hunt et al. (2019) found that the mineral-to-matrix ratio was increased in the T2D group compared to the non-T2D, while no differences were found in crystallinity, carbonate: phosphate ratio, and acid phosphate content across groups. Similarly, Wolfel et al. (2020) also found a higher regional

mineralisation heterogeneity and increased mineral-to-matrix ratio in the periosteal regions in the T2D compared to the control and T2DwHP groups. Additionally, crystallinity of the endocortical region was significantly lower in T2DwHP compared to T2D and mineral maturity was significantly lower in the T2DwHP group compared to the control and T2D group. Conversely, Sihota et al. (2021) found that T2D bone post fracture had lower mineral-to-matrix ratio but no changes in crystallinity, carbonate-to-phosphate ratio or acid phosphate content compared to non T2D bone post fracture Starr et al. (2018) performed an in vivo study finding an increased radial and tibial trabecular bone volume fraction, plate volume fraction and areal BMD and no change in cortical porosity in T2D women compared to non-T2D women using HR-pQCT. They also found unchanged or increased trabecular volumetric BMD at the femoral neck and tibia. Similarly, Farr et al. (2014) used in vivo DXA and HR-pQCT and found the radial cortical thickness, trabecular number and trabecular separation of T2D higher than non-T2D patients. This study also found increased BMD for T2D patients compared to controls. However, when adjusted for BMI, there was no significant difference to the controls. Burghardt et al. (2010) found that T2D patients had higher trabecular volumetric BMD, trabecular thickness, and increased cortical porosity through in vivo HR-pQCT. Patsch et al. (2013) using DXA and HR-pQCT imaging of the distal radius found increased cortical porosity in T2D postmenopausal women with fragility fractures (T2DFx) compared to T2D postmenopausal women without fragility fractures. When T2DFx was compared to non-T2D post-menopausal women without fragility fractures, there was no significant differences. Comparably, Heilmeier et al. (2016) found that T2D patients with fragility fracture history had an elevated global porosity compared to T2D patients with no previous fractures, suggesting that elevated cortical porosity is a potential contributor to the high skeletal fragility in T2D. Yu et al. (2014) found increased radial cortical porosity and decreased volumetric BMD and TMD in African American women with T2D compared to non-T2D controls. No differences were

seen in total radial volumetric BMD or trabecular vBMD between groups. T2D patients with microvascular complications have also been found to have a lower cortical volumetric BMD, cortical thickness and a higher cortical porosity at the radius (Shanbhogue et al. 2016). Interestingly, Osima et al. (2017) found that women with T2D have a lower cortical porosity at the proximal femoral shaft. It is therefore apparent that T2D affects trabecular and cortical bone differently.

Ex vivo studies by Cirovic et al. (2022) and Karim et al. (2018) examined the microarchitecture at the femoral neck in T2D tissue. Cirovic et al. (2022) found that cortical porosity was higher and cortical thickness was lower in T2D with previous fractures compared to non-T2D controls. In contrast to this, Karim et al. (2018) found no significant differences in cortical porosity in the femoral neck in T2D and controls. Cirovic et al. (2022) found that, of the trabecular microarchitectural properties, only SMI was slightly higher in T2D samples compared to controls. More generally, ex vivo studies have generally found no change (Karim et al. 2018; Hunt et al. 2019; Parle et al. 2020; Piccoli et al. 2020) in trabecular microarchitectural properties in human T2D trabecular bone, however one study (Sihota et al. 2021) that investigated T2D bone after a fragility fracture found impaired trabecular microarchitectural properties.

2.6 Biomechanical implications of T2D

2.6.1 General

Despite the fact that micro-architectural changes have been observed in people with T2D, the functional effects of these structural modifications remain largely unknown. Furthermore, while several population-level studies have shown an increased risk of fracture in T2D, there are limited studies that actually demonstrate that the mechanical properties of T2D tissue is impaired in humans (see Table 2.9). In fact, much of the evidence that T2D adversely impairs the mechanical properties of bone tissue has been derived from either animal models of T2D

(Saito et al. 2006b; Reinwald et al. 2009; Zhang et al. 2009) or in vitro glycation models that have been used to study the effect of AGE accumulation on mechanical properties. For the purposes of this literature review, the focus will be on mechanical investigations of tissue from in vitro glycation models (Section 2.6.2) and human T2D studies (Section 2.6.3).

2.6.2 In Vitro Glycation Models and AGE Accumulation

It has been widely hypothesised that AGE accumulation has a negative impact on bone quality because it reduces collagen molecular sliding, resulting in reduced energy dissipation of the collagen fibrils and inherent toughness of the tissue (Fessel et al. 2014). It has been proposed that AGE accumulation in T2D leads to increased fracture risk (Saito and Marumo 2010). For example, even in patients without diabetes, the pentosidine content is significantly higher in patients with hip fracture compared to patients without a hip fracture (Vaculík et al. 2016). This has led to the hypothesis that increases in AGE crosslinks and adducts in the collagenous phase of bone may contribute to the deterioration of bone strength and be responsible for increased fragility in T2D (Saito et al. 2006c; Saito et al. 2006a). However, the relationship between AGE accumulation and bone fragility has not been fully established (Willett et al. 2022).

The difficulty in obtaining large volumes of human tissue in T2D has meant that many studies have used in vitro glycation models to simulate the effects of T2D. In vitro glycation models use solutions containing sugars to mimic the state of hyperglycaemia that is present in T2D. It must be noted that these in vitro glycation models are not capable of capturing other complex physiological and biological effects of T2D on bone. In addition, these in vitro studies have provided conflicting results (Willett et al. 2022). Table 2.8 provides a summary of studies that have investigate the mechanical properties of bone tissue using in vitro glycation models.

Vashishth et al. (2001) investigated bovine cortical bone subject to in vitro glycation. Through uniaxial compression and tension, an increase in yield stress and strain, and secant modulus

and a decrease in damage fraction was found. There was no change in the post-yield properties of the bone in the glycated samples. Stress relaxation tests on demineralised glycated samples had increased stiffness compared to control. Tang et al. (2007) tested glycated individual human trabeculae using four point-bend tests and trabecular bone cores in uniaxial compression. The four-point bend tests showed reduced stiffness for the glycated sample and the compression tests showed reduced post-yield strain energy and damage fraction (Tang et al. 2007). Viguet-Carrin et al. (2008), tested in vitro glycated bovine cortical bone using three-point bend and microhardness and found no difference in either the pre-or post-yield mechanical properties. It was suggested that this was due to the 3-point bend test being unable to capture the mechanical changes of the sample due to AGE accumulation. However, Willet et al. (2013) also tested in vitro glycated bovine cortical bone using three-point bend tests and found an increased secant modulus but reduced ultimate and post-yield strain, post-yield strain energy, toughness, and damage fraction. Similarly, Jia et al. (2021) tested glycated cortical bone using three-point bend tests and found an increased secant modulus, decreased post-yield strain, post-yield strain energy and damage fraction. Jia et al. also measured the fracture toughness of the bone and found that glycated sample had a reduced plastic contribution of fracture toughness in quasi static conditions but no differences in overall fracture toughness. Using stress-relaxation tests, an increase in stiffness was also seen (Jia et al. 2021). Merlo et al. (2020) carried out an in vitro glycation study on human cortical bone and examined mechanical properties using fracture toughness, microhardness and cyclic reference point indentation (cRPI) tests. From the fracture toughness test, the critical fracture toughness of the glycated samples was reduced, while the microhardness test also showed reduced mechanical properties for the glycated samples. No differences were found from the cRPI test (Merlo et al. 2020). Interestingly, Tang and Vashishth (2007) investigated microdamage accumulation of in vitro glycated human tibial trabecular bone and found increased microdamage in the glycated

samples compared to the controls.

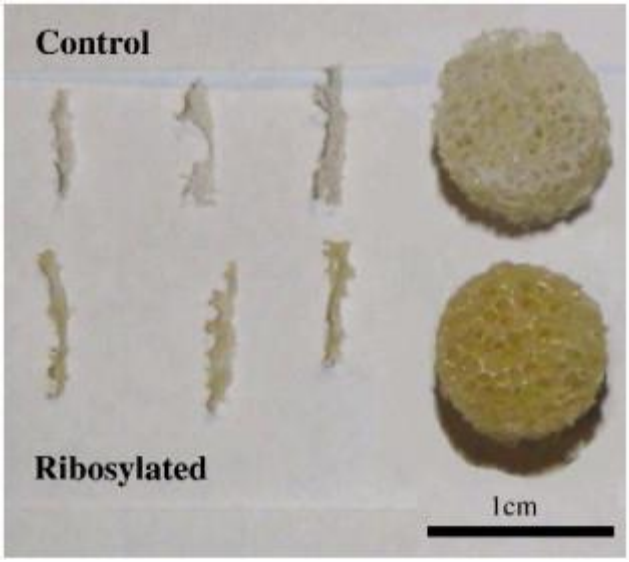

Figure 2.19 Cancellous bone cores and individual trabeculae show changes from a white (appears as a lighter shade) to a yellow colour (a darker shade) after in vitro ribosylation (Tang et al. 2007)

Overall, the data derived from in vitro glycation models has provided conflicting results on the pre- and post-fracture behaviour (Vashishth et al. 2001; Tang et al. 2007; Viguet-Carrin et al. 2008; Willett et al. 2013; Merlo et al. 2020; Jia et al. 2021), with many studies using different incubation times, varying from 7 days (Tang et al. 2007) to 38 days (Vashishth et al. 2001) (Figure 2.20) and being limited by substantial inter-specimen variability (Viguet-Carrin et al. 2008). The precise role of AGE accumulation on both tissue mechanics in the elastic range and fracture mechanics has proven difficult to identify and approaches to reduce specimen variability are required.

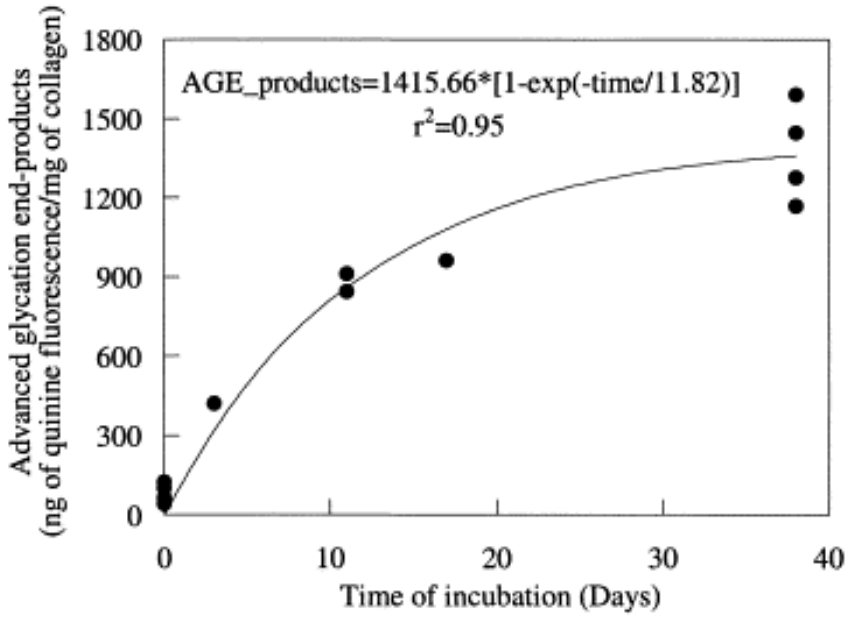

Figure 2.20 Accumulation of AGEs in bone specimens.
After 3, 11, 17, and 38 days of incubation in ribose, fluorescent AGEs were quantified and normalised to the content of collagen (Vashishth et al.*2001).*

Table 2.8 Summary of in vitro AGE accumulation of bone and mechanical tests studies. Did not measure(DNM), fluorescent AGE (fAGE), uniaxial compression (UC), uniaxial tension (UT), three-point bend (3PB), four-point bend, (4PB), stress-relaxation (SR), microhardness (MH), fracture toughness (FT), secant modulus (Esec), yield stress (σ_Y), yield strain (ε_Y), ultimate strain (εult), post-yield strain (ε_{PY}), post-yield strain energy (UPY), damage fraction (DF), toughness (T)

	Vashishth et al.**, 2001**	**Tang** et al.**, 2007**	**Viguet-Carrin** et al.**, 2008**	**Willet** et al.**, 2013**	**Merlo** et al.**, 2019**	**Jia** et al.**, 2021**
Bone	Bovine Cortical	Human Trabecular	Bovine Cortical	Bovine Cortical	Human Cortical	Bovine Cortical
fAGE	1576% ↑	**190%** ↑	DNM	DNM	**236%** ↑	DNM
AGE other	DNM	DNM	PEN ↑	PEN ↑	DNM	DNM
TEST	UC,UT, SR	4PB, UC	3PB, MH	3PB	FT, MH	3PB, FT, SR
4PB	DNM	stiffness ↓	DNM	DNM	DNM	DNM
3PB	DNM	DNM	No Difference	E_{sec} ↑ ε_{ult} ↓ ε_{PY}↓ U_{PY} ↓ T ↓ DF ↓	DNM	E_{sec} ↑ ε_{PY} ↓ U_{PY} ↓ DF↓
Fracture	DNM	DNM	DNM	DNM	K_{Ic} ↓ Initiation Load ↓ Initiation Time ↓	J_{pl} ↓
Compression	DNM	U_{PY} ↓ DF ↓	DNM	DNM	DNM	DNM
Compression /Tension	σ_Y↑ ε_Y↑ E_{sec} ↑ DF ↓	DNM	DNM	DNM	DNM	DNM
Micro Hardness	DNM	DNM	No Difference	DNM	Mech Props ↓	DNM
Stress Relaxation	Stiffness ↑	DNM	DNM	DNM	DNM	Stiffness ↑
Cyclic RPI	DNM	DNM	DNM	DNM	No difference	DNM

2.6.3 Human Tissue

Table 2.9 summarises the results from studies that have investigated the mechanical properties of human T2D bone tissue. The results from these studies have been conflicting, with the mechanical behaviour of T2D human tissue varying substantially across the different tissue types tested. Farr et al. (2014) has presented the only in vivo data to demonstrate that the mechanical properties of T2D tissue are impaired, where in vivo RPI was used to establish that bone material strength was lower in the cortical bone of T2D patients compared to non-T2D controls. Interestingly, many other studies on ex vivo tissue have actually found improved or unchanged mechanical properties of the trabecular bone (Karim et al. 2018; Hunt et al. 2018; Parle et al. 2020; Wölfel et al. 2020). However, a study (Sihota et al. 2021) looking at T2D trabecular bone after first fragility fracture found impaired mechanical properties.

Karim et al. (2018) tested trabecular cores from the femoral head under uniaxial compression and found no change in the mechanical properties. However, cortical bone from the femoral neck was also tested using cRPI, revealing a greater creep indentation distance and indentation distance increase in T2D bone compared to non-T2D suggesting a reduction in the mechanical properties of T2D cortical bone. No significant differences were found in microarchitecture or AGE accumulation of T2D bone compared to non-T2D bone and measured AGEs in bone were unrelated to bone biomechanical properties. Hunt et al. (2019) found that trabecular specimens from the femoral neck of T2D patients had increased modulus, yield stress, and ultimate stress. Additionally, the T2D samples trended toward a greater BV/TV and had significantly higher mineral content than the non-T2D samples. Parle et al. (2020) used similar approaches to evaluate the mechanical response of trabecular specimens from the femoral head, finding no difference in mechanical behaviour, although the bone mineral in T2D samples was more heterogeneously distributed compared to non-diabetic controls. Wölfel et al. (2020) found that high cortical porosity was occasionally present in T2D bone and that this generally coincided

with changes in the mineralisation pattern. Tissue-level biomechanical properties were measured using nanoindentation and no differences were found in T2D patients with or without high porosity, compared to non-T2D patients. Additionally, Wölfel et al. (2022) used cRPI and found impaired mechanical properties in cortical bone, from the femur and vertebrae, in T2D patients with high porosity (T2DwHP). Piccoli et al. (2020) tested trabecular bone from femoral heads of postmenopausal women using uniaxial compression and found similar BMD and biomechanical properties in T2D and non-T2D samples. However, they found that T2D affected the expression of several genes that are linked to bone formation. Furthermore, they observed that the accumulation of AGEs, in both T2D and non-diabetic bone, was negatively correlated with volumetric BMD, BV/TV and positively correlated with trabecular separation and spacing. Sihota et al. (2021) found impaired mechanical properties of T2D trabecular bone, from the femoral head, after a first hip fragility fracture using compression and nanoindentation testing, when compared to non-T2D samples. Yadav et al. (2022) investigated the viscoelastic behaviour of T2D trabecular bone in comparison to OP and osteopoenic samples. The findings showed that T2D does not affect the time-dependent response of human femoral trabecular bone. Cirovic et al. (2022) used Vickers microhardness testing to show that T2D had lower cortical and trabecular bone microhardness, in the femoral neck, compared to non-T2D samples. Lekkala et al. (2023) examined T2D trabecular and cortical bone from the iliac crest of postmenopausal women using nanoindentation and found that T2D had a higher stiffness and hardness compared to non-T2D samples. Sacher et al. (2022) examined microdamage accumulation in T2D trabecular bone, in the femoral neck, after monotonic compression to 3% strain and found that samples altered distribution of microdamage in the T2D group compared to the non-T2D group. The non-T2D samples displayed a higher proportion of damaged rods per volume compared to plates per volume, in contrast this difference was not present in the T2D samples. However, the total damage accumulation did not differ between groups. To date,

the cyclic behaviour and the role of microdamage accumulation on the biomechanical performance of human T2D bone has not yet been investigated.

Table 2.9 Mechanical results from human T2D bone studies. (↑= T2D bone increase compared to non-T2D, ↓= T2D decreased compared to non-T2D, - = no difference, blank did not measure or report) xlink=crosslink

Mechanical Properties	**Karim et al. 2018**	**Hunt et al. 2019**	**Parle et al. 2020**	**Wölfel et al. 2020**	**Picolli et al. 2020**	**Sihota et al. 2021**	**Yadav et al. 2022**	**Cirovic et al. 2022**	**Wölfel et al. 2022**	**Lekkala et al. 2023**
Modulus	-	↑	-		-	↓				
Yield Stress	-	↑	-		-	↓				
Yield Strain		-	-			-				
Ultimate Stress	-	↑	-		-	↓				
Ultimate Strain		-	-			-				
Post-yield Toughness	-	-	-			↓				
Post-yield Strain			-			-				
Apparent level toughness						↓				
Modulus (Nanoindented)				-		↓			-	↑ Cortical
Hardness (Nanoindented)				-		↓			-	↑ Cortical
Micro Hardness								↓		
Total Indentation Distance									↑T2DwHP	
Creep Indentation Distance	↑								↑T2DwHP	
Indentation Distance Increase	↑								↑T2DwHP	
Normalised shear moduli (G1 Viscoelastic)							-			
Normalised shear moduli (G2 Viscoelastic)							-			
Short Relaxation (Stress Relaxed)							-			
Long Relaxation (Stress Relaxed)							-			
Mean Storage Modulus (Stress Relaxed)							↓			
Mean Loss Modulus (Stress Relaxed)							-			
Compositional Properties										
Mineral-to-matrix Raio		↑		↑		↓	↓		-	-
Sugar Matrix Ratio		↑								
Carbonate to Phosphate Ratio		-		-		-			-	-
Crystallinity		-		-		-			-	-
Mineral Maturity		-		-						-
Acid Phosphate Content		-		-		-				
Enzymatic xlink Ratio		-				↓	↓			
Non-enzymatic xlink Ratio		↑	-			↑	↑			↑ Cortical
Fluorescent AGE	-	-		-	↑	↑	↑		-	↑
Pentosidine Serum	-						↑			
Pentosidine Bone		↑								↑
CML				↑						
Morphology										
BV/TV	-	-	-		-	↓	↓	-		
Tb.Th	-	-	-		-	↓	↓	-		
Tb.Sp	-	↓	-		-	-		-		
Tb.N	-	-	-		-	↓		-		
SMI	-		-			↑		↑		
Conn. D	-	-	-		-			-		
TMD	-				-					
BMD					-					
Cortical Porosity	-			↑T2DwHP					↑T2DwHP	

2.7 References

Adachi, T., K. I. Tsubota, Y. Tomita, and J. H. Scott. 2001. 'Trabecular surface remodeling simulation for cancellous bone using microstructural voxel finite element models', *Journal of Biomechanical Engineering*, 123: 403-09.

Ahn, Sang Bong, Elizabeth E Powell, Anthony Russell, Gunter Hartel, Katharine M Irvine, Chris Moser, and Patricia C Valery. 2020. 'Type 2 diabetes: a risk factor for hospital readmissions and mortality in Australian patients with cirrhosis', *Hepatology communications*, 4: 1279-92.

Allison, Hollie, and Laoise M McNamara. 2019. 'Inhibition of osteoclastogenesis by mechanically stimulated osteoblasts is attenuated during estrogen deficiency', *American Journal of Physiology-Cell Physiology*, 317: C969-C82.

Ansari, Nadeem A, and Debabrata Dash. 2013. 'Amadori glycated proteins: role in production of autoantibodies in diabetes mellitus and effect of inhibitors on non-enzymatic glycation', *Aging and disease*, 4: 50.

Arakawa, Shoutaro, Ryusuke Suzuki, Daisaburo Kurosaka, Ryo Ikeda, Hiroteru Hayashi, Tomohiro Kayama, Rei-ichi Ohno, Ryoji Nagai, Keishi Marumo, and Mitsuru Saito. 2020. 'Mass spectrometric quantitation of AGEs and enzymatic crosslinks in human cancellous bone', *Scientific Reports*, 10: 18774.

Ashman, RB, JY Rho, and CH Turner. 1989. 'Anatomical variation of orthotropic elastic moduli of the proximal human tibia', *Journal of Biomechanics*, 22: 895-900.

Bayraktar, Harun H., Elise F. Morgan, Glen L. Niebur, Grayson E. Morris, Eric K. Wong, and Tony M. Keaveny. 2004. 'Comparison of the elastic and yield properties of human femoral trabecular and cortical bone tissue', *Journal of Biomechanics*, 37: 27-35.

Bonds, Denise E., Joseph C. Larson, Ann V. Schwartz, Elsa S. Strotmeyer, John Robbins, Beatriz L. Rodriguez, Karen C. Johnson, and Karen L. Margolis. 2006. 'Risk of Fracture in Women with Type 2 Diabetes: the Women's Health Initiative Observational Study', *The Journal of Clinical Endocrinology & Metabolism*, 91: 3404-10.

Boskey, Adele L., and Laurianne Imbert. 2017. 'Bone quality changes associated with aging and disease: a review', *Annals of the New York Academy of Sciences*, 1410: 93-106.

Bouxsein, Mary L., Stephen K. Boyd, Blaine A. Christiansen, Robert E. Guldberg, Karl J. Jepsen, and Ralph Müller. 2010. 'Guidelines for assessment of bone microstructure in rodents using micro-computed tomography', *JOURNAL OF BONE AND MINERAL RESEARCH*, 25: 1468-86.

Brandi, Maria Luisa. 2009. 'Microarchitecture, the key to bone quality', *Rheumatology (United Kingdom)*, 48.

Burghardt, Andrew J., Ahi S. Issever, Ann V. Schwartz, Kevin A. Davis, Umesh Masharani, Sharmila Majumdar, and Thomas M. Link. 2010. 'High-Resolution Peripheral Quantitative Computed Tomographic Imaging of Cortical and Trabecular Bone Microarchitecture in Patients with Type 2 Diabetes Mellitus', *The Journal of Clinical Endocrinology & Metabolism*, 95: 5045-55.

Burr, David B, and Matthew R Allen. 2019. *Basic and applied bone biology* (Academic Press).

Burstein, A. H., D. T. Reilly, and M. Martens. 1976. 'Aging of bone tissue: mechanical properties', *J Bone Joint Surg Am*, 58: 82-6.

Busse, Björn, Michael Hahn, Markus Soltau, Jozef Zustin, Klaus Püschel, Georg N. Duda, and Michael Amling. 2009. 'Increased calcium content and inhomogeneity of mineralization render bone toughness in osteoporosis: Mineralization, morphology and biomechanics of human single trabeculae', *Bone*, 45: 1034-43.

Carter, D. R., M. C. H. Van der Meulen, and G. S. Beaupré. 1996. 'Mechanical factors in bone growth and development', *Bone*, 18: S5-S10.

Chao Le Meng, Bao, Y. Teo Erin, S. K. Chong Mark, Liu Yuchun, Choolani Mahesh, and K. Y. Chan Jerry. 2013. 'Advances in Bone Tissue Engineering.' in A. Andrades Jose (ed.), *Regenerative Medicine and Tissue Engineering* (IntechOpen: Rijeka).

Cho, N. H., J. E. Shaw, S. Karuranga, Y. Huang, J. D. da Rocha Fernandes, A. W. Ohlrogge, and B. Malanda. 2018. 'IDF Diabetes Atlas: Global estimates of diabetes prevalence for 2017 and projections for 2045', *Diabetes Research and Clinical Practice*, 138: 271-81.

Ciarelli, TE, DP Fyhrie, MB Schaffler, and SA Goldstein. 2000. 'Variations in three-dimensional cancellous bone architecture of the proximal femur in female hip fractures and in controls', *JOURNAL OF BONE AND MINERAL RESEARCH*, 15: 32-40.

Cirovic, Aleksandar, Jelena Jadzic, Danica Djukic, Danijela Djonic, Vladimir Zivkovic, Slobodan Nikolic, Marija Djuric, and Petar Milovanovic. 2022. 'Increased Cortical Porosity, Reduced Cortical Thickness, and Reduced Trabecular and Cortical Microhardness of the Superolateral Femoral Neck Confer the Increased Hip Fracture Risk in Individuals with Type 2 Diabetes', *Calcified Tissue International*, 111: 457-65.

Clynes, Michael A, Nicholas C Harvey, Elizabeth M Curtis, Nicholas R Fuggle, Elaine M Dennison, and Cyrus Cooper. 2020. 'The epidemiology of osteoporosis', *British medical bulletin*.

Cuppone, M., B. B. Seedhom, E. Berry, and A. E. Ostell. 2004. 'The Longitudinal Young's Modulus of Cortical Bone in the Midshaft of Human Femur and its Correlation with CT Scanning Data', *Calcified Tissue International*, 74: 302-09.

Currey, John D. 2012. 'The structure and mechanics of bone', *Journal of Materials Science*, 47: 41-54.

Dall'Ara, E., D. Pahr, P. Varga, F. Kainberger, and P. Zysset. 2012. 'QCT-based finite element models predict human vertebral strength in vitro significantly better than simulated DEXA', *Osteoporosis International*, 23: 563-72.

Damrath, John G, Amy Creecy, Joseph M Wallace, and Sharon M Moe. 2021. 'The impact of advanced glycation end products on bone properties in chronic kidney disease', *Current Opinion in Nephrology and Hypertension*, 30: 411-17.

Danielsson, Per-Erik. 1980. 'Euclidean distance mapping', *Computer Graphics and image processing*, 14: 227-48.

Diabetes-Ireland. 2018. "Diabetes Ireland. Diabetes Ireland highlights escalating cost of treating diabetes complications to TDs on World Diabetes Day." In.: Diabetes Ireland.

Dong, X Neil, and X Edward Guo. 2004. 'The dependence of transversely isotropic elasticity of human femoral cortical bone on porosity', *Journal of Biomechanics*, 37: 1281-87.

Dong, X. Neil, An Qin, Jiake Xu, and Xiaodu Wang. 2011. 'In situ accumulation of advanced glycation endproducts (AGEs) in bone matrix and its correlation with osteoclastic bone resorption', *Bone*, 49: 174-83.

Dong, Xuanliang N, Rae L Acuna, Qing Luo, and Xiaodu Wang. 2012. 'Orientation dependence of progressive post-yield behavior of human cortical bone in compression', *Journal of Biomechanics*, 45: 2829-34.

Donnelly, E. 2011. 'Methods for assessing bone quality: a review', *Clin Orthop Relat Res*, 469: 2128-38.

Dyer, Daniel G, John A Dunn, Suzanne R Thorpe, Karen E Bailie, Timothy J Lyons, David R McCance, and John W Baynes. 1993. 'Accumulation of Maillard reaction products in skin collagen in diabetes and aging', *The Journal of clinical investigation*, 91: 2463-69.

Fantner, Georg E., Tue Hassenkam, Johannes H. Kindt, James C. Weaver, Henrik Birkedal, Leonid Pechenik, Jacqueline A. Cutroni, Geraldo A. G. Cidade, Galen D. Stucky, Daniel E. Morse, and Paul K. Hansma. 2005. 'Sacrificial bonds and hidden length dissipate energy as mineralized fibrils separate during bone fracture', *Nature Materials*, 4: 612-16.

Farr, Joshua N., Matthew T. Drake, Shreyasee Amin, L. Joseph Melton, Louise K. McCready, and Sundeep Khosla. 2014. 'In vivo assessment of bone quality in postmenopausal women with type 2 diabetes', *JOURNAL OF BONE AND MINERAL RESEARCH*, 29.

Ferreira, F., M. A. Vaz, and J. A. Simões. 2006. 'Mechanical properties of bovine cortical bone at high strain rate', *Materials Characterization*, 57: 71-79.

Fessel, Gion, Yufei Li, Vincent Diederich, Manuel Guizar-Sicairos, Philipp Schneider, David R. Sell, Vincent M. Monnier, and Jess G. Snedeker. 2014. 'Advanced Glycation End-Products Reduce Collagen Molecular Sliding to Affect Collagen Fibril Damage Mechanisms but Not Stiffness', *PLOS ONE*, 9: e110948.

Frost, H. M. 1987. 'Bone "mass" and the "mechanostat": A proposal', *The Anatomical Record*, 219: 1-9.

Frost, Harold M. 2003. 'Bone's mechanostat: A 2003 update', *The Anatomical Record Part A: Discoveries in Molecular, Cellular, and Evolutionary Biology*, 275A: 1081-101.

Gangoiti, María Virginia, Verónica Arnol, Ana María Cortizo, and Antonio Desmond McCarthy. 2013. 'Advanced glycation endproducts and alendronate differentially inhibit early and late osteoclastogenesis in vitro', *Journal of Diabetes and Metabolism*, 4.

Gautieri, Alfonso, Fabian S. Passini, Unai Silván, Manuel Guizar-Sicairos, Giulia Carimati, Piero Volpi, Matteo Moretti, Herbert Schoenhuber, Alberto Redaelli, Martin Berli, and Jess G. Snedeker. 2017. 'Advanced glycation end-products: Mechanics of aged collagen from molecule to tissue', *Matrix Biology*, 59: 95-108.

Genant, Harry K, Cyrus Cooper, Gyula Poor, Ian Reid, George Ehrlich, J Kanis, BE Christopher Nordin, Elizabeth Barrett-Connor, Dennis Black, and JP Bonjour. 1999. 'Interim report and recommendations of the World Health Organization task-force for osteoporosis', *Osteoporosis International*, 10: 259.

Ghodsi, M., B. Larijani, A. A. Keshtkar, E. Nasli-Esfahani, S. Alatab, and M. R. Mohajeri-Tehrani. 2016. 'Mechanisms involved in altered bone metabolism in diabetes: a narrative review', *J Diabetes Metab Disord*, 15: 52.

Giangregorio, Lora M, William D Leslie, Lisa M Lix, Helena Johansson, Anders Oden, Eugene McCloskey, and John A Kanis. 2012. 'FRAX underestimates fracture risk in patients with diabetes', *JOURNAL OF BONE AND MINERAL RESEARCH*, 27: 301-08.

Gibson, L. J. 1985. 'The mechanical behaviour of cancellous bone', *Journal of Biomechanics*, 18: 317-28.

Gibson, Lorna J. 2005. 'Biomechanics of cellular solids', *Journal of Biomechanics*, 38: 377-99.

Goulet, Robert W, Steven A Goldstein, Michael J Ciarelli, Janet L Kuhn, MB Brown, and LA Feldkamp. 1994. 'The relationship between the structural and orthogonal compressive properties of trabecular bone', *Journal of Biomechanics*, 27: 375-89.

Gourlay, Margaret L, Jason P Fine, John S Preisser, Ryan C May, Chenxi Li, Li-Yung Lui, David F Ransohoff, Jane A Cauley, and Kristine E Ensrud. 2012. 'Bone-density testing interval and transition to osteoporosis in older women', *New England journal of medicine*, 366: 225-33.

Grandhee, SK, and VM Monnier. 1991. 'Mechanism of formation of the Maillard protein cross-link pentosidine. Glucose, fructose, and ascorbate as pentosidine precursors', *Journal of Biological Chemistry*, 266: 11649-53.

Graves, D. T., and R. A. Kayal. 2008. 'Diabetic complications and dysregulated innate immunity', *Front Biosci*, 13: 1227-39.

Green, Jessica O., Jason Wang, Tamim Diab, Brani Vidakovic, and Robert E. Guldberg. 2011. 'Age-related differences in the morphology of microdamage propagation in trabecular bone', *Journal of Biomechanics*, 44: 2659-66.

Hadjidakis, D. J., and I. I. Androulakis. 2006. 'Bone Remodeling', *Annals of the New York Academy of Sciences*, 1092: 385-96.

Hahn, GT. 1984. 'The influence of microstructure on brittle fracture toughness', *Metallurgical and Materials Transactions A*, 15: 947-59.

Hauschka, Peter V, and Steven A Carr. 1982. 'Calcium-dependent. alpha.-helical structure in osteocalcin', *Biochemistry*, 21: 2538-47.

Hayes, WC, and DR Carter. 1976. 'Postyield behavior of subchondral trabecular bone', *Journal of Biomedical Materials Research*, 10: 537-44.

Hayes, Wilson C. 1991. 'Biomechanics of cortical and trabecular bone: implications for assessment of fracture risk', *Basic orthopaedic biomechanics*: 93-142.

Hayes, Wilson C., Stephen J. Piazza, and Philippe K. Zysset. 1991. 'Biomechanics of Fracture Risk Prediction of the Hip and Spine by Quantitative Computed Tomography', *Radiologic Clinics of North America*, 29: 1-18.

Heilmeier, U., K. Cheng, C. Pasco, R. Parrish, J. Nirody, J. M. Patsch, C. A. Zhang, G. B. Joseph, A. J. Burghardt, A. V. Schwartz, T. M. Link, and G. Kazakia. 2016. 'Cortical bone laminar analysis reveals increased midcortical and periosteal porosity in type 2 diabetic postmenopausal women with history of fragility fractures compared to fracture-free diabetics', *Osteoporosis International*, 27: 2791-802.

Hein, G, R Wiegand, G Lehmann, G Stein, and S Franke. 2003. 'Advanced glycation end-products pentosidine and Nϵ-carboxymethyllysine are elevated in serum of patients with osteoporosis', *Rheumatology*, 42: 1242-46.

Hernandez, C. J., G. S. Beaupré, T. S. Keller, and D. R. Carter. 2001. 'The influence of bone volume fraction and ash fraction on bone strength and modulus', *Bone*, 29: 74-78.

Hernlund, Emma, A Svedbom, M Ivergård, J Compston, Cyrus Cooper, J Stenmark, Eugene V McCloskey, BKJA Jönsson, and John A Kanis. 2013. 'Osteoporosis in the European Union: medical management, epidemiology and economic burden: a report prepared in collaboration with the International Osteoporosis Foundation (IOF) and the European Federation of Pharmaceutical Industry Associations (EFPIA)', *Archives of Osteoporosis*, 8: 1-115.

Hildebrand, T., and P. Rüegsegger. 1997a. 'A new method for the model-independent assessment of thickness in three-dimensional images', *Journal of Microscopy*, 185: 67-75.

Hildebrand, Tor, Andres Laib, Ralph Müller, Jan Dequeker, and Peter Rüegsegger. 1999. 'Direct three-dimensional morphometric analysis of human cancellous bone: microstructural data from spine, femur, iliac crest, and calcaneus', *JOURNAL OF BONE AND MINERAL RESEARCH*, 14: 1167-74.

Hildebrand, TOR, and Peter Rüegsegger. 1997b. 'Quantification of bone microarchitecture with the structure model index', *Computer Methods in Biomechanics and Bio Medical Engineering*, 1: 15-23.

Hillier, Maria L., and Lynne S. Bell. 2007. 'Differentiating Human Bone from Animal Bone: A Review of Histological Methods', *Journal of Forensic Sciences*, 52: 249-63.

Homminga, J., B. R. McCreadie, T. E. Ciarelli, H. Weinans, S. A. Goldstein, and R. Huiskes. 2002. 'Cancellous bone mechanical properties from normals and patients with hip fractures differ on the structure level, not on the bone hard tissue level', *Bone*, 30: 759-64.

Huiskes, Rik, HHJG Weinans, HJ Grootenboer, M Dalstra, B Fudala, and TJ Slooff. 1987. 'Adaptive bone-remodeling theory applied to prosthetic-design analysis', *Journal of Biomechanics*, 20: 1135-50.

Hunt, H. B., and E. Donnelly. 2016. 'Bone quality assessment techniques: geometric, compositional, and mechanical characterization from macroscale to nanoscale', *Clin Rev Bone Miner Metab*, 14: 133-49.

Hunt, Heather B, Jared C Pearl, David R Diaz, Karen B King, and Eve Donnelly. 2018. 'Bone tissue collagen maturity and mineral content increase with sustained hyperglycemia in the KK-Ay murine model of type 2 diabetes', *JOURNAL OF BONE AND MINERAL RESEARCH*, 33: 921-29.

Hunt, Heather B., Ashley M. Torres, Pablo M. Palomino, Eric Marty, Rehan Saiyed, Matthew Cohn, Jonathan Jo, Stephen Warner, Grazyna E. Sroga, Karen B. King, Joseph M. Lane, Deepak Vashishth, Christopher J. Hernandez, and Eve Donnelly. 2019. 'Altered Tissue Composition, Microarchitecture, and Mechanical Performance in Cancellous Bone From Men With Type 2 Diabetes Mellitus', *JOURNAL OF BONE AND MINERAL RESEARCH*: jbmr.3711-jbmr.11.

Janghorbani, M., R. M. Van Dam, W. C. Willett, and F. B. Hu. 2007. 'Systematic Review of Type 1 and Type 2 Diabetes Mellitus and Risk of Fracture', *American Journal of Epidemiology*, 166: 495-505.

Jia, Shaowei, He Gong, Haipeng Cen, Peipei Shi, Rui Zhang, Zhaowei Li, and Xuewei Bi. 2021. 'Influence of non-enzymatic glycation on the mechanical properties of cortical bone', *Journal of the Mechanical Behavior of Biomedical Materials*, 119: 104553-53.

Kabel, J., A. Odgaard, B. van Rietbergen, and R. Huiskes. 1999. 'Connectivity and the elastic properties of cancellous bone', *Bone*, 24: 115-20.

Kanis, J. A., A. Oden, H. Johansson, F. Borgström, O. Ström, and E. McCloskey. 2009. 'FRAX and its applications to clinical practice', *Bone*, 44: 734-43.

Karim, Lamya, and Mary L. Bouxsein. 2016. 'Effect of type 2 diabetes-related non-enzymatic glycation on bone biomechanical properties', *Bone*, 82: 21-27.

Karim, Lamya, Julia Moulton, Miranda Van Vliet, Kelsey Velie, Ann Robbins, Fatemeh Malekipour, Ayesha Abdeen, Douglas Ayres, and Mary L. Bouxsein. 2018. 'Bone microarchitecture, biomechanical properties, and advanced glycation end-products in the proximal femur of adults with type 2 diabetes', *Bone*, 114: 32-39.

Katayama, Yasuyuki, Takuhiko Akatsu, Michiko Yamamoto, Nobuo Kugai, and Naokazu Nagata. 1996. 'Role of nonenzymatic glycosylation of type I collagen in diabetic osteopenia', *JOURNAL OF BONE AND MINERAL RESEARCH*, 11: 931-37.

Katzenberger, Michael J., Devon L. Albert, Amanda M. Agnew, and Andrew R. Kemper. 2020. 'Effects of sex, age, and two loading rates on the tensile material properties of human rib cortical bone', *Journal of the Mechanical Behavior of Biomedical Materials*, 102: 103410.

Keaveny, T. M., T. P. Pinilla, R. P. Crawford, D. L. Kopperdahl, and A. Lou. 1997. 'Systematic and random errors in compression testing of trabecular bone', *Journal of Orthopaedic Research*, 15: 101-10.

Keaveny, Tony M., Edward F. Wachtel, and David L. Kopperdahl. 1999. 'Mechanical behavior of human trabecular bone after overloading', *Journal of Orthopaedic Research*, 17: 346-53.

Keller, Tony S. 1994. 'Predicting the compressive mechanical behavior of bone', *Journal of Biomechanics*, 27: 1159-68.

Kennedy, Oran D., Damien M. Laudier, Robert J. Majeska, Hui B. Sun, and Mitchell B. Schaffler. 2014. 'Osteocyte apoptosis is required for production of osteoclastogenic signals following bone fatigue in vivo', *Bone*, 64: 132-37.

Khan, Moien Abdul Basith, Muhammad Jawad Hashim, Jeffrey Kwan King, Romona Devi Govender, Halla Mustafa, and Juma Al Kaabi. 2020. 'Epidemiology of Type 2 diabetes

- Global burden of disease and forecasted trends', *Journal of Epidemiology and Global Health*, 10: 107-11.

Klose-Jensen, R., J. J. Tse, K. K. Keller, C. Barnabe, A. J. Burghardt, S. Finzel, L. S. Tam, E. M. Hauge, K. S. Stok, and S. L. Manske. 2020. 'High-Resolution Peripheral Quantitative Computed Tomography for Bone Evaluation in Inflammatory Rheumatic Disease', *Front Med (Lausanne)*, 7: 337.

Kopperdahl, David L., and Tony M. Keaveny. 1998. 'Yield strain behavior of trabecular bone', *Journal of Biomechanics*, 31: 601-08.

Kume, Shinichiro, Seiya Kato, Sho-ichi Yamagishi, Yosuke Inagaki, Seiji Ueda, Nobuyuki Arima, Takahiro Okawa, Masamichi Kojiro, and Kensei Nagata. 2005. 'Advanced Glycation End-Products Attenuate Human Mesenchymal Stem Cells and Prevent Cognate Differentiation Into Adipose Tissue, Cartilage, and Bone', *JOURNAL OF BONE AND MINERAL RESEARCH*, 20: 1647-58.

Kunutsor, Setor Kwadzo, Tanefa Antoinette Apekey, and Jari Antero Laukkanen. 2015. 'Association of serum total osteocalcin with type 2 diabetes and intermediate metabolic phenotypes: systematic review and meta-analysis of observational evidence', *European journal of epidemiology*, 30: 599-614.

Lacroix, Damien. 2019. '3 - Biomechanical aspects of bone repair.' in Kendell M. Pawelec and Josep A. Planell (eds.), *Bone Repair Biomaterials (Second Edition)* (Woodhead Publishing).

Laib, A, T Hildebrand, HJ Häuselmann, and P Rüegsegger. 1997. 'Ridge number density: a new parameter for in vivo bone structure analysis', *Bone*, 21: 541-46.

Landis, Eric N, and Denis T Keane. 2010. 'X-ray microtomography', *Materials Characterization*, 61: 1305-16.

Launey, Maximilien E., Markus J. Buehler, and Robert O. Ritchie. 2010. 'On the Mechanistic Origins of Toughness in Bone', *Annual Review of Materials Research*, 40: 25-53.

Lekkala, Sashank, Sara E Sacher, Erik A Taylor, Rebecca M Williams, Kendall F Moseley, and Eve Donnelly. 2023. 'Increased advanced glycation endproducts, stiffness, and hardness in iliac crest bone from postmenopausal women with type 2 diabetes mellitus on insulin', *JOURNAL OF BONE AND MINERAL RESEARCH*, 38: 261-77.

Lerner, UH. 2006. 'Bone remodeling in post-menopausal osteoporosis', *Journal of dental research*, 85: 584-95.

Levinger, Itamar, Ego Seeman, George Jerums, Glenn K McConell, Mark S Rybchyn, Samantha Cassar, Elizabeth Byrnes, Steve Selig, Rebecca S Mason, and Peter R Ebeling. 2016. 'Glucose-loading reduces bone remodeling in women and osteoblast function in vitro', *Physiological reports*, 4: e12700.

Liang, Wenqing, Xudong Wu, Yongqiang Dong, Xuerong Chen, Ping Zhou, and Fangming Xu. 2021. 'Mechanical stimuli-mediated modulation of bone cell function—implications for bone remodeling and angiogenesis', *Cell and Tissue Research*, 386: 445-54.

Linde, Frank, and Ivan Hvid. 1989. 'The effect of constraint on the mechanical behaviour of trabecular bone specimens', *Journal of Biomechanics*, 22: 485-90.

Lochmüller, E. M., J. B. Zeller, D. Kaiser, F. Eckstein, J. Landgraf, R. Putz, and R. Steldinger. 1998. 'Correlation of femoral and lumbar DXA and calcaneal ultrasound, measured in situ with intact soft tissues, with the in vitro failure loads of the proximal femur', *Osteoporos Int*, 8: 591-8.

Loder, R. T. 1988. "The influence of diabetes mellitus on the healing of closed fractures." In *Clinical Orthopaedics and Related Research*, 210-16.

Lorensen, William E, and Harvey E Cline. 1987. 'Marching cubes: A high resolution 3D surface construction algorithm', *ACM siggraph computer graphics*, 21: 163-69.

Lucksanasombool, P., W. A. J. Higgs, R. J. E. D. Higgs, and M. V. Swain. 2001. 'Fracture toughness of bovine bone: influence of orientation and storage media', *Biomaterials*, 22: 3127-32.

Mandair, Gurjit S, and Michael D Morris. 2015. 'Contributions of Raman spectroscopy to the understanding of bone strength', *BoneKEy Reports*, 4: 620.

Mansell, J. P., and A. J. Bailey. 2003. 'Increased metabolism of bone collagen in post-menopausal female osteoporotic femoral heads', *The International Journal of Biochemistry & Cell Biology*, 35: 522-29.

Maquer, G., S. N. Musy, J. Wandel, T. Gross, and P. K. Zysset. 2015. 'Bone volume fraction and fabric anisotropy are better determinants of trabecular bone stiffness than other morphological variables', *J Bone Miner Res*, 30: 1000-8.

Martin, R Bruce, and David B Burr. 1989. *Structure, function, and adaptation of compact bone* (New York: Raven Press).

McCalden, Richard W, and Joseph A McGeough. 1997. 'Age-related changes in the compressive strength of cancellous bone. The relative importance of changes in density and trabecular architecture', *JBJS*, 79: 421-7.

McCarthy, Antonio Desmond, Toshimasa Uemura, Susana Beatriz Etcheverry, and Ana María Cortizo. 2004. 'Advanced glycation endproducts interfere with integrin-mediated osteoblastic attachment to a type-I collagen matrix', *International Journal of Biochemistry and Cell Biology*, 36: 840-48.

McNally, Elizabeth A, Henry P Schwarcz, Gianluigi A Botton, and A Larry Arsenault. 2012. 'A model for the ultrastructure of bone based on electron microscopy of ion-milled sections', *PLOS ONE*, 7: e29258.

McNamara, LM. 2010. 'Perspective on post-menopausal osteoporosis: establishing an interdisciplinary understanding of the sequence of events from the molecular level to whole bone fractures', *Journal of the Royal Society Interface*, 7: 353-72.

Melton, L. J., 3rd. 1995. 'How many women have osteoporosis now?', *J Bone Miner Res*, 10: 175-7.

Mercer, Natalia, Hafiz Ahmed, Susana B Etcheverry, Gerardo R Vasta, and Ana Maria Cortizo. 2007. 'Regulation of advanced glycation end product (AGE) receptors and apoptosis by AGEs in osteoblast-like cells', *Molecular and cellular biochemistry*, 306: 87-94.

Merlo, Kelly, Jacob Aaronson, Rachana Vaidya, Taraneh Rezaee, Vijaya Chalivendra, and Lamya Karim. 2020. 'In Vitro-Induced High Sugar Environments Deteriorate Human Cortical Bone Elastic Modulus and Fracture Toughness', *Journal of Orthopaedic Research®*, 38: 972-83.

Mirzaali, Mohammad J., J. Jakob Schwiedrzik, Suwanwadee Thaiwichai, James P. Best, Johann Michler, Philippe K. Zysset, and Uwe Wolfram. 2016. 'Mechanical properties of cortical bone and their relationships with age, gender, composition and microindentation properties in the elderly', *Bone*, 93: 196-211.

Miyata, Toshio, Kohei Notoya, Keiji Yoshida, Katsunori Horie, Kenji Maeda, Kiyoshi Kurokawa, and Shigehisa Taketomi. 1997. 'Advanced glycation end products enhance osteoclast-induced bone resorption in cultured mouse unfractionated bone cells and in rats implanted subcutaneously with devitalized bone particles', *Journal of the American Society of Nephrology*, 8: 260-70.

Monahan, Genna E, Jessica Schiavi-Tritz, Marissa Britton, and Ted J Vaughan. 2023. 'Longitudinal alterations in bone morphometry, mechanical integrity and composition in Type-2 diabetes in a Zucker diabetic fatty (ZDF) rat', *Bone*, 170: 116672.

Morgan, E. F., and T. M. Keaveny. 2001. 'Dependence of yield strain of human trabecular bone on anatomic site', *J Biomech*, 34: 569-77.

Morgan, E. F., G. U. Unnikrisnan, and A. I. Hussein. 2018. 'Bone Mechanical Properties in Healthy and Diseased States', *Annu Rev Biomed Eng*, 20: 119-43.

Morgan, Elise F., Harun H. Bayraktar, and Tony M. Keaveny. 2003. 'Trabecular bone modulus–density relationships depend on anatomic site', *Journal of Biomechanics*, 36: 897-904.

Morgan, S., A. A. Poundarik, and D. Vashishth. 2015. 'Do Non-collagenous Proteins Affect Skeletal Mechanical Properties?', *Calcif Tissue Int*, 97: 281-91.

Morris, M. D., and G. S. Mandair. 2011. 'Raman assessment of bone quality', *Clin Orthop Relat Res*, 469: 2160-9.

Musy, Sarah N., Ghislain Maquer, Jarunan Panyasantisuk, Jasmin Wandel, and Philippe K. Zysset. 2017. 'Not only stiffness, but also yield strength of the trabecular structure determined by non-linear µFE is best predicted by bone volume fraction and fabric tensor', *Journal of the Mechanical Behavior of Biomedical Materials*, 65: 808-13.

Nagai, Ryoji, Jun-ichi Shirakawa, Yukio Fujiwara, Rei-ichi Ohno, Narumi Moroishi, Noriyuki Sakata, and Mime Nagai. 2014. 'Detection of aGEs as markers for carbohydrate metabolism and protein denaturation', *Journal of clinical biochemistry and nutrition*, 55: 1-6.

Napoli, Nicola, Elsa S. Strotmeyer, Kristine E. Ensrud, Deborah E. Sellmeyer, Douglas C. Bauer, Andrew R. Hoffman, Thuy Tien L. Dam, Elizabeth Barrett-Connor, Lisa Palermo, Eric S. Orwoll, Steven R. Cummings, Dennis M. Black, and Ann V. Schwartz. 2014. 'Fracture risk in diabetic elderly men: The MrOS study', *Diabetologia*, 57: 2057-65.

Nazarian, Ara, John Muller, David Zurakowski, Ralph Müller, and Brian D Snyder. 2007. 'Densitometric, morphometric and mechanical distributions in the human proximal femur', *Journal of Biomechanics*, 40: 2573-79.

Norman, Timothy L, D Vashishth, and DB Burr. 1995. 'Fracture toughness of human bone under tension', *Journal of Biomechanics*, 28: 309-20.

Novitskaya, Ekaterina, Po-Yu Chen, Steve Lee, Ana Castro-Ceseña, Gustavo Hirata, Vlado A. Lubarda, and Joanna McKittrick. 2011. 'Anisotropy in the compressive mechanical properties of bovine cortical bone and the mineral and protein constituents', *Acta Biomaterialia*, 7: 3170-77.

O'Mahony, Aisling M, John L Williams, Jerald O Katz, and Paulette Spencer. 2000. 'Anisotropic elastic properties of cancellous bone from a human edentulous mandible', *Clinical Oral Implants Research*, 11: 415-21.

O'Sullivan, Laura. 2020. "Time-sequence of Biomechanical Adaption in Trabecular Tissue during Estrogen Deficiency." In.

O'Sullivan, L. M., H. Allison, E. E. Parle, J. Schiavi, and L. M. McNamara. 2020. 'Secondary alterations in bone mineralisation and trabecular thickening occur after long-term estrogen deficiency in ovariectomised rat tibiae, which do not coincide with initial rapid bone loss', *Osteoporosis International*, 31: 587-99.

Odgaard, A, and HJG Gundersen. 1993. 'Quantification of connectivity in cancellous bone, with special emphasis on 3-D reconstructions', *Bone*, 14: 173-82.

Odgaard, Anders, and Frank Linde. 1991. 'The underestimation of Young's modulus in compressive testing of cancellous bone specimens', *Journal of Biomechanics*, 24: 691-98.

Oei, Ling, M. Carola Zillikens, Abbas Dehghan, Gabriëlle H. S. Buitendijk, Martha C. Castaño-Betancourt, Karol Estrada, Lisette Stolk, Edwin H. G. Oei, Joyce B. J. Van Meurs, Joseph A. M. J. L. Janssen, Albert Hofman, Johannes P. T. M. Van Leeuwen, Jacqueline C. M. Witteman, Huibert A. P. Pols, André G. Uitterlinden, Caroline C. W. Klaver, Oscar H. Franco, and Fernando Rivadeneira. 2013. 'High bone mineral density

and fracture risk in type 2 diabetes as skeletal complications of inadequate glucose control: The Rotterdam study', *Diabetes Care*, 36: 1619-28.

Oftadeh, Ramin, Miguel Perez-Viloria, Juan C. Villa-Camacho, Ashkan Vaziri, and Ara Nazarian. 2015. 'Biomechanics and mechanobiology of trabecular bone: a review', *Journal of Biomechanical Engineering*, 137: 0108021-21.

Ogawa, N, T Yamaguchi, S Yano, M Yamauchi, M Yamamoto, and T Sugimoto. 2007. 'The combination of high glucose and advanced glycation end-products (AGEs) inhibits the mineralization of osteoblastic MC3T3-E1 cells through glucose-induced increase in the receptor for AGEs', *Hormone and metabolic research*, 39: 871-75.

Öhman, Caroline, Massimiliano Baleani, Egon Perilli, Enrico Dall'Ara, Simone Tassani, Fabio Baruffaldi, and Marco Viceconti. 2007. 'Mechanical testing of cancellous bone from the femoral head: Experimental errors due to off-axis measurements', *Journal of Biomechanics*, 40: 2426-33.

Oliver, Warren C, and Georges M Pharr. 2004. 'Measurement of hardness and elastic modulus by instrumented indentation: Advances in understanding and refinements to methodology', *Journal of materials research*, 19: 3-20.

Oliver, Warren Carl, and George Mathews Pharr. 1992. 'An improved technique for determining hardness and elastic modulus using load and displacement sensing indentation experiments', *Journal of materials research*, 7: 1564-83.

Osima, Marit, Rita Kral, Tove T. Borgen, Ingvild K. Høgestøl, Ragnar M. Joakimsen, Erik F. Eriksen, and Åshild Bjørnerem. 2017. 'Women with type 2 diabetes mellitus have lower cortical porosity of the proximal femoral shaft using low-resolution CT than nondiabetic women, and increasing glucose is associated with reduced cortical porosity', *Bone*, 97: 252-60.

Ottewell, P. D. 2016. 'The role of osteoblasts in bone metastasis', *J Bone Oncol*, 5: 124-27.

Parfitt, A. M., C. H. E. Mathews, A. B. Villanueva, M. Kleerekoper, B. Frame, and D. S. Rao. 1983. 'Relationships between surface, volume, and thickness of iliac trabecular bone in aging and in osteoporosis. Implications for the microanatomic and cellular mechanisms of bone loss', *Journal of Clinical Investigation*, 72: 1396-409.

Parle, Eoin, Sherdya Tio, Annie Behre, John J. Carey, Colin G. Murphy, Timothy F. O'Brien, William A. Curtin, Stephen R. Kearns, John P. McCabe, Cynthia M. Coleman, Ted J. Vaughan, and Laoise M. McNamara. 2020. 'Bone Mineral Is More Heterogeneously Distributed in the Femoral Heads of Osteoporotic and Diabetic Patients: A Pilot Study', *JBMR Plus*, 4: e10253-e53.

Paschou, Stavroula A, Anastasia D Dede, Panagiotis G Anagnostis, Andromachi Vryonidou, Daniel Morganstein, and Dimitrios G Goulis. 2017. 'Type 2 Diabetes and Osteoporosis: A Guide to Optimal Management', *The Journal of Clinical Endocrinology & Metabolism*, 102: 3621-34.

Patsch, Janina M., Andrew J. Burghardt, Samuel P. Yap, Thomas Baum, Ann V. Schwartz, Gabby B. Joseph, and Thomas M. Link. 2013. 'Increased cortical porosity in type 2 diabetic postmenopausal women with fragility fractures', *JOURNAL OF BONE AND MINERAL RESEARCH*, 28: 313-24.

Peterlik, Herwig, Paul Roschger, Klaus Klaushofer, and Peter Fratzl. 2006. 'From brittle to ductile fracture of bone', *Nature Materials*.

Pezzotti, Giuseppe, Alfredo Rondinella, Elia Marin, Wenliang Zhu, Nicolò Nicoli Aldini, Gianfranco Ulian, and Giovanni Valdrè. 2017. 'Raman spectroscopic investigation on the molecular structure of apatite and collagen in osteoporotic cortical bone', *Journal of the Mechanical Behavior of Biomedical Materials*, 65: 264-73.

Piccoli, Alessandra, Francesca Cannata, Rocky Strollo, Claudio Pedone, Giulia Leanza, Fabrizio Russo, Valentina Greto, Camilla Isgrò, Carlo Cosimo Quattrocchi, Carlo

Massaroni, Sergio Silvestri, Gianluca Vadalà, Tiziana Bisogno, Vincenzo Denaro, Paolo Pozzilli, Simon Y. Tang, Matt J. Silva, Caterina Conte, Rocco Papalia, Mauro Maccarrone, and Nicola Napoli. 2020. 'Sclerostin Regulation, Microarchitecture, and Advanced Glycation End-Products in the Bone of Elderly Women With Type 2 Diabetes', *JOURNAL OF BONE AND MINERAL RESEARCH*, 35: 2415-22.

Purnamasari, Dyah, Melisa D Puspitasari, Bambang Setiyohadi, Pringgodigdo Nugroho, and Harry Isbagio. 2017. 'Low bone turnover in premenopausal women with type 2 diabetes mellitus as an early process of diabetes-associated bone alterations: a cross-sectional study', *BMC endocrine disorders*, 17: 1-8.

Reilly, Donald T, Albert H Burstein, and Victor H Frankel. 1974. 'The elastic modulus for bone', *Journal of Biomechanics*, 7: 271-75.

Reinwald, Susan, Richard G. Peterson, Matt R. Allen, and David B. Burr. 2009. 'Skeletal changes associated with the onset of type 2 diabetes in the ZDF and ZDSD rodent models', *American Journal of Physiology - Endocrinology and Metabolism*, 296: E765-E65.

Reitsma, S., D. W. Slaaf, H. Vink, M. A. van Zandvoort, and M. G. oude Egbrink. 2007. 'The endothelial glycocalyx: composition, functions, and visualization', *Pflugers Arch*, 454: 345-59.

Rho, Jae-Young, Liisa Kuhn-Spearing, and Peter Zioupos. 1998. 'Mechanical properties and the hierarchical structure of bone', *Medical Engineering & Physics*, 20: 92-102.

Rho, Jae-Young, Ting Y Tsui, and George M Pharr. 1997. 'Elastic properties of human cortical and trabecular lamellar bone measured by nanoindentation', *Biomaterials*, 18: 1325-30.

Riggs, B. L., S. Khosla, and L. J. Melton, 3rd. 2002. 'Sex steroids and the construction and conservation of the adult skeleton', *Endocr Rev*, 23: 279-302.

Ritchie, R. O., K. J. Koester, S. Ionova, W. Yao, N. E. Lane, and J. W. Ager, 3rd. 2008. 'Measurement of the toughness of bone: a tutorial with special reference to small animal studies', *Bone*, 43: 798-812.

Ritter, Nadine M, Mary C Farach-Carson, and William T Butler. 1992. 'Evidence for the formation of a complex between osteopontin and osteocalcin', *JOURNAL OF BONE AND MINERAL RESEARCH*, 7: 877-85.

Robling, Alexander G., and Lynda F. Bonewald. 2020. 'The Osteocyte: New Insights', *Annual Review of Physiology*, 82: 485-506.

Røhl, Lisbeth, Ejnar Larsen, Frank Linde, Anders Odgaard, and Jørgen Jørgensen. 1991. 'Tensile and compressive properties of cancellous bone', *Journal of Biomechanics*, 24: 1143-49.

Rucci, N. 2008. 'Molecular biology of bone remodelling', *Clin Cases Miner Bone Metab*, 5: 49-56.

Saito, M, K Fujii, S Soshi, and T Tanaka. 2006a. 'Reductions in degree of mineralization and enzymatic collagen cross-links and increases in glycation-induced pentosidine in the femoral neck cortex in cases of femoral neck fracture', *Osteoporosis International*, 17: 986-95.

Saito, M., K. Fujii, Y. Mori, and K. Marumo. 2006b. 'Role of collagen enzymatic and glycation induced cross-links as a determinant of bone quality in spontaneously diabetic WBN/Kob rats', *Osteoporosis International*, 17: 1514-23.

Saito, Marumo, and KMSKM Marumo. 2010. 'Collagen cross-links as a determinant of bone quality: a possible explanation for bone fragility in aging, osteoporosis, and diabetes mellitus', *Osteoporosis International*, 21: 195-214.

Saito, Mitsuru, Katsuyuki Fujii, and Keishi Marumo. 2006c. 'Degree of mineralization-related collagen crosslinking in the femoral neck cancellous bone in cases of hip fracture and controls', *Calcified Tissue International*, 79: 160-68.

Saito, Mitsuru, and Keishi Marumo. 2015. 'Effects of Collagen Crosslinking on Bone Material Properties in Health and Disease', *Calcified Tissue International*, 97: 242-61.

Sanguineti, Roberta, Daniela Storace, Fiammetta Monacelli, Alberto Federici, and Patrizio Odetti. 2008. "Pentosidine effects on human osteoblasts in vitro." In *Annals of the New York Academy of Sciences*, 166-72. Blackwell Publishing Inc.

Sassi, Francesca, Ilaria Buondonno, Chiara Luppi, Elena Spertino, Emanuela Stratta, Marco Di Stefano, Marco Ravazzoli, Gianluca Isaia, Marina Trento, and Pietro Passera. 2018. 'Type 2 diabetes affects bone cells precursors and bone turnover', *BMC endocrine disorders*, 18: 1-8.

Scanco. 'SCANCO Medical FAQ', Accessed 13 March.

Schwartz, A. V. 2003. 'Diabetes Mellitus: Does it Affect Bone?', *Calcified Tissue International*, 73: 515-19.

Schwartz, Ann V., and Deborah E. Sellmeyer. 2007. 'Diabetes, fracture, and bone fragility', *Current Osteoporosis Reports*, 5: 105-11.

Schwartz, Ann V., Eric Vittinghoff, Douglas C. Bauer, Teresa A. Hillier, Elsa S. Strotmeyer, Kristine E. Ensrud, Meghan G. Donaldson, Jane A. Cauley, Tamara B. Harris, Annemarie Koster, Catherine R. Womack, Lisa Palermo, and Dennis M. Black. 2011. 'Association of BMD and FRAX score with risk of fracture in older adults with type 2 diabetes', *JAMA - Journal of the American Medical Association*, 305: 2184-92.

Seeman, Ego, and Pierre D. Delmas. 2006. "Mechanisms of Disease Bone Quality-The Material and Structural Basis of Bone Strength and Fragility." In.

Sell, David R. 1997. 'Ageing promotes the increase of early glycation Amadori product as assessed by ϵ-N-(2-furoylmethyl)-l-lysine (furosine) levels in rodent skin collagen: The relationship to dietary restriction and glycoxidation', *Mechanisms of ageing and development*, 95: 81-99.

Sensi, Maurizio, Flavia Pricci, Giuseppe Pugliese, Maria Grazia De Rossi, Antonio FG Petrucci, Angelo Cristina, Susanna Morano, Giuseppe Pozzessere, Elvira Valle, and Domenico Andreani. 1995. 'Role of advanced glycation end-products (AGE) in late diabetic complications', *Diabetes Research and Clinical Practice*, 28: 9-17.

Seref-Ferlengez, Z., O. D. Kennedy, and M. B. Schaffler. 2015. 'Bone microdamage, remodeling and bone fragility: how much damage is too much damage?', *Bonekey Rep*, 4: 644.

Shanbhogue, Vikram V., Stinus Hansen, Morten Frost, Niklas Rye Jørgensen, Anne Pernille Hermann, Jan Erik Henriksen, and Kim Brixen. 2016. 'Compromised cortical bone compartment in type 2 diabetes mellitus patients with microvascular disease', *European Journal of Endocrinology*, 174: 115-24.

Shi, Xiutao, Xiang Wang, and Glen L. Niebur. 2009. 'Effects of Loading Orientation on the Morphology of the Predicted Yielded Regions in Trabecular Bone', *Annals of Biomedical Engineering*, 37: 354-62.

Sihota, Praveer, Ram Naresh Yadav, Ruban Dhaliwal, Jagadeesh Chandra Bose, Vandana Dhiman, Deepak Neradi, Shailesh Karn, Sidhartha Sharma, Sameer Aggarwal, Vijay G. Goni, Vishwajeet Mehandia, Deepak Vashishth, Sanjay Kumar Bhadada, and Navin Kumar. 2021. 'Investigation of mechanical, material and compositional determinants of human trabecular bone quality in type 2 diabetes', *The Journal of Clinical Endocrinology & Metabolism*, XX: 1-19.

Singh, Varun Parkash, Anjana Bali, Nirmal Singh, and Amteshwar Singh Jaggi. 2014. 'Advanced glycation end products and diabetic complications', *The Korean journal of physiology & pharmacology: official journal of the Korean Physiological Society and the Korean Society of Pharmacology*, 18: 1.

Snedeker, J. G., and A. Gautieri. 2014. 'The role of collagen crosslinks in ageing and diabetes - the good, the bad, and the ugly', *Muscles Ligaments Tendons J*, 4: 303-8.

Sroga, Grażyna E, and Deepak Vashishth. 2012. 'Effects of bone matrix proteins on fracture and fragility in osteoporosis', *Current Osteoporosis Reports*, 10: 141-50.

Stefan, Unger, Blauth Michael, and Schmoelz Werner. 2010. 'Effects of three different preservation methods on the mechanical properties of human and bovine cortical bone', *Bone*, 47: 1048-53.

Strotmeyer, Elsa S., Jane A. Cauley, Ann V. Schwartz, Michael C. Nevitt, Helaine E. Resnick, Douglas C. Bauer, Frances A. Tylavsky, Nathalie de Rekeneire, Tamara B. Harris, and Anne B. Newman. 2005. 'Nontraumatic Fracture Risk With Diabetes Mellitus and Impaired Fasting Glucose in Older White and Black Adults', *Archives of Internal Medicine*, 165: 1612-12.

Suzuki, Akinobu, Akito Yabu, and Hiroaki Nakamura. 2022. 'Advanced glycation end products in musculoskeletal system and disorders', *Methods*, 203: 179-86.

Tanaka-Kamioka, Kayo, Hiroshi Kamioka, Hans Ris, and Soo-Siang Lim. 1998. 'Osteocyte shape is dependent on actin filaments and osteocyte processes are unique actin-rich projections', *JOURNAL OF BONE AND MINERAL RESEARCH*, 13: 1555-68.

Tanaka, Hiroaki, Takenori Yamashita, Misao Yoneda, Satoshi Takagi, and Toshihiro Miura. 2018. 'Characteristics of bone strength and metabolism in type 2 diabetic model Tsumura, Suzuki, Obese Diabetes mice', *Bone reports*, 9: 74-83.

Tang, S. Y. Y., U. Zeenath, and D. Vashishth. 2007. 'Effects of non-enzymatic glycation on cancellous bone fragility', *Bone*, 40: 1144-51.

Tavakol, Mahdi, and Ted J. Vaughan. 2020. 'The structural role of osteocalcin in bone biomechanics and its alteration in Type-2 Diabetes', *Scientific Reports*, 10: 17321-21.

———. 2022. 'Energy dissipation of osteopontin at a HAp mineral interface: Implications for bone biomechanics', *Biophysical Journal*, 121: 228-36.

Teo, J. C. M., K. M. Si-Hoe, J. E. L. Keh, and S. H. Teoh. 2007. 'Correlation of cancellous bone microarchitectural parameters from microCT to CT number and bone mechanical properties', *Materials Science and Engineering: C*, 27: 333-39.

Turner, C. H. 1992. 'Functional determinants of bone structure: Beyond Wolff's law of bone transformation', *Bone*, 13: 403-09.

Turner, Charles H, Jae Rho, Yuichi Takano, Ting Y Tsui, and George M Pharr. 1999. 'The elastic properties of trabecular and cortical bone tissues are similar: results from two microscopic measurement techniques', *Journal of Biomechanics*, 32: 437-41.

Twarda-Clapa, Aleksandra, Aleksandra Olczak, Aneta M Białkowska, and Maria Koziołkiewicz. 2022. 'Advanced Glycation End-Products (AGEs): Formation, Chemistry, Classification, Receptors, and Diseases Related to AGEs', *Cells*, 11: 1312.

Unal, Mustafa, Sasidhar Uppuganti, Calen J Leverant, Amy Creecy, Mathilde Granke, Paul Voziyan, and Jeffry S Nyman. 2018. 'Assessing glycation-mediated changes in human cortical bone with Raman spectroscopy', *Journal of biophotonics*, 11: e201700352.

Unnanuntana, A., B. P. Gladnick, E. Donnelly, and J. M. Lane. 2010. 'The assessment of fracture risk', *J Bone Joint Surg Am*, 92: 743-53.

Vaculík, J., M. Braun, P. Dungl, K. Pavelka, and J. J. Stepan. 2016. 'Serum and bone pentosidine in patients with low impact hip fractures and in patients with advanced osteoarthritis', *BMC Musculoskelet Disord*, 17: 308.

Valcourt, Ulrich, Blandine Merle, Evelyne Gineyts, Stéphanie Viguet-Carrin, Pierre D. Delmas, and Patrick Garnero. 2007. 'Non-enzymatic glycation of bone collagen modifies osteoclastic activity and differentiation', *Journal of Biological Chemistry*, 282: 5691-703.

Vashishth, D., G. J. Gibson, J. I. Khoury, M. B. Schaffler, J. Kimura, and D. P. Fyhrie. 2001. 'Influence of nonenzymatic glycation on biomechanical properties of cortical bone', *Bone*, 28: 195-201.

Vashishth, Deepak. 2007. 'Hierarchy of bone microdamage at multiple length scales', *International Journal of Fatigue*, 29: 1024-33.

Verbruggen, Stefaan W., Bernhard Kainz, Susan C. Shelmerdine, Joseph V. Hajnal, Mary A. Rutherford, Owen J. Arthurs, Andrew T. M. Phillips, and Niamh C. Nowlan. 2018. 'Stresses and strains on the human fetal skeleton during development', *Journal of the Royal Society Interface*, 15: 20170593.

Vestergaard, P. 2007. 'Discrepancies in bone mineral density and fracture risk in patients with type 1 and type 2 diabetes—a meta-analysis', *Osteoporosis International*, 18: 427-44.

Viguet-Carrin, S., D. Farlay, Y. Bala, F. Munoz, M. L. Bouxsein, and P. D. Delmas. 2008. 'An in vitro model to test the contribution of advanced glycation end products to bone biomechanical properties', *Bone*, 42: 139-49.

Wang, Ji, Bin Zhou, X. Sherry Liu, Aaron J. Fields, Arnav Sanyal, Xiutao Shi, Mark Adams, Tony M. Keaveny, and X. Edward Guo. 2015. 'Trabecular plates and rods determine elastic modulus and yield strength of human trabecular bone', *Bone*, 72: 71-80.

Wang, Jie, Wenjun You, Zhaohai Jing, Robin Wang, Zhengju Fu, and Yangang Wang. 2016. 'Increased risk of vertebral fracture in patients with diabetes: a meta-analysis of cohort studies', *International Orthopaedics*, 40: 1299-307.

Wang, Xin, Yu Wang, Wenlong Gou, Qiang Lu, Jiang Peng, and Shibi Lu. 2013. 'Role of mesenchymal stem cells in bone regeneration and fracture repair: a review', *International Orthopaedics*, 37: 2491-98.

Wang, XJ, XB Chen, PD Hodgson, and Cui'E Wen. 2006. 'Elastic modulus and hardness of cortical and trabecular bovine bone measured by nanoindentation', *Transactions of nonferrous metals society of china*, 16: s744-s48.

Webster, SS Jee, and S Jee. 1983. 'The skeletal tissues', *Histology. Elsevier Biomedical Press, Amsterdam*: 200-54.

Weiner, S., and H. D. Wagner. 1998. 'The material bone: Structure-mechanical function relations', *Annual Review of Materials Science*, 28: 271-98.

Whitehouse, WJ. 1974. 'The quantitative morphology of anisotropic trabecular bone', *Journal of Microscopy*, 101: 153-68.

Willett, Thomas L., Sibi Sutty, Anne Gaspar, Nick Avery, and Marc Grynpas. 2013. 'In vitro non-enzymatic ribation reduces post-yield strain accommodation in cortical bone', *Bone*, 52: 611-22.

Willett, Thomas L., Paul Voziyan, and Jeffry S. Nyman. 2022. 'Causative or associative: A critical review of the role of advanced glycation end-products in bone fragility', *Bone*, 163: 116485.

Wölfel, Eva M., Imke A. K. Fiedler, Sofie Dragoun Kolibova, Johannes Krug, Mei-Chun Lin, Bashar Yazigi, Anna K. Siebels, Herbert Mushumba, Birgit Wulff, Benjamin Ondruschka, Klaus Püschel, Claus C. Glüer, Katharina Jähn-Rickert, and Björn Busse. 2022. 'Human tibial cortical bone with high porosity in type 2 diabetes mellitus is accompanied by distinctive bone material properties', *Bone*, 165: 116546.

Wölfel, Eva M., Katharina Jähn-Rickert, Felix N. Schmidt, Birgit Wulff, Herbert Mushumba, Grazyna E. Sroga, Klaus Püschel, Petar Milovanovic, Michael Amling, Graeme M. Campbell, Deepak Vashishth, and Björn Busse. 2020. 'Individuals with type 2 diabetes mellitus show dimorphic and heterogeneous patterns of loss in femoral bone quality', *Bone*, 140: 115556-56.

Wolfram, Uwe, Hans-Joachim Wilke, and Philippe K Zysset. 2010. 'Valid μ finite element models of vertebral trabecular bone can be obtained using tissue properties measured with nanoindentation under wet conditions', *Journal of Biomechanics*, 43: 1731-37.

Woodside, Mitchell, and Thomas L. Willett. 2016. 'Elastic–plastic fracture toughness and rising JR-curve behavior of cortical bone is partially protected from irradiation–sterilization-induced degradation by ribose protectant', *Journal of the Mechanical Behavior of Biomedical Materials*, 64: 53-64.

Wu, Dan, Per Isaksson, Stephen J. Ferguson, and Cecilia Persson. 2018. 'Young's modulus of trabecular bone at the tissue level: A review', *Acta Biomaterialia*, 78: 1-12.

Yadav, Ram Naresh, Praveer Sihota, Deepak Neradi, Jagadeesh Chandra Bose, Vandana Dhiman, Shailesh Karn, Sidhartha Sharma, Sameer Aggarwal, Vijay G. Goni, Sanjay Kumar Bhadada, and Navin Kumar. 2022. 'Effects of type 2 diabetes on the viscoelastic behavior of human trabecular bone', *Medical Engineering & Physics*, 104: 103810.

Yamagishi, Sho-ichi. 2011. 'Role of advanced glycation end products (AGEs) and receptor for AGEs (RAGE) in vascular damage in diabetes', *Experimental gerontology*, 46: 217-24.

Yan, Jiahau, Amit Daga, Rajendra Kumar, and John J. Mecholsky. 2008. 'Fracture toughness and work of fracture of hydrated, dehydrated, and ashed bovine bone', *Journal of Biomechanics*, 41: 1929-36.

Yu, E. W., M. S. Putman, N. Derrico, G. Abrishamanian-Garcia, J. S. Finkelstein, and M. L. Bouxsein. 2014. 'Defects in cortical microarchitecture among African-American women with type 2 diabetes', *Osteoporosis International*, 26: 673-79.

Zhang, Liping, Yaping Liu, Dong Wang, Xinbo Zhao, Zhanjun Qiu, Hong Ji, and Haiqin Rong. 2009. 'Bone biomechanical and histomorphometrical investment in type 2 diabetic Goto-Kakizaki rats', *Acta Diabetologica*, 46: 119-26.

Zimmermann, Elizabeth A., Eric Schaible, Hrishikesh Bale, Holly D. Barth, Simon Y. Tang, Peter Reichert, Bjoern Busse, Tamara Alliston, Joel W. Ager, and Robert O. Ritchie. 2011. 'Age-related changes in the plasticity and toughness of human cortical bone at multiple length scales', *Proceedings of the National Academy of Sciences of the United States of America*, 108: 14416-21.

Zysset, P. K. 2009. 'Indentation of bone tissue: a short review', *Osteoporosis International*, 20: 1049-55.

Zysset, P. K., and A. Curnier. 1995. 'An alternative model for anisotropic elasticity based on fabric tensors', *Mechanics of Materials*, 21: 243-50.

Zysset, Philippe K, X Edward Guo, C Edward Hoffler, Kristin E Moore, and Steven A Goldstein. 1999. 'Elastic modulus and hardness of cortical and trabecular bone lamellae measured by nanoindentation in the human femur', *Journal of Biomechanics*, 32: 1005-12.

Zysset, Philippe K. 2003. 'A review of morphology–elasticity relationships in human trabecular bone: theories and experiments', *Journal of Biomechanics*, 36: 1469-85.

CHAPTER 3

An Investigation on the Effects of In Vitro Induced Advanced Glycation End-products on Cortical Bone Fracture Mechanics at Fall-Related Loading Rates

This Chapter has been adapted from a published article, 'Britton et al., (2023), An investigation on the effects of in vitro induced advanced glycation end-products on cortical bone fracture mechanics at fall-related loading rates, which has been published in the Journal of Mechanical Behaviour of Biomedical Materials.'.

3.1 Introduction

Bone strength is governed by tissue composition and structure (Cowin, 2001; Currey, 2006). Bone must be sufficiently stiff to provide adequate support to the surrounding tissues and organs, while having sufficient flexibility to absorb energy by deforming without cracking (Currey, 2012) (Seeman and Delmas, 2006). Bone's ability to carry out its vital functions is reduced if the mechanical integrity of the tissue is compromised. A phenomenon which is thought to have a deleterious effect on bone quality is non-enzymatic glycation of the organic phase of bone, where sugars in the extracellular space cause the formation of unwanted

crosslinks and adducts that alter the microenvironment of the collagen network by modifying the structure of the amino acid (Willett et al. 2022). These crosslinks and adducts are known as advanced glycation end-products (AGEs) and are believed to alter the mechanics of the collagen protein network in bone (Vashishth et al. 2001; Tang et al. 2007; Tang and Vashishth 2010; Karim et al. 2018; Hunt et al. 2019) and other collagenous tissues (Werbner et al. 2022; Moshtagh et al. 2018; Bank et al. 1998). Increased accumulation of AGEs in bone are linked with aging (Zimmermann et al. 2011), chronic kidney disease (Damrath et al. 2021) and type 2 diabetes (T2D) (Karim and Bouxsein 2016). In particular, T2D patients have a higher bone fracture risk than non-diabetic patients (Bonds et al. 2006; Janghorbani et al. 2007; Vestergaard 2007; Schwartz et al. 2011; Napoli et al. 2014), despite having normal, or even higher, bone mineral density (BMD). Previous studies have proposed that these unwanted AGE crosslinks may stiffen the overall collagen network leading to more brittle behaviour and increased bone fragility (Vashishth et al. 2001). However, the difficulty in obtaining direct measurements from bone tissue in vivo means that quantitative data describing precisely how bone tissue properties are affected by AGE accumulation in diseased patients is limited.

It is important to note that, while it has been widely assumed that AGEs accumulate in bone tissue of people with T2D, the evidence for this is actually limited and even conflicting. For example, there are limited examples of studies that observe an increase in fluorescent AGEs in human T2D tissue (Sihota et al., 2021), while many other recent studies (Karim et al. 2018; Hunt et al. 2019) have observed no difference in fluorescent AGEs in T2D tissue compared to non-T2D controls, although increases in pentosidine have been observed (Hunt et al. 2019). The complex hierarchical structural organisation of bone tissue and associated damage accumulation process means that there is a limited understanding of the relationship between AGE accumulation and bone tissue properties. Recently, it was found that trabecular cores tested under uniaxial compression had an increased Young's modulus, yield stress, ultimate

stress and AGEs in male T2D bone compared to non-diabetic controls (Hunt et al. 2019), implying that the T2D bone was actually stiffer and stronger. Several similar studies have reported no significant differences in the mechanical properties of human T2D bone measured by compression testing of trabecular cores (Karim et al. 2018; Parle et al. 2020). However, Sihota and colleagues (Sihota et al. 2021) have found increased AGEs and impaired mechanical properties in trabecular bone, with apparent toughness, post-yield energy, tissue level modulus and hardness, lower in the T2D group compared to non-T2D controls. This is in line with the findings of others (Zimmermann et al. 2011) that have examined the difference between young and old human cortical bone and found reduced fracture resistance as non-enzymatic collagen crosslinking was increased with aging. On the other hand, Karim and colleagues (Karim et al. 2018) examined cortical bone using cyclic reference point indentation, and did observe an increase in indentation distance (ID) and indentation distance increase (IDI), suggesting impaired cortical bone tissue properties in T2D, however there was no change found in the level of AGEs in the bone. These studies highlight the challenges in understanding the precise role of AGE accumulation on bone tissue mechanics.

The difficulty in obtaining large volumes of human tissue with AGE accumulation has meant that several studies have used in vitro glycation models to study the effect of AGE accumulation on mechanical properties. In vitro glycation models use solutions containing sugars to mimic the state of hypergylcaemia that is present in T2D, although it must be noted that these in vitro glycation models are not capable of capturing the complex physiological and biological effects of T2D on bone. However, these in vitro studies have still provided conflicting results (Willett et al. 2022). It has been found that bovine cortical bone subject to in vitro glycation showed an increase in yield stress and strain, but no change in the post-yield properties of the bone in the glycated samples (Vashishth et al. 2001). Meanwhile, other studies have found no differences in the pre-yield properties but significantly impaired post-yield

properties of glycated samples (Tang et al. 2007; Willett et al. 2013; Jia et al. 2021). In all cases, these studies found decreases in the damage fraction for the glycated samples and most studies observed an increase in the secant modulus of the tissue (Vashishth et al. 2001; Willett et al. 2013; Jia et al. 2021). Conversely, another study using in vitro glycated bovine bone found no differences in either the pre-or post-yield mechanical properties (Viguet-Carrin et al. 2008) and it was suggested that this was due to the 3-point bend test being insufficient in capturing the mechanical changes of the sample due to AGE accumulation. The vast majority of these studies have focussed on compression, tension or demineralised test specimens, and these testing approaches provide little insight into the fracture mechanics of the tissue. Critical quantities related to crack propagation, such as fracture toughness, have rarely been quantified. Most recently, fracture toughness tests have been carried out on in vitro glycated human (Merlo et al. 2020) and bovine (Jia et al. 2021) cortical bone, finding impaired fracture toughness in human glycated bone and a reduced plastic contribution but no differences in overall fracture toughness for bovine bone. Overall, the data derived from in vitro glycation models has provided conflicting results on the pre- and post-fracture behaviour (Vashishth et al. 2001; Tang et al. 2007; Viguet-Carrin et al. 2008; Willett et al. 2013; Merlo et al. 2020; Jia et al. 2021), with many studies using different incubation times of anywhere from 7 (Tang et al. 2007) to 38 (Vashishth et al. 2001) days and being limited by substantial inter-specimen variability (Viguet-Carrin et al. 2008). This implies that the precise role of AGE accumulation on both tissue mechanics in the elastic range and fracture mechanics has proven difficult to identify and approaches to reduce specimen variability are required.

The objective of this study is to investigate the relationship between AGE accumulation and the fracture mechanics of cortical bone tissue. An in vitro glycation model was used to simulate diabetic conditions in twenty anatomically adjacent pairs of bone from a single bovine femur, which reduced the possibility of inter-specimen variability. Mechanical characterisation

was carried out using 3-point bend, fracture toughness and nanoindentation testing, while bone composition was analysed by quantifying the accumulation of fluorescent AGEs, which allowed us to systematically investigate the effect of AGE accumulation on bone fracture mechanics.

3.2 Methods

3.2.1 In vitro Incubation

Two bovine femurs from one animal were machined into forty rectangular specimens using a band saw, followed by a low-speed saw (ISOMET^{TM} Low Speed Saw, Beuhler, IL, USA) under constant irrigation. The specimens were taken longitudinally and were paired so that they consisted of twenty anatomically adjacent pairs, with the dimensions of 3-point bend and fracture toughness specimens, as shown in Figure 3.1. The specimens were then grouped into a glycated group and a control group, with the anatomically adjacent pairs split so that one was in each group. The glycated samples were incubated at 37°C in 100 mg/ml ribose in Hanks' buffer with 1.3 mM $CaCl_2$ (Vashishth et al. 2001) to induce in vitro glycation. To prevent bacterial growth, the solution also contained 5 mg/10 ml of gentamicin and 100 μl/10ml of toluene and chloroform. The controls were incubated in the same solution but without the ribose. For both groups, the bone specimens were incubated for a total of 40 days, with solutions changed every 7 days. The 40-day incubation period was chosen to ensure high levels of AGE accumulation.

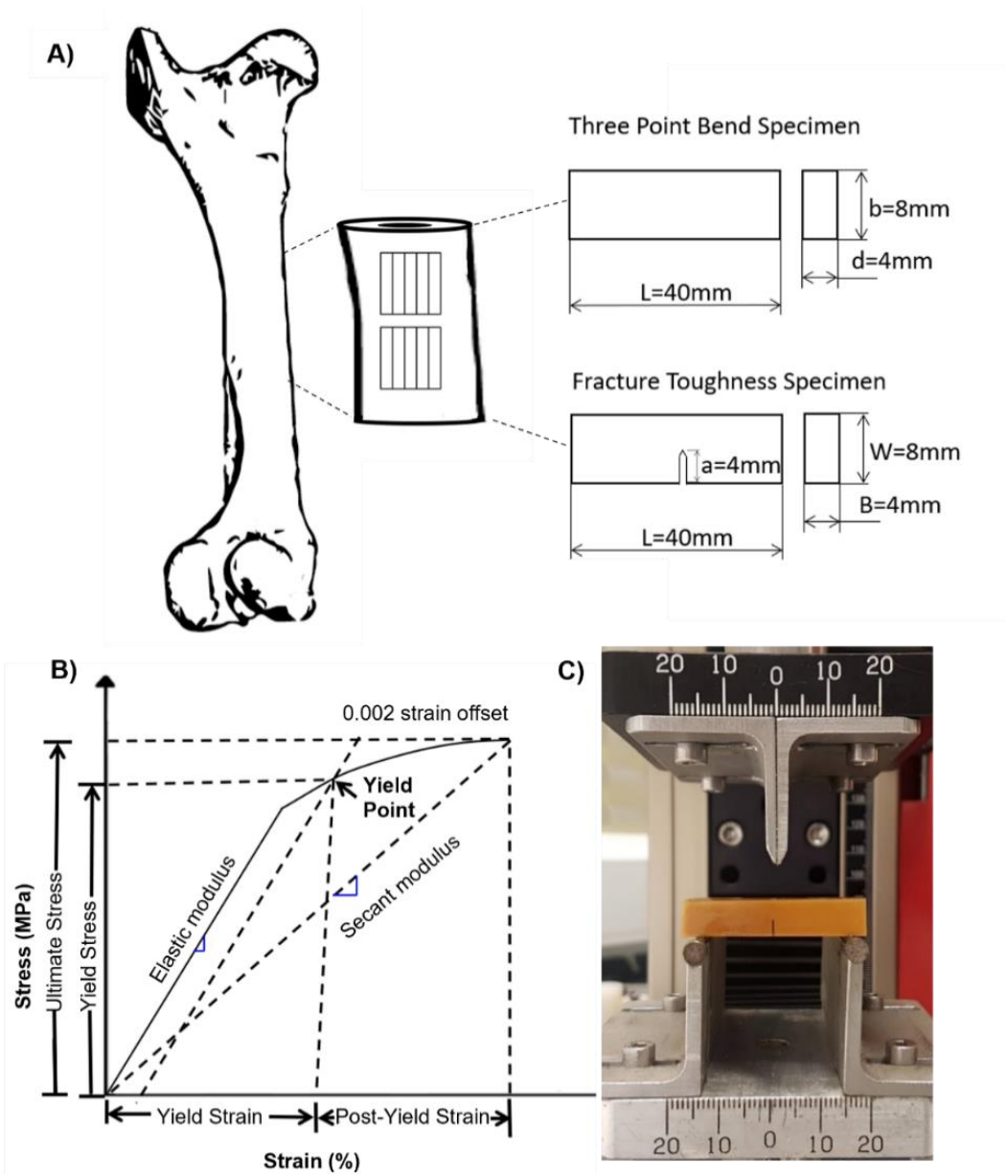

Figure 3.1A) Schematic of specimens. B) Schematic of Stress-Strain curve for cortical bone. C) Experimental configuration for the fracture toughness test.

3.2.2 AGE Quantification -Fluorometric Analysis

A fluorometric assay was performed on the bone tissue samples to determine the bulk measurement of fluorescent AGEs present in the organic collagen matrix. This assay was carried out post-mechanical testing, whereby approximately 100 mg of each bone was demineralised in 45% formic acid with a 1 mM sodium citrate buffer. Once the samples were demineralised, the collagen was digested in a papain digest solution of 0.4 mg/ml papain in 0.1 mM sodium acetate buffer at 65°C in an oven for 16 hours. The samples were then centrifuged

to separate the supernatant from any non-digested material. To determine the fluorescent AGEs present in the papain digested samples, they were compared against a quinine standard of 0, 0.5, 1, 2, 3.5, 5, 10, and 20 µg/ml, which were made using a stock solution of 50 µg/mL quinine per 0.1 N sulfuric acid. 200 µl of each sample was carefully pipetted into a 96-well plate and put into a Biotek plate reader at 360/460 nm excitation/emission. A hydroxyproline assay (Capella-Monsonís et al. 2018) was also carried out to determine the amount of collagen in each sample so that the nanograms of quinine per milligram of collagen could be measured.

3.2.3 Three Point Bend

Specimens were tested in a three-point bending configuration using a Zwick uniaxial testing machine (Zwick/Roell, Ulm, Germany) with a 2.5 kN load cell. Three-point bending was applied assuming a span width of 32mm, with the load (F) applied transverse to the long axis of the cortical beams at a strain rate of 0.0025/s. After testing, load-displacement data were analysed using Equation 3.1 and Equation 3.2 to obtain a stress-strain curve and the flexural modulus (E_f), yield stress (σ_Y), yield strain (ε_Y), ultimate flexural strength, ultimate strain, modulus of resilience, secant modulus (E_{sec}), damage fraction, post-yield toughness, and post-yield strain energy were determined,

$$\sigma_f = \frac{3FL}{2bd^2} \tag{3.1}$$

$$\varepsilon_f = \frac{6Dd}{L^2} \tag{3.2}$$

where F is the load applied, L is the support span, b is width, d is the depth, and D is the maximum deflection.

3.2.4 Fracture Toughness

Following ASTM E399-90 as closely as possible, three-point bending tests were performed to determine the fracture toughness using a support span of 32 mm. The specimens were kept in PBS until immediately before testing with a Zwick uniaxial testing machine, with a 2.5 kN load cell and a 10 mm/min test speed. Specimens were loaded to failure, and the fracture toughness K_Q was calculated using Equations 3.3 and 3.4. Further fracture toughness measurements were analysed following the ASTM Standard E1820 (E1820-08a 2014) using the nonlinear elastic J-integral (J_{int}) measurements, Equations 3.5, 3.6 and 3.7, to include the contribution of elastic phase (J_{el}) and plastic deformation (J_{el}) in the calculation of the fracture toughness

$$Y = \frac{3\left(\frac{a}{W}\right)^{\frac{1}{2}}\left[1.99 - \frac{a}{b}\left(1 - \frac{a}{W}\right)\left(2.15 - 3.93\frac{a}{W} + 2.7\left(\frac{a}{W}\right)^{2}\right)\right]}{2\left(1 + 2\frac{a}{W}\right)\left(1 - \frac{a}{W}\right)^{\frac{3}{2}}} \tag{3.3}$$

$$K_Q = \frac{P_Q S}{BW^{\frac{3}{2}}} Y \tag{3.4}$$

$$J_{int} = J_{el} + J_{pl} \tag{3.5}$$

$$J_{el} = \frac{K_Q^2(1 - v^2)}{E} \tag{3.6}$$

$$J_{pl} = \frac{n_{pl}^{E} A_{pl}}{Bb} \tag{3.7}$$

where Y is a geometric correction term, a is the notch depth, W is the depth of the specimen, B is the width of the sample, P_Q is the maximum load, v is the Poisson's ratio, E is the Youngs' modulus obtained from nanoindentation of the interstitial tissue, n_{pl} is 1.9, A_{pl} is the plastic area underneath the load-displacement curve, b is the width W minus the crack length a.

3.2.5 Nanoindentation

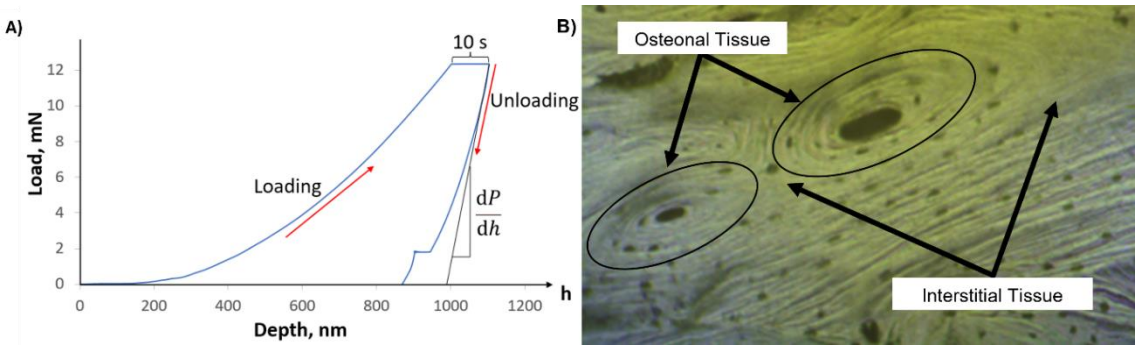

Figure 3.2 A) Schematic for nanoindentation loading profile. B) Image detailing interstitial and osteonal tissue.For nanoindentation testing, the samples, glycated n=6 and control n=6, were mounted in epoxy to enable surface preparation. First, the specimens were dehydrated using a series of alcohol baths. The specimens were then put into moulds and embedded in epoxy, placed in a vacuum to remove any air and left to cure for 72 hours. The samples were then cut parallel using the low-speed saw and polished using the Buehler MetaServ 250 polisher (Buehler, Lake Bluff, IL, USA) at 5 N of force with soft ChemoMet polishing cloths and diamond suspensions of decreasing size (9, 3, 1, 0.05 µm). A Keysight G200 Nano Indenter (Keysight Technologies, Santa Rosa, USA), with a Berkovich tip, was used for the nanoindentation. Indentations were performed in two distinct regions of the bone. One set of 2 × 2 indentations was performed in the osteonal lamellae and the other was performed in the interstitial lamellae. First, the elastic modulus of fused silica was measured to ensure that the

machine was calibrated correctly. The loading profile can be seen in A. The sample is loaded to a maximum depth of 1000 nm, the load was held for a period of 10 s before unloading to account for any viscoelastic effects during the test. The samples were then unloaded, and the load is held at 15% peak load for 75 s to account for the thermal drift, the thermal drift correction factor is applied to the test displacement data prior to further data analysis.

The Oliver and Pharr method was used to determine the modulus and hardness using Equations 3.8-3.10. Experimentally measured quantities used include the peak load P_{max}, the contact area A and the rate of change of load with respect to the displacement, dP/dh. During loading the sample undergoes both elastic and plastic deformation, during unloading only the elastic deformation is recovered and thus the unloading curve was used to calculate the modulus.

$$H = \frac{P_{max}}{A} \tag{3.8}$$

$$E^* = \frac{dP}{dh}\frac{\sqrt{\pi}}{2\sqrt{A}} \tag{3.9}$$

$$\frac{1}{E^*} = \frac{1 - {v_s}^2}{E_s} + \frac{1 - {v_i}^2}{E_i} \tag{3.10}$$

Where H is hardness, P is the load, A is the area of contact of the indenter, E_s and E_i are the substrate and indenter moduli, v_s and v_i are the substrate and indenter Poisson's ratio and h is the depth.

3.2.6 Statistical Analysis

All statistical analyses were performed using Minitab statistical software using paired t-tests. For all tests, $p < 0.05$, was considered statistically significant.

3.3 Results

3.3.1 AGE Accumulation

Figure 3.3.1A shows the colour change of the glycated specimens from white to a brownish colour following the period of incubation. This colour change signifies that the Maillard reaction has taken place and is a visual confirmation that non-enzymatic glycation has occurred. Figure 3.3 shows that bulk fluorescent AGE accumulation in the glycated samples was significantly higher compared to the control sample. After 40 days of incubation, the nanograms of quinine fluorescence per milligram of collagen increased significantly ($p < 0.001$) in the glycated group (1084 ± 251 ng/mg) when compared to the control group (137 ± 111 ng/mg) of six paired specimens.

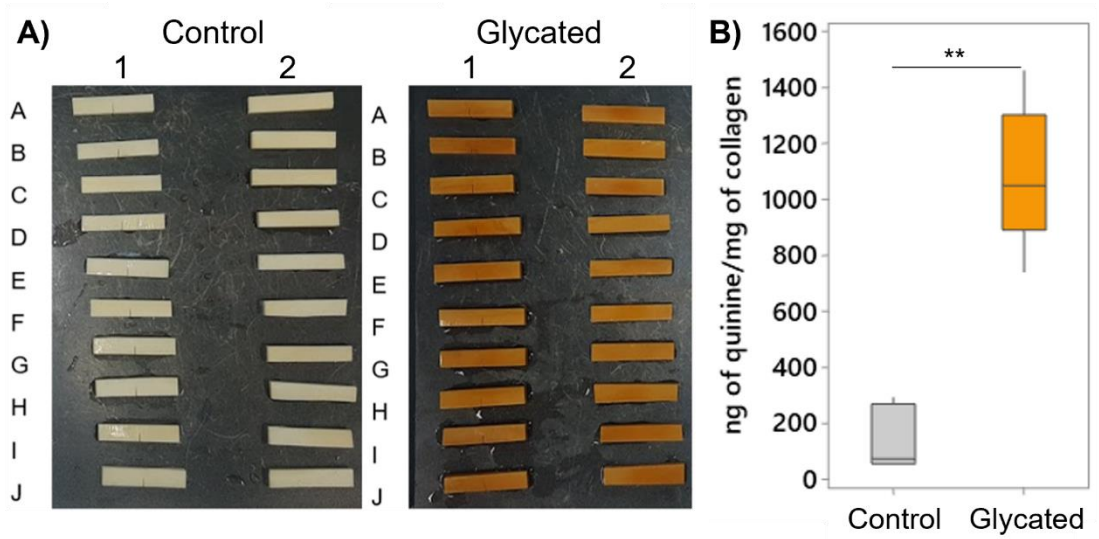

Figure 3.3 A) Control and glycated bones after removal from the solution. B) Boxplot of fluorescent AGEs.

3.3.2 Macro Mechanical Results

Figure 3.4 shows representative stress-strain curves from the three-point bend (Figure 3.4A) and fracture toughness testing (Figure 3.4B) with boxplots comparing specific mechanical properties of control and glycated groups also shown (Figure 3.4C-J). These results are also summarised in Table 3.1. Paired t-tests showed that there was a significant increase in yield stress (Figure 3.4D), Ultimate Flexural Strength (Figure 3.4F), and the Secant Modulus

(Figure 3.4I) in the glycated samples, compared to controls ($p < 0.05$). Interestingly, it was found that the glycated samples had significantly higher critical fracture toughness, K_Q ($p < 0.01$), and J_{el} ($p < 0.05$) compared to control samples ($p < 0.01$). There was no difference seen in J_{pl} or J_{int}.

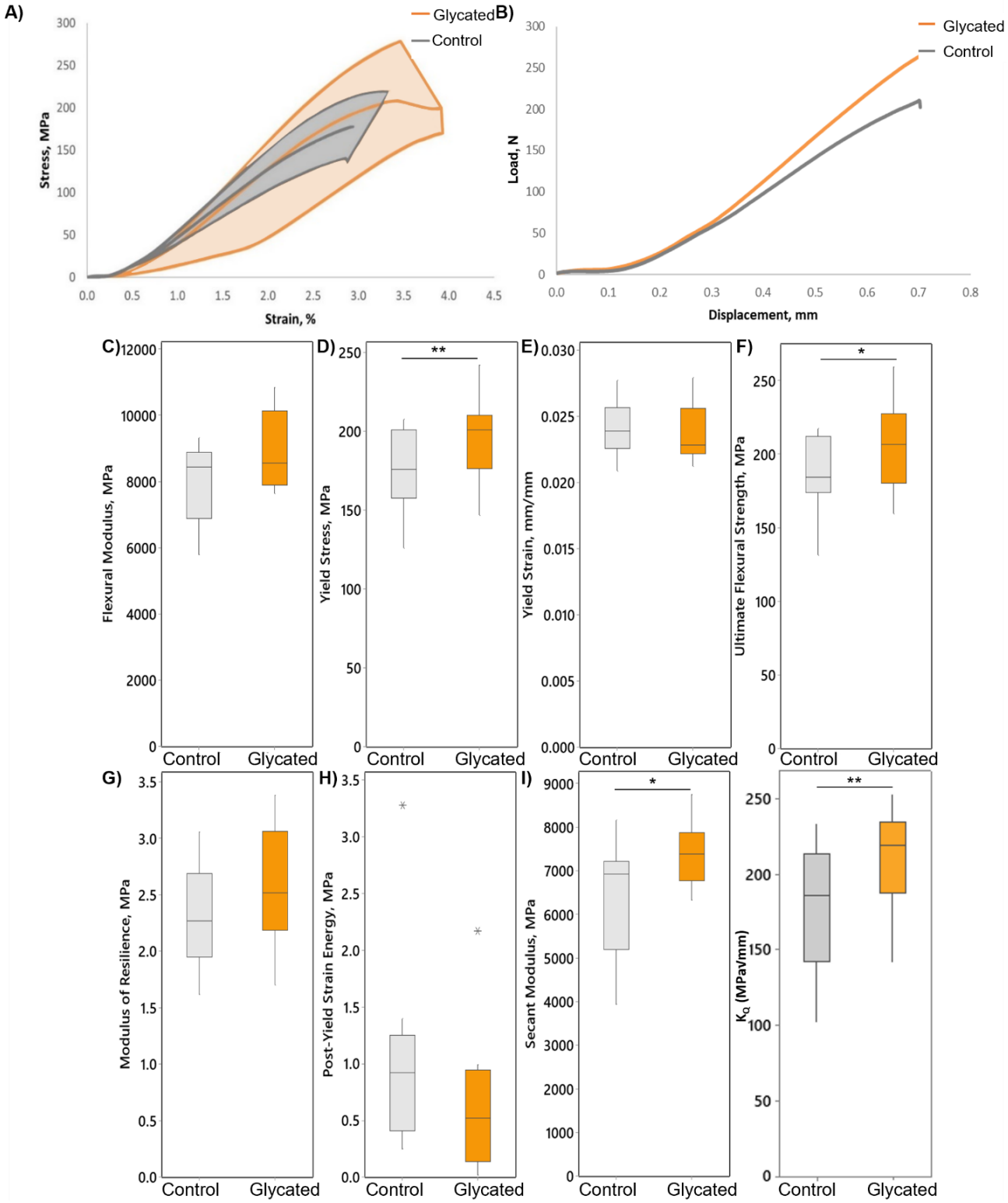

Figure 3.4 A) Three-point bend representative stress-strain curves, B) representative fracture toughness stress-strain curves. Boxplots for C) flexural modulus, D) yield stress, E) yield strain, F) ultimate flexural strength, G) modulus of resilience, H) post-yield strain energy, I) secant modulus and J) critical fracture toughness K_Q

*Table 3.1 Three-point bend and fracture toughness results for bovine cortical in vitro bone compared to control (*p ≤ 0.05, **p < 0.01).*

	Control (*n*=10)	**Glycated (*n*=10)**	**p-value**	**Confidence Interval**
Flexural Modulus (MPa)	7,929 ± 1,224	8,889 ± 1,157	0.063	-1,985, 65
Yield Stress (MPa)	174.95 ± 26.02	195.77 ± 27.63	**0.001****	-30.93, -10.71
Yield Strain	0.024174 ± 0.002	0.02381 ± 0.00214	0.707	-0.001639, 0.00236
Ultimate Flexural Strength (MPa)	186.98±26.98	205.83±30.30	**0.018***	-33.62, -4.09
Ultimate Strain	0.02960±0.005	0.02771±0.00377	0.455	-0.00359; 0.00737
Post-Yield Toughness (MJ/mm^3)	1.028±0.882	0.642±0.626	0.310	-0.426, 1.199
Modulus of Resilience (MPa)	2.306±0.450	2.553±0.516	0.154	-0.606, 0.112
Secant Modulus (MPa)	6,319±1346	7,389±742	**0.050***	-2,140, -1
Damage Fraction	0.2067±0.0893	0.1619±0.0852	0.298	-0.0470, 0.1366
Post Yield Strain	0.00543 ±0.00513	0.00390± 0.00357	0.508	-0.00654,0.00348
K_Q (MPa√m)	176.56±45.40	210.11±32.78	**0.007****	11.88, 55.23
J_{el} ($kJ\ m^{-2}$)	1.835±0.841	2.455±0.703	**0.011***	0.180,1.060
J_{pl} ($kJ\ m^{-2}$)	1.646±1.028	1.133±0.486	0.228	-1.410, 0.384
J_{int} ($kJ\ m^{-2}$)	3.481±1.438	3.588±0.757	0.796	-0.801,1015

3.3.3 Nanoindentation Results

From nanoindentation testing, the average modulus and hardness for the osteonal and interstitial spaces were determined using the Oliver and Pharr method, with results shown as box plots in Figure 3.5 and summarised in Table 3.2. It was found that the elastic modulus and hardness were not significantly different between the control and glycated groups.

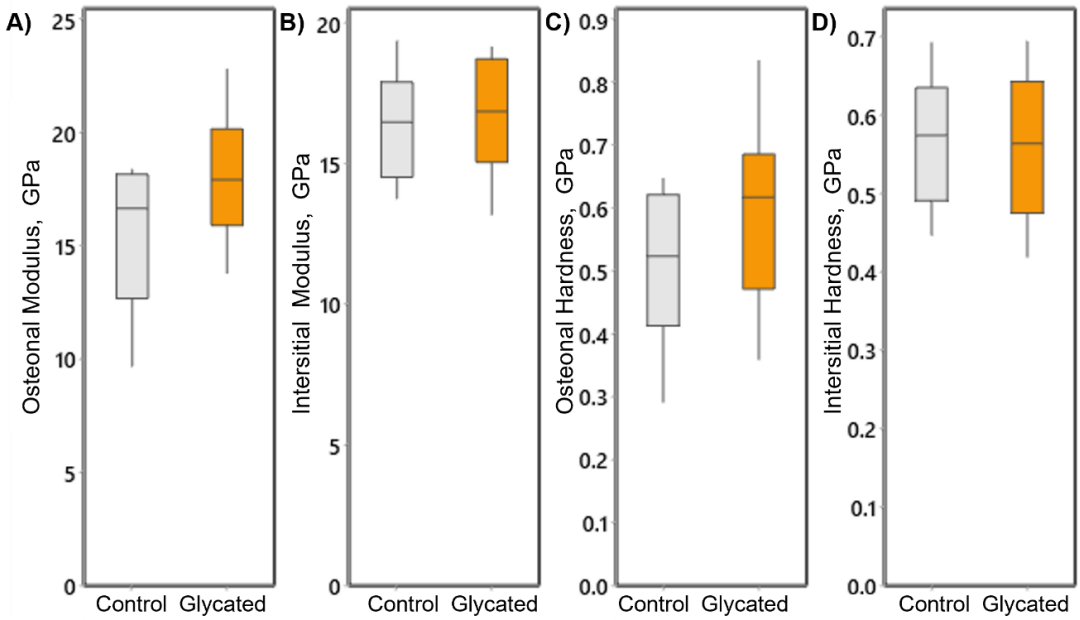

Figure 3.5 A) Nanoindentation results from control and ribosylated groups: A) osteonal modulus, B) interstitial modulus, C) osteonal hardness and D) interstitial hardness and D) details the osteonal and interstitial tissue.

Table 3.2 Nanoindentation results showing hardness and modulus of osteonal and interstitial bone tissue.

	Control (*n*=6)	**Ribose (*n*=6)**	**p-value**	**Confidence Interval**
Osteonal Modulus (GPa)	15.53±3.39	18.06±2.99	0.289	-2.95, 8.00
Osteonal Hardness (GPa)	0.5092±0.1330	0.5960±0.1565	0.436	-0.1046, 0.0546
Interstitial Modulus (GPa)	16.381±1.965	16.723±2.138	0.31	-2.51, 3.20
Interstitial Hardness (GPa)	0.5687±0.0853	0.5603±0.0978	0.842	-0.1102, 0.0935

3.4 Discussion

This Chapter used an in vitro glycation model to investigate the relationship between AGE accumulation and fracture mechanics of bone tissue. Anatomically adjacent pairs of bovine bone from a single femur were subject to in vitro glycation to eliminate the effects of inter-subject variability and investigate the accumulation of AGEs under controlled conditions. It was found that the AGE accumulation resulted in significant changes in the mechanical response, with mechanical properties enhanced in glycated samples. Under three-point bend testing, it was found that the yield stress, ultimate flexural strength, and secant modulus of the glycated samples were significantly higher than the controls. Furthermore, fracture toughness testing showed that the critical fracture toughness was increased by 16% in glycated samples compared to controls. These results provide no evidence that the accumulation of AGEs plays a role in bone fragility, with AGE accumulation actually found to enhance several pre- and post-yield properties of the tissue.

Previous studies have linked AGE accumulations with alterations in mechanical properties of collagenous tissues (Werbner et al. 2022; Moshtagh et al. 2018; Vashishth et al. 2001; Bank et al. 1998) and it has been suggested that the presence of these undesired crosslinks may result in the stiffening of the entire collagen network, which could cause the bone to become more brittle and fragile (Vashishth et al. 2001). While the effect of AGE accumulation on bone tissue properties has previously been evaluated through experimental tests (Vashishth et al. 2001; Tang et al. 2007; Viguet-Carrin et al. 2008; Willett et al. 2013; Merlo et al. 2020; Jia et al. 2021), the experimental evidence on their contribution to bone fragility is still limited. Previous studies have used similar in vitro approaches to this study (Tang et al. 2007) although these have tended to use much shorter incubation periods, typically between 7 and 15 days (Tang et al. 2007; Viguet-Carrin et al. 2008; Willett et al. 2013; Merlo et al. 2020; Jia et al. 2021). Together, the results from these studies have been very contradictory when both the measured

alterations in pre-yield (Vashishth et al. 2001) and post-yield properties (Tang et al. 2007; Willett et al. 2013; Jia et al. 2021) are considered. Using an in vitro glycation model, these results showed that bone samples had AGE levels that were significantly higher following the incubation period, confirmed visually by a prominent colour change and evaluated through fluoroscopy measurements. It was found through 3-point bend testing that samples with AGE accumulation had a higher resistance to deformation and increased yield stress and ultimate flexural strength. Others who have previously performed 3-point bend testing have found no difference in properties (Viguet-Carrin et al. 2008) or found reduction in post-yield properties with an increase in secant modulus (Willett et al. 2013) for glycated samples. The differences observed in the results here may be due to the different incubation times, 15 and 14 days, and strain rates of 0.003/s and 0.000167/s (1%/min), respectively compared to the incubation time of 40-days and strain rate of 0.0025/s. The findings of this Chapter are in line with several authors who have observed increases in secant moduli (Vashishth et al. 2001; Willett et al. 2013; Jia et al. 2021) and yield stress (Vashishth et al. 2001). This has led to the conclusion that these increases in tissue stiffness and strength were a consequence of the tissue becoming more brittle due to AGE accumulation, with several authors hypothesising that this tissue would be less resistant to crack propagation (Vashishth et al. 2001; Tang et al. 2007). While an increase in stiffness and strength can be at the expense of ductility and toughness in certain material systems (Currey 1969; Ritchie 2011), the results here showed that there was no significant reduction in the post-yield properties or damage fraction in glycated samples. Furthermore, this study evaluated the critical fracture toughness, K_Q, using ASTM 399 and J-integrals using ASTM E1820 where it was found that K_Q and J_{el} was higher for the glycated samples compared to controls with no difference seen in J_{pl} or J_{int} at a deflection rate of 0.167 mm/s. Similarly, a study (Woodside and Willett 2016) on fracture toughness on irradiation-sterilized bone tissue showed that fracture toughness can be protected, in part with a ribose pre-treatment.

Conversely, others (Jia et al. 2021) that have used bovine cortical bone subject to a shorter incubation periods have found a reduction in the plastic contribution of fracture toughness in glycated samples, at a lower displacement rate of 0.0001/s, compared to controls, but found no significant differences in the overall fracture toughness. Jia et al. (2021) using a higher displacement 0.1/s rate, closer to the level used in the current study, found no differences in J_{el}, J_{pl} or J_{int}. Although their study (Jia et al. 2021) was limited by the fact that AGE accumulation was not measured. A recent study on in vitro glycated human (Merlo et al. 2020) cortical bone did observe a reduced fracture toughness with increased levels of AGE accumulation. However, their study (Merlo et al. 2020) had a shorter incubation period of only 15 days and actually showed a significant reduction in elastic properties, at a displacement rate of 0.005mm/s, which is contrary to many other observations from in vitro glycation models (Vashishth et al. 2001; Willett et al. 2013; Jia et al. 2021). Through nanoindentation, no changes were observed in modulus or hardness of the glycated samples compared to the control. which is comparable with microhardness (Viguet-Carrin et al. 2008) and cyclic reference point indentation (Merlo et al. 2020) in other studies. However, microhardness results from Merlo et al. (2020) showed a reduction in modulus and mechanical properties of glycated samples. While results from in vitro glycation models to date have been highly contradictory, this Chapter has used one of the longer incubation periods to produce highly significant changes in AGE levels, with all testing taking place on matched bone specimens reduce inter-specimen variability, where no deterioration in mechanical properties in glycated samples were found.

These results contradict the current perception that prevails across the literature, which is that AGE accumulation in the collagenous network of bone tissue is responsible for increased brittleness and overall bone fragility in T2D. While the effect of AGEs on mechanical properties has been found to vary across different studies, the findings of this Chapter have important implications in the understanding of bone fragility. Firstly, studies that have

quantified the accumulation of fluorescent AGEs in human T2D patients have been quite conflicting. In particular, several recent studies have found no significant differences between either fluorescent AGEs in bone tissue (Karim et al. 2018; Hunt et al. 2019) or serum pentosidine levels (Karim et al. 2018; Hunt et al. 2020) in T2D patients, when compared to non-diabetic controls. Others have only observed relatively small increases in fluorescent AGEs (Sihota et al. 2021) or pentosidine levels in bone (Hunt et al. 2019) compared to controls. Of these, there is only limited evidence that AGE accumulation resulted in any deterioration in mechanical properties (Sihota et al. 2021), with others finding no significant difference (Karim et al. 2018), or even finding enhanced mechanical properties in T2D (Hunt et al. 2019). Much of the evidence for altered mechanical properties with AGE accumulation has been derived from in vitro models. However, it is important note that these in vitro glycation models (Vashishth et al. 2001; Tang et al. 2007; Viguet-Carrin et al. 2008) induce supra-physiological levels of AGEs in the tissue. Typically, these AGE levels tend to be between 2 and 16-fold higher to controls, whereas the largest increase observed in fluorescent AGEs from human T2D tissue has been ~30%. The in vitro glycation model used in this Chapter showed a supra-physiological increase of 800% in fluorescent AGE levels, and, despite this, there was no reduction in the mechanical properties of the bone and, in fact, the mechanical properties of the cortical bone tissue were enhanced. In the context of the conflicting data that exists across human and in vitro studies, these results provide no evidence the biomechanical effects of AGE accumulation alone could be a contributing factor to bone fragility.

It should be noted that this study has several limitations. Firstly, this study used a well-established in vitro glycation model for AGE accumulation in bone. However, it is difficult to say that this model provides a meaningful representation of T2D bone tissue. While the model clearly induces glycation within the samples, which was confirmed visually and through fluorescent AGE quantification, the levels induced are supra-physiological, being several

orders of magnitude higher than what has been observed from in vivo T2D tissue. Regarding AGE accumulation, an increase in the bulk fluorescent AGE accumulation was observed, however the method does not capture all of the complex chemistry of AGEs or distinguish between crosslinks and adducts. Furthermore, the model does not capture other tissue-level changes that are known to take place physiologically during T2D (e.g changes in osteoblastic (Kume et al. 2005; Sanguineti et al. 2008; McCarthy et al. 2004) and osteoclastic activity (Dong et al. 2011; Valcourt et al. 2007), and could induce other unwanted effects in the tissue due to incubation, such as dehydration due to the presence of chloroform and toluene, which may affect the behaviour of the bone samples. Additionally, the water content or the tensile properties and dynamic modulus of the samples under cyclic loading were not measured, where the effect of the collagen network can become more dominant. Moreover, it has been suggested that changes in the organic phase of bone, including those caused by AGEs show up more readily in the ASTM J-R curve, which were not investigated in this study. Despite these limitations, the established protocols were followed for this model and therefore can provide a direct comparison to other published work using this in vitro model. While the model used in this Chapter used bovine bone and not human tissue, this study is one of the first to quantify critical fracture toughness in glycated samples. Furthermore, this study was carried out on anatomically adjacent pairs from a single femur, which reduced the possibility of inter-specimen variability. In this context, these results provide no evidence that AGE accumulation that could be a contributing factor to bone fragility However, given the conflicting data that exists across in vitro glycation studies and the supra-physiological AGE levels that are induced using the in vitro model, future studies should focus on examining tissue from either animal or human patients with T2D.

3.5 Conclusion

It was found that AGE accumulation resulted in significant changes in the mechanical response of bone tissue, with mechanical properties enhanced in glycated samples. From three-point bend testing, it was found that the yield stress, ultimate flexural strength, and secant modulus of the glycated samples were significantly increased compared to the controls. Additionally, fracture toughness testing showed that the critical fracture toughness K_Q was higher by 16% in glycated samples compared to controls. These findings do not support the theory that the mechanical effects of AGEs alone, when isolated from the effects that AGE accumulation may have on the cellular interaction, play a prominent role in bone fragility, with AGE accumulation found to enhance several pre- and post-yield properties of the tissue. Although the mechanical effects of AGE accumulation may not increase the fracture risk of bone, the mechanical changes on the microenvironment does induce changes on the cellular behaviour and this needs to be investigated further.

3.6 References

Bank, Ruud A., Michael T. Bayliss, Floris P. J. G. Lafeber, Alice Maroudas, and Johan M. Tekoppele. 1998. "Ageing and zonal variation in post-translational modification of collagen in normal human articular cartilage The age-related increase in non-enzymatic glycation affects biomechanical properties of cartilage." In *Biochem. J*, 345-51.

Bonds, Denise E., Joseph C. Larson, Ann V. Schwartz, Elsa S. Strotmeyer, John Robbins, Beatriz L. Rodriguez, Karen C. Johnson, and Karen L. Margolis. 2006. 'Risk of Fracture in Women with Type 2 Diabetes: the Women's Health Initiative Observational Study', *The Journal of Clinical Endocrinology & Metabolism*, 91: 3404-10.

Capella-Monsonís, Héctor, João Q. Coentro, Valeria Graceffa, Zhuning Wu, and Dimitrios I. Zeugolis. 2018. 'An experimental toolbox for characterization of mammalian collagen type i in biological specimens', *Nature Protocols*, 13: 507-29.

Currey, J. D. 1969. 'The mechanical consequences of variation in the mineral content of bone', *Journal of Biomechanics*, 2: 1-11.

Damrath, John G, Amy Creecy, Joseph M Wallace, and Sharon M Moe. 2021. 'The impact of advanced glycation end products on bone properties in chronic kidney disease', *Current Opinion in Nephrology and Hypertension*, 30: 411-17.

Dong, X. Neil, An Qin, Jiake Xu, and Xiaodu Wang. 2011. 'In situ accumulation of advanced glycation endproducts (AGEs) in bone matrix and its correlation with osteoclastic bone resorption', *Bone*, 49: 174-83.

E1820-08a. 2014. "Standard test method for measurement of fracture toughness." In *ASTM International*.

Hunt, Heather B., Nicholas A. Miller, Kimberly J. Hemmerling, Maho Koga, Kelsie A. Lopez, Erik A. Taylor, Deborah E. Sellmeyer, Kendall F. Moseley, and Eve Donnelly. 2020. 'Bone Tissue Composition in Postmenopausal Women Varies With Glycemic Control From Normal Glucose Tolerance to Type 2 Diabetes Mellitus', *JOURNAL OF BONE AND MINERAL RESEARCH*, 36: 334-46.

Hunt, Heather B., Ashley M. Torres, Pablo M. Palomino, Eric Marty, Rehan Saiyed, Matthew Cohn, Jonathan Jo, Stephen Warner, Grazyna E. Sroga, Karen B. King, Joseph M. Lane, Deepak Vashishth, Christopher J. Hernandez, and Eve Donnelly. 2019. 'Altered Tissue Composition, Microarchitecture, and Mechanical Performance in Cancellous Bone From Men With Type 2 Diabetes Mellitus', *JOURNAL OF BONE AND MINERAL RESEARCH*: jbmr.3711-jbmr.11.

Janghorbani, M., R. M. Van Dam, W. C. Willett, and F. B. Hu. 2007. 'Systematic Review of Type 1 and Type 2 Diabetes Mellitus and Risk of Fracture', *American Journal of Epidemiology*, 166: 495-505.

Jia, Shaowei, He Gong, Haipeng Cen, Peipei Shi, Rui Zhang, Zhaowei Li, and Xuewei Bi. 2021. 'Influence of non-enzymatic glycation on the mechanical properties of cortical bone', *Journal of the Mechanical Behavior of Biomedical Materials*, 119: 104553-53.

Karim, Lamya, and Mary L. Bouxsein. 2016. 'Effect of type 2 diabetes-related non-enzymatic glycation on bone biomechanical properties', *Bone*, 82: 21-27.

Karim, Lamya, Julia Moulton, Miranda Van Vliet, Kelsey Velie, Ann Robbins, Fatemeh Malekipour, Ayesha Abdeen, Douglas Ayres, and Mary L. Bouxsein. 2018. 'Bone microarchitecture, biomechanical properties, and advanced glycation end-products in the proximal femur of adults with type 2 diabetes', *Bone*, 114: 32-39.

Kume, Shinichiro, Seiya Kato, Sho-ichi Yamagishi, Yosuke Inagaki, Seiji Ueda, Nobuyuki Arima, Takahiro Okawa, Masamichi Kojiro, and Kensei Nagata. 2005. 'Advanced Glycation End-Products Attenuate Human Mesenchymal Stem Cells and Prevent

Cognate Differentiation Into Adipose Tissue, Cartilage, and Bone', *JOURNAL OF BONE AND MINERAL RESEARCH*, 20: 1647-58.

McCarthy, Antonio Desmond, Toshimasa Uemura, Susana Beatriz Etcheverry, and Ana María Cortizo. 2004. 'Advanced glycation endproducts interfere with integrin-mediated osteoblastic attachment to a type-I collagen matrix', *International Journal of Biochemistry and Cell Biology*, 36: 840-48.

Merlo, Kelly, Jacob Aaronson, Rachana Vaidya, Taraneh Rezaee, Vijaya Chalivendra, and Lamya Karim. 2020. 'In Vitro-Induced High Sugar Environments Deteriorate Human Cortical Bone Elastic Modulus and Fracture Toughness', *Journal of Orthopaedic Research®*, 38: 972-83.

Moshtagh, Parisa R., Nicoline M. Korthagen, Mattie H. P. van Rijen, Rene M. Castelein, Amir A. Zadpoor, and Harrie Weinans. 2018. 'Effects of non-enzymatic glycation on the micro- and nano-mechanics of articular cartilage', *Journal of the Mechanical Behavior of Biomedical Materials*, 77: 551-56.

Napoli, Nicola, Elsa S. Strotmeyer, Kristine E. Ensrud, Deborah E. Sellmeyer, Douglas C. Bauer, Andrew R. Hoffman, Thuy Tien L. Dam, Elizabeth Barrett-Connor, Lisa Palermo, Eric S. Orwoll, Steven R. Cummings, Dennis M. Black, and Ann V. Schwartz. 2014. 'Fracture risk in diabetic elderly men: The MrOS study', *Diabetologia*, 57: 2057-65.

Parle, Eoin, Sherdya Tio, Annie Behre, John J. Carey, Colin G. Murphy, Timothy F. O'Brien, William A. Curtin, Stephen R. Kearns, John P. McCabe, Cynthia M. Coleman, Ted J. Vaughan, and Laoise M. McNamara. 2020. 'Bone Mineral Is More Heterogeneously Distributed in the Femoral Heads of Osteoporotic and Diabetic Patients: A Pilot Study', *JBMR Plus*, 4: e10253-e53.

Ritchie, Robert O. 2011. 'The conflicts between strength and toughness', *Nature Materials*, 10: 817-22.

Sanguineti, Roberta, Daniela Storace, Fiammetta Monacelli, Alberto Federici, and Patrizio Odetti. 2008. "Pentosidine effects on human osteoblasts in vitro." In *Annals of the New York Academy of Sciences*, 166-72. Blackwell Publishing Inc.

Schwartz, Ann V., Eric Vittinghoff, Douglas C. Bauer, Teresa A. Hillier, Elsa S. Strotmeyer, Kristine E. Ensrud, Meghan G. Donaldson, Jane A. Cauley, Tamara B. Harris, Annemarie Koster, Catherine R. Womack, Lisa Palermo, and Dennis M. Black. 2011. 'Association of BMD and FRAX score with risk of fracture in older adults with type 2 diabetes', *JAMA - Journal of the American Medical Association*, 305: 2184-92.

Sihota, Praveer, Ram Naresh Yadav, Ruban Dhaliwal, Jagadeesh Chandra Bose, Vandana Dhiman, Deepak Neradi, Shailesh Karn, Sidhartha Sharma, Sameer Aggarwal, Vijay G. Goni, Vishwajeet Mehandia, Deepak Vashishth, Sanjay Kumar Bhadada, and Navin Kumar. 2021. 'Investigation of mechanical, material and compositional determinants of human trabecular bone quality in type 2 diabetes', *The Journal of Clinical Endocrinology & Metabolism*, XX: 1-19.

Tang, S. Y. Y., and D. Vashishth. 2010. 'Non-enzymatic glycation alters microdamage formation in human cancellous bone', *Bone*, 46: 148-54.

Tang, S. Y. Y., U. Zeenath, and D. Vashishth. 2007. 'Effects of non-enzymatic glycation on cancellous bone fragility', *Bone*, 40: 1144-51.

Valcourt, Ulrich, Blandine Merle, Evelyne Gineyts, Stéphanie Viguet-Carrin, Pierre D. Delmas, and Patrick Garnero. 2007. 'Non-enzymatic glycation of bone collagen modifies osteoclastic activity and differentiation', *Journal of Biological Chemistry*, 282: 5691-703.

Vashishth, D., G. J. Gibson, J. I. Khoury, M. B. Schaffler, J. Kimura, and D. P. Fyhrie. 2001. 'Influence of nonenzymatic glycation on biomechanical properties of cortical bone', *Bone*, 28: 195-201.

Vestergaard, P. 2007. 'Discrepancies in bone mineral density and fracture risk in patients with type 1 and type 2 diabetes—a meta-analysis', *Osteoporosis International*, 18: 427-44.

Viguet-Carrin, S., D. Farlay, Y. Bala, F. Munoz, M. L. Bouxsein, and P. D. Delmas. 2008. 'An in vitro model to test the contribution of advanced glycation end products to bone biomechanical properties', *Bone*, 42: 139-49.

Werbner, Benjamin, Matthew Lee, Allan Lee, Linda Yang, Mohamed Habib, Aaron J. Fields, and Grace D. O'Connell. 2022. 'Non-enzymatic glycation of annulus fibrosus alters tissue-level failure mechanics in tension', *Journal of the Mechanical Behavior of Biomedical Materials*, 126: 104992.

Willett, Thomas L., Sibi Sutty, Anne Gaspar, Nick Avery, and Marc Grynpas. 2013. 'In vitro non-enzymatic ribation reduces post-yield strain accommodation in cortical bone', *Bone*, 52: 611-22.

Willett, Thomas L., Paul Voziyan, and Jeffry S. Nyman. 2022. 'Causative or associative: A critical review of the role of advanced glycation end-products in bone fragility', *Bone*, 163: 116485.

Woodside, Mitchell, and Thomas L. Willett. 2016. 'Elastic–plastic fracture toughness and rising JR-curve behavior of cortical bone is partially protected from irradiation–sterilization-induced degradation by ribose protectant', *Journal of the Mechanical Behavior of Biomedical Materials*, 64: 53-64.

Zimmermann, Elizabeth A., Eric Schaible, Hrishikesh Bale, Holly D. Barth, Simon Y. Tang, Peter Reichert, Bjoern Busse, Tamara Alliston, Joel W. Ager, and Robert O. Ritchie. 2011. 'Age-related changes in the plasticity and toughness of human cortical bone at multiple length scales', *Proceedings of the National Academy of Sciences of the United States of America*, 108: 14416-21.

CHAPTER 4

Investigating the Composition, Morphology, Mechanical Properties and Microdamage Accumulation of Human Type 2 Diabetic Bone

This Chapter has been adapted from a manuscript that is under preparation, 'Britton et al., Investigating the mechanical properties and microdamage accumulation of human type 2 diabetic bone.'

4.1 Introduction

Type 2 Diabetic (T2D) patients have up to a 3-fold increase in bone fracture risk (Janghorbani et al. 2007; Epstein and LeRoith 2008; Schwartz 2003; Schwartz and Sellmeyer 2007; Melton et al. 2008; Leslie et al. 2012; Shanbhogue et al. 2016) when compared to non-T2D patients. However, there are clinical challenges associated with predicting fracture risk in T2D patients as the level of bone mineral density (BMD) tends to be normal, or even higher than non-diabetic controls (Strotmeyer et al. 2004). This implies that type 2 diabetes impairs the quality of the bone matrix itself, whereby the intrinsic properties of bone tissue matrix are

deteriorated. However, the precise factors that contribute to sub-tissue alterations in the bone matrix and their effect on whole-bone fragility remain poorly understood.

It is thought that the hyperglycaemic state in type 2 diabetes impairs tissue properties by forming non enzymatic cross-links and adducts known as advanced glycation end products (AGEs) in the collagenous proteins of the bone matrix. The accumulation of AGEs is known to lead to a disruption of bone homeostasis (Paschou et al. 2017)and affect the bone cells, leading to decreased osteoblast activity (Mercer et al. 2007; Sanguineti et al. 2008), decreased osteoblast attachment to the collagen matrix (McCarthy et al. 2004), and decreased osteoclastogenisis (Valcourt et al. 2007). Consequently, these alterations have repercussions on the mineral and collagen components of bone with lower levels, of bone formation and resorption markers found in T2D leading to the implication that bone turnover in T2D is lower (Sassi et al. 2018; Purnamasari et al. 2017). The presence of AGEs causes a decline in the solubility of collagen (Valcourt et al. 2007). The mineralisation of the tissue is also affected due to T2D with hyperglycaemia disrupting the mineralisation phase of osteoblasts (Ghodsi et al. 2016). Additionally, the mineralisation quality is thought to possibly be altered due to secondary mineralisation not developing as it should (Monahan et al. 2023).

The accumulation of AGEs in the bone matrix is thought to lead to a more brittle behaviour. Despite this common assertion (Willett et al. 2022; Khosla et al. 2021; Carnevale et al. 2014), there is a lack of experimental data that quantitatively demonstrates any mechanistic relationship between AGE accumulation and mechanical properties in human T2D bone (Unal et al. 2023). In fact, much of the current understanding of the mechanics of bone fragility in type 2 diabetes has been generated using in vitro models (Vashishth et al. 2001; Tang et al. 2007; Viguet-Carrin et al. 2008; Willett et al. 2013; Jia et al. 2021; Merlo et al. 2020), whereby animal or human tissue has been immersed in a ribose solution to promote non-enzymatic glycation of the protein network. However, in Chapter 3, it was demonstrated that in vitro

glycation models are severely limited by the fact that they induce AGEs levels that are much higher than what occurs physiologically (Britton et al. 2022). In contrast, many human studies (Hunt et al. 2019; Karim et al. 2018) have reported no significant differences in fluorescent AGEs in T2D femoral neck and head trabecular bone tissue compared to non-T2D controls. Only a limited number of human studies have actually seen elevations in either bulk fluorescent AGEs (Sihota et al. 2021) or pentosidine (Hunt et al. 2019) in trabecular bone tissue from the femoral head and neck, respectively. It should be noted that the Sihota et al. (2021) study involved patients that had experienced their first fragility fracture, whereas other studies involved patients with osteoarthritis, this may explain the increased levels of AGEs found in the bulk fluorescent measurement by Sihota et al. (2021) as osteoporosis is also associated with an increase in levels of AGEs. Furthermore, there is a poor understanding of the relationship between AGE accumulation and bone tissue mechanics in T2D due to the complicated hierarchical structural organisation of bone tissue and the related damage accumulation process. Uniaxial compression testing of trabecular cores from femoral heads has revealed no discernible differences in the mechanical properties of human T2D bone (Karim et al. 2018; Parle et al. 2020), compared to non-T2D controls, with Hunt et al. (2019) actually showing that male T2D bone had higher Young's modulus, yield stress, and ultimate stress in trabecular cores than non-diabetic controls (Hunt et al. 2019). Only one study (Sihota et al. 2021) has found impaired mechanical properties in trabecular bone, although Karim et al. (2018) have observed an increase in indentation distance in cortical bone using reference point indentation testing, although, the mechanical properties were not correlated to AGE accumulation in this study. These are the only results in the literature that have shown impaired tissue-level properties in T2D. This highlights that, rather than AGE accumulation, other mechanisms must be responsible for fragility in T2D, which are yet to be elucidated.

During their lifetime, bones are subjected to repeated cyclic loading that leads to the accumulation of microdamage in the tissue. Microdamage is thought to be a biomechanically significant component of bone quality (Hernandez and Keaveny 2006), which more frequently develops in vivo in older people (Schaffler et al. 1995; Mori et al. 1997; Fazzalari et al. 1998a; Fazzalari et al. 1998b). Microdamage is generally repaired through the process of bone remodelling, whereby osteoblast and osteoclast cells actively maintain a healthy bone tissue matrix (Mori and Burr 1993; Burr et al. 1985). However, the onset of T2D leads to complex pathophysiological changes that ultimately disrupts normal bone homeostasis (Paschou et al. 2017) and alters the bone remodelling process (Sassi et al. 2018; Purnamasari et al. 2017). The altered remodelling process in diabetes has been hypothesised to lead to an increase in microdamage accumulation in bone (Sacher et al. 2022), possibly leading to impaired properties. However, there have been limited experimental investigations on the accumulation of microdamage in diabetic bone. While Tang and Vashishth (2010) showed using an in vitro glycation model of human bone that higher levels of microdamage accumulated in glycated samples compared to control bones, only one study has characterised microdamage in actual T2D tissue, to date. Here, Sacher et al (2022) used uniaxial compression testing to show that, while there was an altered distribution of microdamage in T2D bone, there was no difference in the total accumulation of microdamage compared to non-T2D controls following uniaxial compression. However, this study used monotonic loading, which does not replicate the repeated cyclic loading that bone experiences in vivo due to daily activities. Many early studies on non-diabetic bone (Michel and Hayes 1993; Moore and Gibson 2003; Lambers et al. 2013) have used cyclic loading to establish relationships between proportion of fatigue life, mechanical properties and microdamage accumulation. In particular, Lambers et al.(2013) showed that even small amounts of microdamage accumulation in human vertebral cancellous bone following cyclic loading may have substantial effects on biomechanical performance.

Such mechanisms could play a role in diabetic bone fragility, however, the relationship between microdamage accumulation and the biomechanical performance of human T2D bone has not yet been investigated.

The objective of this study is to investigate the roles of bone composition and microdamage accumulation on the mechanical properties T2D femoral head trabecular bone tissue under both monotonic and cyclic loading. Cylindrical cores from human femoral heads were extracted and mechanically tested using monotonic, cyclic compression and nanoindentation testing. Morphological analysis was conducted using micro computed tomography (micro-CT) imaging, while microdamage accumulation was quantified through barium sulphate staining. The collagen content, AGE concentration and mineralisation of the bone were compositionally analysed using fluorometric analysis, HPLC and Raman spectroscopy.

4.2 Materials and Methods

4.2.1 Bone Samples

Figure 4.1 shows a schematic that describes the study design. Femoral heads were obtained from age and sex-matched patients, with T2D (74 ± 9 years) and without T2D (74 ± 9 years). These were from patients who underwent total hip replacement for clinically diagnosed osteoarthritis (OA) and osteoporosis (OP) at two Galway hospital sites, Merlin Park University Hospital and University Hospital Galway. All research procedures were approved by the Clinical Research Ethics Committee, Galway University Hospitals, Galway, Ireland. The research was performed in accordance with relevant guidelines and regulations of the University of Galway. The groups were categorised as follows; T2D (*n*=17) (T2D+OA *n*=9, T2D+OP *n*=8) and non-T2D (*n*=17). None of the patients examined had any recorded comorbidities or were on medications known to affect bone metabolism (e.g. glucocorticoids, antiretroviral medications, bisphosphonates, teriparatide, or denosumab). HbA1C levels for *n*=10 of the T2D group were collected prior to surgery (57.6 ± 14.2 mmol/mol or 7.4 ± 1.3%), the HbA1C for the remaining T2D samples were unavailable. Three cylindrical cores of trabecular bone were removed from the femoral head, with one of these cores undergoing monotonic compression, another undergoing cyclic compression and the third core being used as a control. Microdamage was measured by staining the samples with barium sulphate and using micro-CT imaging to measure the accumulation of damage. Sections from the femoral head were also tested using nanoindentation to measure tissue-level mechanical properties. Compositional analysis using fluorometric assays, HPLC and Raman spectroscopy was carried out on both trabecular and cortical tissue to measure the accumulation of AGEs.

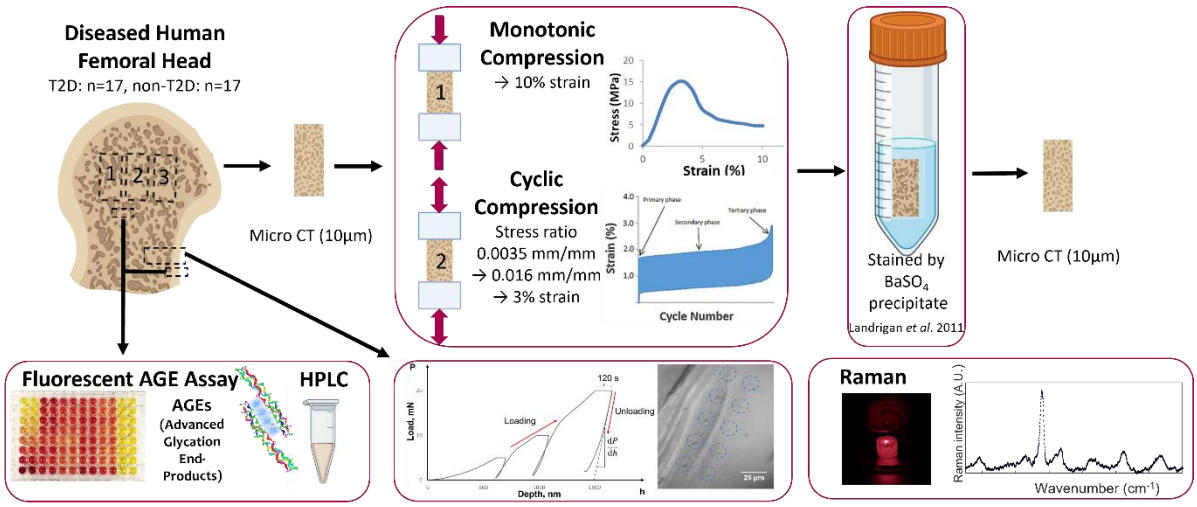

Figure 4.1 Study design showing bone cores removed from the femoral head, and the characterisation methods used to evaluate the bone cores morphologically, mechanically and compositionally.

4.2.2 Sample Preparation

Upon removal from the patient, femoral heads were wrapped in PBS-soaked gauze and stored in a sterile container. Samples were then frozen at -20°C before processing. Samples were defrosted and scanned using a micro-CT scanner (µCT100, Scanco Medical AG, Basseldorf, Switzerland) (see Section 2.2). The bone was then cut in a plane orthogonal to main trabecular direction (MTD), using a low-speed saw (ISOMET^{TM} Low Speed Saw, Beuhler, IL, USA) under constant water irrigation. A second cut parallel to the first cut was performed to obtain a ~21 mm thick bone slice. Figure 4.1 shows a schematic of the three cylindrical samples that were extracted from the central trabecular region of the femoral head using a diamond-tipped coring tool with an inner diameter of 8 mm. Bone marrow was removed from the sample using a water jet while the sample was underwater to reduce any additional microdamage. The cores were then scanned at a 10 µm resolution to measure the morphological properties. The samples to undergo mechanical testing were glued using cyanoacrylate (Prism 401, Loctite, Newington, CT, USA) into brass endcaps, to limit end-artefacts, and allowed to cure at 4°C overnight while the sample remained wrapped in PBS-soaked gauze.

4.2.3 Micro CT Scanning

Micro-CT images of the full femoral heads were obtained at a voxel size of 36.8 × 36.8 × 36.8 μm^3 using a high-resolution micro-CT scanner (μCT100, Scanco Medical AG, Basseldorf, Switzerland) with settings of 70 kVp, 114 mA and 300 ms (Ryan et al. 2020). Samples were placed in a sample holder to allow for the anatomical positions to be aligned with the axis of the micro-CT machine. The sample holder was then filled with PBS to cover the femoral head. The bone morphology evaluation script was used to determine the MTD. Cores one and two from each of the femoral heads were also scanned at 10 μm resolution to determine the morphological properties: bone volume fraction (BV/TV), connectivity density (Conn.D, $1/mm^3$), bone mineral density (mg HA/cm^3), tissue mineral density (mg HA/cm^3), bone surface fraction (BS/BV), trabecular number (Tb.N, 1/mm), trabecular thickness (Tb.Th, mm) and trabecular separation (Tb.Sp, mm). Images were segmented using a threshold of 617 mg HA/cm^3 and a Gaussian filter of sigma 1.2 and support 2 was used on the raw images to remove noise.

4.2.4 Mechanical Analysis

4.2.4.1 Uniaxial Monotonic Compression

All monotonic mechanical testing was carried out on a uniaxial testing machine (Zwick/Roell, Ulm, Germany) with a 2.5 kN load cell. The cores were wrapped in PBS-soaked gauze to maintain hydration during the test and all tests were carried out at a strain rate of 0.5% s^{-1}. Ten preconditioning cycles between 0-0.3% strain were carried out as is standard in the literature (Bevill et al. 2009). Core one from each femoral head underwent monotonic compression until a strain of 10%. A schematic of the monotonic compression stress-strain curve is shown in Figure 4.2A. The apparent modulus was determined from the linear best fit to the steepest 0.2% of the linear portion of the curve. The yield point was determined using the 0.2% offset method.

The pre-yield toughness was evaluated as the total area under the curve before the yield point and the toughness was calculated as the total area under the curve.

4.2.4.2 Cyclic Compression

All cyclic mechanical testing was carried out on a uniaxial testing machine (Zwick/Roell, Ulm, Germany) with a 2.5 kN load cell. The cores were wrapped in PBS-soaked gauze to maintain hydration during the test and all tests were carried out at a strain rate of 0.5% s^{-1}. Ten preconditioning cycles between 0-0.4% strain were carried out. Core two from each femoral head underwent cyclic compression testing at a normalised stress (Lambers et al. 2013; Green et al. 2011) of 0.0035 mm/mm to 0.016 mm/mm until a predefined failure threshold of 3% strain was reached, which was chosen based on preliminary testing that were found to capture the three phases of cyclic behaviour. Figure 4.2 illustrates these three phases where (i) in the primary phase, the strain accumulation per cycle falls, (ii) in the secondary phase, the strain accumulation per cycle is constant and (iii) in the tertiary phase, the strain accumulation per cycle increases. The initial apparent modulus was determined from the linear best fit to the steepest 0.2% of the first loading cycle of the cyclic fatigue curve, while the final apparent modulus was determined from the steepest 0.2% of the final loading cycle. Across the tests carried out, the mechanical properties that were evaluated will be the number of cycles to failure (N_f), initial apparent modulus ($E_{initial}$), final apparent modulus (E_{final}), percentage reduction in modulus, and energy dissipation as the area of the cyclic loading curves.

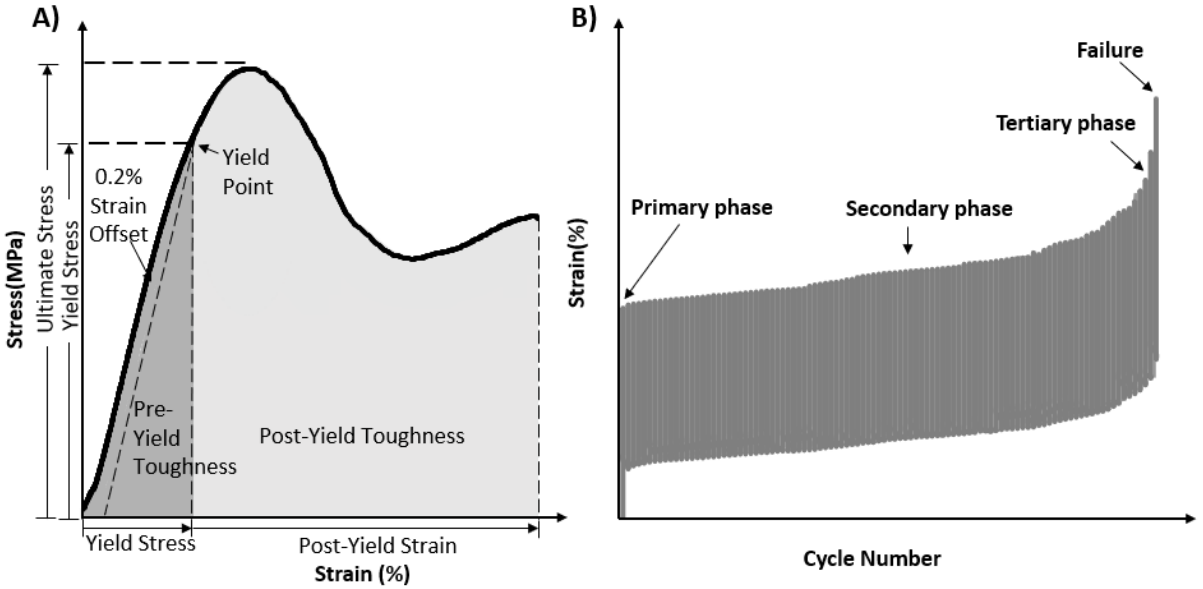

Figure 4.2 A) Stress-strain curve schematic of monotonic compression to 10% strain applied to the core one cohort, B) strain versus cycle number schematic of cyclic compression to 3% strain applied to the core two cohort.

4.2.4.3 Nanoindentation Testing

The tissue-level material properties were determined using nanoindentation. The samples were dehydrated in a series of ascending ethanol baths to prepare for embedding, whereby the cores were embedded an epoxy resin (EpoThin2^{TM}, Beuhler, IL, USA) and placed under vacuum to allow the epoxy to fill all spaces. While drying does influence the nanoindentation modulus and hardness of bone (Hengsberger et al. 2002), it is widely used across literature (Mittra et al. 2006; Mulder et al. 2007; O'Sullivan 2020). Silicon carbide paper was used to remove epoxy to expose the test surface, which was then polished using a series of descending diamond suspension pastes (9 µm, 3 µm, 1.5 µm and 0.05 µm) with polishing cloths on a polishing machine (MetaServ® 250 Grinder-Polisher with Vector® LC Power Head, Beuhler, IL, USA). Using an ultrasonic bath and deionised water, the samples were washed between each polishing phase. The nanoindentation was carried out on a NanoIndenter G200 (Keysight Technologies, CA, USA) with a Berkovich diamond indenter tip, with calibration of the machine performed using fused silica. Ten indents were made on the trabecular bone and cortical interstitial bone of each sample, with all indents positioned at least 10 µm away from the edge of the sample

and 15 µm from neighbouring indents within the array. Figure 4.3 shows a schematic of the loading profile used, which consisted of two conditioning steps that reached loads of 25% max load and 50% max load, followed by a third step that reached the max load of 20 mN. A hold period of 120 s was included after each loading peak was reached, which together with the multiple loading cycles, reduced the effects of time-dependent plasticity (Mittra et al. 2006; Mulder et al. 2007; Brennan et al. 2009; O'Sullivan 2020). Upon unloading, the rate of thermal expansion was measured by holding the indenter at 10% of the max load for 120 s to calibrate the thermal drift correction factor ahead of further data analysis.

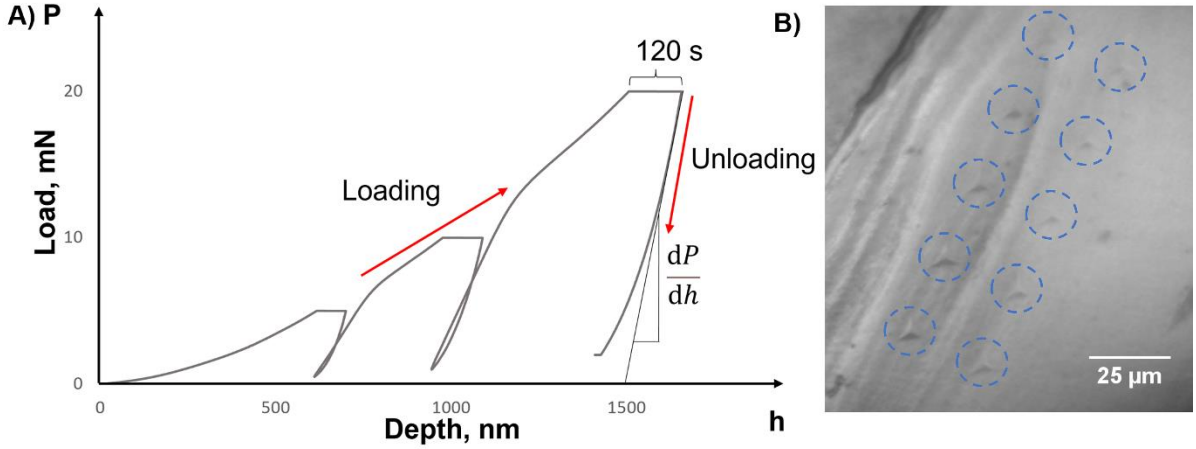

Figure 4.3 (A) Schematic for nanoindentation loading profile. (B) Embedded trabecular bone that shows indented regions.

The data obtained from the indentation tests were analysed to determine the Young's modulus and hardness of the samples, assuming a Poisson's ratio of 0.3, using the in-built Oliver and Pharr method (Keysight NanoSuite Software) and the same methodology described in Chapter 3.

4.2.4.4 Microdamage Analysis

After core one and two had undergone monotonic and cyclic tests, microdamage was measured by barium sulphide staining and micro-CT analysis in both the T2D and non-T2D groups. From each femoral head, core three, which had not undergone any mechanical testing, was used as a control to measure the pre-existing microdamage. To quantify microdamage accumulation, the

damaged specimens and the control specimen were stained with a barium sulphate solution (Landrigan et al. 2011) by soaking in an aqueous solution of equal parts 0.5 M $BaCl_2$, acetone and PBS for 72 hours followed by 0.5 M $NaSO_4$, acetone and PBS for 72 hours, all under vacuum. Finally, the specimens were agitated in buffered saline solution to remove excess $BaSO_4$ precipitates for 1 hour. All specimens were scanned at 10 μm resolution, 70 kVp voltage and 114 μA current with 200 ms integration time. A Gaussian filter of sigma 1 and support 2 was used on the raw images to remove noise (Wang et al. 2007). Different thresholds were used to determine the volume of bone and the volume of $BaSO_4$. Voxels with intensities greater than native 9,000, corresponding to 631.1 mg HA/cm^3, and less than native 23,500, corresponding to 1965.6 mg HA/cm^3, were taken to be bone and voxels with intensities greater than native 23,500 were taken to be $BaSO_4$.The damaged volume was defined as the volume of $BaSO_4$ divided by the total volume of bone.

4.2.5 Bone Compositional Analysis

4.2.5.1 Raman micro-spectroscopy and spectral analysis

Raman micro-spectroscopy was used to evaluate the compositional properties of T2D, and non-T2D bone tissue. The properties measured where the mineral-to-matrix ratio, carbonate substitution, crystallinity, the matrix maturity, the helical status, the hydroxyproline-to-proline ratio and the amide I-to-amide III ratio. This work was carried out using a similar methodology to Van Gulick et al. (2022). A HE-785 Raman spectrometer (Jobin-Yvon-Horiba, Longjumeau, France) was used to record the Raman spectra. This system included a high efficiency (HE) spectrometer with a fixed 950 g/mm grating coupled to a matrix charge coupled device (CCD) detector that was cooled by the Peltier effect at 200 K (Andor Technologies, Belfast, Northern Ireland). The excitation source and the detecting system were connected with a fibre probe (InPhotonics, MA, USA). The probe head included a bandpass filter, a beam splitter, a lens, a mirror, and a long pass filter. The 5 mm-focal-distance fibre probe was mounted on a z-

adjustable holder to ensure optimum acquisition repeatability and enhance focus on the sample. The excitation wavelength of the laser source for illumination was set at 785 nm and was provided by an OEM diode laser (Process Instruments Inc., UT, USA) This device offers high throughput, sensitivity, and wavelength stability even when the temperature fluctuates. A 10-second integration time was used to gather all of the spectra. Per sample, 10 measurements were made. Data acquisition was performed using the Labspec 5.0 software (Jobin-Yvon-Horiba).

Matlab (Mathworks, MA, USA) was used to process the Raman data. The raw spectra required multiple data processing steps, which consisted of instrument response correction, wave number calibration, fluorescence background subtraction, cosmic ray removal and baseline corrected using a fifth polynomial fit. The data was smoothed using a seven-point Savitzky-Golay technique. A Standard Normal Variate (SNV) technique was used to normalise the resultant spectra.

4.2.5.2 High Performance Liquid Chromatography

As the glycation reaction is a complex process involving early and late steps, two different glycation products have been quantified to evaluate each phase of the process. Firstly, furosine concentrations were evaluated to provide information about the formation of Amadori products during the early phase of glycation. Furosine is an analytical surrogate for the adduct Nε-1-deoxyfructosyl (FL) and is a by-product formed during acid hydrolysis of FL (Schleicher et al. 1981; Sell 1997). Secondly, Carboxymethyl Lysate (CML) was evaluated to provide information about the later phase of glycation that involved oxidative reactions (e.g. formation of AGEs).

All samples were subjected to acid hydrolysis with 6 M hydrochloric acid for 18 h at 110 °C. Hydrolysates were evaporated to dryness twice under a nitrogen stream. Furosine and CML

were then quantified by liquid chromatography coupled to tandem mass spectrometry (LC-MS/MS). Briefly, dried hydrolysates were resuspended in 100 µl of 125 mM ammonium formate containing 1 µM of d2-CML and 1 µM d4-furosine, used as internal standards, and filtered using Uptidisc PTFE filters (4 mm, 0.45 µm, Interchim, France) prior to LC-MS/MS analysis.

Furosine quantification was performed using a LC20 chromatographic system (Shimadzu, Kyoto, Japan) equipped with a Kinetex XB-C18 column (100 × 3.0 mm, 2.6 µm – Phenomenex, CA, USA) with a gradient program composed of 5 mM ammonium formate (pH 2.9) as mobile phase A and 100% acetonitrile as mobile phase B. The flow rate was constant at 0.3 mL/min during all separation steps. The gradient program was as follows: 0–0.1 min: 5% B; 0.1–4.1 min: gradient to 95% B; 4.1–6.1 min: 95% B; 6.1–7.1 min: gradient to 5% B; 7.1–13.1 min: 5% B. The injection volume was 3 µl and the oven temperature was set at 40°C. Detection was performed using an API4000 system (ABSciex, France) in positive-ion mode with an electrospray ionization (ESI) source. Multiple reaction monitoring (MRM) transitions used for quantification were as follows: 255.1 > 84.2 for furosine and 259.0 > 88.2 for d4-furosine.

CML quantification was performed using a LC20 chromatographic system (Shimadzu) equipped with a Kinetex HILIC column (100 × 4.6 mm, 2.6 µm - Phenomenex) with a gradient program composed of 5 mM ammonium formate (pH 2.9) as mobile phase A and 100% acetonitrile as mobile phase B. The flow rate was constant at 0.9 mL/min during all separation steps. The gradient program was as follows: 0–0.3 min: 90% B; 0.3–1.5 min: gradient to 50% B; 1.5–2.0 min: 50% B; 2.0–3.1 min: gradient to 40% B; 3.1–3.5 min: 40% B; 3.5–4.0 min: gradient to 90% B. The injection volume was 10 µl and oven temperature was set at 25°C. Detection was performed using an API4000 system (ABSciex, France) in positive-ion mode with an electrospray ionization (ESI) source. Multiple reaction monitoring (MRM) transitions used for quantification were as follows: 205.1 > 130.1 for CML and 207.1 > 84.1 for d2-CML.

Calibration curves were performed by preparing diluted serum solutions spiked with increased amounts of CML (ranging from 2.5 μM to 80 μM), which have been submitted to the same preanalytical treatments as patient samples. In addition, the lysine content in the hydrolysate was quantified by LC-MS/MS to normalise the expression of results.

4.2.5.3 Fluorescent AGE quantification

To quantify fluorescent cross-links present in the collagen of the bone, a fluorometric assay (Karim et al. 2018) was performed, using a similar approach to Chapter 3. After the specimens had been mechanically tested, approximately 100 mg of each bone was demineralised in 45% formic acid with a 1 mM sodium citrate buffer. Once the samples were demineralised, all that remained was the organic components from each sample. The collagen was digested in a papain digest solution of 3.88 units of papain in 0.1 mM sodium acetate buffer at 65°C in an oven for 16 hours. The samples were then centrifuged to separate the supernatant from any-non-digested material. The papain digested samples were then hydrolysed by placing equal parts of the supernatant and HCL ~38% into an Eppendorf and incubating at 100°C for 18 hours. The samples were then allowed to dry out and be rehydrated. To determine the fluorescent AGEs, the rehydrated samples were compared against a quinine standard of 0, 0.5, 1, 2, 3.5,5,10, and 20 μg/ml, which were made using a stock solution of 50 μg/mL quinine per 0.1 N sulfuric acid. 200 μl of each sample was carefully pipetted into a 96 well plate and a Biotek plate reader used at 360/460 nm excitation/emission. A hydroxyproline assay was also carried out to determine the amount of collagen in each sample, so that the nanograms of quinine per milligram of collagen could be measured.

4.2.6 Statistical Analyses

All statistical analyses were performed using Minitab statistical software, using 2-sample t-tests, with the T2D group being compared to non-T2D group. For all tests, $p < 0.05$, was considered statistically significant. Boxplots were prepared using GraphPad. The distribution

of mechanical properties was analysed to detect potential outliers, and data from samples that were two standard deviations from the mean being removed. This resulted in a total of five samples being removed in the analysis (non-T2D (*n*=2), and T2D (*n*=3)). Additionally, insufficient cortical bone was present in some femoral heads from the femoral neck, leading to the following sample numbers for cortical bone analysis: T2D (n=15) and non-T2D (n=11) for nanoindentation, fluorescent AGE analysis, Raman, and HPLC results.

4.3 Results

4.3.1 Bone Morphology

Figure 4.4 and Table 4-1 show the morphological properties determined through micro-CT scanning, with significant differences observed between the T2D and non-T2D samples for several parameters. T2D bone had significantly higher BV/TV (+22%, p=0.006), trabecular number (+13%, p=0.015) and bone mineral density (+17%, p=0.019) compared to non-T2D controls. T2D bone had significantly lower tissue mineral density (-2%, p<0.001) and trabecular separation (-17%, p=0.002) compared to the non-T2D controls. T2D bone had a significantly lower structural model index compared to non-T2D. Here, the T2D bone had a negative mean, which is indicative of a concave surface, while the non-T2D bone had a positive mean, which is indicative of a convex surface. The SMI was also closer to zero for the T2D group, meaning the structure was more plate-like compared to the There were no differences in connectivity density or trabecular thickness between groups.

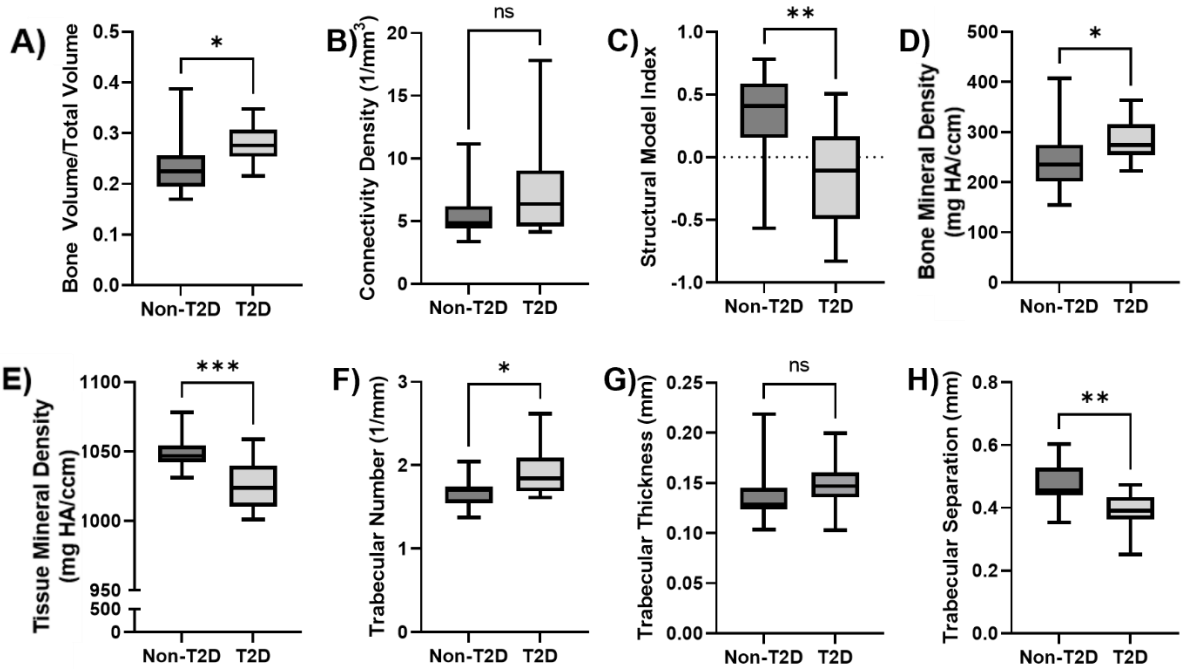

*Figure 4.4 Micro-CT results A) BV/TV, B) connectivity density, C) structural model index, D) bone mineral density, E) tissue mineral density, F) trabecular number, G) trabecular thickness and H) trabecular separation. *(p<0.05), **(p<0.01), ***(p<0.001)*

Table 4.1 Trabecular bone microarchitecture results measured using micro-CT.

	Non-T2D (*n*=15)	T2D (*n*=14)	CI	p-value
Connectivity Density (1/mm3)	5.47±1.86	7.21±3.68	(-4.18,0.43)	0.104
Structural Model Index	0.31±0.344	-0.16±0.398	(0.184,0.755)	**0.002**
Bone Mineral Density (mg HA/cm^3)	245.8±57.4	287.5±43.8	(-80.5, -2.8)	**0.036**
Tissue Mineral Density (mg HA/cm^3)	1049±13.9	1026±17.4	(10.33,34.60)	**<0.001**
Bone Volume/Total Volume	0.23±0.0530	0.28±0.0383	(0.0114, 0.0817)	**0.012**
Bone Surface/Bone Volume	14.9±2.23	13.8±2.20	(-0.577, 2.808)	0.187
Trabecular Number (1/mm)	1.68±0.166	1.89±0.271	(-0.040, -0.39)	**0.018**
Trabecular Thickness (mm)	0.15±0.0226	0.14±0.0259	(-0.02938, 0.00766)	0.239
Trabecular Separation (mm)	0.47±0.0679	0.39±0.0581	(0.0280, 0.1243)	**0.003**

4.3.2 Mechanical Results

4.3.2.1 Monotonic Results

Figure 4.5A shows a representative stress-strain curve for T2D and non-T2D under monotonic compression. Figure 4.5B-H show boxplots of the mechanical properties that were evaluated across both groups. The data were analysed by comparing T2D with OA to non-T2D with OA, as well as T2D with OP to non-T2D with OP. The results of these comparisons are presented in Appendix 4.1. It was found that the T2D samples had a significantly higher apparent modulus (+26%, p=0.021), yield stress (+39%, p=0.026), max stress (+47%, p=0.012), pre-yield toughness (+57%, p=0.013), post-yield toughness (+48%, p=0.041) and toughness (+59%, p=0.011) (see

Table 4.2). The results were normalised by BV/TV as it is the best morphological determinant of bone stiffness (Maquer et al. 2015; Voumard et al. 2022). When normalised against BV/TV (by dividing by BV/TV), all the previously significant properties remained significantly higher in T2D group compared to the non-T2D. The data was also normalised using both a generalised

linear model (GLM) and a power law model (PLM), which involved fitting a linear and power law trendline, respectively, to the data. These are both common ways to normalise mechanical properties when dealing with bone, to separate the effect of the porous structure. The equations of each trendline were then used to normalise the data using the GLM and PLM methods, respectively, resulting in the normalised GLM and PLM data, which are summarised in Table 4.4. After GLM and PLM normalisation, none of the properties remained significantly higher in the T2D group.

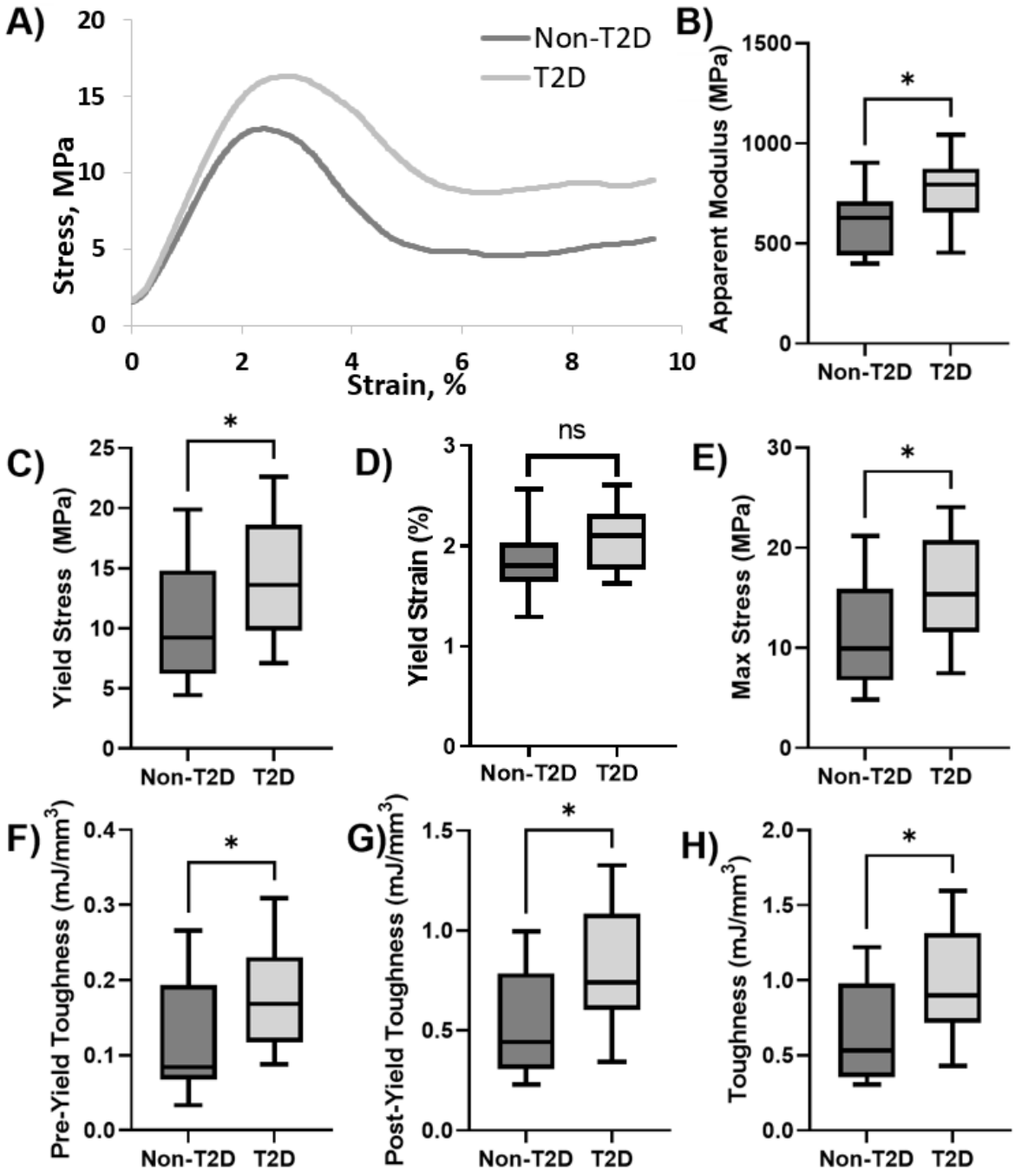

*Figure 4.5 Monotonic compression mechanical properties A) representative stress-strain curve, B) apparent modulus), C) yield stress, D) yield strain (inclusive of toe region), E) max stress, F) pre-yield toughness, G) post-yield toughness, and H) toughness. *($p<0.05$)*

4.3.2.2 Microdamage Accumulation under Cyclic Loading

Figure 4.6A shows the creep-fatigue curve consisting of the primary, secondary and tertiary phases of the creep response. Figure 4.6B shows the cyclic mechanical properties. It was found

that the T2D group had higher initial modulus (+20%, p=0.25) and final modulus (+24%, p=0.032) compared to the non-T2D group. The T2D group also underwent significantly higher number of cycles before failure (p=0.039). There were no significant differences in the percentage reduction in modulus, initial energy dissipation, final energy dissipation or increase in energy dissipation when comparing the T2D samples with the non-T2D samples.

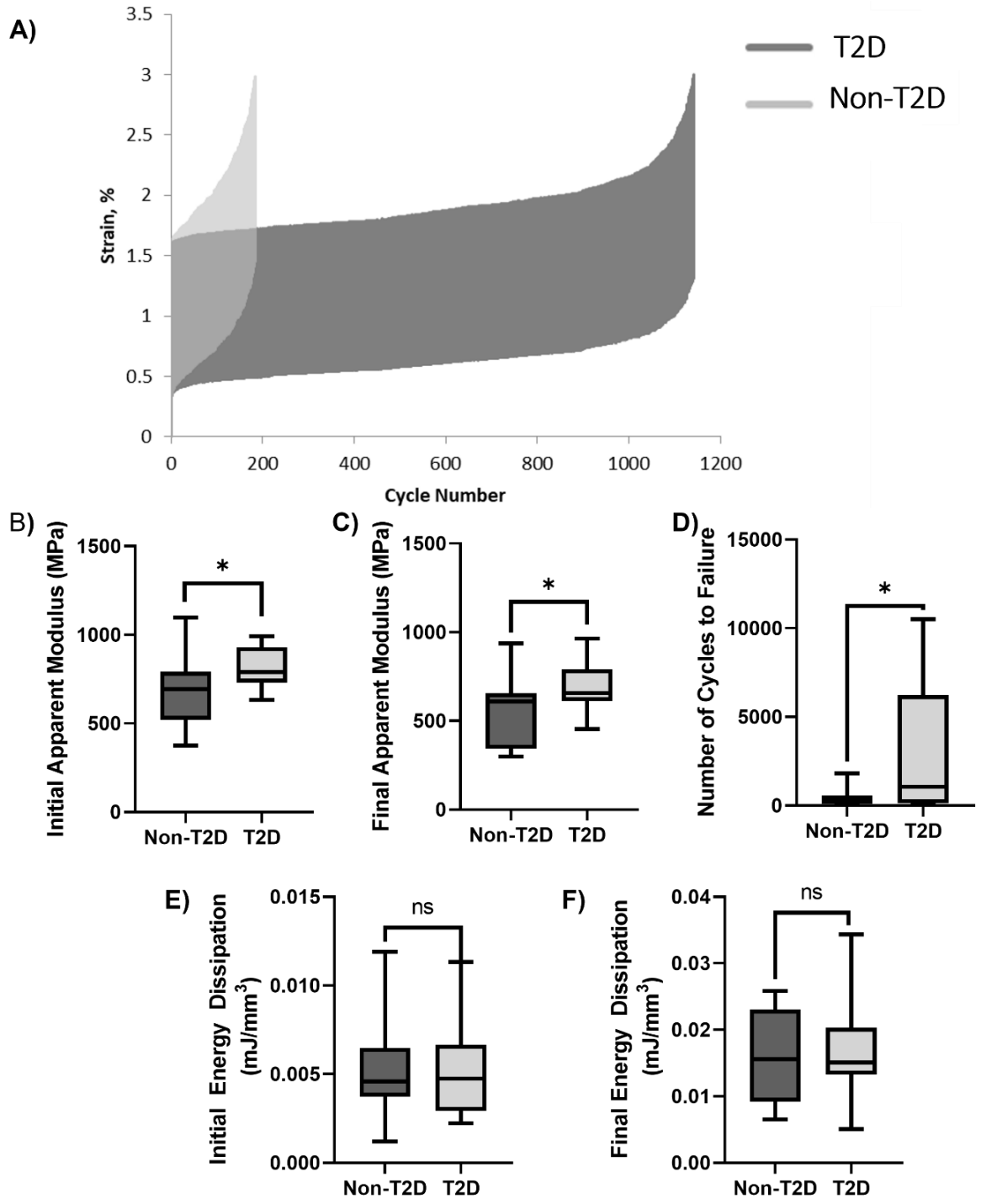

*Figure 4.6 Cyclic compression mechanical properties A) representative creep-fatiguecurve, B) initial apparent modulus, C) final apparent modulus, D) number of cycles to failure, E) initial energy dissipation, and F) final energy dissipation. *($p<0.05$)*

Table 4.2 Trabecular bone monotonic compression and cyclic compression measured mechanical properties.

	Non-T2D (*n*=15)	**T2D (*n*=14)**	**95% Confidence Interval**	***p*-value**
Monotonic Compression				
Apparent Modulus (MPa)	605±175	763±171	(-290.0, -25.7)	**0.021**
Yield Stress (MPa)	10.21±4.7	14.19±4.4	(-7.46, -0.51)	**0.026**
Yield Strain (%)	1.87±0.32	2.09±0.32	(-0.46, 0.02)	0.075
Max Stress (MPa)	10.98±5.08	16.11±5.15	(-9.05, -1.22)	**0.012**
Post-yield Strain (%)	7.55±0.54	7.31±0.55	(-0.173 0.66)	0.241
Pre-Yield Toughness (mJ/mm^3)	0.11±0.07	0.17±0.07	(-0.11, -0.003)	**0.042**
Post-Yield Toughness (mJ/mm^3)	0.51±0.25	0.81±0.32	(-0.52, -0.08)	**0.011**
Toughness (mJ/mm^3)	0.62±0.32	0.98±0.39	(-0.63, -0.08)	**0.013**
Mean Intercept Length Tensor (°)	18.9±12.4	12.9±6.71	(-13.70, 1.53)	0.111
Cyclic Compression				
Initial Apparent Modulus (MPa)	676±188	814±166	(-257.5, 18.9)	**0.025**
Final Apparent Modulus (MPa)	561±187	695±151	(-264.4, - 5.1)	**0.042**
% Reduction in Modulus	16.8±17.6	15±11.3	(-9.42, 13.10)	0.738
Initial Energy Dissipation (mJ/mm^3)	0.005±0.003	0.005±0.003	(-0.002, 0.002)	0.907
Final Energy Dissipation (mJ/mm^3)	0.016±0.007	0.016±0.007	(-0.006, 0.005)	0.885
% Increase in Energy Dissipation	262±205	241±206	(-143, 186)	0.791
Number of Cycles to Failure (N_f)	484±553	3988±4385	(-4791, -144)	**0.039**

Table 4.3 Monotonic results normalised three ways, firstly by dividing by BV/TV, secondly by using a general linear model and finally by using a power law model.

Normalised	Non-T2D (*n*=15)		T2D (*n*=14)		*p*-value
Monotonic Compression Divided by BV/TV					
Apparent Modulus (MPa/(BV/TV))	2633	±760	3320	±746	**0.021**
Yield Stress (MPa/(BV/TV))	44.4	±20.4	61.8	±19.2	**0.026**
Max Stress (MPa/(BV/TV))	47.8	±22.1	70.1	±22.4	**0.012**
Pre-Yield Toughness (mJ/mm^3) /(BV/TV)	0.50	±0.29	0.73	±0.30	**0.042**
Post-Yield Toughness (mJ/mm^3/(BV/TV))	2.21	±1.09	3.52	±1.41	**0.011**
Toughness (mJ/mm^3/(BV/TV))	2.71	±1.37	4.25	±1.68	**0.013**
General Linear Model					
Apparent Modulus (MPa)	0.93	±0.20	1.07	±0.23	0.078
Yield Stress (MPa)	0.91	±0.25	1.09	±0.32	0.110
Max Stress (MPa)	0.88	±0.23	1.11	±0.36	0.073
Pre-Yield Toughness (mJ/mm^3)	0.90	±0.30	1.09	±0.42	0.166
Post-Yield Toughness (mJ/mm^3)	0.85	±0.21	1.13	±0.49	0.063
Toughness (mJ/mm^3)	0.86	±0.21	1.13	±0.47	0.067
Power Law Model					
Apparent Modulus (MPa)	0.97	±0.20	1.08	±0.24	0.181
Yield Stress (MPa)	0.97	±0.26	1.12	±0.36	0.198
Max Stress (MPa)	0.95	±0.25	1.15	±0.41	0.128
Pre-Yield Toughness (mJ/mm^3)	0.98	±0.33	1.17	±0.46	0.211
Post-Yield Toughness (mJ/mm^3)	0.93	±0.23	1.19	±0.55	0.116
Toughness (mJ/mm^3)	0.93	±0.23	1.18	±0.52	0.118

4.3.2.3 Microdamage Accumulation

Figure 4.7 shows a box plot of microdamage accumulation volume across each group, expressed as the damage volume/bone volume, and an example of scanned trabecular samples showing microdamage accumulation. There was no significant difference in the level of microdamage accumulation between T2D and non-T2D samples. However, there was a significant difference in the microdamage accumulation across the mechanical tests carried out. In the T2D group, the monotonic compression sample had a significantly higher level of microdamage compared to the cyclic sample and the non-mechanically tested control sample. The same significant differences were present for the non-T2D group, with the monotonic samples having a significantly higher level of microdamage accumulation than the cyclic and control samples. One non-T2D sample was incorrectly stained during this process and was removed from the analysis.

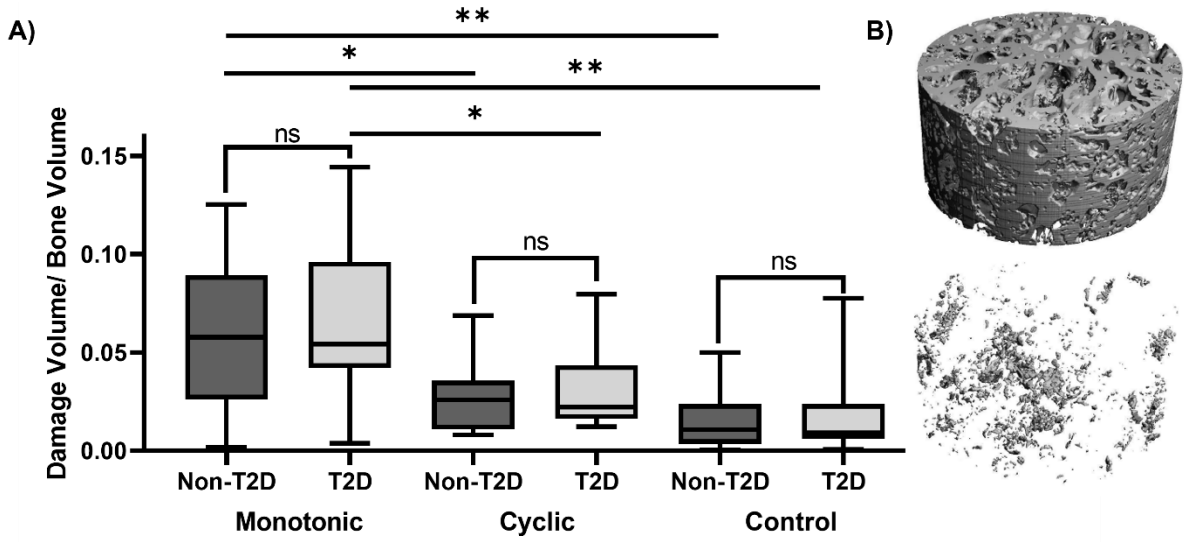

*Figure 4.7 A) Microdamage accumulation results, B) micro-CT scan of damage. *($p<0.05$), **($p<0.01$)*

4.3.2.4 Nanoindentation testing

Figure 4.8 shows results from nanoindentation testing for trabecular and cortical tissue. No significant differences were found in either elastic modulus or hardness between the non-T2D and T2D groups in any of the cortical or trabecular regions examined.

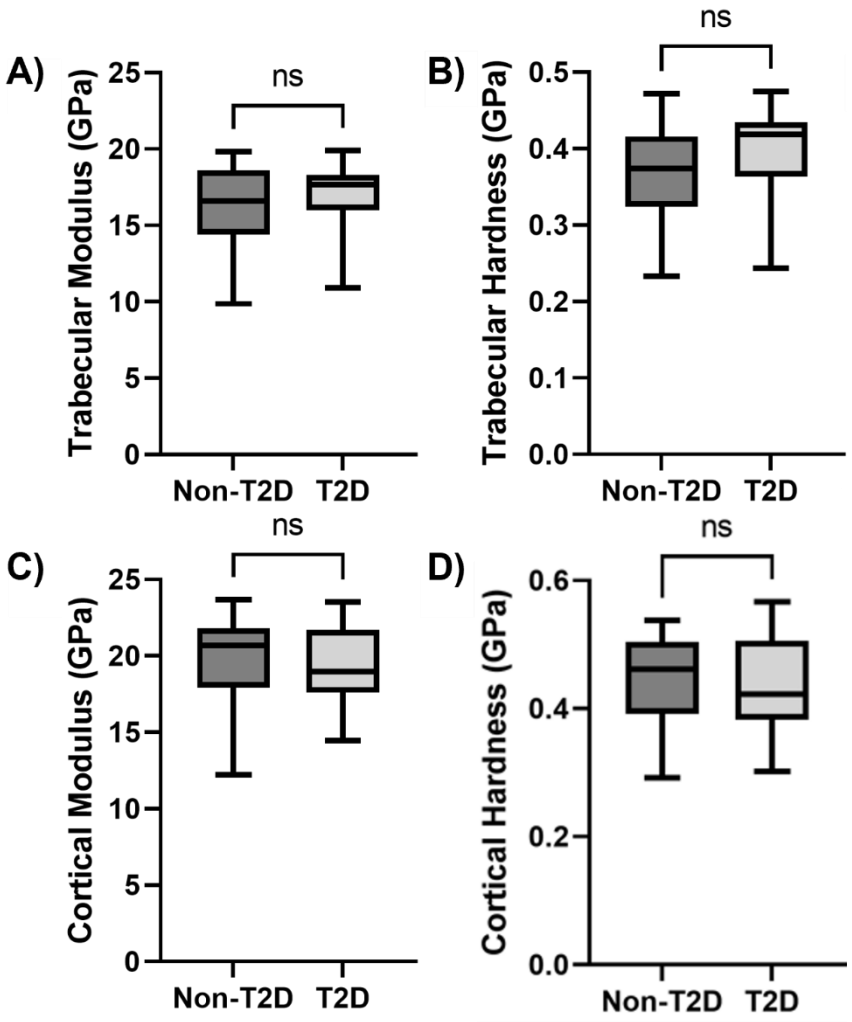

Figure 4.8 Nanoindentation results A) trabecular modulus, B) trabecular hardness, C) cortical modulus and D) cortical hardness.

4.3.3 Compositional Results

4.3.3.1 Fluorescent AGE Analysis and High-Performance Liquid Chromatography

Figure 4.9 shows the results from the compositional analysis of bone. The results of the fluorescent AGE analysis are shown in Figures 4A-C for cortical bone and Figures 4D-F for trabecular bone. No differences were found in the levels of fluorescent AGE in cortical or trabecular bone of non-T2D compared to T2D. Levels of glycation were significantly higher in T2D compared to the non-T2D group, with higher measurements of trabecular furosine (+40%, $p<0.001$), cortical furosine (+65%, $p=0.001$) and cortical CML (+97%, $p=0.004$), as shown in Figure 4.9B, C and E respectively. Trabecular CML (+10%, $p=0.604$) was not significantly different.

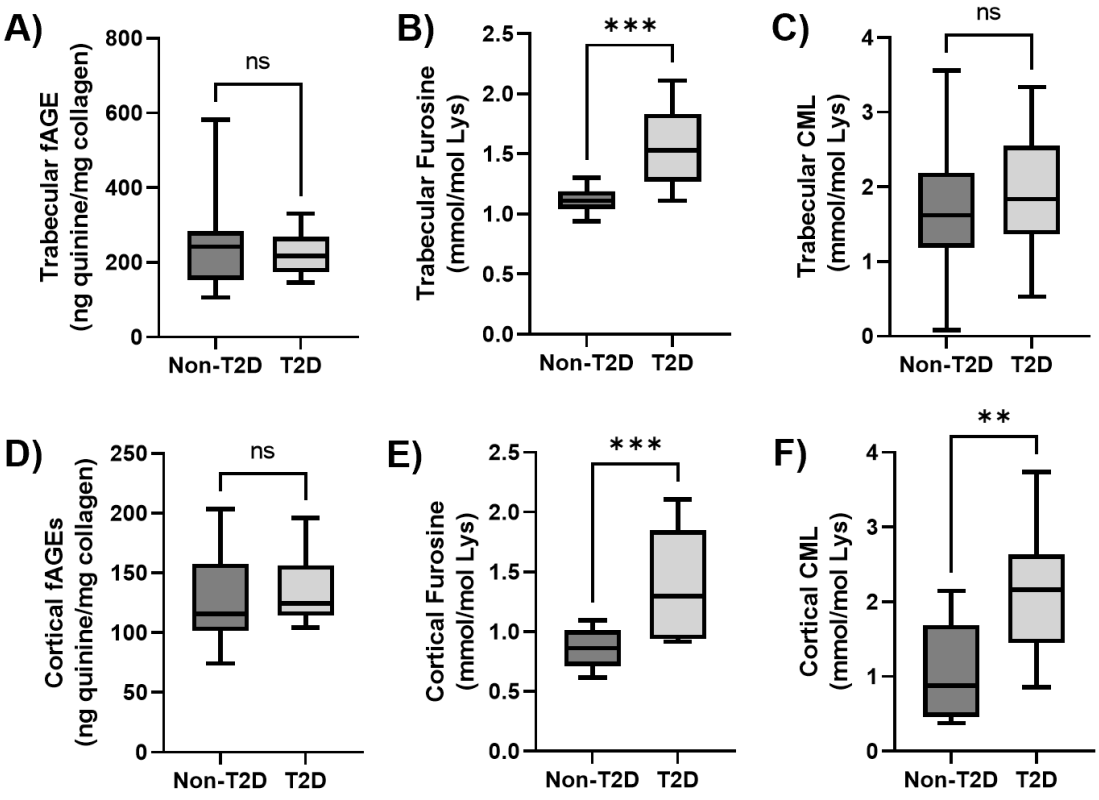

*Figure 4.9 Compositional analysis of bone A) trabecular fluorescent AGEs, B) trabecular furosine, C) trabecular CML, D) cortical fluorescent AGEs, E) cortical furosine, and cortical CML. *(p<0.05), **(p<0.01), ***(p<0.001)*

Table 4.4 Compositional analysis of bone with results from HPLC and fluorometric analysis. fAGE = fluorescent AGE

	Non-T2D		T2D		CI	p-value
Trabecular Furosine (mmol/mol Lys)	1.12	±0.1	1.57	±0.33	(-0.64, -0.25)	**<0.001**
Trabecular CML (mmol/mol Lys)	1.78	±0.88	1.95	±0.8	(-0.80, 0.48)	0.604
Cortical Furosine (mmol/mol Lys)	0.86	±0.16	1.42	±0.44	(-0.84, -0.27)	**0.001**
Cortical CML (mmol/mol Lys)	1.05	±0.66	2.07	±0.8	(-1.68, -0.38)	**0.004**
Trabecular fAGE ng quinine/ mg collagen	255	±127	226.6	±58.6	(-47.7, 104.5)	0.444
Cortical fAGE ng quinine/ mg collagen	128.5	±39.6	135.3	±29.7	(-40.3, 26.5)	0.665

4.3.3.2 Raman Spectroscopy

The results of the Raman spectroscopy are presented in Table 4.5. The T2D trabecular bone had significantly higher mineral to matrix ratios for ν_1PO_4/Amide I, ν_1PO_4/Amide III, ν_1PO_4/Proline, and ν_1PO_4/CH_2, an altered carbonate to amide I ratio with higher (1065/1653 cm^{-1}) and lower (1065/1674 cm^{-1}) values, lower carbonate substitution, lower crystallinity, and a higher amide I/amide III ratio compared to the non-T2D bone. The mineral maturity, helical status, and hydroxyproline to proline ratio were similar across groups.

The cortical bone had a lower mineral-to-matrix ratio for ν_1PO_4/Amide I, and higher mineral-to-matrix ratios for ν_1PO_4/Proline and ν_1PO_4/CH_2, higher crystallinity, and a higher hydroxyproline to proline ratio. The carbonate to amide I ratio, carbonate substitution, matrix maturity, helical status, and amide I/amide III ratio were similar across groups.

*Table 4.5 Cortical and trabecular bone compositional properties determined by Raman spectroscopy. Hyp is hydroxyproline (*p<0.05, **p<0.01, ***p<0.001)*

				Cortical			Trabecular		
Phase			Bands (cm^{-1})	**Non-T2D**	**T2D**	**Non-T2D vs T2D**	**Non-T2D**	**T2D**	**Non-T2D vs T2D**
Mineral phase/ Organic phase	**Mineral /Matrix ratio**	$\nu1PO_4$ /Amide I	957/1624	0.21±0.06	0.17±0.04	**(↓19%) *****	0.25±0.07	0.29±0.07	NS
			957/1653	0.49±0.14	0.42±0009	NS	0.81±0.28	1.32±0.35	**(↑ 63%)*****
			957/1674	0.26±0.07	0.26±0.06	NS	0.35±0.10	0.32±0.09	NS
			957/1698	0.31±0.09	0.33±0.08	NS	0.51±0.15	0.73±0.19	**(↑43%)*****
		$\nu1PO_{4arbonate}$ /Amide III	957/1243	0.72±0.15	0.74±0.02	NS	0.67±0.14	0.72±0.14	NS
			957/1267	0.22±0.05	0.21±0.04	NS	0.30±0.08	0.44±0.10	**(↑27%)*****
		$\nu1PO_4$/Proline	957/853	1.77±0.44	2.18±0.58	**(↑23%) ****	1.5±0.35	2.14±0.55	**(↑53%)*****
		$\nu1PO_4/CH_2$	957/1440	0.28±0.07	0.36±0.08	**(↑29%) *****	0.31±0.08	0.37±0.09	**(↑19%)*****
		CO_3/1628-1680	1065/1624	0.65±0.08	0.60±0.07	NS	0.74±0.09	0.69±0.10	NS
			1065/1653	1.89±0.27	1.84±0.31	NS	2.63±0.44	3.27±0.62	**(↑24%)*****
			1065/1674	1.03±0.14	0.94±0.14	NS	1.10±0.15	0.97±0.16	**(↓11%)****
			1065/1698	1.14±0.17	1.25±0.18	NS	1.77±0.33	1.60±0.25	NS
Mineral phase	**Carbonate substitution**	CO_3 /$1PO_4$	1065/957	0.95±0.67	3.36±0.68	NS	2.74±0.56	2.32±0.46	**(↓15%) ****
	Crystallinity	FWHM($\nu1$ PO_4) 1 / FWHM(PO_4)	957(i)	32.76±11.0	3301±1.00	NS	29.99±1.14	28.40±1.06	**(↓5%) *****
			957(width)	24.99±0.43	25.00±0.4	NS	25.45±0.42	25.67±0.45	NS
			957(height)	7.70±0.24	7.85±0.23	**(↑2%) ***	6.95±0.24	6.71±0.25	**(↓3%) *****
			1/957	0.07±0.00	0.07±0.00	NS	0.07±0.00	0.07±0.00	NS
Organic phase	**Matrix maturity**	I1661/I1690	1674/1698	1.13±0.21	1.09±0.21	NS	1.31±0.31	1.40±0.31	NS
	Helical status	I1661/I1640	1674/1653	1.75±0.29	1.68±0.32	NS	2.49±0.63	2.62±0.58	NS
	Hyp to proline	I875/I850	875/853	7.33±1.84	9.24±2.31	**(↑ 26%)*****	4.37±0.92	4.78±1.00	NS
	Amide I / Amide III	I1628↓I1680 / I1236↓1270	1624/1243	2.69±0.61	3.21±1.04	NS	1.82±0.38	1.84±0.41	NS
			1653/1243	1.01±0.33	1.10±0.38	NS	0.41±0.14	0.44±0.13	NS
			1674/1243	1.84±0.48	1.94±0.67	NS	1.43±0.37	1.30±0.33	NS
			1698/1243	1.33±0.37	1.61±0.55	NS	0.82±0.25	0.80±0.22	NS
			1624/1267	1.38±0.10	1.41±0.13	NS	1.38±0.13	1.50±1.18	**(↑ 9%) *****
			1653/1267	0.45±0.05	0.46±0.06	NS	0.32±0.07	0.30±0.06	NS
			1674/1267	0.84±0.09	0.82±0.12	NS	0.81±0.13	1.00±0.17	**(↑23%)*****
			1698/1267	0.66±0.11	0.66±0.08	NS	0.55±0.10	0.56±0.11	NS

4.4 Discussion

Previous population-level studies have found that T2D patients have an increased fracture risk when compared to non-diabeticT2D patients. The present study evaluated bone composition, mechanical properties and microdamage accumulation of T2D femoral head trabecular bone tissue under monotonic and cyclic loading and has added more information to the limited experimental data on human T2D bone. Cylindrical cores from the femoral head were tested in monotonic and cyclic compression, morphologically analysed using micro-CT, stained for microdamage accumulation using barium sulphate and compositionally analysed using fluorometric analysis, HPLC and Raman. Nanoindentation was also carried out on sections of trabecular and cortical bone from these femoral heads. It was found that T2D does not have a detrimental effect on the mechanical properties of trabecular bone from the femoral head of T2D patients. In fact, T2D bone had higher strength, and resistance to deformation, with higher apparent modulus, yield stress, max stress, pre- and post-yield toughness, and toughness. These findings are similar to the majority other recent studies that have also found no reduction in mechanical properties of T2D trabecular bone (Karim et al. 2018; Hunt et al. 2019; Parle et al. 2020) compared to non-T2D controls. Furthermore, under cyclic loading, the T2D diabetic samples could withstand a greater number of cycles-to-failure, compared to controls. While elevated levels of AGEs were found in T2D bone, along with distinct changes in the mineral-to-matrix ratio, mineral phase and organic phase, it was found that T2D does not impair the mechanical properties of trabecular bone from the femoral heads of T2D patients. This suggests that other mechanisms may be responsible for the increase fracture risk seen in T2D patients.

These results are broadly in line with earlier research showing that T2D patients have either a denser or preserved trabecular microarchitecture compared to non-diabetic controls (Andrade et al. 2020; Starr et al. 2018; Nilsson et al. 2017; Sacher et al. 2022; Hunt et al. 2019). Structural analysis revealed a greater BV/TV and trabecular number in the T2D samples compared to

non-T2D samples, although lower tissue mineral density and trabecular separation were found in the T2D samples, while connectivity density and trabecular thickness were not significantly different. Other studies have found denser or maintained trabecular microarchitecture in populations with predominantly well-controlled or early-stage T2D (Sacher et al. 2022; Andrade et al. 2020). However, longer disease duration or the presence of comorbidities can result in impaired microarchitecture, with reductions in bone volume fraction reported in T2D patients who have undergone a fragility fracture with a mean duration of disease of 7.5 years (Sihota et al. 2021). The preserved trabecular microarchitecture in T2D could be a result of an anabolic reaction brought on by hyperinsulinemia (Thrailkill et al. 2005), remodelling adjustment to higher BMI or the altered remodelling process seen in T2D. In the current study, the BMI of the T2D patients was unfortunately not available. However, generally, patients with T2D tend to have higher BMI compared to people in good health (Nilsson et al. 2017).

Raman spectroscopy indicated that the composition of the bone matrix was altered in the T2D group compared to the non-T2D bone. The T2D trabecular bone had a higher mineral-to-matrix ratio, a lower carbonate substitution and crystallinity compared to the non-T2D trabecular bone. These compositional changes could be, in part, linked to the altered mechanical properties in T2D trabecular bone found in this Chapter. Higher mineral-to-matrix ratio has been linked to higher strength in cortical bone (Unal et al. 2018; Unal 2021) so this could contribute to the higher effective strength of the trabecular samples obtained here under monotonic loading. Additionally, the higher mineral-to-matrix ratio could also explain the higher fatigue life of the T2D trabecular cores. However, it should be noted that if the bone becomes too mineralised, it can become brittle and be more likely to fracture. The precise role of both carbonate substitution and crystallinity and their effect on the mechanical properties of bone remains poorly understood (Unal 2021). Some studies have found that higher carbonate substitution was linked to reduced strength (Unal 2021) and fragility (McCreadie et al. 2006),

while others have found that lower carbonate substitution was linked to fragility (Boskey et al. 2016). Higher crystallinity has also been linked with increased strength (Unal 2021) and stiffness and decreased ductility (Yerramshetty and Akkus 2008), suggesting lower crystallinity would lead to the opposite. However, despite the T2D group having lower crystallinity there was no reduction in mechanical properties. Additionally, the differences in mineral-to-matrix ratio, carbonate substitution and crystallinity suggest an altered remodelling process is occurring in T2D compared to non-T2D. Studies that investigated the bone tissue composition of T2D patients using different methods found varying results, with several studies finding no difference in compositional features (Wölfel et al. 2022; Lekkala et al. 2023) Other studies have observed different matrix composition. Sihota et al. (2021) used FTIR and found a lower mineral-to-matrix ratio and enzymatic crosslink ratio, and a higher non-enzymatic crosslink ratio in T2D patients. Rokidi et al. (2020) also used Raman and found no difference in the mineral-to-matrix ratio but an increase in mineral crystallinity in T2D patients compared to non-T2D controls. Wölfel et al. (2022) used Raman and found a higher carbonate substitution in the cortical bone of the buccal cortex of T2D patients but no difference in the mineral-to-matrix ratio. Further research is needed to elucidate the precise compositional characteristics of T2D bone.

Bulk measurement of total fluorescent AGEs revealed no significant differences between T2D and non-T2D, which is similar to findings across several recent studies that have also measured bulk fluorescent AGEs (Karim et al. 2018; Hunt et al. 2019). However, other studies have found differences in bulk fluorescent AGE accumulation (Sihota et al. 2021; Andrade et al. 2020; Piccoli et al. 2020). In the current study, there were significant changes in non-fluorescent AGEs in T2D bone, reporting for the first time higher levels of furosine present in cortical and trabecular bone, while also observing higher levels of CML in cortical bone, which has been shown previously (Dhaliwal et al. 2022; Rokidi et al. 2020). Recently, Arakawa and

colleagues found that, of the AGEs that are currently quantifiable, adducts are considerably more abundant than cross links by at least an order of magnitude (Arakawa et al. 2020). This highlights the importance of measuring not only the bulk fluorescent AGEs but also specific non-fluorescent and adduct AGEs such as CML.

Under monotonic loading, it was found that the apparent modulus, yield stress, maximum stress, pre-yield toughness, post-yield toughness and toughness were significantly greater for the T2D samples compared to the non-T2D samples. When normalised by dividing by BV/TV, the max stress, pre-yield toughness, post-yield toughness, and toughness remained significantly higher. These results suggest that the T2D samples had improved tissue-level properties, with higher strength and resistance to deformation, although these significant differences were no longer evident when normalised using GLM and PLM. These findings are similar to Hunt et al. (2019) who found a higher modulus, yield stress and ultimate stress in T2D samples (when normalised by dividing by BV/TV), although the post-yield properties were not different. Several other studies (Karim et al. 2018; Piccoli et al. 2020) have found no differences in the apparent mechanical properties of T2D bone, while others (Sihota et al. 2021) have found impaired properties. Similarly, the results from cyclic testing of the bone revealed that the initial apparent modulus and the final modulus were higher for the T2D samples. There was no difference in the percentage reduction in modulus between the first and final cycles, nor were there differences between the initial or final energy dissipation or strain energies. Interestingly, this current study found that the numbers of cycles to failure for T2D samples were significantly higher compared to non-T2D samples, although the overall damage volume accumulation between groups was similar for all loading scenarios. Sacher et al. (2022) also found that total damage accumulation did not differ in T2D compared to non-T2D samples following monotonic testing. Nanoindentation results fell within the range reported for human trabecular and cortical bone at the femoral neck (Zysset et al. 1999), but no differences in tissue

level properties were observed. Other studies have found impaired tissue-level mechanical properties through nanoindentation (Sihota et al. 2021) and cyclic reference point indentation (Karim et al. 2018). This may be explained by the fact that the cohort used in Sihota and colleagues study consisted of first fragility fracture patients and the different test method used by Karim and colleagues. While AGE accumulation is hypothesised to cause increased fracture risk in T2D patients, no supporting evidence of this was found, with no significant difference in microdamage accumulation between groups and the T2D samples actually withstanding a greater number of fatigue cycles before failure. Compositional analysis revealed distinct changes in both organic and mineral phases of the bone tissue matrix of the T2D bone compared to the non-T2D, including a higher mineral-to-matrix ratio, a lower carbonate substitution and crystallinity. These changes coincided with higher mechanical properties under both monotonic and cyclic loading. Currently, there is a lack of in vivo and ex vivo human experimental evidence that quantitatively links AGE accumulation to increased bone fragility in T2D. Given these findings, there is still much to be understood about AGEs and their effects on bone and, in particular, the impact that AGE adducts have on the mechanical properties of bone needs to be better understood (Willett et al. 2022). This understanding needs to apply to both cortical and trabecular bone as they both play an important role in resisting fracture (Thomas et al. 2009) (Ritchie et al. 2005), particularly as it has been suggested that cortical bone may be primarily responsible for hip fracture that occur in the femoral neck (Crabtree et al. 2001).

There are some limitations associated with this study. The primary limitation of the study was the patient data information, which had limited information on factors such as BMI, HbA1C, disease duration and long-term disease management. Fracture risk is influenced by T2D disease control and duration and therefore the results cannot be related to control or duration. While the results of this study are not controlled for disease control or duration, the samples came

from sex, age, and disease-matched individuals with (clinically diagnosed osteoporosis) and without fractures (clinically diagnosed osteoarthritis). When the results of the overall group where further broken down to osteoarthritis with and without T2D and osteoporosis with and without T2D, the mechanical and morphological results for the OA were similar to the results of the overall group and there was no notable difference observed in the OP group. Additionally, there AGE accumulation did not differ significantly between T2D and non-T2D in either OA or OP. Another limitation is that bone from the femoral head was used instead of the femoral neck, which is a more common fracture site. This was done to ensure the results were comparable as not all explants had sufficient tissue in the femoral neck to extract samples. Finally, the applied cyclic strain was higher than physiological strain (Yang et al. 2011), however they are still below levels of uniaxial yield strain (Morgan and Keaveny 2001). By using the selected strain range it was possible to induce detectable microdamage while preventing excessive degradation of the material caused by external is the first study to report an increase in the early AGE marker furosine in T2D bone. This study is also the first to characterise the cyclic behaviour and subsequent microdamage accumulation of T2D bone.

4.5 Conclusions

This study complements the increasing body of recent research of the biomechanics of T2D trabecular bone. It was found that the mechanical properties of trabecular bone from the femoral head of T2D patients were not impaired by the condition. In fact, even when normalised against BV/TV, T2D bone had higher yield and maximum strength and greater resistance to deformation compared to controls, despite a significant increase in AGE levels. Distinct changes were observed in both the organic and mineral phases of the bone tissue matrix through compositional analysis, including a higher mineral-to-matrix ratio, a lower carbonate substitution and crystallinity. These changes were found to correspond with higher mechanical properties under both monotonic and cyclic loading. These results are consistent with earlier

investigations that also found no significant reduction in mechanical properties of trabecular bone from T2D. In addition, the T2D samples could endure more cycles before failing under cyclic loading than controls. According to this study, T2D does not impair the mechanical properties of trabecular bone in the femoral head, suggesting that other processes may be responsible for the increased risk of fractures in T2D.

4.6 Appendix 4.1

When the mechanical results are split further and looked at in groups of OA and OP, the monotonic mechanical properties generally remained higher in the T2D samples with OA compared to the non-T2D samples with OA. These T2D samples with OA also exhibited a significantly higher number of cycles to failure compared to the non-T2D samples with OA. However, for the OP group no difference in monotonic or cyclic mechanical properties was observed between the T2D and non-T2D samples. Furthermore, the T2D samples with OA demonstrated denser morphological properties than the non-T2D samples with OA. Conversely, no difference was observed in the OP group between T2D and non-T2D samples. In terms of composition, T2D bone had higher levels of trabecular and cortical furosine in both OA and OP groups. T2D samples with OA also had a higher level of cortical CML compared to the non-T2D OA samples. No differences were observed in the level of AGE accumulation in either OA or OP.

Table A4.1 Monotonic, cyclic, morphology and AGE results when split by osteoarthritis (OA) and osteoporosis (OP). Where CML is carboxymethyl-lysine and fAGE is fluorescent advanced glycation end-products.

	OA			OP		
	Non-T2D (*n*=7)	T2D (*n*=7)	p-value	Non-T2D (*n*=8)	T2D (*n*=7)	p-value
Monotonic Compression						
Apparent Modulus (MPa)	638 ±127	817 ±149	0.034	576 ±213	709 ±186	0.222
Yield Stress (MPa)	10.11 ±3.23	15.20 ±4.28	0.029	10.29 ±5.93	13.19 ±4.62	0.309
Yield Strain (%)	2.26 ±0.56	2.62 ±0.51	0.236	2.61 ±0.51	2.76 ±0.32	0.614
Max Stress (MPa)	10.79 ±3.38	17.31 ±4.89	0.016	11.15 ±6.47	14.92 ±5.51	0.246
Post-yield Strain (%)	7.74 ±0.56	7.78 ±0.51	0.236	7.39 ±0.51	7.24 ±0.62	0.614
Pre-Yield Toughness (mJ/mm^3)	0.11 ±0.05	0.18 ±0.08	0.048	0.13 ±0.09	0.17 ±0.07	0.377
Post-Yield Toughness (mJ/mm^3)	0.48 ±0.14	0.88 ±0.35	0.027	0.53 ±0.33	0.74 ±0.31	0.235
Toughness (mJ/mm^3)	0.59 ±0.19	1.06 ±0.42	0.026	0.66 ±0.41	0.90 ±0.37	0.249
Cyclic Compression						
Initial Apparent Modulus (MPa)	668 ±150	840 ±149	0.054	683 ±227	788 ±73	0.253
Final Apparent Modulus (MPa)	587 ±146	755 ±179	0.079	538 ±225	636 ±97	0.294
% Reduction in Modulus	11.2 ±19.4	10.6 ±11.2	0.949	21.8 ±15.4	19.3 ±10.4	0.724
Initial Energy Dissipation (mJ/mm^3)	0.006 ±0.003	0.005 ±0.003	0.47	0.005 ±0.003	0.006 ±0.002	0.495
Final Energy Dissipation (mJ/mm^3)	0.19 ±0.007	0.013 ±0.006	0.11	0.013 ±0.006	0.191 ±0.007	0.112
% Increase in Energy Dissipation	385 ±231	284 ±155	0.386	342 ±194	382 ±238	0.733
Number of Cycles to Failure (N_f)	342 ±449	5491 ±4385	0.021	608 ±634	413 ±447	0.499
Morphology						
Connectivity Density (1/mm3)	4.447 ±0.75	8.67 ±4.49	0.05	6.04 ±2.29	5.76 ±2.07	0.804
Structural Model Index	0.419 ±0.21	-0.324 ±0.49	0.01	0.25 ±0.40	-0.078 ±0.30	0.095
Bone Mineral Density (mg HA/cm^3)	232.1 ±21.6	306.6 ±53.2	0.011	253.6 ±75.9	268.4 ±22	0.614
Tissue Mineral Density (mg HA/cm^3)	1055.5 ±15.7	1026.7 ±18.2	0.009	1044.2 ±11.9	1025.8 ±18.1	0.044
Bone Volume/Total Volume	0.2196 ±0.02	0.2938 ±0.04	0.005	0.2408 ±0.07	0.2656 ±0.02	0.37
Bone Surface/Bone Volume	14.95 ±1.28	14 ±3.03	0.466	14.95 ±1.28	14 ±3.03	0.466
Trabecular Number (1/mm)	1.628 ±0.13	2.008 ±0.31	0.017	1.707 ±0.20	1.775 ±0.18	0.498
Trabecular Thickness (mm)	0.1342 ±0.01	0.1457 ±0.03	0.304	0.1398 ±0.03	0.1493 ±0.01	0.483
Trabecular Separation (mm)	0.4839 ±0.05	0.3599 ±0.05	0.001	0.4569 ±0.08	0.4212 ±0.05	0.316
Advanced Glycation End-Products						
Trabecular Furosine (mmol/mol Lys)	1.08±0.1	1.5±0.2	0.004	1.16±0.1	1.68±0.4	0.015
Trabecular CML (mmol/mol Lys)	1.35±0.7	1.8±0.9	0.285	2.16±0.9	2.06±0.7	0.813
Cortical Furosine (mmol/mol Lys)	0.9±0.2	1.3±0.3	0.020	0.83±0.1	1.58±0.5	0.020
Cortical CML (mmol/mol Lys)	1.0±0.7	1.9±0.6	0.030	1.23±0.7	2.30±1.0	0.114
Trabecular fAGE (ng quinine/mg collagen)	274±183	237±54	0.626	239±53	216±65.3	0.487
Cortical fAGE (ng quinine/mg collagen)	142±41	145±37.2	0.900	102±24	125±14	0.266

Table 4.6 Monotonic results normalised by mean intercept length tensor (MIL)by using a general linear model and a power law model.

Normalised to MIL	**Non-T2D (*n*=15)**		**T2D (*n*=14)**		***p*-value**
Monotonic Compression General Linear Model					
Apparent Modulus (MPa)	0.94	±0.22	1.07	± 0.23	0.120
Max Stress (MPa)	**0.86**	**±0.34**	**1.15**	**±0.37**	**0.037**
Yield Stress (MPa)	0.90	±0.35	1.12	±0.33	0.099
Pre-Yield Toughness (mJ/mm^3)	0.88	±0.46	1.15	±0.45	0.121
Post-Yield Toughness (mJ/mm^3)	0.81	±0.36	1.20	±0.48	0.026
Toughness (mJ/mm^3)	**0.82**	**±0.38**	**1.19**	**±0.47**	**0.031**
Power Law Model					
Apparent Modulus (MPa)	0.95	± 0.20	1.12	± 0.26	0.059
Yield Stress (MPa)	0.94	±0.37	1.22	±0.38	0.056
Max Stress (MPa)	**0.92**	**±0.38**	**1.27**	**±0.43**	**0.027**
Pre-Yield Toughness (mJ/mm^3)	0.96	±0.53	1.32	±0.53	0.077
Post-Yield Toughness (mJ/mm^3)	**0.90**	**±0.42**	**1.36**	**±0.57**	**0.022**
Toughness (mJ/mm^3)	**0.90**	**±0.43**	**1.34**	**±0.55**	**0.025**

4.7 References

Andrade, Vicente FC, Domingos C Chula, Fábio P Sabbag, Daniel D da S Cavalheiro, Lorena Bavia, Altair Rogério Ambrósio, Cleber Rafael V Da Costa, Luciene M Dos Reis, Victória ZC Borba, and Carolina Aguiar Moreira. 2020. 'Bone histomorphometry in young patients with type 2 diabetes is affected by disease control and chronic complications', *The Journal of Clinical Endocrinology & Metabolism*, 105: 506-14.

Arakawa, Shoutaro, Ryusuke Suzuki, Daisaburo Kurosaka, Ryo Ikeda, Hiroteru Hayashi, Tomohiro Kayama, Rei-ichi Ohno, Ryoji Nagai, Keishi Marumo, and Mitsuru Saito. 2020. 'Mass spectrometric quantitation of AGEs and enzymatic crosslinks in human cancellous bone', *Scientific Reports*, 10: 18774.

Bevill, G., F. Farhamand, and T. M. Keaveny. 2009. 'Heterogeneity of yield strain in low-density versus high-density human trabecular bone', *J Biomech*, 42: 2165-70.

Boskey, Adele L, Eve Donnelly, Elizabeth Boskey, Lyudmila Spevak, Yan Ma, Wei Zhang, Joan Lappe, and Robert R Recker. 2016. 'Examining the relationships between bone tissue composition, compositional heterogeneity, and fragility fracture: a matched case-controlled FTIRI study', *JOURNAL OF BONE AND MINERAL RESEARCH*, 31: 1070-81.

Brennan, O., O. D. Kennedy, T. C. Lee, S. M. Rackard, and F. J. O'Brien. 2009. 'Biomechanical properties across trabeculae from the proximal femur of normal and ovariectomised sheep', *Journal of Biomechanics*, 42: 498-503.

Britton, Marissa, Eoin Parle, and Ted Vaughan. 2022. 'An investigation on the effects of in vitro induced advanced glycation end-products on cortical bone fracture mechanics at fall-related loading rates', *Journal of the Mechanical Behavior of Biomedical Materials*: 105619.

Burr, David B., R. Bruce Martin, Mitchell B. Schaffler, and Eric L. Radin. 1985. 'Bone remodeling in response to in vivo fatigue microdamage', *Journal of Biomechanics*, 18: 189-200.

Carnevale, V., E. Romagnoli, L. D'Erasmo, and E. D'Erasmo. 2014. 'Bone damage in type 2 diabetes mellitus', *Nutrition, Metabolism and Cardiovascular Diseases*, 24: 1151-57.

Crabtree, N, N Loveridge, M Parker, N Rushton, J Power, KL Bell, TJ Beck, and J Reeve. 2001. 'Intracapsular hip fracture and the region-specific loss of cortical bone: analysis by peripheral quantitative computed tomography', *JOURNAL OF BONE AND MINERAL RESEARCH*, 16: 1318-28.

Dhaliwal, R., S. K. Ewing, D. Vashishth, R. D. Semba, and A. V. Schwartz. 2022. 'Greater Carboxy-Methyl-Lysine Is Associated With Increased Fracture Risk in Type 2 Diabetes', *J Bone Miner Res*, 37: 265-72.

Epstein, Sol, and Derek LeRoith. 2008. "Diabetes and fragility fractures - A burgeoning epidemic?" In *Bone*.

Fazzalari, N. L., M. R. Forwood, B. A. Manthey, K. Smith, and P. Kolesik. 1998a. 'Three-dimensional confocal images of microdamage in cancellous bone', *Bone*, 23: 373-78.

Fazzalari, N. L., M. R. Forwood, K. Smith, B. A. Manthey, and P. Herreen. 1998b. 'Assessment of cancellous bone quality in severe osteoarthrosis: Bone mineral density, mechanics, and microdamage', *Bone*, 22: 381-88.

Ghodsi, M., B. Larijani, A. A. Keshtkar, E. Nasli-Esfahani, S. Alatab, and M. R. Mohajeri-Tehrani. 2016. 'Mechanisms involved in altered bone metabolism in diabetes: a narrative review', *J Diabetes Metab Disord*, 15: 52.

Green, Jessica O., Jason Wang, Tamim Diab, Brani Vidakovic, and Robert E. Guldberg. 2011. 'Age-related differences in the morphology of microdamage propagation in trabecular bone', *Journal of Biomechanics*, 44: 2659-66.

Hengsberger, S., A. Kulik, and Ph Zysset. 2002. 'Nanoindentation discriminates the elastic properties of individual human bone lamellae under dry and physiological conditions', *Bone*, 30: 178-84.

Hernandez, C. J., and T. M. Keaveny. 2006. "A biomechanical perspective on bone quality." In *Bone*, 1173-81. NIH Public Access.

Hunt, Heather B., Ashley M. Torres, Pablo M. Palomino, Eric Marty, Rehan Saiyed, Matthew Cohn, Jonathan Jo, Stephen Warner, Grazyna E. Sroga, Karen B. King, Joseph M. Lane, Deepak Vashishth, Christopher J. Hernandez, and Eve Donnelly. 2019. 'Altered Tissue Composition, Microarchitecture, and Mechanical Performance in Cancellous Bone From Men With Type 2 Diabetes Mellitus', *JOURNAL OF BONE AND MINERAL RESEARCH*: jbmr.3711-jbmr.11.

Janghorbani, M., R. M. Van Dam, W. C. Willett, and F. B. Hu. 2007. 'Systematic Review of Type 1 and Type 2 Diabetes Mellitus and Risk of Fracture', *American Journal of Epidemiology*, 166: 495-505.

Jia, Shaowei, He Gong, Haipeng Cen, Peipei Shi, Rui Zhang, Zhaowei Li, and Xuewei Bi. 2021. 'Influence of non-enzymatic glycation on the mechanical properties of cortical bone', *Journal of the Mechanical Behavior of Biomedical Materials*, 119: 104553-53.

Karim, Lamya, Julia Moulton, Miranda Van Vliet, Kelsey Velie, Ann Robbins, Fatemeh Malekipour, Ayesha Abdeen, Douglas Ayres, and Mary L. Bouxsein. 2018. 'Bone microarchitecture, biomechanical properties, and advanced glycation end-products in the proximal femur of adults with type 2 diabetes', *Bone*, 114: 32-39.

Khosla, Sundeep, Parinya Samakkarnthai, David G Monroe, and Joshua N Farr. 2021. 'Update on the pathogenesis and treatment of skeletal fragility in type 2 diabetes mellitus', *Nature Reviews Endocrinology*, 17: 685-97.

Lambers, Floor M., Amanda R. Bouman, Clare M. Rimnac, and Christopher J. Hernandez. 2013. 'Microdamage caused by fatigue loading in human cancellous bone: Relationship to reductions in bone biomechanical performance', *PLOS ONE*, 8: 1-9.

Landrigan, Matthew D., Jiliang Li, Travis L. Turnbull, David B. Burr, Glen L. Niebur, and Ryan K. Roeder. 2011. 'Contrast-enhanced micro-computed tomography of fatigue microdamage accumulation in human cortical bone', *Bone*, 48: 443-50.

Lekkala, Sashank, Sara E Sacher, Erik A Taylor, Rebecca M Williams, Kendall F Moseley, and Eve Donnelly. 2023. 'Increased advanced glycation endproducts, stiffness, and hardness in iliac crest bone from postmenopausal women with type 2 diabetes mellitus on insulin', *JOURNAL OF BONE AND MINERAL RESEARCH*, 38: 261-77.

Leslie, William D., Mishaela R. Rubin, Ann V. Schwartz, and John A. Kanis. 2012. 'Type 2 diabetes and bone', *JOURNAL OF BONE AND MINERAL RESEARCH*, 27: 2231-37.

Maquer, G., S. N. Musy, J. Wandel, T. Gross, and P. K. Zysset. 2015. 'Bone volume fraction and fabric anisotropy are better determinants of trabecular bone stiffness than other morphological variables', *J Bone Miner Res*, 30: 1000-8.

McCarthy, Antonio Desmond, Toshimasa Uemura, Susana Beatriz Etcheverry, and Ana María Cortizo. 2004. 'Advanced glycation endproducts interfere with integrin-mediated osteoblastic attachment to a type-I collagen matrix', *The International Journal of Biochemistry & Cell Biology*, 36: 840-48.

McCreadie, Barbara R., Michael D. Morris, Tso-ching Chen, D. Sudhaker Rao, William F. Finney, Effendi Widjaja, and Steven A. Goldstein. 2006. 'Bone tissue compositional differences in women with and without osteoporotic fracture', *Bone*, 39: 1190-95.

Melton, L. J., Cynthia L. Leibson, Sara J. Achenbach, Terry M. Therneau, and Sundeep Khosla. 2008. 'Fracture Risk in Type 2 Diabetes: Update of a Population-Based Study', *JOURNAL OF BONE AND MINERAL RESEARCH*, 23: 1334-42.

Mercer, Natalia, Hafiz Ahmed, Susana B Etcheverry, Gerardo R Vasta, and Ana Maria Cortizo. 2007. 'Regulation of advanced glycation end product (AGE) receptors and apoptosis by AGEs in osteoblast-like cells', *Molecular and cellular biochemistry*, 306: 87-94.

Merlo, Kelly, Jacob Aaronson, Rachana Vaidya, Taraneh Rezaee, Vijaya Chalivendra, and Lamya Karim. 2020. 'In Vitro-Induced High Sugar Environments Deteriorate Human Cortical Bone Elastic Modulus and Fracture Toughness', *Journal of Orthopaedic Research®*, 38: 972-83.

Michel, Markijs C., and Wilson C. Hayes. 1993. 'Fatigue Behavior of', 26.

Mittra, Erik, Sailaja Akella, and Yi-Xian Qin. 2006. 'The effects of embedding material, loading rate and magnitude, and penetration depth in nanoindentation of trabecular bone', *Journal of Biomedical Materials Research Part A*, 79A: 86-93.

Monahan, Genna E, Jessica Schiavi-Tritz, Marissa Britton, and Ted J Vaughan. 2023. 'Longitudinal alterations in bone morphometry, mechanical integrity and composition in Type-2 diabetes in a Zucker diabetic fatty (ZDF) rat', *Bone*, 170: 116672.

Moore, Tara L. A., and Lorna J. Gibson. 2003. 'Fatigue of Bovine Trabecular Bone', *Journal of Biomechanical Engineering*, 125: 761-68.

Morgan, E. F., and T. M. Keaveny. 2001. 'Dependence of yield strain of human trabecular bone on anatomic site', *J Biomech*, 34: 569-77.

Mori, S, R Harruff, W Ambrosius, and DB Burr. 1997. 'Trabecular bone volume and microdamage accumulation in the femoral heads of women with and without femoral neck fractures', *Bone*, 21: 521-26.

Mori, S., and D. B. Burr. 1993. 'Increased intracortical remodeling following fatigue damage', *Bone*, 14: 103-09.

Mulder, Lars, Jan Harm Koolstra, Jaap M. J. den Toonder, and Theo M. G. J. van Eijden. 2007. 'Intratrabecular distribution of tissue stiffness and mineralization in developing trabecular bone', *Bone*, 41: 256-65.

Nilsson, Anna G, Daniel Sundh, Lisa Johansson, Martin Nilsson, Dan Mellström, Robert Rudäng, Michail Zoulakis, Märit Wallander, Anna Darelid, and Mattias Lorentzon. 2017. 'Type 2 diabetes mellitus is associated with better bone microarchitecture but lower bone material strength and poorer physical function in elderly women: a population-based study', *JOURNAL OF BONE AND MINERAL RESEARCH*, 32: 1062-71.

O'Sullivan, Laura. 2020. "Time-sequence of Biomechanical Adaption in Trabecular Tissue during Estrogen Deficiency." In.

Parle, Eoin, Sherdya Tio, Annie Behre, John J. Carey, Colin G. Murphy, Timothy F. O'Brien, William A. Curtin, Stephen R. Kearns, John P. McCabe, Cynthia M. Coleman, Ted J. Vaughan, and Laoise M. McNamara. 2020. 'Bone Mineral Is More Heterogeneously Distributed in the Femoral Heads of Osteoporotic and Diabetic Patients: A Pilot Study', *JBMR Plus*, 4: e10253-e53.

Paschou, Stavroula A, Anastasia D Dede, Panagiotis G Anagnostis, Andromachi Vryonidou, Daniel Morganstein, and Dimitrios G Goulis. 2017. 'Type 2 Diabetes and Osteoporosis: A Guide to Optimal Management', *The Journal of Clinical Endocrinology & Metabolism*, 102: 3621-34.

Piccoli, Alessandra, Francesca Cannata, Rocky Strollo, Claudio Pedone, Giulia Leanza, Fabrizio Russo, Valentina Greto, Camilla Isgrò, Carlo Cosimo Quattrocchi, Carlo Massaroni, Sergio Silvestri, Gianluca Vadalà, Tiziana Bisogno, Vincenzo Denaro, Paolo Pozzilli, Simon Y. Tang, Matt J. Silva, Caterina Conte, Rocco Papalia, Mauro Maccarrone, and Nicola Napoli. 2020. 'Sclerostin Regulation, Microarchitecture, and Advanced Glycation End-Products in the Bone of Elderly Women With Type 2 Diabetes', *JOURNAL OF BONE AND MINERAL RESEARCH*, 35: 2415-22.

Purnamasari, Dyah, Melisa D Puspitasari, Bambang Setiyohadi, Pringgodigdo Nugroho, and Harry Isbagio. 2017. 'Low bone turnover in premenopausal women with type 2 diabetes mellitus as an early process of diabetes-associated bone alterations: a cross-sectional study', *BMC endocrine disorders*, 17: 1-8.

Ritchie, Robert O, John H Kinney, Jamie J Kruzic, and Ravi K Nalla. 2005. 'A fracture mechanics and mechanistic approach to the failure of cortical bone', *Fatigue & Fracture of Engineering Materials & Structures*, 28: 345-71.

Rokidi, Stamatia, Vicente F. C. Andrade, Victoria Borba, Elizabeth Shane, Adi Cohen, Jochen Zwerina, Eleftherios P. Paschalis, and Carolina A. Moreira. 2020. 'Bone tissue material composition is compromised in premenopausal women with Type 2 diabetes', *Bone*, 141: 115634.

Ryan, M., L. Barnett, J. Rochester, J. M. Wilkinson, and E. Dall'Ara. 2020. 'A new approach to comprehensively evaluate the morphological properties of the human femoral head: example of application to osteoarthritic joint', *Scientific Reports*, 10: 5538.

Sacher, S. E., H. B. Hunt, S. Lekkala, K. A. Lopez, J. Potts, A. K. Heilbronner, E. M. Stein, C. J. Hernandez, and E. Donnelly. 2022. 'Distributions of Microdamage Are Altered Between Trabecular Rods and Plates in Cancellous Bone From Men With Type 2 Diabetes Mellitus', *J Bone Miner Res*, 37: 740-52.

Sanguineti, Roberta, Daniela Storace, Fiammetta Monacelli, Alberto Federici, and Patrizio Odetti. 2008. "Pentosidine effects on human osteoblasts in vitro." In *Annals of the New York Academy of Sciences*, 166-72. Blackwell Publishing Inc.

Sassi, Francesca, Ilaria Buondonno, Chiara Luppi, Elena Spertino, Emanuela Stratta, Marco Di Stefano, Marco Ravazzoli, Gianluca Isaia, Marina Trento, and Pietro Passera. 2018. 'Type 2 diabetes affects bone cells precursors and bone turnover', *BMC endocrine disorders*, 18: 1-8.

Schaffler, M. B., K. Choi, and C. Milgrom. 1995. 'Aging and matrix microdamage accumulation in human compact bone', *Bone*, 17: 521-25.

Schleicher, E., L. Scheller, and O. H. Wieland. 1981. 'Quantitation of lysine-bound glucose of normal and diabetic erythrocyte membranes by HPLC analysis of furosine [ε-N(L-furoylmethyl)-L-lysine]', *Biochemical and Biophysical Research Communications*, 99: 1011-19.

Schwartz, A. V. 2003. 'Diabetes Mellitus: Does it Affect Bone?', *Calcified Tissue International*, 73: 515-19.

Schwartz, Ann V., and Deborah E. Sellmeyer. 2007. 'Diabetes, fracture, and bone fragility', *Current Osteoporosis Reports*, 5: 105-11.

Sell, David R. 1997. 'Ageing promotes the increase of early glycation Amadori product as assessed by ϵ-N-(2-furoylmethyl)-l-lysine (furosine) levels in rodent skin collagen: The relationship to dietary restriction and glycoxidation', *Mechanisms of ageing and development*, 95: 81-99.

Shanbhogue, Vikram V., Deborah M. Mitchell, Clifford J. Rosen, and Mary L. Bouxsein. 2016. 'Type 2 diabetes and the skeleton: new insights into sweet bones', *The Lancet Diabetes & Endocrinology*, 4: 159-73.

Sihota, Praveer, Ram Naresh Yadav, Ruban Dhaliwal, Jagadeesh Chandra Bose, Vandana Dhiman, Deepak Neradi, Shailesh Karn, Sidhartha Sharma, Sameer Aggarwal, Vijay G. Goni, Vishwajeet Mehandia, Deepak Vashishth, Sanjay Kumar Bhadada, and Navin Kumar. 2021. 'Investigation of mechanical, material and compositional determinants of human trabecular bone quality in type 2 diabetes', *The Journal of Clinical Endocrinology & Metabolism*, XX: 1-19.

Starr, Jessica F, Leonardo C Bandeira, Sanchita Agarwal, Ankit M Shah, Kyle K Nishiyama, Yizhong Hu, Donald J McMahon, X Edward Guo, Shonni J Silverberg, and Mishaela

R Rubin. 2018. 'Robust trabecular microstructure in type 2 diabetes revealed by individual trabecula segmentation analysis of HR-pQCT images', *JOURNAL OF BONE AND MINERAL RESEARCH*, 33: 1665-75.

Strotmeyer, Elsa S., Jane A. Cauley, Ann V. Schwartz, Michael C. Nevitt, Helaine E. Resnick, Joseph M. Zmuda, Douglas C. Bauer, Frances A. Tylavsky, Nathalie De Rekeneire, Tamara B. Harris, and Anne B. Newman. 2004. 'Diabetes is associated independently of body composition with BMD and bone volume in older white and black men and women: The health, aging, and body composition study', *JOURNAL OF BONE AND MINERAL RESEARCH*, 19: 1084-91.

Tang, S. Y. Y., and D. Vashishth. 2010. 'Non-enzymatic glycation alters microdamage formation in human cancellous bone', *Bone*, 46: 148-54.

Tang, S. Y. Y., U. Zeenath, and D. Vashishth. 2007. 'Effects of non-enzymatic glycation on cancellous bone fragility', *Bone*, 40: 1144-51.

Thomas, C David L, Paul M Mayhew, Jon Power, Kenneth ES Poole, Nigel Loveridge, John G Clement, Chris J Burgoyne, and Jonathan Reeve. 2009. 'Femoral neck trabecular bone: loss with aging and role in preventing fracture', *JOURNAL OF BONE AND MINERAL RESEARCH*, 24: 1808-18.

Thrailkill, Kathryn M, Charles K Lumpkin Jr, R Clay Bunn, Stephen F Kemp, and John L Fowlkes. 2005. 'Is insulin an anabolic agent in bone? Dissecting the diabetic bone for clues', *American Journal of Physiology-Endocrinology and Metabolism*, 289: E735-E45.

Unal, Mustafa. 2021. 'Raman spectroscopic determination of bone matrix quantity and quality augments prediction of human cortical bone mechanical properties', *Journal of Biomechanics*, 119: 110342.

Unal, Mustafa, Amy Creecy, and Jeffry S. Nyman. 2018. 'The Role of Matrix Composition in the Mechanical Behavior of Bone', *Current Osteoporosis Reports*, 16: 205-15.

Unal, Mustafa, Sasidhar Uppuganti, Daniel Y. Dapaah, Rafay Ahmed, Jacquelyn S. Pennings, Thomas L. Willett, Paul Voziyan, and Jeffry S. Nyman. 2023. 'Effect of ribose incubation on physical, chemical, and mechanical properties of human cortical bone', *Journal of the Mechanical Behavior of Biomedical Materials*, 140: 105731.

Valcourt, Ulrich, Blandine Merle, Evelyne Gineyts, Stéphanie Viguet-Carrin, Pierre D. Delmas, and Patrick Garnero. 2007. 'Non-enzymatic glycation of bone collagen modifies osteoclastic activity and differentiation', *Journal of Biological Chemistry*, 282: 5691-703.

Van Gulick, Laurence, Charles Saby, Stéphane Jaisson, Anaïs Okwieka, Philippe Gillery, Emilie Dervin, Hamid Morjani, and Abdelilah Beljebbar. 2022. 'An integrated approach to investigate age-related modifications of morphological, mechanical and structural properties of type I collagen', *Acta Biomaterialia*, 137: 64-78.

Vashishth, D., G. J. Gibson, J. I. Khoury, M. B. Schaffler, J. Kimura, and D. P. Fyhrie. 2001. 'Influence of nonenzymatic glycation on biomechanical properties of cortical bone', *Bone*, 28: 195-201.

Viguet-Carrin, S., D. Farlay, Y. Bala, F. Munoz, M. L. Bouxsein, and P. D. Delmas. 2008. 'An in vitro model to test the contribution of advanced glycation end products to bone biomechanical properties', *Bone*, 42: 139-49.

Voumard, Benjamin, Pia Stefanek, Michael Pretterklieber, Dieter Pahr, and Philippe Zysset. 2022. 'Influence of aging on mechanical properties of the femoral neck using an inverse method', *Bone reports*, 17: 101638.

Wang, Xiang, Daniel B. Masse, Huijie Leng, Kevin P. Hess, Ryan D. Ross, Ryan K. Roeder, and Glen L. Niebur. 2007. 'Detection of trabecular bone microdamage by micro-computed tomography', *Journal of Biomechanics*, 40: 3397-403.

Willett, Thomas L., Sibi Sutty, Anne Gaspar, Nick Avery, and Marc Grynpas. 2013. 'In vitro non-enzymatic ribation reduces post-yield strain accommodation in cortical bone', *Bone,* 52: 611-22.

Willett, Thomas L., Paul Voziyan, and Jeffry S. Nyman. 2022. 'Causative or associative: A critical review of the role of advanced glycation end-products in bone fragility', *Bone*, 163: 116485.

Wölfel, Eva M., Imke A. K. Fiedler, Sofie Dragoun Kolibova, Johannes Krug, Mei-Chun Lin, Bashar Yazigi, Anna K. Siebels, Herbert Mushumba, Birgit Wulff, Benjamin Ondruschka, Klaus Püschel, Claus C. Glüer, Katharina Jähn-Rickert, and Björn Busse. 2022. 'Human tibial cortical bone with high porosity in type 2 diabetes mellitus is accompanied by distinctive bone material properties', *Bone,* 165: 116546.

Yang, Pengfei, Gert-Peter Brüggemann, and Jörn Rittweger. 2011. 'What do we currently know from in vivo bone strain measurements in humans?', *Journal of Musculoskeletal and Neuronal Interactions*, 11: 8-20.

Yerramshetty, Janardhan S., and Ozan Akkus. 2008. 'The associations between mineral crystallinity and the mechanical properties of human cortical bone', *Bone,* 42: 476-82.

Zysset, Philippe K, X Edward Guo, C Edward Hoffler, Kristin E Moore, and Steven A Goldstein. 1999. 'Elastic modulus and hardness of cortical and trabecular bone lamellae measured by nanoindentation in the human femur', *Journal of Biomechanics*, 32: 1005-12.

CHAPTER 5

An Investigation of Regional Heterogeneity within the Ex Vivo Femoral Head of Type-2 Diabetic Patients

5.1 Introduction

While this thesis thus far has focused primarily on the mechanical properties of T2D bone, the mechanical performance of bone is controlled by the size, shape, distribution, organisation and characteristic properties of the bone tissue (Cowin 2001; Currey 2006). To date, the regional microarchitecture of T2D femoral head trabecular bone tissue has not been investigated. In this Chapter, the regional microarchitecture of the femoral head is considered by performing microarchitectural analysis on 37 distinct regions of interest (Ryan et al. 2020).

T2D patients are at an increased risk of fractures, particularly at the hip where the incidence of fragility fractures can be up to three times more frequent than in non-T2D patients (Bonds et al. 2006; Janghorbani et al. 2007; Vestergaard 2007; Schwartz et al. 2011; Napoli et al. 2014). This is despite the fact that T2D is generally associated with similar, or in some cases higher, areal BMD in a range of anatomical locations, including the hip, femoral neck and spine, as

measured by Dual-energy x-ray absorptiometry (DXA). However, this technique is not an adequate method for predicting hip fracture in T2D patients as it measures only bone quantity, and fails to measure specific aspects of bone quality, which include the three-dimensional regional distribution of bone mass, cortical and trabecular microarchitecture and intrinsic properties of the bone matrix. High-resolution peripheral quantitative computed tomography (HR-pQCT) has been used to study T2D patients, revealing increased trabecular BMD in the tibia as well as morphological changes such as increasing trabecular thickness. (Burghardt et al. 2010). Current micro computed tomography (micro-CT) imaging facilitates the high-resolution scanning and detailed evaluation of microarchitectural and densitometric properties of specimens, which provide a better indication of structural performance of the tissue than areal BMD (Voumard et al. 2022).Studies using micro-CT that have examined T2D microarchitecture of the femoral head and neck have looked at isolated sections (Karim et al. 2018; Hunt et al. 2019; Parle et al. 2020; Sihota et al. 2021), generally along the primary loading zone. From these isolated samples, only one study has found impaired microarchitectural properties (Sihota et al. 2021), while the majority of studies show either a preserved trabecular microarchitecture (Karim et al. 2018; Hunt et al. 2019; Parle et al. 2020; Sihota et al. 2021) or a denser structure, with a more plate-like trabecular microarchitecture found in Chapter 4 and by others (Sacher et al. 2022). In Chapter 4, it was found that this denser micro-architecture in T2D bone in the central region of the femoral head coincided with enhanced mechanical properties, suggesting that other factors must be responsible for fragility in T2D. In particular, regional changes in bone density and microarchitecture across the entire femoral head have not yet been investigated in T2D, and there is no information on the cross-sectional distribution of bone density and microarchitecture over the femoral head of T2D patients. Such information may improve our understanding of a structural basis of T2D hip fracture risk.

The onset of several bone-related diseases can cause distinct changes in trabecular bone properties and microarchitecture. For example, Homminga et al. (2004) showed that the trabecular microarchitecture in osteoporotic vertebrae becomes highly anisotropic along the primary direction of loading, which is thought to be a compensatory mechanism to the bone loss that takes place. Several other studies have investigated regional differences in trabecular bone with the onset of disease, with many of these focussing on the femoral head. Li and Aspden (1997) performed one of the first such studies, measuring the mechanical and material properties of extracted bone cores at five different regions of the femoral head in osteoarthritis (OA), osteoporosis (OP), and healthy samples. They found greater regional heterogeneity in bone density and stiffness in OA compared to healthy specimens, providing evidence for regional alterations in the bone tissue arising with the onset of disease. Tamaddon et al. (2017) used peripheral quantitative computed tomography (pQCT) to evaluate the volumetric bone mineral density (vBMD) in 36 regions of interest of the femoral head of OA patients and showed heterogeneity of vBMD throughout the evaluated regions. Chiba et al. (2013) also used HR-pQCT to perform a detailed evaluation of regional variations in osteoporotic trabecular bone microarchitecture by dividing the femoral head into ten volumes of interest, looking at the influence of depth and anatomic position. It was found that the femoral head had denser structures in the centre, superior and supero-posterior regions, with higher bone volume, trabecular number, thickness and anisotropy, and more plate-like structures compared to the other regions. Ryan et al. (2020) built on these findings by developing a new approach to comprehensively evaluate the microarchitectural properties of the human femoral head by dividing the trabecular bone region into 37 volumes of interest based on anatomic locations and applied this approach to analyse OA samples and healthy controls. While no significant differences were found between groups, possibly due to the small sample number (n = 5), this study demonstrated how the developed approach could be used to study the heterogeneous

properties of the human femoral head. However, to date, these regional analyses and comparisons between disease states of macro- and micro-regions have not yet been used to study T2D bone. Additionally, the heterogeneity within macro-regions of T2D bone has not yet been investigated.

The objective of this study is to investigate the regional morphological properties of the trabecular architecture in ex vivo T2D femoral heads using micro-CT imaging. The study uses the approach developed by Ryan et al. (2020), whereby the regional microarchitecture of T2D and non-T2D specimens is evaluated across pre-defined macro- and micro-regions of the femoral head. Additionally, this study will evaluate the inter- and intra-regional heterogeneity across these macro-regions in the femoral head. This will help to understand if there is any regional structural basis for T2D fragility fractures, which could better inform the clinical evaluation of fracture risk for T2D patients.

5.2 Methods

5.2.1 Ex Vivo Micro-CT Scanning

Femoral heads were obtained from age and sex-matched patients, with T2D (72.1 ± 9.5 years) and without T2D (72.6 ± 10.4 years), who underwent total hip replacement for clinically diagnosed osteoarthritis (OA) at two Galway hospital sites, Merlin Park University Hospital and University Hospital Galway. All research procedures were approved by the Clinical Research Ethics Committee, Galway University Hospitals, Galway, Ireland. The groups were categorised as follows; T2D (n = 9) and non-T2D (n = 9). None of the patients examined had any recorded comorbidities or were on medications known to affect bone metabolism (e.g. glucocorticoids, antiretroviral medications, bisphosphonates, teriparatide, or denosumab). HbA1C levels for n=4 of the T2D group were collected prior to surgery (54.5 ± 5.7 mmol/mol or 7.1 ± 0.5%), the HbA1C for the remaining T2D samples were unavailable. Micro-CT images of T2D and non-T2D full femoral heads were obtained at a voxel size of 36.8 × 36.8 × 36.8 μm^3 using micro-CT 100, (Scanco Medical, Switzerland) with settings of 70 kVp, 114 mA and 300 ms (Ryan et al. 2020).

5.2.2 Image Analysis

The Matlab imaging toolbox was used to segment the femoral head into multiple volumes of interest (VOIs) within the femoral head through the development of a custom Matlab script. This script segmented the femoral head into five macro-regions, which are shown in Figure 5.2. These were the central trabecular region (CTB), the inferior middle trabecular region (inf MTB), the superior middle trabecular region (sup MTB), the inferior subchondral trabecular region (inf STB), and the superior subchondral trabecular region (sup STB). Once the macro-regions were created, the inf MTB, sup MTB, inf STB and sup STB were further segmented in 8 sub regions based on anatomical location, which were defined as posterior postero-lateral (PPL), anterior postero-lateral (APL), posterior antero-lateral (PAL), anterior antero-lateral

(AAL), anterior antero-medial (AAM), posterior antero-medial (PAM) anterior postero-medial (APM), and posterior postero-medial (PPM). Overall, this script created thirty-seven unique VOIs.

The workflow of the segmentation script is shown in Figure 5.1. First, the images were converted into DICOM format using the Scanco Medical CT software and exported to ImageJ. The trabecular bone was manually delineated from the cortical bone by drawing a region of interest every 25 slices and interpolating between these slices, resulting in a binary trabecular bone mask. The mask was exported from ImageJ to Matlab as a Tiff file and converted back to DICOM format using Matlab. Next, the sphereFit function (Jennings 2013) was applied to the binarized trabecular bone mask to determine the fitted sphere centroid and radius. Based on these values, three binary semi-spheres were created with radii of one third, two thirds, and the full radius of the trabecular bone. The smaller spheres were then subtracted from their immediately larger sphere to create two distinct regions of interest. A cone with a 45-degree angle was created, and Boolean subtractions were performed to create the five macro-regions (e.g. inferior MTB, superior MTB, inferior STB, superior STB, and a central region). Finally, the inferior and superior MTB and STB regions were further divided into the eight sub-regions of interest using a segmentation of a sphere with an angle of 45 degrees and Boolean subtractions. The Matlab script used to segment these regions is included in Section 5.6 Appendix 5.1.

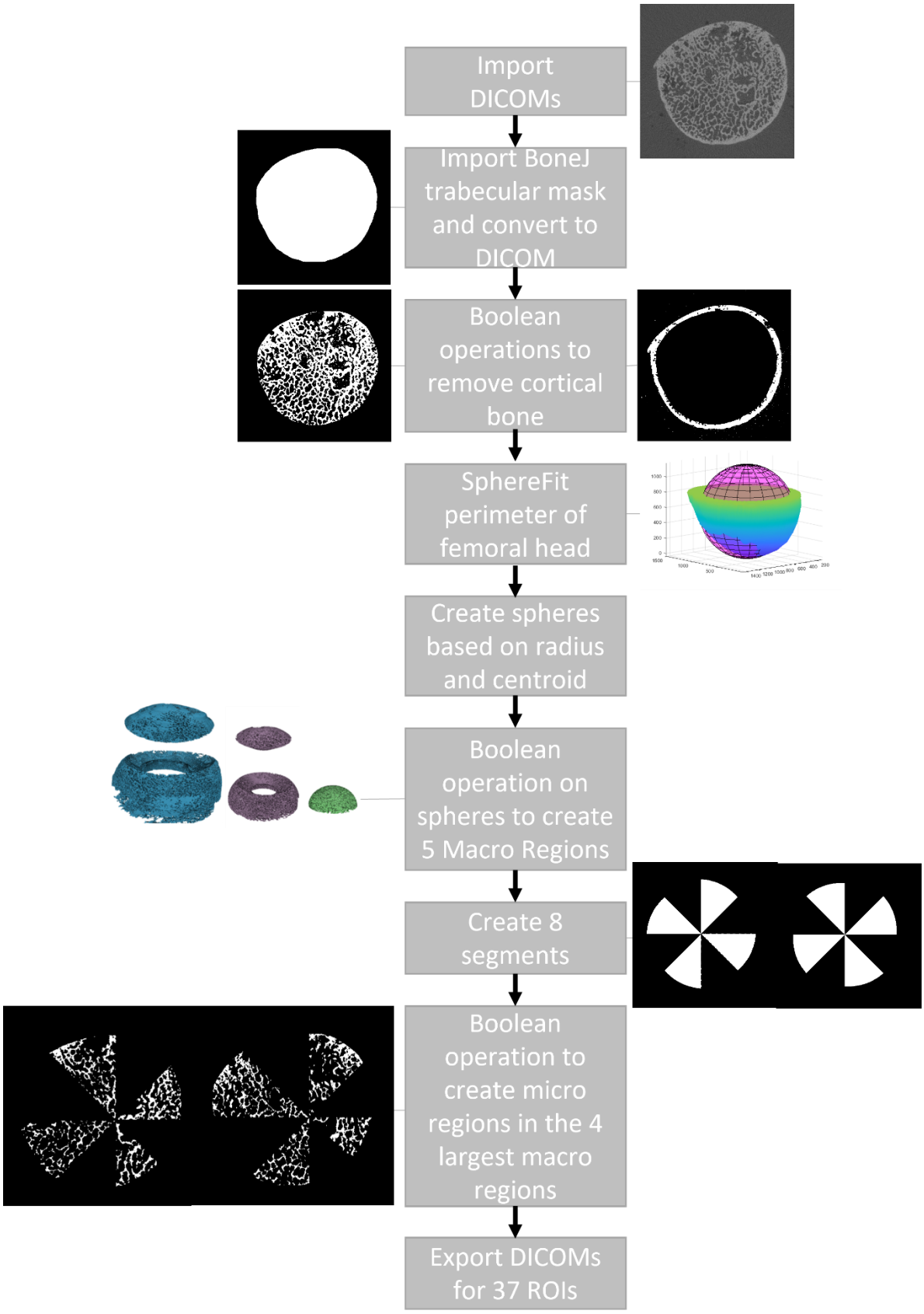

Figure 5.1 Workflow for MATLAB script to create the 37 regions of interest.

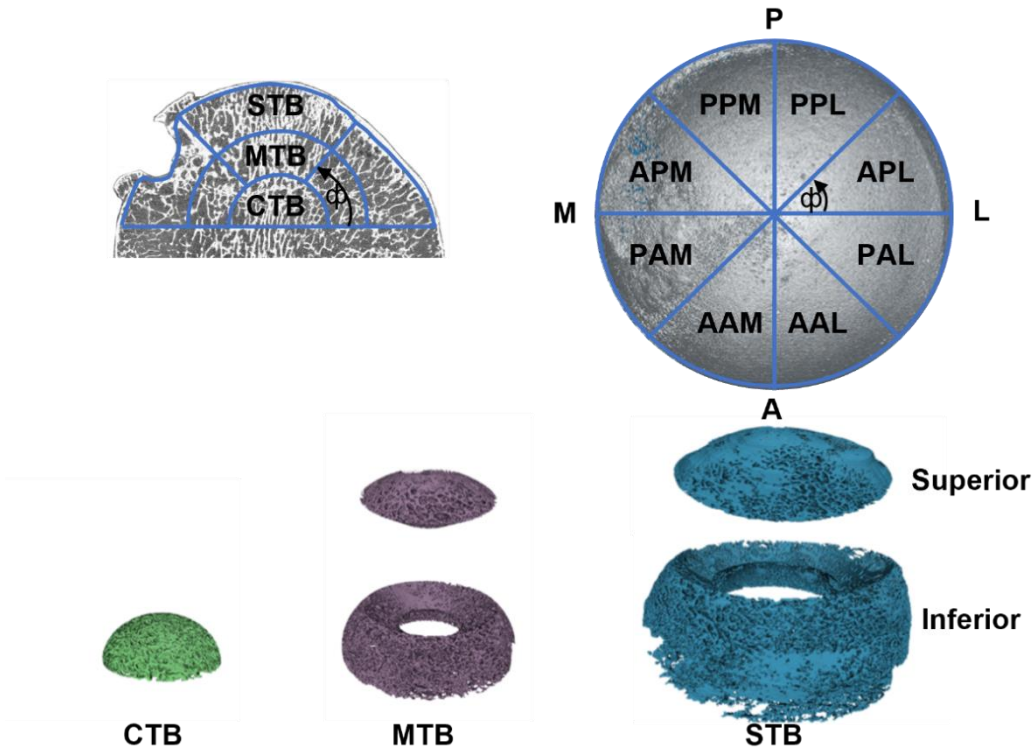

Figure 5.2 37 regions of interest with the five macro-regions are created the central trabecular region (CTB) the inferior middle trabecular region (inf MTB) the superior middle trabecular region (sup MTB), the inferior subchondral trabecular region (inf STB) and the superior subchondral trabecular region (sup STB). The macro-regions were then further segmented in 8 sub regions based on anatomical location posterior postero-lateral (PPL), anterior postero-lateral (APL), posterior antero-lateral (PAL), anterior antero-lateral (AAL), anterior antero-medial (AAM), posterior antero-medial (PAM) anterior postero-medial (APM), and posterior postero-medial (PPM).

5.2.3 Microarchitectural Analysis

Various microarchitectural parameters were measured for each VOI in the trabecular bone to enable quantitative comparison between the morphology of the T2D and non-T2D bone using Scanco Medical CT software v.6.6. Specifically, BV/TV, trabecular thickness (Tb.Th), trabecular separation (Tb.Sp), trabecular number (Tb.N), connectivity density of the trabecular network (Conn.D), structural model index (SMI) and degree of anisotropy (DA) were determined for each VOI. Images were segmented using a threshold of 466.2 mg HA/cm^3 and a Gaussian filter of sigma 1.2 and support 3 was used on the raw images to remove noise.

5.2.4 Bone Mineral Density Distribution Analysis

Bone mineral density distribution (BMDD) was used to evaluate differences in bone composition of the CTB in T2D and non-T2D samples. This method enabled a thorough assessment of the bone volume at various stages of mineralisation, providing a detailed description of bone quality. Raw micro-CT data files were analysed quantitatively to generate BMDD measurements for each trabecular data set. Grey level histograms were generated from the micro-CT images, depicting the frequency of voxels occurring at a particular grey level or tissue mineral density (mg HA/cm^3). To avoid underestimation of trabecular bone mineral density due to partial volume effects, the outer surface voxels (one layer) from each trabecula were excluded from the histograms. A custom Matlab script was employed to characterise specific aspects of each distribution, including the weighted mean tissue mineral density (mean mineral density, mgHA/cm^3), the most frequent mineral density (mode mineral density, mgHA/cm^3), the full width at half maximum (FWHM) of the mineral distribution curve (mineral heterogeneity, mgHA/cm^3), and the bone volume at low, medium or high mineral densities. The bone volume at low mineral density was quantified below the 25th percentile mineral density value of the baseline BMDD curves, whereas high mineral density bone was above the 75th percentile value of the baseline BMDD curves, and medium mineral bone volume was the volume of bone between these limits (O'Sullivan et al. 2020). This BMDD analysis approach provides a comprehensive and quantitative assessment of the mineral composition of trabecular bone from the central region, enabling an accurate description of any differences that may result from T2D.

5.2.5 Statistics

Due to low sample numbers, all data was tested for normality using the Kolmogorov-Smirnov normality. For data that was normal, two sample t-tests were used to compare morphological properties between diseases, while for non-normal data, a non-parametric Mann-Whitney test

was used. A one-way ANOVA with Tukey's post hoc test was used to determine if there was a location-based difference within each group.

5.3 Results

5.3.1 Macro-regions

5.3.1.1 Central Trabecular Region the Most Dense and Structurally Robust

In the five macro regions considered, trabecular microarchitectural properties did not differ significantly between T2D and non-T2D groups, as shown in Figure 5.3. Similarly, when the five macro regions were considered in combination (e.g. the bulk femoral head), there were no significant differences in the trabecular microarchitecture (see Figure A.5.1 in Appendix 5). However, several of the micro-architectural properties showed significant differences inter-regionally, across these different macro-regions. The central region (CTB) was generally the densest region and had the highest BV/TV of all regions and was significantly higher than the inferior middle region (MTB) (Non-T2D: +73%, $p<0.001$, T2D: +72%, $p<0.001$) and inferior subchondral region (STB) (Non-T2D: +75%, $p<0.001$, T2D: +72%, $p<0.001$) for both groups, and was also higher than the superior middle region (MTB) in the non-T2D group (Non-T2D: +75%, $p<0.05$). In line with the higher density observed the Tb.Sp was lower in the central region (CTB) compared to the inferior middle region (MTB) (Non-T2D: -56%, $p<0.01$, T2D: -60%, $p<0.001$) and inferior subchondral region (STB) (Non-T2D: -85%, $p<0.01$, T2D: -80%, $p<0.001$) for both groups. Again keeping with the higher density in the central region (CTB) the Tb.N of this region was higher than the inferior middle region (MTB) (Non-T2D: +25%, $p<0.01$, T2D: +28%, $p<0.001$) and inferior subchondral region (STB) (Non-T2D: +50%, $p<0.001$, T2D: +45%, $p<0.001$) for both groups and higher than the superior middle region (MTB) (Non-T2D: +22%, $p<0.05$) for non-T2D, and the superior subchondral region (STB) (T2D: +21%, $p<0.01$) for the T2D group. The Tb.Th in the central region (CTB) was generally similar to other regions, only being significantly higher when compared to the inferior middle region (MTB) (Non-T2D: +40%, $p<0.05$) for the non-T2D group. Additionally, the Conn.D was higher in the central (CTB) compared to the inferior subchondral region (STB) (Non-T2D:

+60%, $p<0.05$, T2D: +51%, $p<0.05$) for both groups. Finally, the SMI of the central (CTB) was lower, and thus more plate like, compared to the inferior middle region (MTB) (Non-T2D $p<0.01$, T2D $p<0.01$) and inferior subchondral region (STB) (Non-T2D: $p<0.001$, T2D: $p<0.001$) across both groups, but not significantly different to either of the superior regions. Overall, the observed results show that the central region (CTB) is the densest and most structurally robust region.

In general, the remaining four regions were more similar to each other, however, some differences still existed. Upon comparing these regions, it was found that the superior subchondral region (STB) exhibited the most significant differences compared to the other three macro-regions. The superior subchondral region (STB) was the next densest region after the central region and had the second-highest BV/TV and showed higher BV/TV compared to the inferior middle region (MTB) (Non-T2D: +58%, $p<0.01$, T2D: +53%, $p<0.01$) and inferior subchondral region (STB) (Non-T2D: +60%, $p<0.01$, T2D: +52%, $p<0.05$) for both groups. The Tb.Th of the superior subchondral region (STB) was significantly higher than the inferior middle region (MTB) (Non-T2D: +50%, $p<0.01$, T2D: +51%, $p<0.01$) for both groups. Similarly, Tb.Sp of the superior subchondral region (STB) was significantly higher than the inferior subchondral region (STB) (Non-T2D: -34%, $p<0.01$, T2D: +28%, $p<0.01$) for both groups. The superior subchondral region (STB) had a higher Tb.N than the inferior subchondral region (STB) (Non-T2D: +28%, $p<0.01$, T2D: +20%, $p<0.05$) for both groups. The SMI was lower, and thus more plate like, in the superior subchondral region (STB) than in the inferior subchondral region (STB) (Non-T2D: $p<0.01$, T2D: $p<0.05$) in both groups. Additionally, a small number of differences existed between the superior middle region (MTB) and the remaining two regions. The comparison between the superior middle region (MTB) and the inferior subchondral region (STB) of the T2D group showed lower Tb.Sp (T2D: -30%, $p<0.001$) and higher Tb.N (T2D: +28%, $p<0.01$) of the superior middle region (MTB). The

DA was higher in the superior middle region (MTB) than in the inferior subchondral region (STB) (Non-T2D: +37%, $p<0.001$, T2D: +31%, $p<0.001$) for both groups and higher than the inferior middle region (MTB) (Non-T2D: +2%, $p<0.01$) for non-T2D.

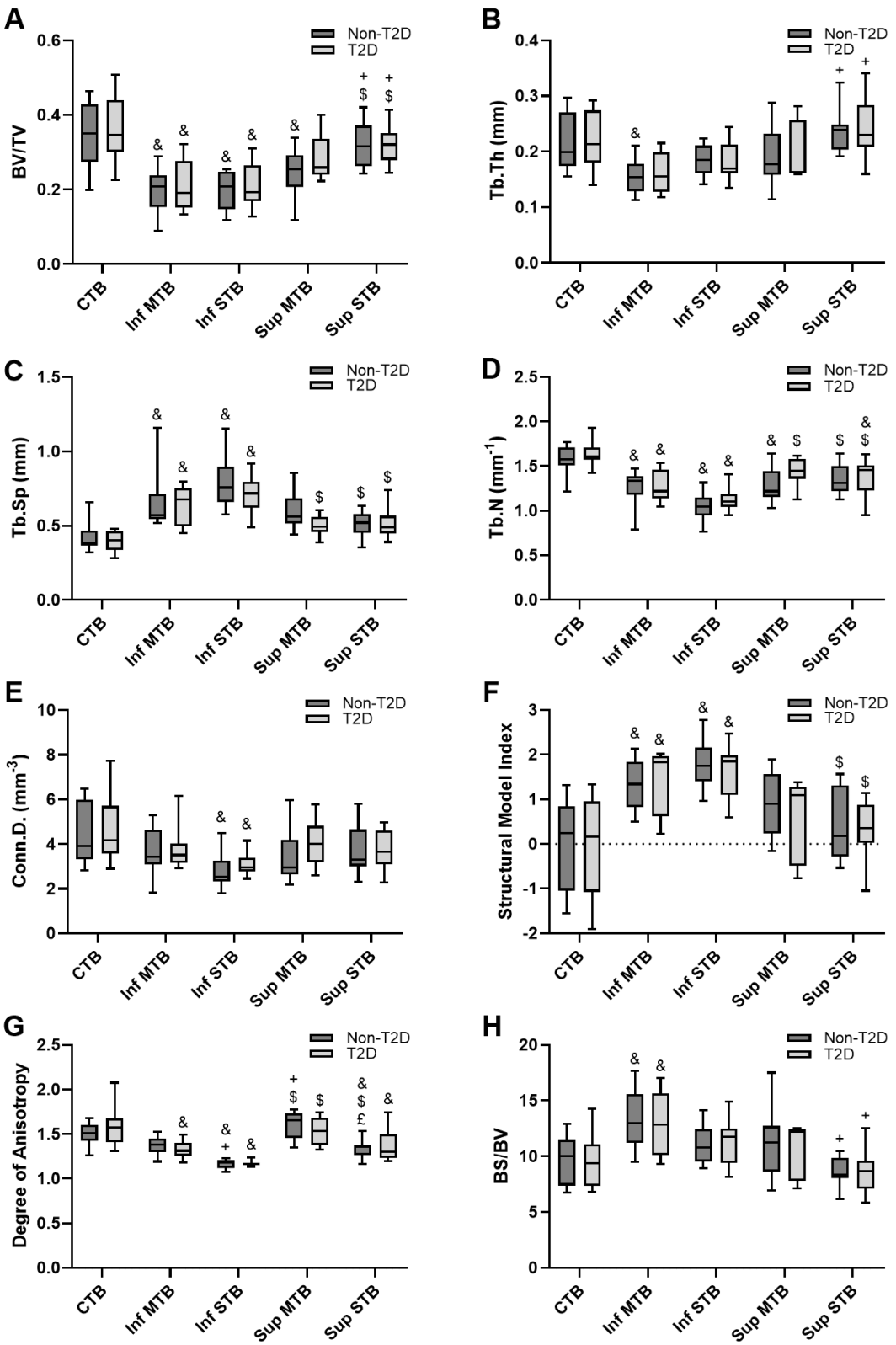

Figure 5.3 Boxplots of the microarchitectural properties of trabecular bone in the five macro volumes of interest, central, inferior middle (MTB), inferior subchondral (STB), superior middle (MTB, and superior STB for T2D (light grey) and non-T2D (dark grey) are shown. The following parameters are displayed: A) BV/TV, B) Tb.Th, C) Tb.Sp, D) Tb.N, E) Conn D, F) Structural Model Index, G) Degree of anisotropy, and H) BS/BV. &,+, $ and £ denote inter-regional differences in microarchitectural parameters from CTB, inferior MTB, inferior STB and superior MTB respectively.

5.3.2 Micro-Regions

5.3.2.1 Posterior and Medial T2D Micro-Regions Denser than non-T2D

Within the thirty-two anatomically defined micro-regions of the bone, the morphological parameters of distinct anatomical locations were compared between groups. Figure 5.4 and Table 5.1 show the results of these comparisons. The results indicate that there were no significant differences in any of the parameters analysed in the inferior or superior middle region (MTB). However, some posterior and medial T2D micro-regions were found to be denser than non-T2D micro-regions, with a significant increase in the BV/TV was observed in the inferior subchondral region (STB) APM region (+100%, $p<0.01$) and the superior middle (MTB) PAM region (+10%, $p<0.05$) in the T2D group. Furthermore, the Tb.Sp was significantly lower in the inferior subchondral (STB) APM (-43%, $p<0.01$) and superior middle (MTB) PPL (-33%, $p<0.05$) regions in the T2D group compared to the non-T2D group. The Tb.N was significantly higher in the inferior subchondral region (STB) APM (+63%, $p<0.01$) and superior middle (MTB) PPL regions (+21%, $p<0.05$) in the T2D group. Lastly, a significantly higher Conn.D was observed in the inferior subchondral region (STB) APM region (+200%, $p<0.01$) in the T2D group compared to the non-T2D group. The Tb.Th did not show any significant differences between the groups despite the T2D group having denser regions.

5.3.2.2 Intra-regionally the Inferior Subchondral Region Most Heterogenous

Furthermore, comparison of morphological parameters inter-regionally, between the eight predefined micro anatomical regions (PPL, APL, PAL, AAL, AAM, PAM, APM, and PPM) within the macro-regions (inferior subchondral (STB), superior subchondral (STB), inferior middle (MTB), superior middle (MTB)) was performed and is summarised in Table 5.2 with significant results being displayed (see Table A.5.1 in Appendix 5 for more detail of non-significant results). The results of the one-way ANOVA analysis revealed that the inferior

subchondral region (STB) showed the most non-uniformity, with the most significant differences observed between the micro-regions in both T2D and non-T2D groups. The inferior subchondral region (STB) was the most heterogeneous with the most significant differences in BV/TV, Tb.Sp, Tb.N, and Conn.D depending on micro-anatomical location, but no significant differences in Tb.Th. Conversely, the inferior middle (MTB), superior middle (MTB) and superior subchondral region (STB) were in general quite uniform, with only a small number of significant differences. In the inferior middle (MTB) and superior middle (MTB) regions for the T2D group less intra-regional heterogeneity was present, significant differences were observed in Tb.N and Conn. D depending on anatomical location with no other differences observed. Additionally, in the inferior middle region (MTB) of the non-T2D group, some intra-regional heterogeneity was present with significant differences in BV/TV and Tb.Th were observed, depending on location. Differences were also observed in the BV/TV based on location in the superior middle region (MTB) of the non-T2D group. Finally, in the superior subchondral region (STB) of the T2D group, several significant differences in Tb.N were observed based on location, while no differences in location-based morphological properties were observed in the superior subchondral region (STB) of the non-T2D group.

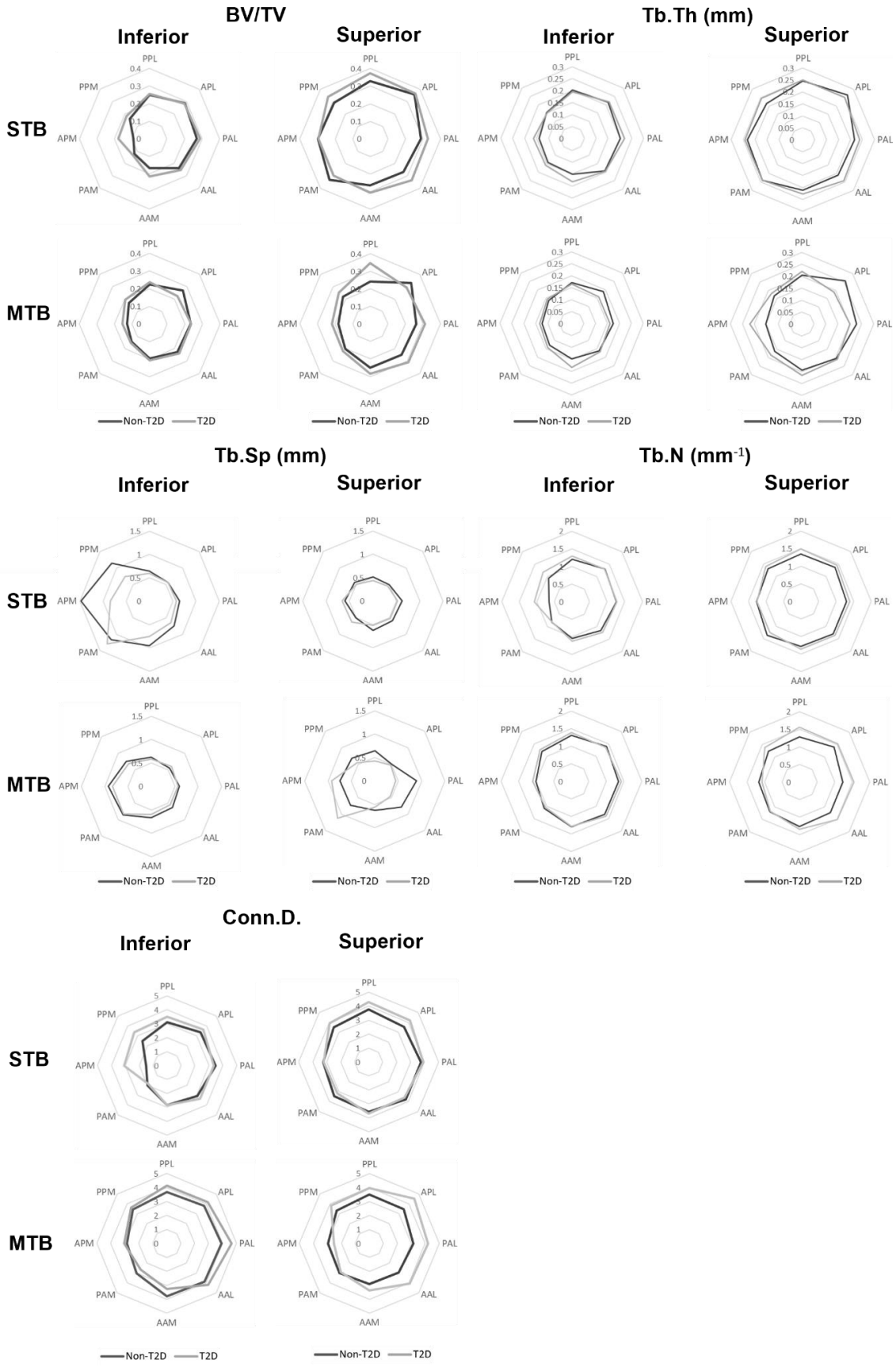

Figure 5.4 Radar plots of the mean value for the microarchitectural parameters evaluated in the 32 smaller volumes of interest are shown.

Table 5.1 Trabecular bone microarchitectural parameters, with each micro-region being compared to the matching micro-region between groups. A figure highlights the regions with significant differences, where MTB and STB mean middle and subchondral regions respectively.

		Inferior MTB			Inferior STB			Superior MTB			Superior STB		
		Non-T2D	T2D	*p*	Non-T2D	T2D	*p*	Non-T2D	T2D	*p*	Non-T2D	T2D	*p*
BV/TV	PPL	0.22 ± 0.08	0.24 ± 0.10	ns	0.25 ± 0.12	0.26 ± 0.07	ns	0.24 ± 0.08	0.35 ± 0.12	***0.04***	0.33 ± 0.09	0.37 ± 0.07	ns
	APL	0.27 ± 0.08	0.22 ± 0.09	ns	0.29 ± 0.10	0.28 ± 0.08	ns	0.33 ± 0.08	0.29 ± 0.07	ns	0.36 ± 0.08	0.36 ± 0.09	ns
	PAL	0.23 ± 0.08	0.24 ± 0.10	ns	0.27 ± 0.13	0.29 ± 0.13	ns	0.26 ± 0.12	0.31 ± 0.08	ns	0.29 ± 0.10	0.33 ± 0.12	ns
	AAL	0.22 ± 0.11	0.24 ± 0.07	ns	0.24 ± 0.12	0.25 ± 0.12	ns	0.25 ± 0.11	0.31 ± 0.06	ns	0.27 ± 0.05	0.33 ± 0.09	ns
	AAM	0.20 ± 0.06	0.21 ± 0.07	ns	0.17 ± 0.10	0.21 ± 0.10	ns	0.25 ± 0.11	0.28 ± 0.07	ns	0.28 ± 0.09	0.31 ± 0.08	ns
	PAM	0.14 ± 0.05	0.15 ± 0.06	ns	0.12 ± 0.07	0.13 ± 0.07	ns	0.20 ± 0.09	0.22 ± 0.12	***0.04***	0.33 ± 0.12	0.30 ± 0.10	ns
	APM	0.13 ± 0.05	0.16 ± 0.08	ns	0.09 ± 0.03	0.18 ± 0.08	***0.005***	0.18 ± 0.06	0.22 ± 0.09	ns	0.30 ± 0.10	0.29 ± 0.08	ns
	PPM	0.17 ± 0.06	0.20 ± 0.11	ns	0.16 ± 0.11	0.18 ± 0.10	ns	0.22 ± 0.13	0.25 ± 0.11	ns	0.29 ± 0.12	0.34 ± 0.13	ns
Tb.Th (mm)	PPL	0.17 ± 0.06	0.17 ± 0.05	ns	0.20 ± 0.08	0.19 ± 0.03	ns	0.21 ± 0.11	0.22 ± 0.07	ns	0.25 ± 0.06	0.25 ± 0.02	ns
	APL	0.19 ± 0.05	0.16 ± 0.04	ns	0.21 ± 0.04	0.22 ± 0.05	ns	0.26 ± 0.13	0.19 ± 0.04	ns	0.26 ± 0.05	0.25 ± 0.04	ns
	PAL	0.17 ± 0.06	0.16 ± 0.04	ns	0.20 ± 0.07	0.22 ± 0.07	ns	0.23 ± 0.07	0.20 ± 0.05	ns	0.22 ± 0.04	0.24 ± 0.09	ns
	AAL	0.16 ± 0.05	0.17 ± 0.04	ns	0.19 ± 0.06	0.20 ± 0.06	ns	0.20 ± 0.06	0.21 ± 0.05	ns	0.21 ± 0.04	0.24 ± 0.05	ns
	AAM	0.15 ± 0.03	0.18 ± 0.05	ns	0.15 ± 0.05	0.18 ± 0.06	ns	0.19 ± 0.07	0.22 ± 0.05	ns	0.21 ± 0.08	0.23 ± 0.07	ns
	PAM	0.13 ± 0.02	0.14 ± 0.04	ns	0.14 ± 0.03	0.16 ± 0.04	ns	0.16 ± 0.05	0.19 ± 0.05	ns	0.24 ± 0.08	0.24 ± 0.07	ns
	APM	0.12 ± 0.02	0.13 ± 0.04	ns	0.14 ± 0.03	0.16 ± 0.03	ns	0.15 ± 0.03	0.22 ± 0.08	ns	0.23 ± 0.05	0.24 ± 0.05	ns
	PPM	0.14 ± 0.02	0.15 ± 0.05	ns	0.15 ± 0.06	0.15 ± 0.05	ns	0.17 ± 0.07	0.18 ± 0.07	ns	0.21 ± 0.07	0.25 ± 0.09	ns
Tb.Sp (mm)	PPL	0.62 ± 0.18	0.59 ± 0.18	ns	0.64 ± 0.17	0.59 ± 0.13	ns	0.64 ± 0.20	0.43 ± 0.10	***0.01***	0.52 ± 0.15	0.44 ± 0.14	ns
	APL	0.54 ± 0.16	0.60 ± 0.20	ns	0.57 ± 0.19	0.57 ± 0.15	ns	0.51 ± 0.15	0.47 ± 0.12	ns	0.50 ± 0.14	0.46 ± 0.15	ns
	PAL	0.60 ± 0.18	0.57 ± 0.21	ns	0.65 ± 0.34	0.57 ± 0.18	ns	0.88 ± 0.82	0.45 ± 0.08	ns	0.62 ± 0.35	0.52 ± 0.24	ns
	AAL	0.63 ± 0.25	0.56 ± 0.11	ns	0.75 ± 0.37	0.65 ± 0.25	ns	0.80 ± 0.74	0.47 ± 0.10	ns	0.59 ± 0.17	0.52 ± 0.21	ns
	AAM	0.67 ± 0.25	0.60 ± 0.09	ns	0.95 ± 0.53	0.76 ± 0.30	ns	0.63 ± 0.21	0.56 ± 0.16	ns	0.62 ± 0.25	0.52 ± 0.10	ns
	PAM	0.86 ± 0.36	0.84 ± 0.18	ns	1.17 ± 0.30	1.29 ± 0.71	ns	0.73 ± 0.30	1.13 ± 1.61	ns	0.51 ± 0.16	0.63 ± 0.34	ns
	APM	0.92 ± 0.30	0.83 ± 0.29	ns	1.48 ± 0.50	0.84 ± 0.29	***0.002***	0.75 ± 0.24	0.93 ± 0.57	ns	0.60 ± 0.24	0.66 ± 0.38	ns
	PPM	0.76 ± 0.29	0.68 ± 0.25	ns	1.15 ± 0.84	0.74 ± 0.23	ns	0.69 ± 0.31	0.54 ± 0.11	ns	0.56 ± 0.17	0.50 ± 0.23	ns

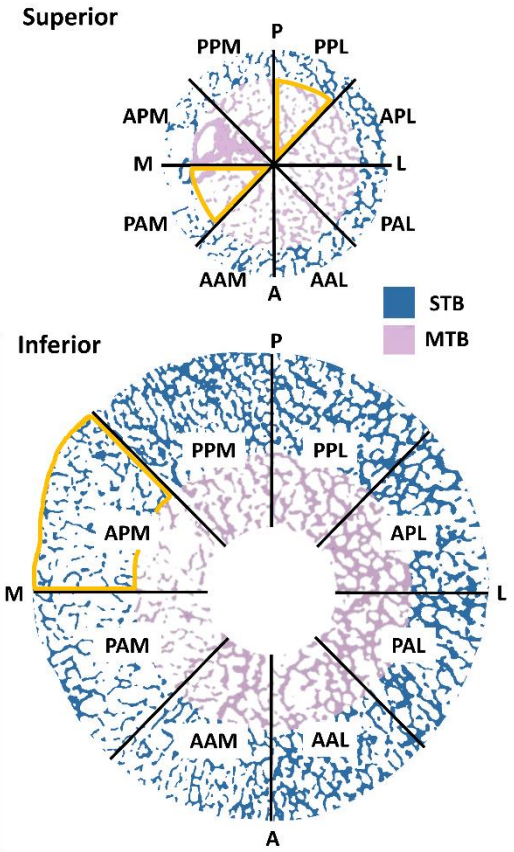

		Inferior MTB			Inferior STB			Superior MTB			Superior STB		
		Non-T2D	T2D	*p*	Non-T2D	T2D	*p*	Non-T2D	T2D	*p*	Non-T2D	T2D	*p*
Tb.N (mm^{-1})	PPL	1.30 ± 0.25	1.39 ± 0.31	ns	1.21 ± 0.17	1.29 ± 0.20	ns	1.28 ± 0.34	1.56 ± 0.12	***0.03***	1.4 ± 0.25	1.49 ± 0.23	ns
	APL	1.41 ± 0.26	1.37 ± 0.28	ns	1.32 ± 0.24	1.31 ± 0.24	ns	1.40 ± 0.33	1.54 ± 0.21	ns	1.36 ± 0.27	1.45 ± 0.23	ns
	PAL	1.34 ± 0.27	1.42 ± 0.27	ns	1.27 ± 0.33	1.29 ± 0.17	ns	1.24 ± 0.51	1.54 ± 0.11	ns	1.30 ± 0.34	1.39 ± 0.30	ns
	AAL	1.33 ± 0.30	1.40 ± 0.21	ns	1.16 ± 0.32	1.24 ± 0.26	ns	1.24 ± 0.39	1.51 ± 0.23	ns	1.30 ± 0.27	1.37 ± 0.32	ns
	AAM	1.30 ± 0.27	1.29 ± 0.12	ns	1.04 ± 0.34	1.13 ± 0.24	ns	1.27 ± 0.28	1.35 ± 0.25	ns	1.28 ± 0.32	1.36 ± 0.18	ns
	PAM	1.09 ± 0.26	1.04 ± 0.15	ns	0.82 ± 0.30	0.81 ± 0.32	ns	1.20 ± 0.30	1.18 ± 0.40	ns	1.36 ± 0.24	1.25 ± 0.29	ns
	APM	1.02 ± 0.24	1.11 ± 0.29	ns	0.66 ± 0.17	1.08 ± 0.36	***0.002***	1.16 ± 0.26	1.07 ± 0.43	ns	1.27 ± 0.31	1.25 ± 0.34	ns
	PPM	1.20 ± 0.30	1.27 ± 0.29	ns	0.95 ± 0.37	1.17 ± 0.29	ns	1.25 ± 0.30	1.39 ± 0.12	ns	1.32 ± 0.19	1.41 ± 0.29	ns
Conn.D ($1/mm^3$)	PPL	3.66 ± 3.66	4.12 ± 2.06	ns	3.12 ± 0.90	3.49 ± 0.81	ns	3.51 ± 1.76	3.98 ± 0.73	ns	3.75 ± 1.39	4.27 ± 0.81	ns
	APL	3.80 ± 3.80	4.16 ± 1.75	ns	3.39 ± 1.26	3.66 ± 1.66	ns	3.48 ± 1.65	4.55 ± 1.41	ns	3.57 ± 1.26	3.90 ± 1.31	ns
	PAL	3.93 ± 3.93	4.64 ± 1.47	ns	3.49 ± 1.53	3.36 ± 0.44	ns	3.15 ± 1.83	4.19 ± 0.72	ns	3.74 ± 1.40	4.19 ± 0.81	ns
	AAL	3.85 ± 3.85	4.21 ± 1.22	ns	3.09 ± 1.21	3.35 ± 0.91	ns	2.95 ± 1.44	4.08 ± 1.28	ns	3.77 ± 1.63	3.62 ± 1.14	ns
	AAM	3.79 ± 3.79	3.26 ± 0.91	ns	2.84 ± 1.44	2.85 ± 0.81	ns	2.91 ± 1.01	3.37 ± 1.12	ns	3.57 ± 1.52	3.69 ± 0.86	ns
	PAM	3.05 ± 3.05	2.64 ± 0.65	ns	2.00 ± 1.26	1.89 ± 1.17	ns	3.01 ± 1.26	2.89 ± 1.17	ns	3.48 ± 1.29	3.23 ± 1.31	ns
	APM	2.84 ± 2.84	3.03 ± 1.05	ns	1.50 ± 0.60	3.09 ± 1.65	***0.004***	2.95 ± 1.09	2.53 ± 1.33	ns	3.25 ± 1.38	3.16 ± 1.08	ns
	PPM	3.40 ± 3.41	3.62 ± 1.19	ns	2.50 ± 1.43	3.36 ± 1.00	ns	3.31 ± 1.37	3.84 ± 0.84	ns	3.52 ± 0.61	3.94 ± 1.41	ns

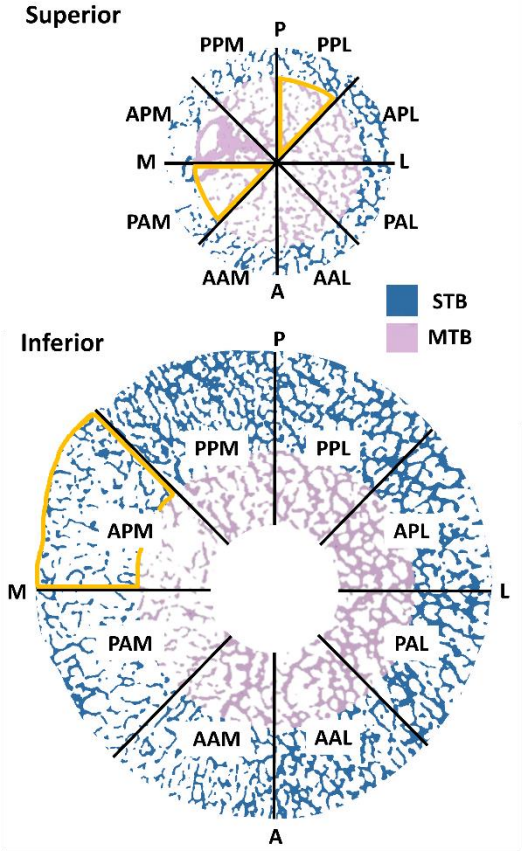

*Table 5.2 Location comparison of significant trabecular bone microarchitectural parameters in the micro-regions done using one way ANOVA. *(p<0.05), **(p<0.01), ***(p<0.001). A schematic displays the labelled regions, where P is posterior, A is anterior, L is lateral, and M is medial.*

		PPL vs. PAM	PPL vs. APM	APL vs. PAM	APL vs. APM	PAL vs. PAM	PAL vs. APM	AAL vs. PAM	AAL vs. APM	AAM vs. PAM	PAM vs. PPM
T2D BV/TV	Inferior STB	ns	ns	*	ns	*	ns	ns	ns	ns	ns
	Superior STB	ns	ns	ns	ns	ns	ns	ns	ns	ns	ns
	Inferior MTB	ns	ns	ns	ns	ns	ns	ns	ns	ns	ns
	Superior MTB	ns	ns	ns	ns	ns	ns	ns	ns	ns	ns
Non -T2D BV/TV	Inferior STB	ns	*	*	**	*	**	ns	ns	ns	ns
	Superior STB	ns	ns	ns	ns	ns	ns	ns	ns	ns	ns
	Inferior MTB	ns	ns	*	**	ns	ns	ns	ns	ns	ns
	Superior MTB	ns	ns	ns	*	ns	ns	ns	ns	ns	ns
T2D Tb.Th (mm)	Inferior STB	ns	ns	ns	ns	ns	ns	ns	ns	ns	ns
	Superior STB	ns	ns	ns	ns	ns	ns	ns	ns	ns	ns
	Inferior MTB	ns	ns	ns	ns	ns	ns	ns	ns	ns	ns
	Superior MTB	ns	ns	ns	ns	ns	ns	ns	ns	ns	ns
Non-T2D Tb.Th (mm)	Inferior STB	ns	ns	ns	ns	ns	ns	ns	ns	ns	ns
	Superior STB	ns	ns	ns	ns	ns	ns	ns	ns	ns	ns
	Inferior MTB	ns	ns	ns	*	ns	ns	ns	ns	ns	ns
	Superior MTB	ns	ns	ns	ns	ns	ns	ns	ns	ns	ns
T2D Tb.Sp (mm)	Inferior STB	***	ns	***	ns	***	ns	**	ns	*	*
	Superior STB	ns	ns	ns	ns	ns	ns	ns	ns	ns	ns
	Inferior MTB	ns	ns	ns	ns	ns	ns	ns	ns	ns	ns
	Superior MTB	ns	ns	ns	ns	ns	ns	ns	ns	ns	ns
Non-T2D Tb.Sp (mm)	Inferior STB	ns	**	ns	**	ns	**	ns	*	ns	ns
	Superior STB	ns	ns	ns	ns	ns	ns	ns	ns	ns	ns
	Inferior MTB	ns	ns	ns	ns	ns	ns	ns	ns	ns	ns
	Superior MTB	ns	ns	ns	ns	ns	ns	ns	ns	ns	ns

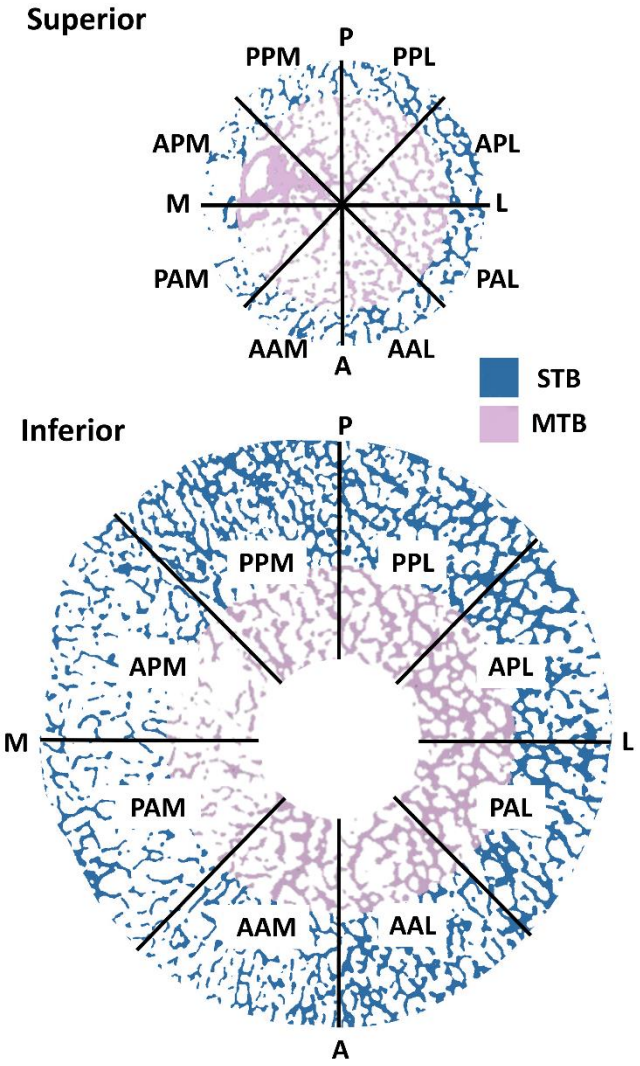

		PPL vs. PAM	PPL vs. APM	APL vs. PAM	APL vs. APM	PAL vs. PAM	PAL vs. APM	AAL vs. PAM	AAL vs. APM	AAM vs. PAM	PAM vs. PPM
T2D Tb.N (mm^{-1})	**Inferior STB**	**	ns	**	ns	*	ns	*	ns	ns	ns
	Superior STB	ns	**	**	***	*	***	ns	*	ns	ns
	Inferior MTB	ns	ns	ns	ns	*	ns	ns	ns	ns	ns
	Superior MTB	ns	**	ns	**	ns	**	ns	*	ns	ns
Non-T2D Tb.N (mm^{-1})	**Inferior STB**	ns	**	*	***	*	***	ns	*	ns	ns
	Superior STB	ns	ns	ns	ns	ns	ns	ns	ns	ns	ns
	Inferior MTB	ns	ns	ns	ns	ns	ns	ns	ns	ns	ns
	Superior MTB	ns	ns	ns	ns	ns	ns	ns	ns	ns	ns
T2D Conn.D ($1/mm^3$)	**Inferior STB**	ns	ns	*	ns	ns	ns	ns	ns	ns	ns
	Superior STB	ns	ns	ns	ns	ns	ns	ns	ns	ns	ns
	Inferior MTB	ns	ns	ns	ns	*	ns	ns	ns	ns	ns
	Superior MTB	ns	ns	*	**	ns	*	ns	ns	ns	ns
Non-T2D Conn.D ($1/mm^3$)	**Inferior STB**	ns	ns	ns	*	ns	*	ns	ns	ns	ns
	Superior STB	ns	ns	ns	ns	ns	ns	ns	ns	ns	ns
	Inferior MTB	ns	ns	ns	ns	ns	ns	ns	ns	ns	ns
	Superior MTB	ns	ns	ns	ns	ns	ns	ns	ns	ns	ns

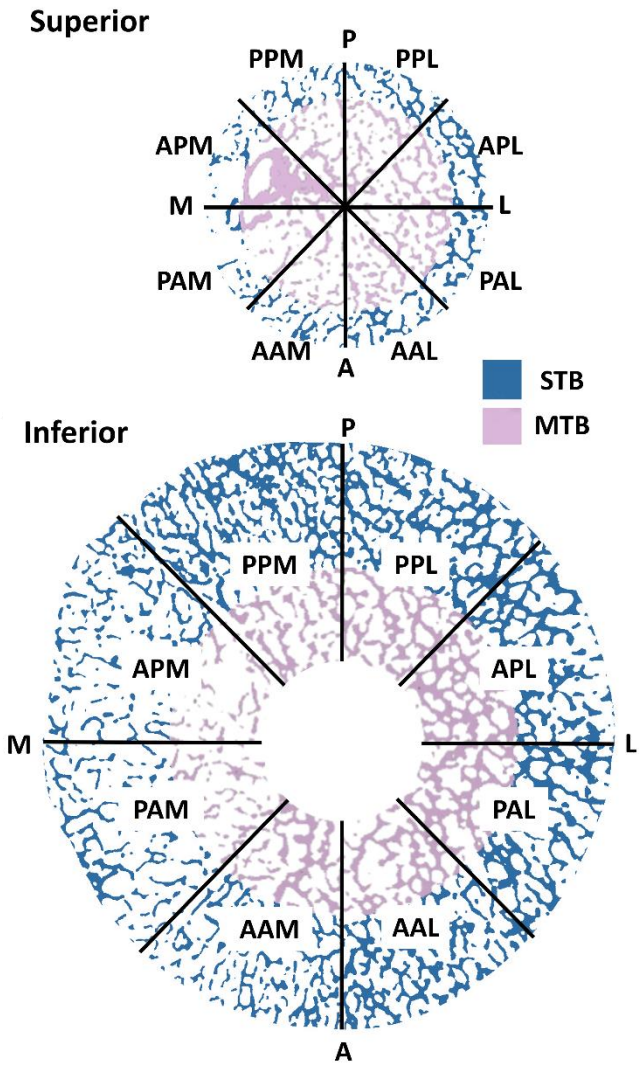

5.3.3 Bone Mineral Density Distribution

The bone mineral density distribution (BMDD) parameters of the central trabecular region were analysed, and the results are shown in Table 5.3 and Figure 5.5. The mode and mean mineral density, mineral heterogeneity, tissue volume at low, medium, and high mineral density did not differ significantly between groups.

Table 5.3 Comparison of bone mineral density distribution (BMDD) parameters of the central trabecular region (CTB) in non-T2D and T2D groups.

	Mode (mg HA/cm^3)	**Mean (mg HA/cm^3)**	**Heterogeneity (mg HA/cm^3)**	**Tissue Volume at Low Mineral Density (mm^3)**	**Tissue Volume at Medium Mineral Density (mm^3)**	**Tissue Volume at High Mineral Density (mm^3)**
Non-T2D	806.96	786.60	283.9	0.184	1.586	0.511
(n=9)	± 24.49	± 29.58	± 48.89	± 0.134	± 0.386	± 0.188
T2D	801.00	778.48	308.4	0.275	1.809	0.585
(n=9)	± 21.68	± 18.83	± 71.03	± 0.249	± 0.265	± 0.301
p	0.6024	0.5046	0.4266	0.3712	0.1816	0.5599

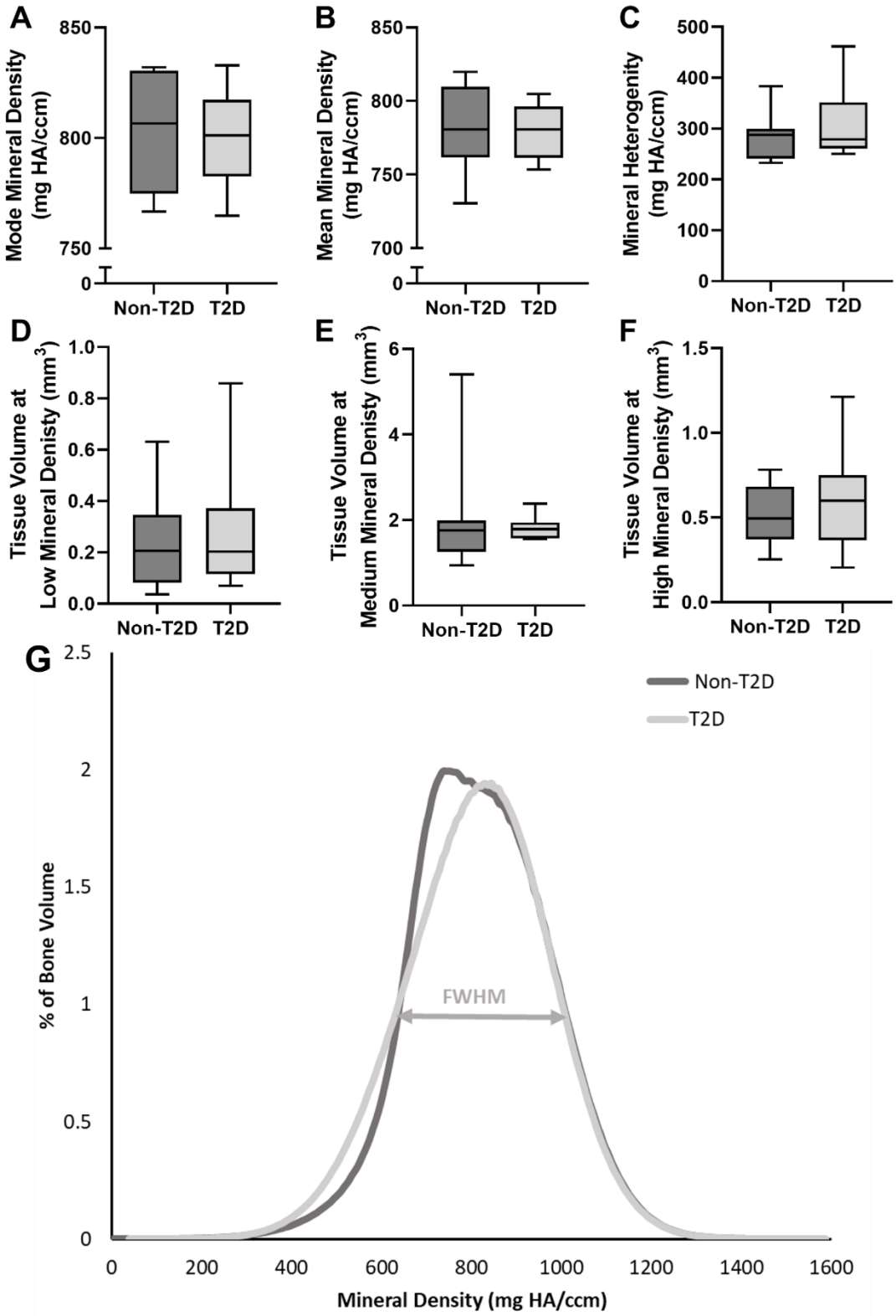

Figure 5.5 Comparison of bone mineral density distribution (BMDD) parameters of the central trabecular region (CTB) in non-T2D and T2D groups. A) mode mineral density, B) mean mineral density, C) mineral heterogeneity, D) tissue volume at low mineral density, E) tissue volume at medium mineral density, F) tissue volume at high mineral density, and G) bone mineral density distribution plot (BMDD) with the average BMDD curve for both the non-T2D and T2D groups.

5.4 Discussion

This study investigated the regional microarchitectural and morphological properties of trabecular bone in both type 2 diabetic and non-type 2 diabetic patients. Femoral heads of type 2 diabetic and non-type 2 diabetic patients who underwent total hip replacement were scanned using micro-CT, and the local microarchitectural properties of thirty-seven distinct regions of interest analysed based on a study by Ryan et al. (2020). It was found that disease status did not significantly affect trabecular microarchitectural properties in the five macro-regions examined. However, significant inter-regional variations were observed between the anatomical macro-regions analysed, with the central region showing the most differences compared to other regions, having a denser structure through a higher number of trabecula than subchondral and middle regions. Furthermore, significant microarchitectural differences were found in distinct micro-regions between disease states, with the type 2 diabetic samples having higher bone volume fraction and denser trabecular microarchitecture in certain locations in the inferior subchondral and superior middle regions of bone. When comparing intra-regional variation within each macro-region, there were significant differences in uniformity observed in both diabetic and non-diabetic groups, with inferior middle, superior middle and superior subchondral regions having a largely uniform structure, while the inferior subchondral showed a more non-uniform structure across the micro-regions analysed. This study represents the first in-depth evaluation of the effects of regional location on the morphological properties of diabetic femoral trabecular bone tissue. These results provide important insights into the microstructural differences of trabecular bone in the femoral head, in both diabetic and non-diabetic patients, which may have implications for bone fragility in individuals with diabetes.

While the microarchitectural properties of diabetic trabecular bone have previously been evaluated using ex vivo samples from the femoral head (Karim et al. 2018; Hunt et al. 2019; Parle et al. 2020; Sihota et al. 2021) and have generally shown that diabetic bone does not have

reduced bone mineral density, these analyses have exclusively focused on the central region of the femoral head. This study examined regional variations in the microarchitectural properties of the femoral head in diabetic patients. Even though no significant differences were found between the diabetic and non-diabetic groups in the five macro-regions analysed, several significant differences were observed in certain micro-regions of the femoral head. Some diabetic micro-regions displayed microarchitectural properties with a higher density than their non-diabetic counterparts. Specifically, the diabetic group showed a significant increase in the bone mass in the inferior subchondral APM region, and the superior middle PAM region compared to the non-diabetic group. The diabetic group also had significantly lower trabecular separation in the inferior subchondral APM and superior middle PPL regions, and a significantly higher trabecular number in the inferior subchondral APM and superior middle PPL regions compared to the non-diabetic. Additionally, a significantly higher connectivity density was observed in the inferior subchondral APM region in the diabetic group compared to the non-diabetic group. These observations suggests that these micro-regions, closer to the medial and posterior location, in the diabetic bone are altered and have a higher density and are more structurally robust. These results are in line with the results from the previous Chapter, which also found that discrete diabetic samples scanned at 10 µm resolution were denser with a higher bone volume fraction, trabecular number and lower trabecular separation than non-diabetic samples. In line with Chapter 4, the preserved and denser morphological properties seen in the diabetic group may be due to the altered remodelling process that is associated with T2D, remodelling to compensate for higher BMI or as a result of an anabolic reaction brought on by hyperinsulinemia (Thrailkill et al. 2005). These findings are also generally consistent with previous studies (Andrade et al. 2020; Starr et al. 2018; Nilsson et al. 2017; Sacher et al. 2022; Hunt et al. 2019, Parle et al. 2020) that have reported preserved or elevated trabecular microarchitecture in diabetic patients. The results from the current study indicate that changes

in the microarchitecture in individuals with diabetes are not necessarily uniform across the structure and can take place in local regions. Therefore, on first glance it may not appear that there are changes in the bulk femoral head, however, it is important to consider changes that may be occurring in precise regions due to diabetes.

According to Wolff's law, trabecular bone tends to be adapted according to the primary loading direction, which has been shown to lead to substantial variation and heterogeneity in trabecular architecture across different trabecular bone structures, including the vertebrae (Hulme et al. 2007; Kennedy et al. 2009). This study considered inter-regional variation of the trabecular architecture and showed substantial heterogeneity between several of the macro-regions considered in both disease states. The central region was generally the densest and most structurally robust with the highest bone volume fraction and trabecular number for both groups, and a lower trabecular separation compared to the inferior middle and subchondral regions. The structural model index of the central region also revealed a significantly more plate-like dense structure compared to the inferior middle and subchondral. However, the trabecular microarchitecture in the central regions were generally more similar to the superior middle and subchondral. Given the central location of these regions, along the primary loading axis of the femoral head, it would be expected that they would have a higher proportion of load-bearing responsibility compared to inferior subchondral and middle regions, which likely explain their denser structures. While other studies have analysed inter-regional variation of the femoral head (Li and Aspden 1997; Tamaddon et al. 2017; Ryan et al. 2020), only Chiba et al. (2013) have conclusively demonstrated inter- or intra-regional heterogeneity in microarchitectural properties in the in the femoral head, similar to this study. Chiba et al. (2013) observed this in osteoporotic samples, which they attributed to the non-uniform distribution of loads within the hip joint and proximal femur. While several previous studies have observed regional heterogeneity, this is the first study to have observed it using the high resolution of

micro-CT, which provides additional information on the microarchitecture of trabeculae such as bone volume fraction, trabecular separation, trabecular thickness, trabecular number, structural model index, connectivity density, and degree of anisotropy. In this study, it was found that regions that were likely situated along the principal loading axis of the femoral head, such as the central, superior middle and subchondral, would exhibit increased values of bone volume fraction, trabecular number, trabecular number, connectivity density and anisotropy, and have a plate-like structure. Conversely, regions that are not aligned with this axis, such as the inferior middle and subchondral tended to have lower values of bone volume fraction, trabecular number, trabecular thickness, connectivity density, anisotropy, and have a rod-like structure. Despite higher bone volume fraction in the central compared to the inferior middle and subchondral, a consistent increase in trabecular thickness was not observed. However, significantly increased trabecular number and decreased trabecular separation was observed, suggesting that in this case the increase bone volume fraction was not due to an increase in trabecular thickness. In summary, the regions along the primary loading axis of the femoral head, in particular the central region, tended to have microarchitectural properties suggesting they were the denser and more structurally robust than the regions that were not along this axis.

Further analysis of the morphological parameters intra-regionally within the eight predefined micro-anatomical regions of each of the macro-regions showed that there were significant differences in microarchitectural properties depending on the location in both disease states. The inferior subchondral region was the most heterogeneous with significant differences in bone volume fraction, trabecular separation, trabecular number, and connectivity density within the region in both diabetic and non-diabetic groups. On the other hand, the inferior and superior middle regions were generally more uniform in both groups. In the diabetic group, the superior subchondral region was also generally more uniform, while in the non-diabetic group, it was completely uniform with no significant differences. These findings are consistent with

the results from Chiba et al. (2013), who found that the four regions surrounding the central region in the section defined as superior, which is the most equivalent anatomical location to the inferior subchondral region in the current study, were the most heterogeneous when compared with one another. The heterogeneity observed in the inferior subchondral bone, seen in both disease states, is likely due to heterogeneous loading patterns experienced in vivo in this region.

In this Chapter, the difference in bone mineral density distribution between patients with and without diabetes was also evaluated. The BMDD parameters analysed in this study included the mode and mean mineral density, mineral heterogeneity, and tissue volume at low, medium, and high mineral density, with no significant differences found in these parameters between the groups. Despite no significant difference in the BMDD parameters the type 2 diabetic bone appears to have, on average, more immature bone, which may be due to the altered remodelling process. Bone mineral density distribution has been investigated previously for diabetic patients (Parle et al. 2020; Wölfel et al. 2020). Wölfel et al. (2020) found that the bone mineral density distribution between control and diabetic patients was similar in the periosteal and endocortical regions. However, Wölfel et al. (2020) also found that a sub-group of diabetic patients with high cortical porosity had a higher percentage area with low calcium content compared to the control group. Similarly, Parle et al. (2020) found an increase in tissue volume at lower mineral density in diabetic patients with osteoarthritis compared to non-diabetic osteoporosis patients. The results of this Chapter showed that the mode and mean mineral density and mineral heterogeneity did not differ significantly between the groups, indicating that the overall mineral density and variability within the central region are similar in bone both groups. There was also no significant difference in tissue volume at low, medium, or high mineral density between the groups. Overall, the results of this evaluation suggest that the bone

mineral density distribution parameters are similar between individuals with and without diabetes.

By examining various anatomical locations within the femoral trabecular bone tissue using micro-CT, this study has contributed valuable additional information to the limited body of experimental data on bone in individuals with diabetes. However, the current study has several limitations that must be taken into account when interpreting the results. This study did not measure the fabric tensor and the resolution used to measure the BMDD may not have been sufficient to capture meaningful differences. Similar to Chapter 4, one of the primary limitations is the lack of information on important factors such as body mass index, HbA1C, disease duration, and long-term disease management in the patient data. Although samples were collected from sex and age matched individuals with osteoarthritis, the other missing information on these factors could have influenced the results. Although significant differences between regions were found in this study, it is important to note the small sample size of n=9 per group, which is a limitation that should be taken into account when generalising the findings to a larger population. Nonetheless, despite the limited sample number, this study provides valuable insights into the variations between regions.

5.5 Conclusions

In conclusion, this Chapter has provided valuable insights into the trabecular microarchitecture and BMDD of individuals with diabetes. Inter-regional results suggest that in both disease states the central region is the densest and most structurally robust. Furthermore, the results of this study suggest that the type 2 diabetic bone was denser than the non-diabetic bone in certain medial and posterior micro-anatomical regions of the bone, with significant differences in bone volume fraction, trabecular separation, trabecular number, and connectivity density. The root cause for this is not clear, although, it could be due to localised altered

remodelling of the bone in the type 2 diabetes. Important insights on the intra-regional heterogeneity within the femoral head in both diabetic and non-diabetic individuals are presented with the most heterogeneous region being the inferior subchondral region. This is the first study to provide an understanding of these regions in type 2 diabetic bone. Further studies are needed to elucidate the underlying mechanisms responsible for these observations and to determine the clinical implications of these findings for individuals with diabetes. Overall, this study contributes to our understanding of the complex relationship between diabetes and bone microarchitecture.

5.6 Appendix 5.1

When the five macro regions were combined (e.g. the bulk femoral head), there were no significant differences in the trabecular microarchitecture when comparing the T2D samples with the non-T2Ds in any of the microarchitectural properties as shown in Figure A.5.1.

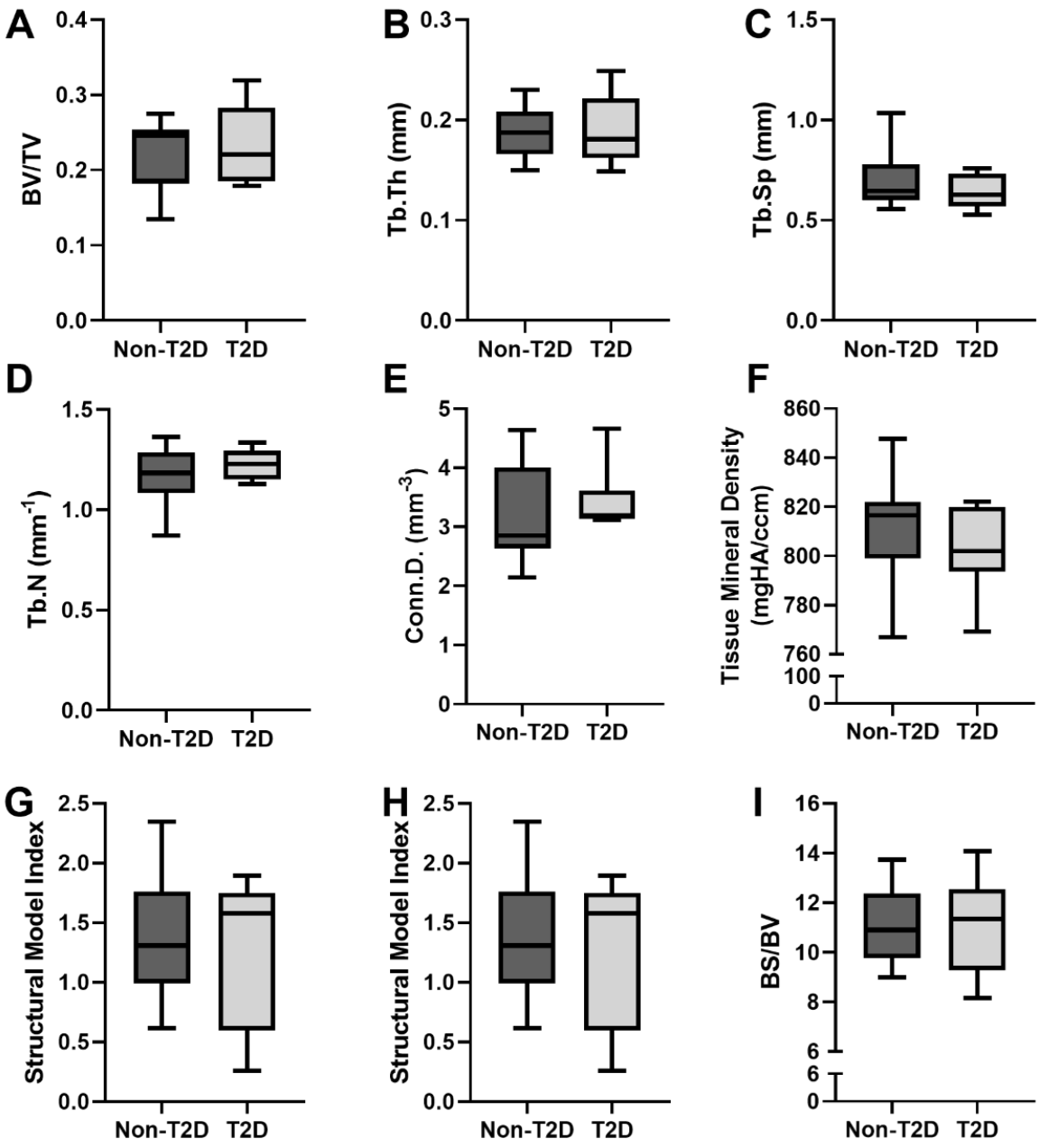

Figure A.5.1 Boxplots of the microarchitectural properties of trabecular bone of the full femoral trabecular region T2D (light grey) and non-T2D (dark grey) are shown. The following parameters are displayed: A) BV/TV, B) Tb.Th, C) Tb.Sp, D) Tb.N, E) Conn D, F) Structural Model Index, G) Degree of anisotropy, and H) BS/BV

*Table A5.1 Location comparison of trabecular bone microarchitectural parameters in the micro-regions done using one way ANOVA. *(p<0.05), **(p<0.01), ***(p<0.001)*

		PPL vs. APL	PPL vs. PAL	PPL vs. AAL	PPL vs. AAM	PPL vs. PAM	PPL vs. APM	PPL vs. PPM	APL vs. PAL	APL vs. AAL	APL vs. AAM	APL vs. PAM	APL vs. APM	APL vs. PPM	PAL vs. AAL	PAL vs. AAM	PAL vs. PAM	PAL vs. APM	PAL vs. PPM	AAL vs. AAM	AAL vs. PAM	AAL vs. APM	AAL vs. PPM	AAM vs. PAM	AAM vs. APM	AAM vs. PPM	PAM vs. APM	PAM vs. PPM	APM vs. PPM
T2D BV/TV	Inferior STB	ns	ns	ns	ns	ns	ns	ns	ns	ns	ns	*	ns	ns	ns	ns	*	ns	ns	ns	ns	ns	ns	ns	ns	ns	ns	ns	ns
	Superior STB	ns	ns	ns	ns	ns	ns	ns	ns	ns	ns	ns	ns	ns	ns	ns	ns	ns	ns	ns	ns	ns	ns	ns	ns	ns	ns	ns	ns
	Inferior MTB	ns	ns	ns	ns	ns	ns	ns	ns	ns	ns	ns	ns	ns	ns	ns	ns	ns	ns	ns	ns	ns	ns	ns	ns	ns	ns	ns	ns
	Superior MTB	ns	ns	ns	ns	ns	ns	ns	ns	ns	ns	ns	ns	ns	ns	ns	ns	ns	ns	ns	ns	ns	ns	ns	ns	ns	ns	ns	ns
Non -T2D BV/TV	Inferior STB	ns	ns	ns	ns	ns	*	ns	ns	ns	ns	*	**	ns	ns	ns	*	**	ns	ns	ns	ns	ns	ns	ns	ns	ns	ns	ns
	Superior STB	ns	ns	ns	ns	ns	ns	ns	ns	ns	ns	ns	ns	ns	ns	ns	ns	ns	ns	ns	ns	ns	ns	ns	ns	ns	ns	ns	ns
	Inferior MTB	ns	ns	ns	ns	ns	ns	ns	ns	ns	ns	*	**	ns	ns	ns	ns	ns	ns	ns	ns	ns	ns	ns	ns	ns	ns	ns	ns
	Superior MTB	ns	ns	ns	ns	ns	ns	ns	ns	ns	ns	ns	*	ns	ns	ns	ns	ns	ns	ns	ns	ns	ns	ns	ns	ns	ns	ns	ns
T2D Tb.Th (mm)	Inferior STB	ns	ns	ns	ns	ns	ns	ns	ns	ns	ns	ns	ns	ns	ns	ns	ns	ns	ns	ns	ns	ns	ns	ns	ns	ns	ns	ns	ns
	Superior STB	ns	ns	ns	ns	ns	ns	ns	ns	ns	ns	ns	ns	ns	ns	ns	ns	ns	ns	ns	ns	ns	ns	ns	ns	ns	ns	ns	ns
	Inferior MTB	ns	ns	ns	ns	ns	ns	ns	ns	ns	ns	ns	ns	ns	ns	ns	ns	ns	ns	ns	ns	ns	ns	ns	ns	ns	ns	ns	ns
	Superior MTB	ns	ns	ns	ns	ns	ns	ns	ns	ns	ns	ns	ns	ns	ns	ns	ns	ns	ns	ns	ns	ns	ns	ns	ns	ns	ns	ns	ns
Non-T2D Tb.Th (mm)	Inferior STB	ns	ns	ns	ns	ns	ns	ns	ns	ns	ns	ns	ns	ns	ns	ns	ns	ns	ns	ns	ns	ns	ns	ns	ns	ns	ns	ns	ns
	Superior STB	ns	ns	ns	ns	ns	ns	ns	ns	ns	ns	ns	ns	ns	ns	ns	ns	ns	ns	ns	ns	ns	ns	ns	ns	ns	ns	ns	ns
	Inferior MTB	ns	ns	ns	ns	ns	ns	ns	ns	ns	ns	ns	*	ns	ns	ns	ns	ns	ns	ns	ns	ns	ns	ns	ns	ns	ns	ns	ns
	Superior MTB	ns	ns	ns	ns	ns	ns	ns	ns	ns	ns	ns	ns	ns	ns	ns	ns	ns	ns	ns	ns	ns	ns	ns	ns	ns	ns	ns	ns
T2D Tb.Sp (mm)	Inferior STB	ns	ns	ns	ns	***	ns	ns	ns	ns	ns	***	ns	ns	ns	ns	***	ns	ns	ns	**	ns	ns	*	ns	ns	ns	*	ns
	Superior STB	ns	ns	ns	ns	ns	ns	ns	ns	ns	ns	ns	ns	ns	ns	ns	ns	ns	ns	ns	ns	ns	ns	ns	ns	ns	ns	ns	ns
	Inferior MTB	ns	ns	ns	ns	ns	ns	ns	ns	ns	ns	ns	ns	ns	ns	ns	ns	ns	ns	ns	ns	ns	ns	ns	ns	ns	ns	ns	ns
	Superior MTB	ns	ns	ns	ns	ns	ns	ns	ns	ns	ns	ns	ns	ns	ns	ns	ns	ns	ns	ns	ns	ns	ns	ns	ns	ns	ns	ns	ns
Non-T2D Tb.Sp (mm)	Inferior STB	ns	ns	ns	ns	ns	**	ns	ns	ns	ns	ns	**	ns	ns	ns	ns	**	ns	ns	ns	*	ns	ns	ns	ns	ns	ns	ns
	Superior STB	ns	ns	ns	ns	ns	ns	ns	ns	ns	ns	ns	ns	ns	ns	ns	ns	ns	ns	ns	ns	ns	ns	ns	ns	ns	ns	ns	ns
	Inferior MTB	ns	ns	ns	ns	ns	ns	ns	ns	ns	ns	ns	ns	ns	ns	ns	ns	ns	ns	ns	ns	ns	ns	ns	ns	ns	ns	ns	ns
	Superior MTB	ns	ns	ns	ns	ns	ns	ns	ns	ns	ns	ns	ns	ns	ns	ns	ns	ns	ns	ns	ns	ns	ns	ns	ns	ns	ns	ns	ns

		PPL vs. APL	PPL vs. PAL	PPL vs. AAL	PPL vs. AAM	PPL vs. PAM	PPL vs. APM	PPL vs. PPM	APL vs. PAL	APL vs. AAL	APL vs. AAM	APL vs. PAM	APL vs. APM	APL vs. PPM	PAL vs. AAL	PAL vs. AAM	PAL vs. PAM	PAL vs. APM	PAL vs. PPM	AAL vs. AAM	AAL vs. PAM	AAL vs. APM	AAL vs. PPM	AAM vs. PAM	AAM vs. APM	AAM vs. PPM	PAM vs. APM	PAM vs. PPM	APM vs. PPM
T2D Tb.N (mm^{-1})	**Inferior STB**	ns	ns	ns	ns	**	ns	ns	ns	ns	ns	**	ns	ns	ns	ns	*	ns	ns	ns	*	ns	ns	ns	ns	ns	ns	ns	ns
	Superior STB	ns	ns	ns	ns	ns	**	ns	ns	ns	ns	**	***	ns	ns	ns	*	***	ns	ns	ns	*	ns	ns	ns	ns	ns	ns	ns
	Inferior MTB	ns	ns	ns	ns	ns	ns	ns	ns	ns	ns	ns	ns	ns	ns	ns	*	ns	ns	ns	ns	ns	ns	ns	ns	ns	ns	ns	ns
	Superior MTB	ns	ns	ns	ns	ns	**	ns	ns	ns	ns	ns	**	ns	ns	ns	ns	**	ns	ns	ns	*	ns	ns	ns	ns	ns	ns	ns
Non-T2D Tb.N (mm^{-1})	**Inferior STB**	ns	ns	ns	ns	ns	**	ns	ns	ns	ns	*	***	ns	ns	ns	*	***	ns	ns	ns	*	ns	ns	ns	ns	ns	ns	ns
	Superior STB	ns	ns	ns	ns	ns	ns	ns	ns	ns	ns	ns	ns	ns	ns	ns	ns	ns	ns	ns	ns	ns	ns	ns	ns	ns	ns	ns	ns
	Inferior MTB	ns	ns	ns	ns	ns	ns	ns	ns	ns	ns	ns	ns	ns	ns	ns	ns	ns	ns	ns	ns	ns	ns	ns	ns	ns	ns	ns	ns
	Superior MTB	ns	ns	ns	ns	ns	ns	ns	ns	ns	ns	ns	ns	ns	ns	ns	ns	ns	ns	ns	ns	ns	ns	ns	ns	ns	ns	ns	ns
T2D Conn.D ($1/mm^3$)	**Inferior STB**	ns	ns	ns	ns	ns	ns	ns	ns	ns	ns	*	ns	ns	ns	ns	ns	ns	ns	ns	ns	ns	ns	ns	ns	ns	ns	ns	ns
	Superior STB	ns	ns	ns	ns	ns	ns	ns	ns	ns	ns	ns	ns	ns	ns	ns	ns	ns	ns	ns	ns	ns	ns	ns	ns	ns	ns	ns	ns
	Inferior MTB	ns	ns	ns	ns	ns	ns	ns	ns	ns	ns	ns	ns	ns	ns	ns	*	ns	ns	ns	ns	ns	ns	ns	ns	ns	ns	ns	ns
	Superior MTB	ns	ns	ns	ns	ns	ns	ns	ns	ns	ns	*	**	ns	ns	ns	ns	*	ns	ns	ns	ns	ns	ns	ns	ns	ns	ns	ns
Non-T2D Conn.D ($1/mm^3$)	**Inferior STB**	ns	ns	ns	ns	ns	ns	ns	ns	ns	ns	ns	*	ns	ns	ns	ns	*	ns	ns	ns	ns	ns	ns	ns	ns	ns	ns	ns
	Superior STB	ns	ns	ns	ns	ns	ns	ns	ns	ns	ns	ns	ns	ns	ns	ns	ns	ns	ns	ns	ns	ns	ns	ns	ns	ns	ns	ns	ns
	Inferior MTB	ns	ns	ns	ns	ns	ns	ns	ns	ns	ns	ns	ns	ns	ns	ns	ns	ns	ns	ns	ns	ns	ns	ns	ns	ns	ns	ns	ns
	Superior MTB	ns	ns	ns	ns	ns	ns	ns	ns	ns	ns	ns	ns	ns	ns	ns	ns	ns	ns	ns	ns	ns	ns	ns	ns	ns	ns	ns	ns

```
%start with clean slate
clearvars % novariables
close all  %no figures
%clc     %empty command window
%% Data Access
%-----------------------------------------------------------------------
%DICOM support
tic
addpath('C:\Users\\OneDrive\Documents\MicroCT\Transfer\SAMPLE_FH');
addpath('C:\Users\\OneDrive\2020\TIFF Trab Masks\');
addpath('C:\Users\\OneDrive\2020\Medical Image Reader and Viewer');
addpath('C:\Users\\OneDrive\2020\Tiff2DicomfromMatlab');
addpath('C:\Users\\OneDrive\2020\BOOLEAN');
addpath('C:\Users\\OneDrive\2020');
addpath('C:\Users\\OneDrive\2020\DICOMSfromPART1');
addpath('C:\Users\\OneDrive\2020\Tiff2DicomfromMatlab\SAMPLE_FH');

%filename convention used in image series
prefix = 'A0004026_';
first=1;%% 100 is near the top and 500 is near the bottom
last=799;%need to check this

imgID=first:last;
ext = '.dcm';
%first filename in series
fname = [prefix num2str(imgID(1),'%05d') ext]; %adding padding zeros
%%
%examine file header
info = dicominfo(fname);
%extract size info from metadata
voxel_size = [info.PixelSpacing; info.SliceThickness]';
%read slice images; populate XYZ matrix
hWaitBar = waitbar(0,'Reading DICOM files');
for i=length(imgID):-1:1
 fname = [prefix num2str(imgID(i),'%05d') ext];
 D(:,:,i) = int16(dicomread(fname)); waitbar((length(imgID)-i)/length(imgID))
end
%%
xy=size(D,1);
halfxy=(xy/2);
delete(hWaitBar)
whos D
v=494;
disp('Done Data Input')
imshow(D(:,:,100))

 for k=1:size(D,3)%only finds the length of the 3rd dimension of matrix
 metadata(k)=dicominfo([prefix num2str(imgID(k),'%05d') ext]);
 end

%% reading in the ROI TIFFs created in ImageJ or someother outside program

mkdir('C:\Users\\OneDrive\2020\FH\');
mkdir('C:\Users\\OneDrive\2020\FH\Macro_CTB');%1
mkdir('C:\Users\\OneDrive\2020\FH\Macro_MTB_SUP_STB_INF');%2
mkdir('C:\Users\\OneDrive\2020\FH\Macro_MTB_INF_STB_SUP');%3
mkdir('C:\Users\\OneDrive\2020\FH\MSTB_APM_PPL_PAL_AAM_INFSUP');%4
mkdir('C:\Users\\OneDrive\2020\FH\MSTB_APM_PPL_PAL_AAM_SUPINF');%5
mkdir('C:\Users\\OneDrive\2020\FH\MSTB_PPM_APL_AAL_PAM_INFSUP');%6
mkdir('C:\Users\\OneDrive\2020\FH\MSTB_PPM_APL_AAL_PAM_SUPINF');%7

disp('directories made')
%%
 Z=zeros(xy,xy,last);
for k = 1:last %last
 Z(:,:,k) = int16(imread('WhiteTrabRegion_SAMPLE_FH.tif', k));%%should i use a gui?
end
disp('TIFFs read in')
%% converting the TIFFs to DICOMs
mkdir('C:\Users\\OneDrive\2020\Tiff2DicomfromMatlab\84');

for q=1:last
```

```
  dicomwrite(Z(:,:,q),['C:\Users\\OneDrive\2020\Tiff2DicomfromMatlab\84\','TrabWhiteMask_01_',
num2str(q,'%05d'), '.dcm'],metadata(q));
end
disp('done dicom write of TIFFs')
%% reading in the converted DICOMS from the previous step.
addpath("C:\Users\\OneDrive\2020\Tiff2DicomfromMatlab\84");

clear Z;

%filename
prefix2 = 'TrabWhiteMask_01_';
fname2 = [prefix2 num2str(imgID(1),'%05d') ext]; %adding padding zeros

%examine file header (nobkpt)
info2 = dicominfo(fname2);
%extract size info from metadata (nobkpt)
voxel_size2 = [info2.PixelSpacing; info2.SliceThickness];
%read slice images; populate XYZ matrix
hWaitBar = waitbar(0,'Reading DICOM files');
for i=length(imgID):-1:1
 fname2 = [prefix2 num2str(imgID(i),'%05d') ext];
 Q(:,:,i) = int16(dicomread(fname2));
 waitbar((length(imgID)-i)/length(imgID))
end

delete(hWaitBar)

whos Q
v=200;
disp('Done Data Input')

bw2 =imbinarize(Q); %convert to binary
imshow(bw2(:,:,v));% number regers to slice and plane
disp('Done Threshold Data and Binarize')
%% SPHERE FIT
M=bwperim(bw2);
imshow(M(:,:,v))

idx = find(M); % find points in M
[rr,cc,pp] = ind2sub(size(M),idx); % sub indices
clear M;
figure;
scatter3(rr,cc,pp,10,pp);
daspect([1,1,1]);
view(-121,36);
axis tight;
% Fit the Sphere:
[cent,radius] = sphereFit([rr, cc, pp]);
fprintf(1,'\nRadius of sphere is %3.1f\nIt is centered at [%3.1f %3.1f %3.1f]\n',radius,cent)
scatter3(cc,rr,pp,25,pp,'*'); %points
hold on;
daspect([1,1,1]); % equal axis
[Base_rr,Base_cc,Base_pp] = sphere(20);
surf(radius*Base_rr+cent(2),...
   radius*Base_cc+cent(1),...
   radius*Base_pp+cent(3),'faceAlpha',0.3,'Facecolor','m')
axis tight;
view(-121,36);

clear pp rr cc idx Base_rr Base_cc Base_pp

disp('done trabecular sphere fit')


%% BOOLEAN SUBTRACTION to Separate cortical bone and trabecular bone
Q=imbinarize(Q);
Q(:,:,(cent(3)+1):last)=[];
figure;
bw =imbinarize(D);%%remove
shape1=bw;%whole bone
shape2=bw2;%trabecular bone mask
clear bw2;
%c is the cortical bone
```

```
c=shape1-shape2;
clear shape1 shape2
imshow(c(:,:,v));
%% Writing Boolean to DICOM
for q=1:size(c,3)
  dicomwrite(c(:,:,q),['C:\Users\\OneDrive\2020\BOOLEAN\CortBOOL2\','CORT_BOOL_01_',
num2str(q,'%05d'), '.dcm'],metadata(q));
end
disp('done dicom write cortical bone')
%%
shapeA=logical(bw);%whole bone
shapeB=logical(c);%cortical bone
figure;
clear bw;
%t is trabecularbone
t=shapeA-shapeB;
clear shapeA shapeB;
imshow(t(:,:,v));
%% Writing Boolean to DICOM
for q=1:size(c,3)
  dicomwrite(t(:,:,q),['C:\Users\\OneDrive\2020\BOOLEAN\TrabBOOL2\','TRAB_BOOL_01_',
num2str(q,'%05d'), '.dcm'],metadata(q));
end
clear c;
disp('done dicom write trabceuls bone')
%%
addpath('C:\Users\\OneDrive\2020\BOOLEAN\TrabBOOL2\');

Z = int16(dicomread('TRAB_BOOL_01_00100'));
bw3 =imbinarize(Z); %convert to binary

imshow(bw3);
clear bw3
disp('Done ');
BWtrab= imbinarize(t);

Trab = BWtrab;
Trab(:,:,(cent(3)+1):last)=[];
D(:,:,(cent(3)+2):last)=[];
clear BWtrab
%%
clear t D
cent=round(cent);
radius=round(radius);

imageSizeX=xy;%348*2;%690;% x and y seem to be mixed up here should x be 658 and y 690
imageSizeY=xy;%348*2;%658; HRB 5 was a smaller image for some reason
imageSizeZ=last;%310*2;%399
[columnsInImage, rowsInImage, pagesInImage] = meshgrid(1:imageSizeX, 1:imageSizeY,1:imageSizeZ);

sphereVoxelsInner = (rowsInImage - cent(1)).^2 ...
  + (columnsInImage - cent(2)).^2 +(pagesInImage - cent(3)).^2<= (radius*1/3).^2;
%delete lower hallf now
sphereVoxelsInner(:,:,(cent(3)+2):last)=[];
sphereVoxelsMiddle = (rowsInImage - cent(1)).^2 ...
  + (columnsInImage - cent(2)).^2 +(pagesInImage - cent(3)).^2<= (radius*2/3).^2;
%delete lower half now
sphereVoxelsMiddle(:,:,(cent(3)+2):last)=[];
sphereVoxelsOuter = (rowsInImage - cent(2)).^2 ...
  + (columnsInImage - cent(1)).^2 +(pagesInImage - cent(3)).^2<= (radius*1.2).^2;
%delete lower half now
sphereVoxelsOuter(:,:,(cent(3)+2):last)=[];

%% Making Cone and Creating sphere quarters to get 45 degree angle

Inner=sphereVoxelsInner;
Middle=sphereVoxelsMiddle;%-sphereVoxelsInner;
Outer=sphereVoxelsOuter;%Q;
clear sphereVoxelsInner sphereVoxelsMiddle sphereVoxelsOuter Q

F=(rowsInImage-cent(1)).^2+(columnsInImage-cent(2)).^2>=((pagesInImage-cent(3))).^2;
F(:,:,(cent(3)+2):last)=[];
clear columnsInImage rowsInImage pagesInImage
```

```
Cone=imbinarize(Outer-F);% changed ZHALF to OUter
clear F;
disp('done sphere halves')
SphereMinusCone=imbinarize(Outer-Cone);
%Macro-region 5
for i=length(imgID):-1:1
 fname = [prefix num2str(imgID(i),'%05d') ext];
 D(:,:,i) = int16(dicomread(fname)); waitbar((length(imgID)-i)/length(imgID))
end

V=D;
clear D;
Macro_CTB=V;
Macro_CTB(~Inner)=0;%%working

%MACRO-REGION1
MiddleRing=imbinarize(Outer-Middle+Inner);
SphereMinusConeminusMiddle=imbinarize(SphereMinusCone-Middle);
Macro_MTB_SUP_STB_INF_B=imbinarize(Trab-imbinarize(SphereMinusCone+MiddleRing))...
  +imbinarize(Trab-imbinarize(Outer-SphereMinusConeminusMiddle));

Macro_MTB_SUP_STB_INF=V;
Macro_MTB_SUP_STB_INF(~Macro_MTB_SUP_STB_INF_B)=0;
clear Macro_MTB_SUP_STB_INF_B

%%MACRO-REGION2
SphereMinusConeplusMiddle=imbinarize(SphereMinusCone+Middle);% macro STB inferior region
clear SphereMinusCone
Macro_MTB_INF_STB_SUP_B=imbinarize(Trab-imbinarize(MiddleRing+Cone))+imbinarize(Trab-
SphereMinusConeplusMiddle);
clear MiddleRing Cone
clear SphereMinusConeplusMiddle
Macro_MTB_INF_STB_SUP=V;
Macro_MTB_INF_STB_SUP(~Macro_MTB_INF_STB_SUP_B)=0;
clear Macro_MTB_INF_STB_SUP_B
clear Trab V SphereMinusConeminusMiddle
%%
for q=1:cent(3)
 dicomwrite(Macro_CTB(:,:,q),['C:\Users\\OneDrive\2020\FH\Macro_CTB\','SET1', num2str(q,'%05d'),
'.dcm'],metadata(q), "CreateMode","copy","WritePrivate",true,"UseMetadataBitDepths", true);

end
disp('Done 1 Macro-regions Dicom Write')
clear Macro_CTB
%%
addpath('C:\Users\\OneDrive\2020\rotateAround');
S1O=Outer;
clear Outer Middle Inner
S1O(1:cent(1),:,:) = 0;
angle=45;
B1 = rotateAround(S1O, cent(1), cent(2), angle);

%%
angle=90;
%B1=imrotate(S1O,45,'crop');%'crop' crops it to the same size as the orignal image
B1(cent(1):xy,:,:) = 0;%APM
B3=rotateAround(B1, cent(1), cent(2), angle);%PPL
B5=rotateAround(B3, cent(1), cent(2), angle);%PAL
B7=rotateAround(B5, cent(1), cent(2), angle);%AAM
B1357=B1+B3+B5+B7;
clear B3 B5 B7
disp ('done odd Bs')
%%
B2=rotateAround(B1, cent(1), cent(2), 45);%PPM
B4=rotateAround(B2, cent(1), cent(2), angle);%APL
B6=rotateAround(B4, cent(1), cent(2), angle);%AAL
B8=rotateAround(B6, cent(1), cent(2), angle);%PAM
clear B1
B2468=B2+B4+B6+B8;
clear B2 B4 B6 B8
disp ('done even Bs')
%%
```

```
MSTB_APM_PPL_PAL_AAM_INFSUP=Macro_MTB_INF_STB_SUP;
MSTB_APM_PPL_PAL_AAM_INFSUP(~B1357)=0;
MSTB_APM_PPL_PAL_AAM_SUPINF=Macro_MTB_SUP_STB_INF;
MSTB_APM_PPL_PAL_AAM_SUPINF(~B1357)=0;
clear B1357

for q=1:cent(3)

dicomwrite(MSTB_APM_PPL_PAL_AAM_INFSUP(:,:,q),['C:\Users\\OneDrive\2020\FH\MSTB_APM_PPL_PAL_AAM_INFSUP
\','SET4', num2str(q,'%05d'), '.dcm'],metadata(q),
"CreateMode","copy","WritePrivate",true,"UseMetadataBitDepths", true);
dicomwrite(MSTB_APM_PPL_PAL_AAM_SUPINF(:,:,q),['C:\Users\\OneDrive\2020\FH\MSTB_APM_PPL_PAL_AAM_SUPINF
\','SET5', num2str(q,'%05d'), '.dcm'],metadata(q),
"CreateMode","copy","WritePrivate",true,"UseMetadataBitDepths", true);
end
disp('done SET 4 AND 5 dicom write')
clear MSTB_APM_PPL_PAL_AAM_SUPINF MSTB_APM_PPL_PAL_AAM_INFSUP
%%
MSTB_PPM_APL_AAL_PAM_INFSUP=Macro_MTB_INF_STB_SUP;
MSTB_PPM_APL_AAL_PAM_INFSUP(~B2468)=0;
MSTB_PPM_APL_AAL_PAM_SUPINF=Macro_MTB_SUP_STB_INF;
MSTB_PPM_APL_AAL_PAM_SUPINF(~B2468)=0;
clear B2468
for q=1:cent(3)

dicomwrite(MSTB_PPM_APL_AAL_PAM_INFSUP(:,:,q),['C:\Users\\OneDrive\2020\FH\MSTB_PPM_APL_AAL_PAM_INFSUP
\','SET6', num2str(q,'%05d'), '.dcm'],metadata(q),
"CreateMode","copy","WritePrivate",true,"UseMetadataBitDepths", true);

dicomwrite(MSTB_PPM_APL_AAL_PAM_SUPINF(:,:,q),['C:\Users\\OneDrive\2020\FH\MSTB_PPM_APL_AAL_PAM_SUPINF
\','SET7', num2str(q,'%05d'), '.dcm'],metadata(q),
"CreateMode","copy","WritePrivate",true,"UseMetadataBitDepths", true);
end
disp('done SET 6 AND 7 dicom write')
clear MSTB_PPM_APL_AAL_PAM_INFSUP MSTB_PPM_APL_AAL_PAM_SUPINF
%%
for q=1:cent(3)

 dicomwrite(Macro_MTB_INF_STB_SUP(:,:,q),['C:\Users\\OneDrive\2020\FH\Macro_MTB_INF_STB_SUP\','SET2',
num2str(q,'%05d'), '.dcm'],metadata(q),
"CreateMode","copy","WritePrivate",true,"UseMetadataBitDepths", true);
 dicomwrite(Macro_MTB_SUP_STB_INF(:,:,q),['C:\Users\\OneDrive\2020\FH\Macro_MTB_SUP_STB_INF\','SET3',
num2str(q,'%05d'), '.dcm'],metadata(q),
"CreateMode","copy","WritePrivate",true,"UseMetadataBitDepths", true);

end
disp('Done 4 Macro-regions DICOM Write')
clear Macro_MTB_INF Macro_MTB_SUP Macro_STB_INF Macro_STB_SUP
toc
disp("doneFH")
```

5.7 References

Bonds, Denise E., Joseph C. Larson, Ann V. Schwartz, Elsa S. Strotmeyer, John Robbins, Beatriz L. Rodriguez, Karen C. Johnson, and Karen L. Margolis. 2006. 'Risk of Fracture in Women with Type 2 Diabetes: the Women's Health Initiative Observational Study', *The Journal of Clinical Endocrinology & Metabolism*, 91: 3404-10.

Burghardt, Andrew J., Ahi S. Issever, Ann V. Schwartz, Kevin A. Davis, Umesh Masharani, Sharmila Majumdar, and Thomas M. Link. 2010. 'High-Resolution Peripheral Quantitative Computed Tomographic Imaging of Cortical and Trabecular Bone Microarchitecture in Patients with Type 2 Diabetes Mellitus', *The Journal of Clinical Endocrinology & Metabolism*, 95: 5045-55.

Chiba, Ko, Andrew J. Burghardt, Makoto Osaki, and Sharmila Majumdar. 2013. 'Heterogeneity of bone microstructure in the femoral head in patients with osteoporosis: An ex vivo HR-pQCT study', *Bone*, 56: 139-46.

Cowin, Stephen C. 2001. *Bone mechanics handbook* (CRC press).

Currey, John D. 2006. *Bones: structure and mechanics* (Princeton university press).

Homminga, J., B. Van-Rietbergen, E. M. Lochmüller, H. Weinans, F. Eckstein, and R. Huiskes. 2004. 'The osteoporotic vertebral structure is well adapted to the loads of daily life, but not to infrequent "error" loads', *Bone*, 34: 510-6.

Hulme, P. A., S. K. Boyd, and S. J. Ferguson. 2007. 'Regional variation in vertebral bone morphology and its contribution to vertebral fracture strength', *Bone*, 41: 946-57.

Hunt, Heather B., Ashley M. Torres, Pablo M. Palomino, Eric Marty, Rehan Saiyed, Matthew Cohn, Jonathan Jo, Stephen Warner, Grazyna E. Sroga, Karen B. King, Joseph M. Lane, Deepak Vashishth, Christopher J. Hernandez, and Eve Donnelly. 2019. 'Altered Tissue Composition, Microarchitecture, and Mechanical Performance in Cancellous Bone From Men With Type 2 Diabetes Mellitus', *JOURNAL OF BONE AND MINERAL RESEARCH*: jbmr.3711-jbmr.11.

Janghorbani, M., R. M. Van Dam, W. C. Willett, and F. B. Hu. 2007. 'Systematic Review of Type 1 and Type 2 Diabetes Mellitus and Risk of Fracture', *American Journal of Epidemiology*, 166: 495-505.

Jennings, Alan. 2013. "Sphere Fit (least squared) (https://www.mathworks.com/matlabcentral/fileexchange/34129-sphere-fit-least-squared)." In, MATLAB Central File Exchange-MATLAB Central File Exchange.

Karim, Lamya, Julia Moulton, Miranda Van Vliet, Kelsey Velie, Ann Robbins, Fatemeh Malekipour, Ayesha Abdeen, Douglas Ayres, and Mary L. Bouxsein. 2018. 'Bone microarchitecture, biomechanical properties, and advanced glycation end-products in the proximal femur of adults with type 2 diabetes', *Bone*, 114: 32-39.

Li, B., and R. M. Aspden. 1997. 'Material properties of bone from the femoral neck and calcar femorale of patients with osteoporosis or osteoarthritis', *Osteoporosis International*, 7: 450-56.

Kennedy, Oran D, Orlaith Brennan, Susan M Rackard, Fergal J O'Brien, David Taylor, and T Clive Lee. 2009. 'Variation of trabecular microarchitectural parameters in cranial, caudal and mid-vertebral regions of the ovine L3 vertebra', *Journal of anatomy*, 214: 729-35.

Napoli, Nicola, Elsa S. Strotmeyer, Kristine E. Ensrud, Deborah E. Sellmeyer, Douglas C. Bauer, Andrew R. Hoffman, Thuy Tien L. Dam, Elizabeth Barrett-Connor, Lisa Palermo, Eric S. Orwoll, Steven R. Cummings, Dennis M. Black, and Ann V. Schwartz. 2014. 'Fracture risk in diabetic elderly men: The MrOS study', *Diabetologia*, 57: 2057-65.

O'Sullivan, L. M., H. Allison, E. E. Parle, J. Schiavi, and L. M. McNamara. 2020. 'Secondary alterations in bone mineralisation and trabecular thickening occur after long-term estrogen deficiency in ovariectomised rat tibiae, which do not coincide with initial rapid bone loss', *Osteoporosis International*, 31: 587-99.

Parle, Eoin, Sherdya Tio, Annie Behre, John J. Carey, Colin G. Murphy, Timothy F. O'Brien, William A. Curtin, Stephen R. Kearns, John P. McCabe, Cynthia M. Coleman, Ted J. Vaughan, and Laoise M. McNamara. 2020. 'Bone Mineral Is More Heterogeneously Distributed in the Femoral Heads of Osteoporotic and Diabetic Patients: A Pilot Study', *JBMR Plus*, 4: e10253-e53.

Ryan, M., L. Barnett, J. Rochester, J. M. Wilkinson, and E. Dall'Ara. 2020. 'A new approach to comprehensively evaluate the morphological properties of the human femoral head: example of application to osteoarthritic joint', *Scientific Reports*, 10: 5538.

Sacher, S. E., H. B. Hunt, S. Lekkala, K. A. Lopez, J. Potts, A. K. Heilbronner, E. M. Stein, C. J. Hernandez, and E. Donnelly. 2022. 'Distributions of Microdamage Are Altered Between Trabecular Rods and Plates in Cancellous Bone From Men With Type 2 Diabetes Mellitus', *J Bone Miner Res*, 37: 740-52.

Schwartz, Ann V., Eric Vittinghoff, Douglas C. Bauer, Teresa A. Hillier, Elsa S. Strotmeyer, Kristine E. Ensrud, Meghan G. Donaldson, Jane A. Cauley, Tamara B. Harris, Annemarie Koster, Catherine R. Womack, Lisa Palermo, and Dennis M. Black. 2011. 'Association of BMD and FRAX score with risk of fracture in older adults with type 2 diabetes', *JAMA - Journal of the American Medical Association*, 305: 2184-92.

Sihota, Praveer, Ram Naresh Yadav, Ruban Dhaliwal, Jagadeesh Chandra Bose, Vandana Dhiman, Deepak Neradi, Shailesh Karn, Sidhartha Sharma, Sameer Aggarwal, Vijay G. Goni, Vishwajeet Mehandia, Deepak Vashishth, Sanjay Kumar Bhadada, and Navin Kumar. 2021. 'Investigation of mechanical, material and compositional determinants of human trabecular bone quality in type 2 diabetes', *The Journal of Clinical Endocrinology & Metabolism*, XX: 1-19.

Tamaddon, Maryam, Shen Mao Chen, Leyre Vanaclocha, Alister Hart, Moataz El-Husseiny, Johann Henckel, and Chaozong Liu. 2017. 'Decrease in Local Volumetric Bone Mineral Density in Osteoarthritic Joints Is Associated with the Increase in Cartilage Damage: A Peripheral Quantitative CT Study', *Frontiers in Materials*, 4.

Thrailkill, Kathryn M, Charles K Lumpkin Jr, R Clay Bunn, Stephen F Kemp, and John L Fowlkes. 2005. 'Is insulin an anabolic agent in bone? Dissecting the diabetic bone for clues', *American Journal of Physiology-Endocrinology and Metabolism*, 289: E735-E45.

Vestergaard, P. 2007. 'Discrepancies in bone mineral density and fracture risk in patients with type 1 and type 2 diabetes—a meta-analysis', *Osteoporosis International*, 18: 427-44.

Voumard, Benjamin, Pia Stefanek, Michael Pretterklieber, Dieter Pahr, and Philippe Zysset. 2022. 'Influence of aging on mechanical properties of the femoral neck using an inverse method', *Bone reports*, 17: 101638.

Wölfel, Eva M., Katharina Jähn-Rickert, Felix N. Schmidt, Birgit Wulff, Herbert Mushumba, Grazyna E. Sroga, Klaus Püschel, Petar Milovanovic, Michael Amling, Graeme M. Campbell, Deepak Vashishth, and Björn Busse. 2020. 'Individuals with type 2 diabetes mellitus show dimorphic and heterogeneous patterns of loss in femoral bone quality', *Bone*, 140: 115556-56.

CHAPTER 6

Concluding Remarks and Future Perspectives

6.1 Summary of Key Contributions

Type 2 diabetic patients experience up to a 3-fold increase in bone fracture risk. Paradoxically, these patients tend to have a normal or increased bone mineral density (BMD) compared to non-diabetic patients. The current leading hypothesis to explain the mechanism(s) of bone fragility in type 2 diabetes is that the hyperglycaemic state leads to non-enzymatic glycation in the collagen network, causing the formation of Advanced Glycation End-products (AGEs), which stiffen the overall collagen network and lead to more brittle behaviour. While the relationship between AGE accumulation and bone biomechanics has been widely proposed, a causal relationship has not yet been established, suggesting that other tissue-level mechanisms could be responsible for fragility. This thesis investigated the biomechanics of type 2 diabetic bone fragility through a multiscale experimental strategy that considered structural, mechanical and compositional features of in vitro and ex vivo human tissue samples.

The overall contribution of this thesis has been to present a detailed biomechanical investigation that provides new insights into the mechanisms of diabetic bone fragility. These

studies have provided much-needed experimental data to the biomechanics community that systematically evaluated the biomechanical and compositional properties of both in vitro AGE accumulated bone and human type 2 diabetic bone. Furthermore, this work has evaluated the morphological properties of the human type 2 diabetic femoral head in both discrete locations and more regional locations. The key scientific contributions have been to show that type 2 diabetes does not impair the trabecular bone's mechanical properties, with some mechanical properties being higher in type 2 diabetes. Additionally, type 2 diabetes has been shown to alter compositional properties of both the mineral and organic phases, and to generally maintain, or in discrete regions, have denser morphological properties. This section outlines in more detail the key contributions and main findings from each of these studies.

Chapter 3 presented an experimental investigation on the effect of in vitro AGE accumulation on bovine cortical bone mechanics using three-point bend, fracture toughness and nanoindentation tests, and fluorometric analysis. It was shown that the mechanical response of bone tissue changed significantly due to AGE accumulation, with glycated samples exhibiting improved mechanical properties. The yield stress, ultimate flexural strength, and secant modulus of the glycated samples were significantly higher than those of the controls, according to the results of three-point bend testing. Furthermore, fracture toughness testing revealed that the critical fracture toughness K_Q in glycated samples was higher by 16% compared to controls. These results contradict the idea that AGE accumulation causes increased brittleness of the tissue or plays any significant role in bone fragility. Instead, AGE accumulation was found to improve several pre-and post-yield tissue properties. Furthermore, the in vitro glycation model was found to induce a supra-physiological increase in the accumulation of AGEs. Specifically, the in vitro glycated samples exhibited an eight-fold rise in AGE accumulation compared to the non-glycated controls.

Chapter 4 presented an experimental investigation into the mechanics, microdamage accumulation, composition, and morphology of type 2 diabetic bone from the femoral head through monotonic and cyclic compression, nanoindentation high-performance liquid chromatography, Raman and fluorometric spectroscopy, and micro computed tomography. It was found that type 2 diabetic bone showed a significant increase in furosine levels, an early biomarker of AGEs, and significant alterations to both the mineral-to-matrix ratio and mineral crystallinity compared to non-diabetic controls. High-resolution micro-CT imaging showed that trabecular cores from the femoral heads of type 2 diabetic patients had higher bone mineral density, bone volume, trabecular thickness and reduced trabecular separation compared to controls. These type 2 diabetic samples also had enhanced macro-mechanical compressive properties, under both monotonic and cyclic compression. These significant differences remained even when normalised against the bone volume, with type 2 diabetic bone exhibiting higher yield, maximum strength, and greater resistance to deformation compared to controls. Furthermore, the type 2 diabetic samples exhibited a greater tolerance for cyclic loading before failing compared to controls. The findings corroborate several recent studies (Karim et al. 2018; Hunt et al. 2019; Parle et al. 2020), which also reported no significant reduction in the mechanical properties of trabecular bone in type 2 diabetes. The study suggests that type 2 diabetes does not impair the mechanical properties of trabecular bone in the femoral head, indicating that other factors may contribute to the heightened risk of fractures in type 2 diabetic patients.

In Chapter 5, a regional morphological assessment of the trabecular region of the type 2 diabetic femoral head was presented, where the trabecular region was segmented into thirty-seven regions of interest and compared against non-diabetic samples. As a whole, this chapter has offered insightful information about the morphological characteristics and BMD of people with type 2 diabetes. The findings suggest that individuals with and without type 2 diabetes have

significant differences in bone volume fraction, trabecular separation, trabecular number, and connectivity density, particularly in specific micro-anatomical regions of the bone. More generally, this Chapter also provided novel insights into the inter-regional and intra-regional heterogeneity of the trabecular structure in human femoral heads. Inter-regional heterogeneity evaluation revealed that the central trabecular region was the densest and structurally robust region. Intra-regionally it was found that the inferior subchondral trabecular region was the most heterogeneous region. This outcome is not surprising as the central trabecular region is where higher stresses and strains occur as it bears much of the load during loading activities, whereas the inferior subchondral trabecular region experiences significantly less loading. In bone, mechanosensors respond to loads experienced by the bone that are transmitted at a cellular level through fluid shear stress and extracellular matrix strain, leading to the release of intracellular signalling and trigger the initiation of mechanotransduction leading to adjustments in the gene expression and subsequent matrix production. These alterations lead to adapted tissue composition and structure for the applied loading conditions (Verbruggen and McNamara 2018).

The denser tissue found in the type 2 diabetic samples, in both Chapter 4 and 5, could be due to the altered remodelling process associated the hyperglycaemic state and accumulation of AGEs in type 2 diabetes, whereby the functions of the osteoblast and osteoblasts are inhibited leading to a lower bone turnover (Sassi et al. 2018; Purnamasari et al. 2017). The higher mechanical properties observed in the type 2 diabetic samples could possibly be explained by the altered morphological and denser properties of the bone, as well as the potentially higher mineral-to-matrix ratio. However, it should be noted that if this ratio becomes excessively high, it can have detrimental effects, which is not the case here. More research is required to clarify the underlying mechanisms causing these observations and ascertain the clinical implications of these findings for people with T2D.

The research presented in this thesis is important as it addresses a disease that affects a large portion of the worldwide population and places a significant burden on healthcare systems, while also filling knowledge gaps that can inform future research. The results challenge the overall assumption that AGE accumulation and type 2 diabetes cause trabecular bone tissue, in particular, to be impaired. Additionally, this research employed a multiscale experimental approach, considering structural, mechanical, and compositional characteristics of type 2 diabetic bone, providing a comprehensive understanding of tissue behaviour. Importantly, this study marked the first instance of cyclic testing on type 2 diabetic trabecular bone with subsequent microdamage measurement. Overall, this research advances our knowledge of the intricate connection between type 2 diabetes and bone health and lays the groundwork for future investigations to create efficient prevention and treatment plans for type 2 diabetic patients who are at risk of bone fractures.

6.2 Future Recommendations

This thesis represents a significant step towards understanding the mechanical behaviour, compositional properties, and morphological properties of trabecular bone in individuals with type 2 diabetes. One of the major contributions of this work was to demonstrate that type 2 diabetes does not necessarily cause impaired mechanical properties in trabecular bone of the femoral head. In fact, it was found that type 2 diabetic trabecular bone had higher strength and resistance to deformation compared to the non-diabetic controls, which coincided with a higher bone volume fraction and denser trabecular structure in the type 2 diabetic bone. Furthermore, an increase in furosine, an early glycation biomarker, was observed in type 2 diabetic trabecular bone for the first time. This is important because, despite the fact that AGE markers were found to be increased in type 2 diabetic bone, no negative effect mechanical on the behaviour of the bone was observed. It is possible that AGE accumulation does not have the negative affect on bone that has widely been assumed. While the results from Chapter 4 focused mainly on

trabecular bone, future work should consider apparent tissue-level mechanical properties of type 2 diabetic cortical bone, as porosity is reportedly higher in type 2 diabetic cortical bone (Burghardt et al. 2010; Patsch et al. 2013; Yu et al. 2014). Specifically, investigating the fatigue, microdamage, and compositional properties of type 2 diabetic cortical bone could provide important insights into bone fragility in this population. A substantial limitation of the majority of the recent studies on the biomechanics of type 2 diabetic bone is that biomechanical testing has been carried out on discrete cores that have been taken from the femoral head. While there are obvious practical reasons for this, as the femoral head is discarded during total hip replacements, the structural complexity of these specimens presents certain confounding factors in trying to determine true biomechanical properties. To gain true insight into bone biomechanics, there is a distinct need for information to be captured at the whole-bone level, whereby bone samples could possibly be obtained through a donor programme similar to previous investigations on whole bone (Mueller et al. 2011). Future investigation of the biomechanics of whole bone through fatigue, compression and fracture toughness studies would provide valuable insights into the mechanical properties of type 2 diabetic bone at a macroscopic level.

The results from this thesis, and other recent publications, present a clear paradox between tissue-level biomechanics and population-level studies, where type 2 diabetic patients have been found to have a higher incidence of fragility fractures than non-diabetic patients (Bonds et al. 2006; Janghorbani et al. 2007; Vestergaard 2007; Schwartz et al. 2011; Napoli et al. 2014). It is important to acknowledge that population level studies can be influenced by biases, and certain factors may not be adequately accounted and controlled for, potentially resulting in the findings of these population-level studies not fully representing the overall picture, which may explain the conflicting results. There is a clear difficulty in understanding the mechanisms of fragility and providing a better link between these population-level and tissue-level studies

is essential. Future studies could make better use of imaging modalities across these scales, through DXA, HR-pQCT and micro-CT imaging to gain a more complete picture of structural alterations taking place at multiple anatomical locations. Furthermore, at the tissue-level, the control of samples remains a challenge as the precise severity of type 2 diabetes is not always known, with other important factors such as BMI, HbA1C and long-term disease management missing from patient data. Larger sample numbers and better stratification of patients and samples could provide further insight into the impact of the disease, with recent work in particular identifying two distinct subgroups of type 2 diabetic bone based on cortical porosity, whereby type 2 diabetic patients have either normal porosity and or high porosity (T2DwHP) (Wölfel et al. 2020; Wölfel et al. 2022). However, it remains unknown whether the increased fracture risk associated with type 2 diabetes is prevalent across all type 2 diabetic individuals or only affects those in the subgroup with high porosity. Therefore, further investigation on these subgroups, across tissue and population-level is warranted to determine if both subgroups of type 2 diabetic bone have an increased fracture risk and whether preventative measures should be focused solely on T2DwHP individuals. Additionally, an interesting future research question could explore whether T2DwHP individuals have high porosity prior to becoming diabetic or is this high porosity induced by type 2 diabetes. To explore this research question, ideally, some longitudinal research on individuals recently diagnosed with type 2 diabetes could be carried out. Such studies would provide valuable information on the relationship between type 2 diabetes and high cortical porosity, and the effect on fragility.

Finally, there is much ongoing work in the general area of type 2 diabetes, as it is a rapidly growing disease. Specifically, efforts are focused on determining the underlying cause of the increase in fracture risk of type 2 diabetic bone. The bone may be denser but possibly have increased cortical porosity and thus may not be stronger in the direction of the falls, which could explain the increased fracture risk. More studies using HR-pQCT should be carried out

at reported fall fracture sites. Further results from ex vivo and in vivo studies using human bone would provide valuable information to help diagnose the cause of the increase in fracture risk. These findings could help inform the development of target preventative strategies to reduce the risk of bone fractures in individuals with type 2 diabetes.

6.3 References

Bonds, Denise E., Joseph C. Larson, Ann V. Schwartz, Elsa S. Strotmeyer, John Robbins, Beatriz L. Rodriguez, Karen C. Johnson, and Karen L. Margolis. 2006. 'Risk of Fracture in Women with Type 2 Diabetes: the Women's Health Initiative Observational Study', *The Journal of Clinical Endocrinology & Metabolism*, 91: 3404-10.

Burghardt, Andrew J., Ahi S. Issever, Ann V. Schwartz, Kevin A. Davis, Umesh Masharani, Sharmila Majumdar, and Thomas M. Link. 2010. 'High-Resolution Peripheral Quantitative Computed Tomographic Imaging of Cortical and Trabecular Bone Microarchitecture in Patients with Type 2 Diabetes Mellitus', *The Journal of Clinical Endocrinology & Metabolism*, 95: 5045-55.

Hunt, Heather B., Ashley M. Torres, Pablo M. Palomino, Eric Marty, Rehan Saiyed, Matthew Cohn, Jonathan Jo, Stephen Warner, Grazyna E. Sroga, Karen B. King, Joseph M. Lane, Deepak Vashishth, Christopher J. Hernandez, and Eve Donnelly. 2019. 'Altered Tissue Composition, Microarchitecture, and Mechanical Performance in Cancellous Bone From Men With Type 2 Diabetes Mellitus', *JOURNAL OF BONE AND MINERAL RESEARCH*: jbmr.3711-jbmr.11.

Janghorbani, M., R. M. Van Dam, W. C. Willett, and F. B. Hu. 2007. 'Systematic Review of Type 1 and Type 2 Diabetes Mellitus and Risk of Fracture', *American Journal of Epidemiology*, 166: 495-505.

Karim, Lamya, Julia Moulton, Miranda Van Vliet, Kelsey Velie, Ann Robbins, Fatemeh Malekipour, Ayesha Abdeen, Douglas Ayres, and Mary L. Bouxsein. 2018. 'Bone microarchitecture, biomechanical properties, and advanced glycation end-products in the proximal femur of adults with type 2 diabetes', *Bone*, 114: 32-39.

Mueller, Thomas L., David Christen, Steve Sandercott, Steven K. Boyd, Bert van Rietbergen, Felix Eckstein, Eva-Maria Lochmüller, Ralph Müller, and G. Harry van Lenthe. 2011. 'Computational finite element bone mechanics accurately predicts mechanical competence in the human radius of an elderly population', *Bone*, 48: 1232-38.

Napoli, Nicola, Elsa S. Strotmeyer, Kristine E. Ensrud, Deborah E. Sellmeyer, Douglas C. Bauer, Andrew R. Hoffman, Thuy Tien L. Dam, Elizabeth Barrett-Connor, Lisa Palermo, Eric S. Orwoll, Steven R. Cummings, Dennis M. Black, and Ann V. Schwartz. 2014. 'Fracture risk in diabetic elderly men: The MrOS study', *Diabetologia*, 57: 2057-65.

Parle, Eoin, Sherdya Tio, Annie Behre, John J. Carey, Colin G. Murphy, Timothy F. O'Brien, William A. Curtin, Stephen R. Kearns, John P. McCabe, Cynthia M. Coleman, Ted J. Vaughan, and Laoise M. McNamara. 2020. 'Bone Mineral Is More Heterogeneously Distributed in the Femoral Heads of Osteoporotic and Diabetic Patients: A Pilot Study', *JBMR Plus*, 4: e10253-e53.

Patsch, Janina M., Andrew J. Burghardt, Samuel P. Yap, Thomas Baum, Ann V. Schwartz, Gabby B. Joseph, and Thomas M. Link. 2013. 'Increased cortical porosity in type 2 diabetic postmenopausal women with fragility fractures', *JOURNAL OF BONE AND MINERAL RESEARCH*, 28: 313-24.

Schwartz, Ann V., Eric Vittinghoff, Douglas C. Bauer, Teresa A. Hillier, Elsa S. Strotmeyer, Kristine E. Ensrud, Meghan G. Donaldson, Jane A. Cauley, Tamara B. Harris, Annemarie Koster, Catherine R. Womack, Lisa Palermo, and Dennis M. Black. 2011. 'Association of BMD and FRAX score with risk of fracture in older adults with type 2 diabetes', *JAMA - Journal of the American Medical Association*, 305: 2184-92.

Verbruggen, Stefaan W., and Laoise M. McNamara. 2018. 'Chapter 6 - Bone mechanobiology in health and disease.' in Stefaan W. Verbruggen (ed.), *Mechanobiology in Health and Disease* (Academic Press).

Vestergaard, P. 2007. 'Discrepancies in bone mineral density and fracture risk in patients with type 1 and type 2 diabetes—a meta-analysis', *Osteoporosis International*, 18: 427-44.

Wölfel, Eva M., Imke A. K. Fiedler, Sofie Dragoun Kolibova, Johannes Krug, Mei-Chun Lin, Bashar Yazigi, Anna K. Siebels, Herbert Mushumba, Birgit Wulff, Benjamin Ondruschka, Klaus Püschel, Claus C. Glüer, Katharina Jähn-Rickert, and Björn Busse. 2022. 'Human tibial cortical bone with high porosity in type 2 diabetes mellitus is accompanied by distinctive bone material properties', *Bone*, 165: 116546.

Wölfel, Eva M., Katharina Jähn-Rickert, Felix N. Schmidt, Birgit Wulff, Herbert Mushumba, Grazyna E. Sroga, Klaus Püschel, Petar Milovanovic, Michael Amling, Graeme M. Campbell, Deepak Vashishth, and Björn Busse. 2020. 'Individuals with type 2 diabetes mellitus show dimorphic and heterogeneous patterns of loss in femoral bone quality', *Bone*, 140: 115556-56.

Yu, E. W., M. S. Putman, N. Derrico, G. Abrishamanian-Garcia, J. S. Finkelstein, and M. L. Bouxsein. 2014. 'Defects in cortical microarchitecture among African-American women with type 2 diabetes', *Osteoporosis International*, 26: 673-79.